



AUBURN UNIVERSITY

SAMUEL GINN
COLLEGE OF ENGINEERING

Final Report
Project Number 930-866R

EVALUATION OF REMEDIATION STRATEGIES FOR SHRINK-SWELL CLAYS IN WESTERN ALABAMA

Submitted to

The Alabama Department of Transportation

Prepared by

J. Brian Anderson, Ph.D., P.E.
Dan T. Jackson, M.E.
Elizabeth Stallings Young, Ph.D., P.E.
Lydia Kennedy, M.S.
Dylan Jones, M.S.

JUNE 2024

Highway Research Center

**Harbert Engineering Center
Auburn University, Alabama 36849**

Chapter 1. Report No.	2. Government Accession No.	Chapter 3. Recipient Catalog No.	
4 Title and Subtitle EVALUATION OF REMEDIATION STRATEGIES FOR SHRINK-SWELL CLAYS IN WESTERN ALABAMA		5 Report Date Fall 2020	6 Performing Organization Code
		8 Performing Organization Report No. ALDOT 930-866R-1	
7. Author(s) J. Brian Anderson, Ph.D., P.E., Dan T. Jackson, M.S., Elizabeth Stallings Young, Ph.D., P.E., Lydia Kennedy, M.S., and Dylan Jones, M.S.		10 Work Unit No. (TRAIS)	
9 Performing Organization Name and Address Highway Research Center Dept. of Civil & Environmental Engineering 238 Harbert Engineering Center Auburn, AL 36849		11 Contract or Grant No.	
		13 Type of Report and Period Covered	
12 Sponsoring Agency Name and Address Alabama Department of Transportation 1409 Coliseum Boulevard Montgomery, AL 36130-3050		14 Sponsoring Agency Code	
		15 Supplementary Notes	
16 Abstract <p>Alabama Highway 5 is a farm-to-market road built over an expansive clay subgrade. Moisture fluctuations cause the soil to shrink and swell, resulting in severe pavement distress. The purpose of this study was to recommend and evaluate remediation strategies that can be implemented on AL 5 and other similar roadways that are affected by swelling clays in Alabama. Specific objectives included to establish the state-of-practice for shrink swell clay remediation for highway construction and maintenance and provide a decision matrix for their use, determine the causal mechanism(s) behind shrink and swell distress on AL 5 and other selected highways in and around the Tuscaloosa area, and demonstrate the effectiveness of selected remediation strategies during resurfacing of AL 5.</p> <p>The state-of-practice was evaluated to examine the behavior of expansive soils and document strategies that could be used for remediation of roadways affected by these soils. Particular emphasis was placed on methods that could be implemented without removing the pavement.</p> <p>Photographic, video, laboratory and field data were collected regarding the preconstruction conditions at AL 5. Laboratory tests, including one dimensional swell, soil water characteristic curves, torsional shear and standard AASHTO classification, were performed. A survey of the trees within 60 ft. of the roadway was conducted to draw correlations with observed pavement distress. International Roughness Index surveys were performed to determine the roadway roughness before and after remediation. The results show that the soils under AL 5 have considerable swell pressures. The shrink/swell cycle is predominately driven by suction pressures either from the soils themselves or nearby vegetation. Torsional ring shear tests revealed very low peak and residual friction angles for the subgrade likely has contributing to the pavement distress. Slope stability analyses concluded the roadway embankments were stable at the end of construction, but quickly failed as the peak and residual shear strength values were reached.</p> <p>Five remediation techniques were investigated at AL 5 in an attempt to identify a method that would the frequency of resurfacing. These remediation techniques included a sand blanket, vertical moisture barriers, lime columns, paved shoulders, and edge drains. Sensors including pavement strain gages, piezometers, moisture sensors and suction sensors were installed to remotely monitor the subgrade and asphalt conditions for the duration of the project. Continuous monitoring of the pavement and subgrade instrumentation revealed that no one method stood out from another in terms of long term performance.</p> <p>Based on the findings, expansive clays were identified at AL 5. These clays also exhibited very low residual shear strength contributing to perceived pavement distress. Paved shoulders, edge drains, and vertical barriers are recommended for mitigating expansive clays while minimizing project cost and inconvenience to the public.</p>			
17 Key Words expansive clay, pavement distress, soil moisture, remediation, trees		18 Distribution Statement No restrictions.	
19 Security Classification (of this report) Unclassified	20 Security Classification (of this page) Unclassified	21 No. of pages	22 Price None

FORM DOT F 1700.7 (8-72)

DRAFT Final Report 930-866R-1

Evaluation of Remediation Strategies for Shrink-Swell Clays in Western Alabama

Submitted to

The Alabama Department of Transportation

Prepared by

J. Brian Anderson, Ph.D., P.E.

Dan T. Jackson, M.S., Ph.D.

Elizabeth Stallings Young, Ph.D., P.E.

Lydia Kennedy, M.S.

Dylan Jones, M.S.

JUNE 2021

Disclaimers

The contents of this report reflect the views of the authors, who are responsible for the facts and the accuracy of the data presented herein. The contents do not necessarily reflect the official views or policies of the Alabama Department of Transportation or the Auburn University Highway Research Center. This report does not constitute a standard, specification, or regulation. Comments contained in this paper related to specific testing equipment and materials should not be considered an endorsement of any commercial product or service; no such endorsement is intended or implied.

NOT INTENDED FOR CONSTRUCTION, BIDDING, OR PERMIT PURPOSES

J. Brian Anderson, Ph.D., P.E.

Research Supervisor

Acknowledgements

This project was sponsored by the Alabama Department of Transportation (ALDOT). Material contained herein was obtained in connection with a research project “Evaluation of Remediation Strategies for Shrink-Swell Clays in Western Alabama,” ALDOT Project 930-866R, conducted by the Auburn University Highway Research Center. The funding, cooperation, and assistance of many individuals from each of these organizations are gratefully acknowledged. The researchers acknowledge the assistance and patience of Bureau of Materials and Tests current and past personnel (Scott George, Kaye Davis, John Jennings, Lyndi Blackburn, and Robert Shugart) and West Central Region current and past personnel (Valerie Branyon, Chris Strickland, Brad Darden, and Benji Cantrell). Students who assisted with this project are acknowledged as well including Jeremy Herman, Meredith Harbison, Connie Fike, Jameson Moulis, Matt Barr, Justin McLaughlin, Jonathan Hogan, Lester Lee, and Pavel Vointeko.

This project would not have been possible without the support of Ronnie Baldwin, Dee Rowe, and the late Buddy Cox.

Table of Contents

Acknowledgements.....	v
Table of Contents.....	vi
List of Figures.....	xi
List of Tables.....	xvii
Abstract.....	xviii
Chapter 1. Introduction.....	1
1.1 Background.....	1
1.2 Objective.....	4
1.3 Scope.....	4
1.4 Source Documents.....	4
Chapter 2. Background and Literature Review.....	6
2.1 Expansive Soils.....	6
2.1.1 Mechanism of Swelling and Shrinking.....	6
2.1.2 Unsaturated Soil Mechanics.....	7
2.1.3 Active Zone and Moisture Fluctuations.....	10
2.1.4 States of Stress.....	10
2.2 Shear Strength of Saturated and Unsaturated Soils.....	12
2.2.1 Typical and Correlated Values for Soils with Plasticity.....	14
2.3 Volume Change in Expansive Soils.....	15
2.3.1 Soil Water Characteristic Curves.....	19
2.3.2 Effect of Swelling on Clay Strength.....	22
2.4 Expansive Soils and Climate.....	23
2.5 Structural Damage to Pavement.....	25
2.6 Expansive Soils and Vegetation.....	26
2.6.1 Structural Damage due to Vegetation.....	30
2.6.2 Remedial Action for Vegetation Related Expansion.....	33
Chapter 3. State-of-Practice Review of Shrink-Swell Soil Stabilization Techniques.....	36
3.1 Mechanistic Designs for Minimizing Moisture Fluctuations.....	36
3.1.1 Vertical Moisture Barriers.....	36
3.1.2 Horizontal Moisture Barriers.....	39
3.1.3 Edge Drains.....	42
3.1.4 Ponding/Prewetting and Water Injection.....	43
3.2 Chemical Treatment.....	46

3.2.1	Traditional Chemical Stabilizers.....	46
3.2.1.1	Lime.....	46
3.2.1.2	Portland Cement	51
3.2.1.3	Fly Ash	52
3.2.2	Nontraditional Chemical Stabilizers	54
3.2.2.1	Potassium and Ammonium.....	54
3.3	Physical Ground Improvements.....	54
3.3.1	Compaction	55
3.3.2	Removal and Replacement/Surcharging.....	55
3.4	New and/or Innovative Designs	56
3.4.1	Geogrids.....	56
3.4.2	Electrochemical Treatment	59
3.4.3	Tire Shreds	60
3.4.4	Deep Soil Mixing (DSM) Columns	60
Chapter 4.	Preliminary Investigation.....	62
4.1	Desk Study	62
4.2	Soil Sample Collection and Subsurface Investigation	69
4.3	Site Observations.....	75
4.3.1	Traffic	75
4.3.2	Site Observations by Damage Type.....	76
4.3.2.1	Heave	76
4.3.2.2	Longitudinal Cracking Associated with Trees	79
4.3.2.3	Slope Distress and Potential Failure	84
4.3.2.4	Standing Water	85
4.3.2.5	Pavement Rutting	86
4.3.3	Site Observations by Location	87
4.3.3.1	Location: Start of Project MP 50.802 to CR12 Intersection at MP 51.82	87
4.3.3.2	Location: MP 50.82 to Start of Project at MP 50.802 (Post Leveling July 2015) 89	
4.3.3.3	Location: MP 50.82 (Post Leveling July 2015).....	89
4.3.3.4	Location: MP 50.84 to MP 50.88 (Post Leveling July 2015).....	89
4.3.3.5	Location: MP 50.93 (Post Leveling July 2015).....	89
4.3.3.6	Location: MP 50.88 to MP 50.97 (Post Leveling July 2015).....	89

4.3.3.7	Location: MP 50.97 to MP 51.00 (Post Leveling July 2015).....	89
4.3.3.8	Location: MP 51.00 to 51.03 (Post Leveling July 2015).....	90
4.3.3.9	Location: MP 51.12 to MP 51.18 (Post Leveling July 2015).....	90
4.3.3.10	Location MP 51.18 to MP 51.21 (Post Leveling July 2015).....	90
4.3.3.11	Location: CR 12 Intersection MP 51.82 to Start of Deciduous Trees at MP 52.82	90
4.3.3.12	Location: MP 51.915 to MP 52.055	92
4.3.3.13	Location: MP 53.11 to MP 53.28	94
4.3.3.14	Location: MP 53.28 to CR 15 Intersection at MP 53.38	96
4.3.3.15	Location: MP 53.52	97
4.3.3.16	Location: Approaches to Bridge at MP 53.68	98
4.3.3.17	Location: MP 54.22	99
4.3.3.18	Location: MP 54.35 to End of Project MP 54.85	100
4.3.4	Tree Survey	101
4.4	International Roughness Index (IRI) Surveys	104
4.5	One Dimensional Swell.....	109
4.6	Torsional Ring Shear Testing.....	113
4.7	Slope Stability Evaluation.....	117
4.8	Synthesis of Preliminary Investigation	121
Chapter 5.	Implementation of Test Sections	125
5.1	Site Description, Layout, and Nomenclature	125
5.2	Remediation Techniques Implemented at AL 5.....	127
5.2.1	Sand Blanket	127
5.2.2	Vertical Moisture Barriers	129
5.2.3	Lime Columns.....	133
5.2.4	Six Foot Paved Shoulders	138
5.2.5	Edge Drains.....	140
5.2.6	Deep Mixing	141
5.3	Instrumentation.....	143
5.3.1	Moisture Sensors.....	143
5.3.2	Suction Sensors	145
5.3.3	Piezometers	146
5.3.4	Neutron Moisture Probe.....	147

5.3.5	Asphalt Strain Gages.....	148
5.3.6	Data Acquisition System and Weather Station.....	149
5.4	Sensor Installation.....	151
5.4.1	Instrumentation Locations	151
5.4.2	Downhole Sensors	153
5.4.2.1	Moisture Sensor Installation.....	153
5.4.2.2	Suction Sensors.....	159
5.4.2.3	Piezometers.....	159
5.4.3	Asphalt Strain Gage Installation	160
5.4.3.1	Sand Blanket Asphalt Strain Gages.....	162
5.4.3.2	All Other Asphalt Strain Gages	164
5.5	Sensor Survivability	165
Chapter 6.	Results and Discussion	167
6.1	Climatological Data.....	167
6.2	Sensor Data	167
6.2.1	Control	167
6.2.2	Sand Blanket – Test Section 1	169
6.2.3	Vertical Barriers – Test Section 2.....	171
6.2.4	Lime Columns – Test Section 3.....	173
6.2.5	Paved Shoulders – Test Section 4.....	175
6.2.6	Edge Drains – Test Section 6.....	177
6.2.7	Trees.....	179
6.3	Interpretation of Sensor Data	180
6.4	Interpretation of IRI Tests	183
6.5	Observations.....	185
6.5.1	December 2016	185
6.5.2	December 2017	186
6.5.3	June 2018	187
6.5.4	November 2018.....	189
6.5.5	October 2019.....	190
6.5.6	February 2020	192
6.5.7	May 2020	196
6.6	Interpretation of Observations.....	199
Chapter 7.	Decision Making and Implementation.....	200

7.1	Analysis of Cost Data.....	200
7.2	Decision Tree for Insitu Remediation Techniques.....	201
7.3	Recommendations on Remediation Options Not Investigated in the Current Study ...	201
Chapter 8.	Summary, Conclusions, Implementation, and Recommendations	204
8.1	Project Summary	204
8.2	Conclusions	205
8.3	Implementation.....	206
8.4	Recommendations for Future Research	206
References	208

List of Figures

Figure 1. Distribution of Expansive Soils in the United States (Patrick and Snethen 1976).....	2
Figure 2. Severity of Expansive Soils in the Southeast (Patrick and Snethen 1976).....	2
Figure 3. Detail of Expansive Soils Showing the AL 5 Study Area.....	3
Figure 4. Recent photograph of AL 5 facing south depicting the condition of the roadway.....	4
Figure 5: Diagram of the Montmorillonite System (Mitchell 1976)	6
Figure 6: Saturated and Unsaturated Soil Zones (after Lu and Likos 2004)	9
Figure 7: Water Content Profiles in the Active Zone (Nelson and Miller 1992)	11
Figure 8: Unsaturated Soil Element (Fredlund and Rahardjo 1993)	12
Figure 9: Mohr-Coulomb Failure Criterion (Saturated Soil) (after Burrage 2016)	13
Figure 10: Extended Mohr-Coulomb Failure Criterion (Unsaturated Soil) (after Burrage 2016)	14
Figure 11: Relationship between $\sin \phi_p$ and plasticity index for normally consolidated soils (After Lambe and Whitman 1969, Kenney 1959)	15
Figure 12: Residual Friction Angle versus Effective Normal Stress Raised to the Minus One Third Power (Data from Chattopadhyay 1972) (Mitchel and Soga 2005)	16
Figure 13: Location of Common Clay Minerals on Casagrande's Plasticity Chart (developed from Casagrande 1948 and data in Mitchell and Soga 2005) (Holtz and Kovacs 1981).....	18
Figure 14: A Diagram Showing the Intercalation of Water Molecules in the Inter-plane Space of Clay Smectites (Taboada 2003).....	19
Figure 15: Three-dimensional Constitutive Surfaces for Soil Structure of an Unsaturated Soil (Fredlund and Rahardjo 1993).....	20
Figure 16: Semi-logarithmic Plot of Void Ratio versus Net Normal Stress and Matric Suction (Fredlund and Rahardjo 1993).....	20
Figure 17: Illustration of McQueen and Miller's (1974) Conceptual Model for General Behavior of the Soil-Water Characteristic Curve (after Lu and Likos 2004)	21
Figure 18: Hysteresis in SWCC (Fredlund et al. 2012).....	21
Figure 19: Representative Soil-Water Characteristic Curves for Sand, Silt and Clay (Lu and Likos 2004)	22
Figure 20: Deformation and Fluid Flow Phenomena in a Near-Surface Deposit of Unsaturated Expansive Soil (after Lu and Likos 2004)	25
Figure 21: Formation of longitudinal cracks during (a) dry and (b) wet seasons (Zornberg and Gupta 2009)	26
Figure 22: Schematic Sketch of Soil-Plant-Atmosphere System (a) Transpiration (b) Soil-plant-atmosphere interaction (c) Active and main roots (Indraratna et al. 2006)	27
Figure 23: Average Soil Water Potential at 20cm Depth During 1993 Growing Season (Dawson 1996)	29
Figure 24: Average Soil Water Potential Around the Root Systems of Three Large and Three Small Trees During the Early July Drought Period (Dawson 1996)	29
Figure 25: A Tentative Classification of the 'Water Demand' of Different Tree Genera in the UK (Biddle 2001)	30
Figure 26: Elevation Contours with Trees (inches) (Tand and Vipulanandan 2011).....	31
Figure 27: Arc-shaped Cracks in HMA Pavement Along 32nd Street, Stillwater, OK (Snethen 2001)	33
Figure 28: Diagram of Remedial Options if Drying is Predominately Seasonal (Biddle 2001) ..	34

Figure 29: Effect of Pruning or Felling if there is a Significant Persistent Moisture Deficit; Stability Not Achieved (Biddle 2001)	34
Figure 30: Installation of a Vertical Moisture Barrier (Evans and McManus 1999).....	37
Figure 31: Detail of Asphalt Seal Extending to Roadside Ditch (Snethen 1979).....	39
Figure 32: WYDOT Vertical and Horizontal Geomembrane Barrier Section Detail (Steinberg 1998)	41
Figure 33: Cross Sectional Schematic of Design Recommendations for IH-15 in Utah (Rollins and Christie 2002).....	42
Figure 35: Sketch of a Drilling Rig in a Pond (McKinney et al. 1974).....	44
Figure 36: Change in Clay Particles Due to Reactivity with Lime (Little 1995)	46
Figure 37: Typical Injection System (Hayward Baker 2010).....	49
Figure 38: Distribution of Lime/Fly Ash Slurry from LSPI (Wilkinson et al. 2010).....	51
Figure 39: Rubber Tired Injection Machines Used in the Beloit Road Project (Hayward Baker 1990)	51
Figure 40: Cross-Section of a Road with Geogrid Reinforcement (Zornberg and Gupta 2009)..	57
Figure 41: Picture of Excavation and Geogrid Edge (Zornberg and Gupta 2009)	58
Figure 42: Electro-osmosis in Clay (Mitchell 1976)	59
Figure 43: Schematic of Deep Mix Columns for the Stabilization of Expansive Soils (Madhyannapu, 2007)	61
Figure 44: Google Map of Alabama Highway 5: MP 50.8-54.3 (Google Earth 2014)	63
Figure 45: Historical Weather Data for Selma Alabama, 1981-2010 (NOAA National Climatic Data Center 2010)	65
Figure 46: Google Map of Alabama Highway 5 (Google Earth 2014) overlaid with USGS Soil Survey Map (Szabo et al. 1988).....	66
Figure 47: Geologic Map of Perry County, AL. Study Area Outlined (Reed 1969).....	66
Figure 48: USDA Soil Survey General Soil Map (Harris 1998)	68
Figure 49: Google Map of Alabama Highway 5 (Google Earth 2014) overlaid with USGS Soil Survey Map (Szabo et al. 1988).....	70
Figure 50: Boring Log Near Mile Marker 53 on AL 5	71
Figure 51: Various Clays Encountered During AL 5 Sampling Operations	71
Figure 52: Illustration of Differential Heave (Not to Scale).....	76
Figure 53: Google Earth Image of AL 5 from Borings B1.0 to B5.0 (after Google Earth 2014). 77	
Figure 54: AL 5 Facing South of Boring B3.0 MP 51.85 (Photo Taken 06/15/15)	78
Figure 55: AL 5 Facing North of CR 12 Intersection MP 51.82 (Photo Taken 06/15/15).....	79
Figure 56: Google Earth Image of AL 5 near Boring B5.0 (Google Earth 2014)	81
Figure 57: Willow Oak, Diameter 41.1 inches (Photo Taken 09/13/16)	82
Figure 58: Driving Factors behind Pavement/Slope Damage near Boring B5.0 MP 52.85	83
Figure 59: Longitudinal Crack due to Shrink Swell near Boring 5.0 MP 52.85 (Photo Taken 06/02/15)	84
Figure 60: Standing Water Observed in Ditch (Photo Taken 4/14/2015)	85
Figure 61: Standing Water Observed between Borings 1.0 and 1.5 (Photo Taken 7/10/15).....	85
Figure 62: Observed Rutting Near Boring 5.0 MP 52.85 (Rut Depth 1 3/8 inch) (Photo Taken 09/13/16)	86
Figure 63: Observed Rutting and Longitudinal Cracking (Photo Taken 09/14/16)	87
Figure 64: Observed Rutting (Photo Taken 09/14/16)	87
Figure 65: AL 5 Facing South MP 51.81 (Photo Taken 11/18/13)	88

Figure 66: AL 5 Facing South MP 51.53 Pre-leveling (Photo Taken 11/18/2013).....	88
Figure 67: AL 5 Facing South of Boring B3.0 MP 51.85 (Photo Taken 06/16/15)	91
Figure 68: AL 5 Facing North of Boring B3.0 MP 51.85 (Photo Taken 06/16/15)	91
Figure 69: AL 5 Facing South of MP 51.915 (Photo Taken 06/16/15)	92
Figure 70: AL 5 Facing South of MP 51.915 (Photo Taken 11/18/2013)	92
Figure 71: AL 5 Facing North MP 51.915 (Photo Taken 06/16/15)	93
Figure 72: AL 5 Facing East MP 51.915 (Photo Taken 06/16/15).....	93
Figure 73: AL 5 Facing North MP 52 (Photo Taken 06/16/15)	94
Figure 74: AL 5 Northbound Lane and Shoulder Facing South MP 53.19 (Photo Taken 06/16/15)	94
Figure 75: AL 5 Northbound Lane Facing South MP 53.19 (Photo Taken 06/16/15)	95
Figure 76: AL 5 Facing Southwest MP 53.19 (Photo Taken 06/16/15)	95
Figure 77: AL 5 Southbound Lane Facing North MP 53.19 (Photo Taken 06/16/15)	95
Figure 78: AL 5 Northbound Lane Facing South MP 53.38 (Photo Taken 06/16/15)	96
Figure 79: Northbound Lane Shoulder and Culvert MP 53.30 (Photo Taken 06/16/15)	97
Figure 80: AL 5 Facing South MP 53.52 (Photo Taken 06/16/15)	97
Figure 81: AL 5 Southbound Approach to Bridge Facing South (Photo Taken 06/16/15)	98
Figure 82: AL 5 Southbound Approach to Bridge Facing North (Photo Taken 06/16/15)	99
Figure 83: AL 5 Facing North MP 54.22 (Photo Taken 06/16/15)	99
Figure 84: AL 5 Facing South East MP 54.59 (Photo Taken 06/16/15).....	100
Figure 85: AL 5 Facing North MP 54.21 (Photo Taken 06/16/15)	100
Figure 86: AL 5 Facing North MP 54.58 (Photo Taken 06/16/15)	101
Figure 87: AL 5 Facing South MP 54.58 (Photo Taken 06/16/15)	101
Figure 88: Tree Roots Observed During Installation of Sensors (Photo Taken 06/28/16).....	103
Figure 89: Tree Root (4" Diameter) Approximately 15' from Edge of Pavement.....	103
Figure 90: Tree Root Extracted from Boring Hole 4.5 (Photo Taken 5/23/16).....	104
Figure 91: Pavement Profiles (Sayers and Karamihas 1998)	104
Figure 92: Inertial Profiler Schematic(Sayers and Karamihas 1998)	105
Figure 93: Northbound, Inside Wheel Path IRI Profiles for May and November 2014.....	107
Figure 94: Northbound, Outside Wheel Path IRI Profiles for May and November 2014	107
Figure 95: Southbound, Inside Wheel Path IRI Profiles for May and November 2014.....	108
Figure 96: Southbound, Outside Wheel Path IRI Profiles for May and November 2014	108
Figure 97: Stress paths of 1-Dimensional Swelling (Tu and Vanapalli 2016)	111
Figure 98: Controls Group Bromhead Ring Shear Apparatus (Controls Group 2019)	114
Figure 99: Plasticity Index versus $\sin \phi_p$ Using Data from Kenney (1959) (After Lambe and Whitman 1969)	116
Figure 100: Comparing Residual Friction Angles versus Effective Normal Stress Raised to the Minus One Third Power from AL 5 (After Mitchel and Soga 2005)	117
Figure 101: Typical Slope for AL 5 Roadway Embankments.....	118
Figure 102: Example of Soil Profile for B1.5 using Residual Strength Values	119
Figure 103: Minimum Failure Surfaces for B1.5 using Residual Strength Values	120
Figure 104: Northbound, Inside Wheel Path IRI Surveys with Site Conditions	122
Figure 105: Northbound, Outside Wheel Path IRI Surveys with Site Conditions.....	123
Figure 106: Southbound, Inside Wheel Path IRI Surveys with Site Conditions	123
Figure 107: Southbound, Outside Wheel Path IRI Surveys with Site Conditions.....	124

Figure 108: Northbound, Outside Wheel Path IRI Surveys Overlain with Swell Pressures and Matric Suction.....	124
Figure 109: Layout of Research Site (Google 2014).....	126
Figure 110: Sand Blanket Cross-Section (ALDOT 2015).....	127
Figure 115: Typical Vertical Moisture Barrier Cross-Section (Snethen 1979).....	130
Figure 116: Vertical Moisture Barrier Cross-Section Plans (ALDOT 2015).....	130
Figure 117: Vertical Moisture Barrier Excavation	131
Figure 118: Vertical Moisture Barrier Cave-In	131
Figure 119: Vertical Moisture Barrier Membrane Placement	132
Figure 120: Vertical Moisture Barrier Filling.....	132
Figure 121: Vertical Moisture Barrier Paving	133
Figure 122: Layout of Lime Columns at AL 5 (ALDOT 2015).....	134
Figure 123: Typical Cross-Section of Lime Columns (ALDOT 2015).....	134
Figure 124: Lime Column Drilling.....	135
Figure 125: Lime Column Drilled Holes	135
Figure 126: Packing Lime Columns	136
Figure 128: Lime Columns Reflecting to Pavement Surface	137
Figure 129: Lime Columns Reflected Through Binder Course and Holding Water	137
Figure 130: Paved Shoulder Cross Section (ALDOT 2015)	138
Figure 131: Longitudinal Cracks in Travel Lane at AL 5 Visible During Construction.....	139
Figure 132: Paved Shoulder Build-Up.....	139
Figure 133: Typical Edge Drain Cross-Section at AL 5 (ALDOT 2015).....	140
Figure 135: Installed Edge Drains	141
Figure 136: Deep Mix Column Layout (ALDOT 2015)	141
Figure 140: Decagon GS1.....	144
Figure 141: Decagon MPS6.....	145
Figure 142: Geokon 4500S	146
Figure 143: Troxler Model 4300 Depth Moisture Gauge.....	147
Figure 144: CTL Asphalt Strain Gage.....	148
Figure 145: Geocomp Asphalt Strain Gage.....	149
Figure 146: Campbell Scientific CR6, AM16/32B, and BP12/CH200	150
Figure 147: Campbell Scientific WTX520	150
Figure 148: Campbell Scientific RF451 and RavenXTV	151
Figure 149: Instrumentation Locations	152
Figure 152: Data Acquisition Installation.....	156
Figure 153: Moisture Sensor Installation Tool	156
Figure 154: GS1 Seated on Installation Tool.....	156
Figure 155: Moisture Sensor and Installation Tool being Lowered down Borehole.....	157
Figure 156: Moisture Sensor Installation.....	158
Figure 157: Fully Installed Moisture Sensor	158
Figure 158: Moisture Sensor Prongs Inserted into Drill Shavings	159
Figure 159: Suction Sensor Preparation	159
Figure 160: Piezometer in Sand-Filled Bag being Lowered Down the Borehole	160
Figure 161: Sand Blanket Strain Gage Layout	161
Figure 162: Strain Gage Layout for Sections Other than Sand Blanket.....	162
Figure 163: ASGs being Tacked with Tack-Sand Mixture	163

Figure 164: Screened Asphalt being Placed and Compacted over Gages	164
Figure 165: Section Milled and Cleaned for placement of ASG Array.....	165
Figure 166: Gage Array on Milled Surface Covered with Screened Asphalt.....	165
Figure 167: Climatological Data at AL 5	168
Figure 168: Strain with Time – Control.....	168
Figure 169: Moisture Content with Time – Control	169
Figure 170: Pore Pressure with Time – Control	169
Figure 171: Strain with Time – Sand Blanket	170
Figure 173: Pore Pressure with Time – Sand Blanket	171
Figure 174: Strain with Time – Vertical Barriers	172
Figure 175: Moisture Content with Time – Vertical Barriers.....	172
Figure 176: Pore Pressure with Time – Vertical Barriers	173
Figure 177: Suction with Time – Vertical Barriers	173
Figure 178: Strain with Time – Lime Columns.....	174
Figure 179: Moisture Content with Time – Lime Columns	174
Figure 180: Pore Pressure with Time – Lime Columns.....	175
Figure 181: Strain with Time – Paved Shoulders	176
Figure 183: Pore Pressure with Time – Paved Shoulders.....	177
Figure 184: Suction with Time – Paved Shoulders	177
Figure 185: Strain with Time – Edge Drains.....	178
Figure 186: Moisture Content with Time – Edge Drains	178
Figure 187: Pore Pressure with Time – Edge Drains.....	179
Figure 188: Suction with Time – Edge Drains	179
Figure 189: Moisture Content with Time – Trees	180
Figure 190: Suction with Time – Trees	180
Figure 191: Relationship Between Strain and Volumetric Moisture Content from the Paved Shoulders Section.....	181
Figure 192: Comparison of Functioning Suction Sensor Measurements	181
Figure 193: Suction and Strain Over Time for Paved Shoulders.....	182
Figure 194: Suction and Strain Over Time for Edge Drains	182
Figure 195: Average IRI by Test Section	184
Figure 196: Comparison of IRI since 2014.....	184
Figure 197: Longitudinal crack in Vertical Barrier section.....	185
Figure 198: Distress of pavement on AL 5 south of the Perry County line.....	186
Figure 199: Off project distress on US80	186
Figure 200: Tree related distress on AL in Dallas County	187
Figure 201: Paved shoulder section of AL 5 in Dallas County	187
Figure 202: Observed Pavement Distress on AL 5 in Dallas County.....	188
Figure 203: Cracking in the paved shoulders section	189
Figure 204: Visible Distress in paved shoulders section	189
Figure 205: Vertical barrier section crack propagation	190
Figure 206: Severe pavement distress south of the Dallas County line.....	190
Figure 207: Vertical Barriers Crack.....	191
Figure 208: Shoulder and Lane Cracking in the Edge Drains	191
Figure 209: Edge Drains Section	192
Figure 210: Paved Shoulders Section	193

Figure 211: Lime Columns Section	193
Figure 212: Lime Vertical Barriers Section.....	194
Figure 213: Sand Blanket Section.....	194
Figure 214: Lime Control Section	195
Figure 215: Off project south of Dalla County Line.....	195
Figure 216: Cracking in Control Near Tree.....	196
Figure 217: Cracking along Safety Widening in Edge Drains Section	197
Figure 218: Shoving in Edge Drain Section	197
Figure 219: Shoving in Paved Shoulder Section	198
Figure 220: Opening Crack with Settlement in Safety Widening of Paved Shoulders	198
Figure 221: Pavement Surface Raveling in Control Section	199

List of Tables

Table 1: Possible Combinations of Stress State Variables for an Unsaturated Soil (Fredlund and Rahardjo 1993).....	12
Table 2: Summary of Friction Angle Data for Use in Preliminary Design (Lambe and Whitman 1969)	16
Table 3: Probable Expansion as Estimated from Classification Test Data (from Holtz and Kovacs 1981)	17
Table 4: Calculated Values for Shear Ratio for all Tested Specimens (Al-Mhaidib and Al-Shamrani 2006).....	24
Table 5: Soil Properties at 32nd Street, Stillwater, Oklahoma (Snethen 2001).....	32
Table 6: Historical Weather Data for Selma, Alabama, 1981-2010 (NOAA National Climatic Data Center 2010)	64
Table 7: Soil Properties from USDA Soil Survey (after Harris 1998)	67
Table 8: Soil Properties from Laboratory Tests on Field Specimens B1A – B7A.....	72
Table 9: Soil Properties from Laboratory Tests on Field Specimens B7A – B8.5A	73
Table 10: Summary of Atterberg Limits determined from Field Specimens	74
Table 11: Descriptive Statistics on Trees Surveyed near Boring B5.0.....	81
Table 12: Summary of Common Trees Surveyed and Size.....	102
Table 13: FHWA IRI Thresholds (Federal Highway Administration 2011).....	106
Table 14: Summary of One-Dimensional Swell Results	110
Table 15: Summary of Water Content and Saturation of Swell Test Specimens	113
Table 16: Summary of Ring Shear Results.....	115
Table 17: Correlated Undrained Shear Strength from Plasticity Index	119
Table 18: Factor of Safety for Slope Stability	120
Table 19: Test Sections	125
Table 20: Instrument Locations	152
Table 21: Sensor Survivability.....	166
Table 22: IRI Record for AL 5	183
Table 23: Costs for AL 5 Test Sections and Overall Project.....	200
Table 24: Comparison of All Remediation Techniques	203

Abstract

Alabama Highway 5 is a farm-to-market road built over an expansive clay subgrade. Moisture fluctuations cause the soil to shrink and swell, resulting in severe pavement distress. The purpose of this study was to recommend and evaluate remediation strategies that can be implemented on AL 5 and other similar roadways that are affected by swelling clays in Alabama. Specific objectives included to establish the state-of-practice for shrink swell clay remediation for highway construction and maintenance and provide a decision matrix for their use, determine the causal mechanism(s) behind shrink and swell distress on AL 5 and other selected highways in and around the Tuscaloosa area, and demonstrate the effectiveness of selected remediation strategies during resurfacing of AL 5.

The state-of-practice was evaluated to examine the behavior of expansive soils and document strategies that could be used for remediation of roadways affected by these soils. Particular emphasis was placed on methods that could be implemented without removing the pavement.

Photographic, video, laboratory and field data were collected regarding the preconstruction conditions at AL 5. Laboratory tests, including one dimensional swell, soil water characteristic curves, torsional shear and standard AASHTO classification, were performed. A survey of the trees within 60 ft. of the roadway was conducted to draw correlations with observed pavement distress. International Roughness Index surveys were performed to determine the roadway roughness before and after remediation. The results show that the soils under AL 5 have considerable swell pressures. The shrink/swell cycle is predominately driven by suction pressures either from the soils themselves or nearby vegetation. Torsional ring shear tests revealed very low peak and residual friction angles for the subgrade likely has contributing to the pavement distress. Slope stability analyses concluded the roadway embankments were stable at the end of construction, but quickly failed as the peak and residual shear strength values were reached.

Five remediation techniques were investigated at AL 5 in an attempt to identify a method that would the frequency of resurfacing. These remediation techniques included a sand blanket, vertical moisture barriers, lime columns, paved shoulders, and edge drains. Sensors including pavement strain gages, piezometers, moisture sensors and suction sensors were installed to remotely monitor the subgrade and asphalt conditions for the duration of the project. Continuous

monitoring of the pavement and subgrade instrumentation revealed that no one method stood out from another in terms of long term performance.

Based on the findings, expansive clays were identified at AL 5. These clays also exhibited very low residual shear strength contributing to perceived pavement distress. Paved shoulders, edge drains, and vertical barriers are recommended for mitigating expansive clays while minimizing project cost and inconvenience to the public.

Chapter 1. Introduction

1.1 Background

Shrinking and swelling, or sometimes called expansive, soils are typically the result of the presence of high plasticity clays that are subject to fluctuations in water content. The mineralogy of these clays results in a high affinity for water. Fluctuations in water content cause significant volume changes. The results of these changes often cause damage to structures and roadways. In 2009 numbers, it is estimated that damage due to expansive clays costs on the order of 13 billion dollars each year in the United States alone (Puppala and Cerato 2009). Steinburg (1985) estimated that approximately half of the damage occurs to the roadway system, while additional damage is incurred by other transportation facilities. These include airport runways, railroads, canals, pipelines, and sidewalks.

Expansive clays consist of colloid sized particles primarily of the smectite or montmorillonite mineral variety that have a large specific surface per unit volume. This is often evidenced in a very high plasticity index. For example, the total surface area of 0.35 oz of montmorillonite, is on the order of 90,000 square feet. (Rendon-Herrero 2011). The amount of swelling depends upon the clay minerals and their arrangement or orientation in the clay soil, as well as the physical-chemical properties such as valence of exchangeable cations, pore water salt concentration, and cementing bonds between clay particles. (Yong and Warkentin 1966).

The consequences of swelling can be significant. Swelling pressures can be as high as 9 tsf in some clays (Yong and Warkentin 1966). Of course, this is extreme and lesser values are seen with lower activity clays; however, there can be enough swelling pressure to heave a building foundation. Even lower pressures are required to heave a roadway.

Expansive soils are an issue in many areas in the United States as depicted in Figure 1. The darker areas represent zones where expansive soils are most common. Focusing in on the southeastern United States, there exists a significant area of low level expansive soils. Based on the maps shown in Figure 2, this problem is relatively widespread in states near Alabama (Texas, Louisiana, Oklahoma, Kansas, and Mississippi). However, within Alabama and Mississippi, there are discrete zones of medium to highly expansive soils. In Alabama, these soils cover between 5 and 10 percent of the state.

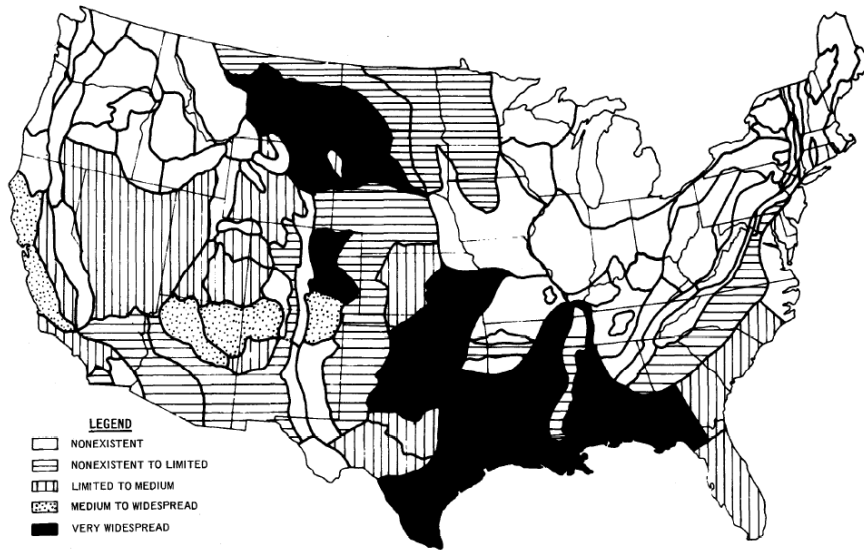


Figure 1. Distribution of Expansive Soils in the United States (Patrick and Snethen 1976)

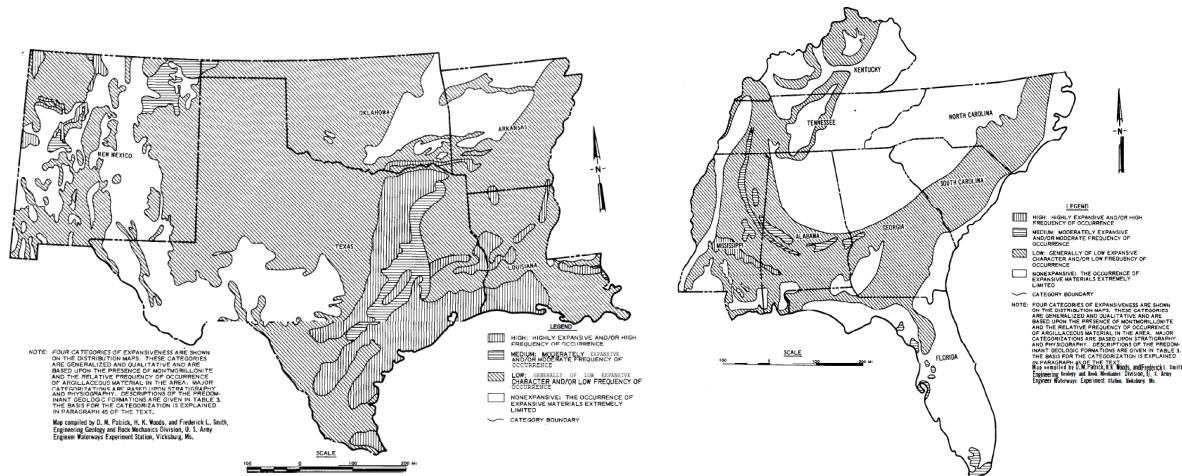


Figure 2. Severity of Expansive Soils in the Southeast (Patrick and Snethen 1976)

Literature and case studies suggest there are several mitigation approaches that are available including compacting wet of optimum, maintenance of water content, chemical treatment, reinforcement, and removal (Holtz and Kovacs 1981). However, these methods are best implemented during initial roadway construction. A much bigger challenge is how to mitigate the potential impacts for existing roadways. Furthermore, many roads just cannot be closed for the amount of time required to perform a permanent repair. Texas has by necessity investigated this issue. Techniques that have been developed for mitigation include horizontal drainage barriers (Steinberg 1992) and vertical drains (Wanyan et al. 2008).

Many roads in Alabama follow "farm to market" routes and were cut and built from materials in the immediate area. These roads typically serve rural areas, yet many have become key shipping and freight routes. A prime example of damage due to shrinking and swelling clays in Alabama is State Route 5 (AL 5) between US 80 and Marion, AL.

Figure 3 shows a Google Map superimposed over an inset of Alabama from Figure 2 (Patrick and Snethen 1976). The portion of AL 5 of interest, point A, falls in a zone of medium expansive clay. During a site visit in July of 2013 with ALDOT Tuscaloosa Area (formerly Division 5) and Materials and Tests Bureau Personnel, severe pavement distress was observed in the form of cracking and an uneven undulating surface. Heavy rain fell at the time and there was dangerous amounts of standing water encountered, resulting in hydroplaning. The distress is evident in Figure 4. After walking a local section then driving the length of the project, an initial hypothesis was made that drainage, or lack thereof, coupled with the character of the clays underneath the roadways, is the root cause of the distress. Of note, often the most severe distress was where there were agricultural ponds along the roadway. A secondary issue could be the pore water chemistry effects due to agricultural runoff and seepage in the area.

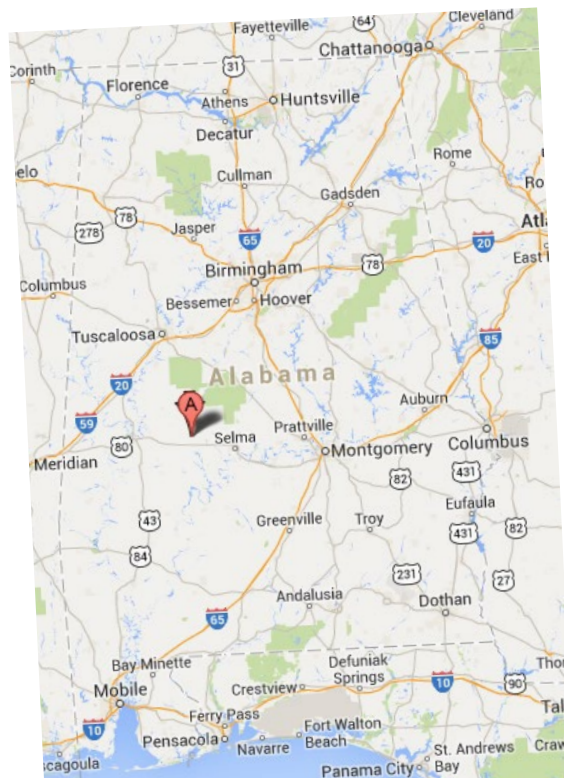


Figure 3. Detail of Expansive Soils Showing the AL 5 Study Area



Figure 4. Recent photograph of AL 5 facing south depicting the condition of the roadway.

1.2 Objective

The overall purpose of this research is to recommend and evaluate remediation strategies that can be implemented on AL 5 and other similar roadways that are affected by swelling clays in Alabama. Specific objectives include:

Establish the state-of-practice for shrink swell clay remediation for highway construction and maintenance and provide a decision matrix for their use.

Determine the causal mechanism(s) behind shrink and swell distress on AL 5 and other selected highways in and around the Tuscaloosa Area.

Demonstrate the effectiveness of selected remediation strategies during resurfacing of AL 5.

1.3 Scope

The research program involves investigation of published remediation strategies for similar soils, characterization, and monitoring of the behavior of existing distressed roadways, recommendation of potential remediation measures, and implementation of a monitoring and verification program to assess the effectiveness of the recommended strategies that will be implemented during resurfacing of AL 5.

1.4 Source Documents

This report is a compilation of the work of several students spanning from 2013 to 2019. Jeremy Herman (2015) compiled the initial site data and state of practice review for expansive soil

remediation. Elizabeth Stallings Young (2016) conducted laboratory tests to characterize the expansive nature of the clay soils present at AL 5. In addition, she conducted a detailed study of the tree species present in close proximity to the study sections in Perry County. The instrumentation program was designed and implemented by Dan Jackson (2016) and continued by Dylan Jones (2017). The residual strength of the expansive prairie clays was investigated by Lydia Kennedy (2019) who continued the monitoring program until the end of the project.

Chapter 2. Background and Literature Review

2.1 Expansive Soils

Expansive clays belong to the smectite mineral group and usually exist as bonded montmorillonite structures (Mitchell 1976, Nelson and Miller 1992). Figure 5 illustrates the montmorillonite particles:

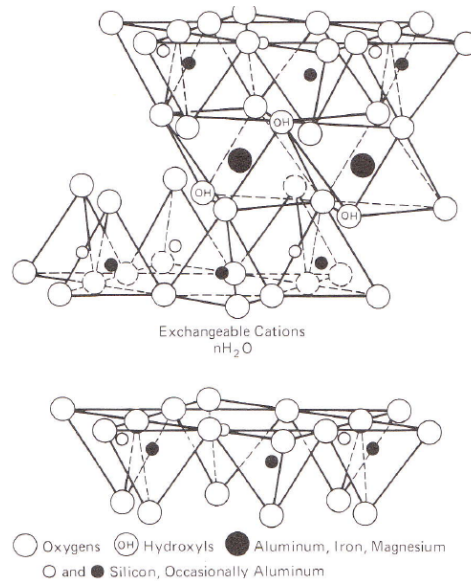


Figure 5: Diagram of the Montmorillonite System (Mitchell 1976)

Montmorillonite consists of an alumina octahedral sheet sandwiched between two silica tetrahedral sheets (Mitchell 1976). The structure is plate-like with negative charges along its surface and positive charges at its edges. Montmorillonite structures, or plates, are bonded together by exchangeable cations and water. Common exchangeable cations include sodium (Na^+), magnesium (Mg^{+2}), and calcium (Ca^{+2}). (The cations are termed “exchangeable” because they may be replaced by other cations). The cations are attracted to the negatively charged clay-plate surfaces. Each exchangeable cation contains a specific hydration energy (i.e. an attraction to a maximum concentration of water molecules) (Pengelly and Addison 2001). Thus, from a microscopic standpoint, expansive clays exist as montmorillonite structures, or plates, bonded together by exchangeable cations and water.

2.1.1 Mechanism of Swelling and Shrinking

The shrink-swell behavior of a montmorillonite clay is governed by its dominant type of exchangeable cation, the adsorptive forces of the clay plates, and the amount of available water

(Pengelly and Addison 2001, Nelson and Miller 1992). The dominant cation contains a specific hydration energy (an attraction to a maximum concentration of water molecules) with a corresponding hydration radius (a maximum possible radius of adsorbed water molecules) (Pengelly and Addison 2001). Additionally, each clay particle exerts short-range electrical and van der Waals forces on nearby water molecules (Lu and Likos 2004). Therefore, as water is made available, the hydration energy of the dominant cation and the short-range adsorptive forces of the clay plates attract water molecules until equilibrium is achieved. This adsorption of water results in the expansion of the diffused water layer surrounding individual clay particles, forcing individual clay particles apart from each other. This phenomenon constitutes swelling (Nelson and Miller 1992). The higher the concentration and/or valence charge of the dominant cation, the lower the swelling potential of a clay (Nelson and Miller 1992). Thus, for example, calcium (Ca^{+2}) montmorillonites are less expansive than sodium (Na^{+1}) montmorillonites (Nelson and Miller 1992).

Water may be removed from the montmorillonite clay system by outside forces, such as suction, which override the attractive forces of the dominant cation and clay particles. When this occurs, the diffused water layer surrounding individual clay particles will shrink, forcing individual clay particles closer together. This phenomenon constitutes shrinkage.

2.1.2 Unsaturated Soil Mechanics

Expansive clays usually exist as unsaturated soils (Fredlund and Rahardjo 1993). According to Terzaghi in *Theoretical Soil Mechanics*, soil mechanics is “the application of the laws of mechanics and hydraulics to engineering problems dealing with sediments and other unconsolidated accumulations of solid particles produced by mechanical and chemical disintegration of rocks, regardless of whether or not they contain an admixture of organic constituents” (Terzaghi 1943). Traditional, or saturated, soil mechanics addresses a variety of engineering problems by making one of the following assumptions: the soil particles are saturated and cohesive, the soil particles are saturated and cohesionless, or the soil particles are completely dry and cohesionless. Use of these assumptions allows for a two phase system of analysis: solids, and water or air. While soils meeting the aforementioned assumptions exist in nature and provide a starting place for analysis, a considerable number of engineering problems deal with soils falling between these extremes. Unsaturated soil mechanics addresses engineering problems and behaviors of cohesive and cohesionless soils that have varying amounts of water and air throughout

the soil mass. These partially saturated or unsaturated soils require a four phase system of analysis: solids, water, air, and a contractile skin – located at the air water interface.

When discussing unsaturated soils, it is important to visualize the different zones of soil under consideration. For the purposes of this section, assume a single homogenous and isotropic soil layer infinitely deep with a water table at a known depth below the ground's surface. The soil layer can then be broken up into four distinct zones based on pore water pressure and degree of saturation. Figure 6 depicts the different zones with their associated saturations and pore water pressures.

Below the water table is the “free water zone,” which has positive pore water pressure and is completely saturated with no air voids. Additionally, free water has no dissolved solutes, including air, has no interactions with other phases that would result in curvature at the air-water interface, and is acted upon only by gravity (Lu and Likos 2004). This state is in thermodynamic and chemical equilibrium and is used as the reference condition as the soil system transitions from saturated to unsaturated conditions. Soil suction is considered to be the decrease in pore water potential relative to the free water potential of zero. It is generally expressed as a positive value (Lu and Likos 2004).

Soil suction can be broken into osmotic and matric suction. Osmotic suction expresses the change in chemical potential of the water as solutes dissolve. Matric suction expresses the change in thermodynamic potential due to the combined effects of capillarity and short range adsorption of water molecules (Lu and Likos 2004). For the purposes of this investigation, osmotic suction is not considered since the ground and pore water are assumed homogenous. Equation 1 shows the combination of matric and osmotic suction to produce total suction.

$$\psi_T = \psi_m + \psi_o \quad (1)$$

where:

$\psi_T = \text{Total Suction}$

$\psi_m = \text{Matric Suction}$

$\psi_o = \text{Osmotic Suction}$

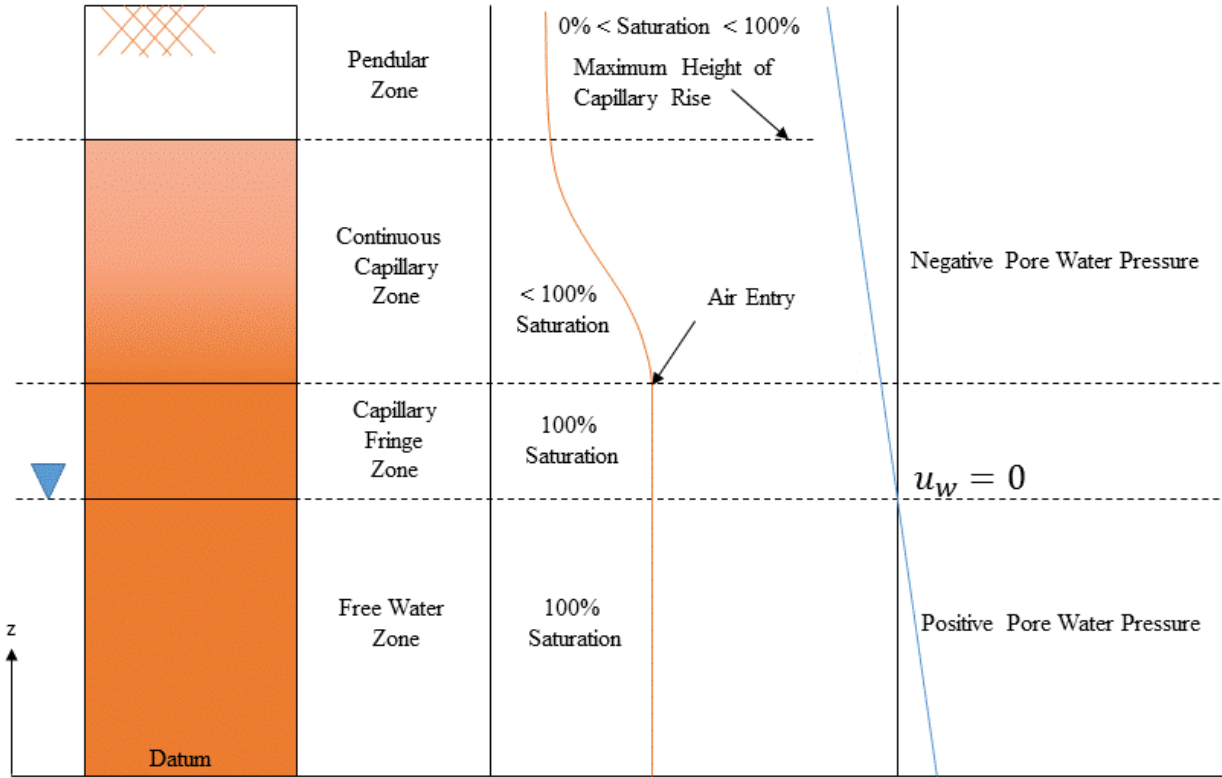


Figure 6: Saturated and Unsaturated Soil Zones (after Lu and Likos 2004)

Matric suction can be quantified by the difference between the pore air pressure and the pore water pressure.

$$\psi_m = u_a - u_w \quad (2)$$

where:

$$u_a = \text{pore air pressure}$$

$$u_w = \text{pore water pressure}$$

Above the water table is the “capillary fringe zone,” which can vary greatly in thickness depending on the grain size distribution of the soil. Within the capillary fringe the soils are fully saturated due to capillary rise but experience negative pore water pressure to maintain hydraulic equilibrium. The pores in a soil matrix form an interconnected pathway of varying diameter, which behaves like a capillary tube. The diameter of the tube drawing water limits the height of capillary rise. Similarly, the capillary fringe zone is limited by the maximum pore diameter in the stratum,

because when the pore diameter becomes sufficiently large for capillary action to cease along a single pathway, air entry occurs and unsaturated soils begin.

The continuous capillary zone begins at the air entry point and continues until the maximum height of capillary rise is achieved. This zone becomes increasingly desaturated with increasing elevation, “reflecting the fact that fewer and smaller capillary fingers are present for a given cross section of the soil column with increasing elevation” (Lu and Likos 2004). Beyond the maximum height of capillary rise pore water primarily exists in the form of pendular water menisci between the solid soil particles. This pendular region has relatively large matric suction and low water content.

Throughout the soil matrix above the water table, short-range adsorbed water plays an important role in matric suction as well. While the capillary effect arises from the curvature of the air-water interface, the short-range adsorption effects are derived from electrical and van der Waals force fields that develop at the solid-liquid interface (Lu and Likos 2004). The properties of adsorbed water and free water are different due to short-range physical and physicochemical interactions with the soil surface. This is especially true at low degrees of saturation and or pendular soil conditions (Lu and Likos 2004). For fine-grained soils, such as clay, the solid particles can carry a net electric charge, which interacts with the polarity of water to maintain a bond between the molecules. Because of the comparatively large surface area and surface charge of clay particles, short-range adsorption can dramatically affect the matric suction at relatively low water contents.

2.1.3 Active Zone and Moisture Fluctuations

The water content, and thus soil suction, in the upper few meters is influenced by environmental factors. This upper few meters where the suction changes seasonally is called the *active zone* (Nelson and Miller 1992). Figure 7 shows the active zone along with some environmental factors that influence the soil suction.

2.1.4 States of Stress

When characterizing the behavior of a given soil, the state of stress of that soil must be considered. State variables are any variables required to describe the state of stress of a system

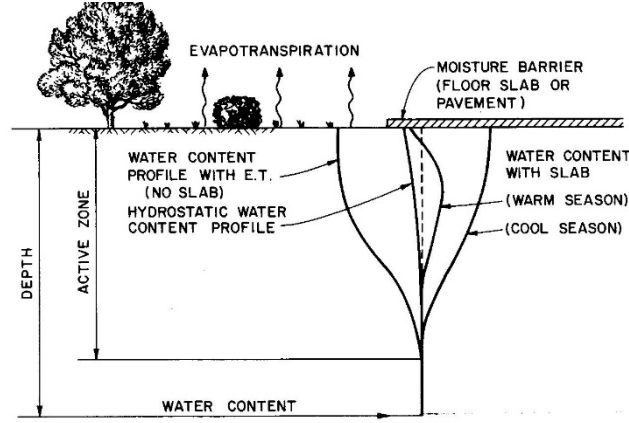


Figure 7: Water Content Profiles in the Active Zone (Nelson and Miller 1992)

for a given phenomenon but are not material variables. Material variables are intrinsic properties to a given material and can vary between material types. Material and state variables can be used in conjunction to describe the state of a system with multiple phases (Fung 1965). In saturated soil mechanics, the effective stress ($\bar{\sigma}$) experienced by the solid phase can be described in terms of total stress (σ) and pore water pressure (u_w).

$$\bar{\sigma} = \sigma - u_w \quad (3)$$

For saturated soils, $(\sigma - u_w)$ is a single stress state variable. The pore water pressure is considered to be compressive (positive), isotropic, and to contribute fully to the effective stress principle. Stress state variables are not dependent on the physical properties of the materials.

Fredlund and Morgenstern (1977) published a “theoretical stress analysis of an unsaturated soil on the basis of multiphase continuum mechanics.” For the purposes of this investigation, Fredlund and Morgenstern’s method of analysis will be used. In Fredlund and Morgenstern’s method of analysis, as summarized by Fredlund and Rahardjo (1993), the soil is considered to be chemically inert, incompressible, and consist of four phases: air, soil solid, water, and the contractile skin. Figure 8 depicts an unsaturated soil element with all four phases.

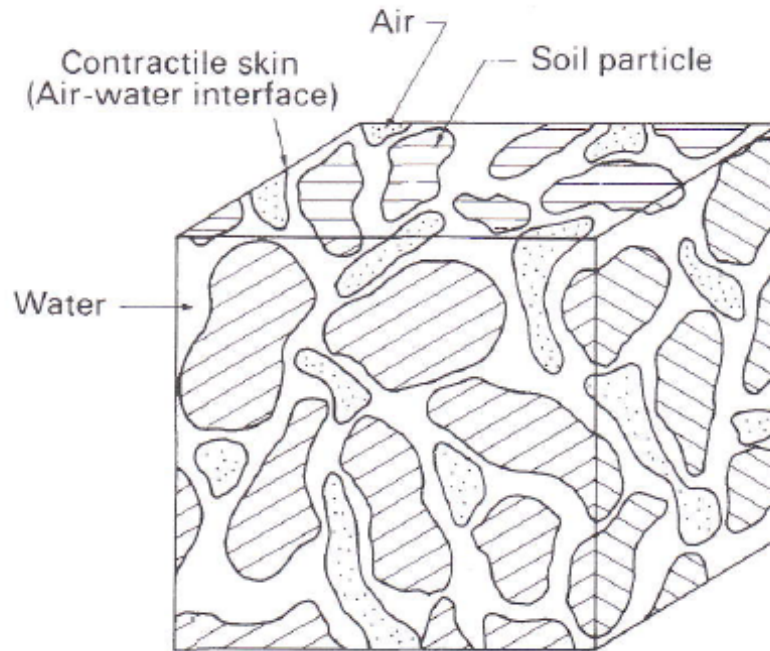


Figure 8: Unsaturated Soil Element (Fredlund and Rahardjo 1993)

Two independent stress states must be used to describe the stress state of an unsaturated soil due to the existence of the contractile skin. Three stress state variables are available for use and a minimum of two must be used in any constitutive relationship. Table 1 describes the possible combinations of stress state variables available for use to describe an unsaturated soil (Fredlund and Rahardjo 1993).

Table 1: Possible Combinations of Stress State Variables for an Unsaturated Soil (Fredlund and Rahardjo 1993)

Reference Pressure	Stress State variables
Pore Air, u_a	$(\sigma - u_a)$ and $(u_a - u_w)$
Pore Water, u_w	$(\sigma - u_w)$ and $(u_a - u_w)$
Total Stress, σ	$(\sigma - u_a)$ and $(\sigma - u_w)$

2.2 Shear Strength of Saturated and Unsaturated Soils

In saturated soil analysis, the Mohr-Coulomb failure criterion is used to determine the shear strength of a given soil in conjunction with Terzaghi's effective stress equation.

$$\tau = \bar{c} + \bar{\sigma} \tan \phi' \quad (4)$$

where:

τ = shear strength

\bar{c} = cohesive intercept

ϕ' = effective angle of internal friction

The slope of the failure criterion is defined by the effective angle of internal friction and the y-intercept by the effective cohesion. Figure 9 depicts the Mohr-Coulomb failure criterion for a saturated soil.

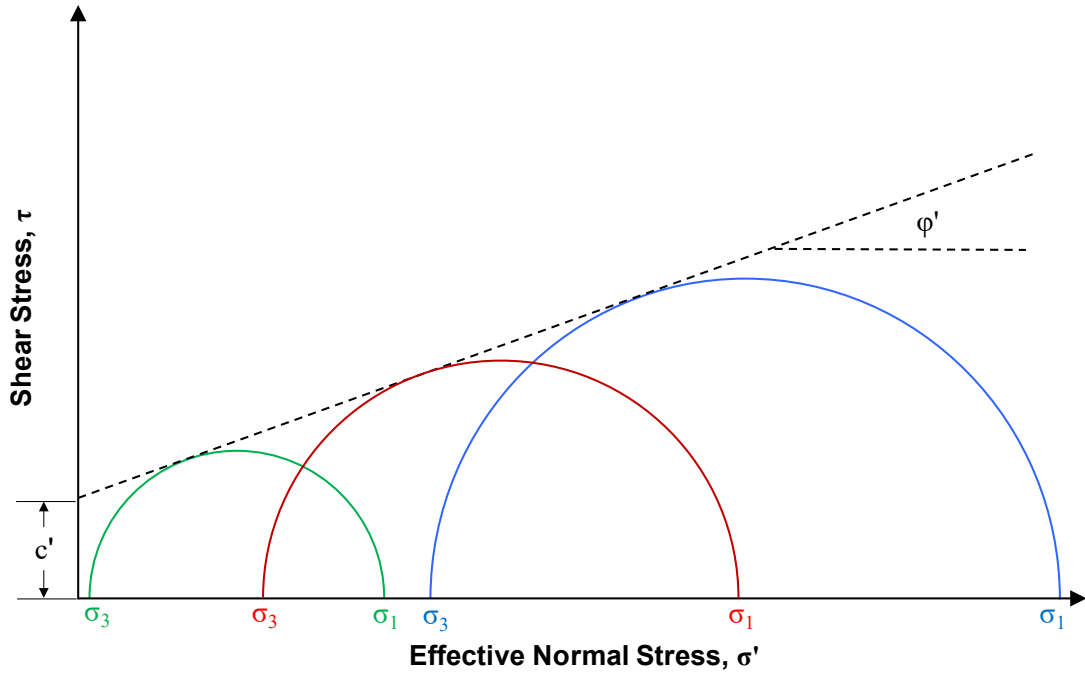


Figure 9: Mohr-Coulomb Failure Criterion (Saturated Soil) (after Burrage 2016)

Using the system of stress analysis developed by Fredlund et al., shear strength is determined using two independent stress state variables (Fredlund et al. 1978). Matric suction ($u_a - u_w$) and net normal stress ($\sigma - u_a$) are used to develop the following shear strength equation for an unsaturated soil.

$$\tau = \bar{c} + (\sigma - u_a) \tan \phi' + (u_a - u_w) \tan \phi^b \quad (5)$$

where:

\bar{c} = the effective cohesion when matric suction and net normal stress is zero

ϕ' = is the angle of internal friction with respect to changes in net normal stress when matric suction is constant

ϕ^b = is an angle that can be regarded as controlling an apparent cohesion which is related to levels of matric suction

Figure 10 depicts the Mohr-Coulomb failure criterion for an unsaturated soil.

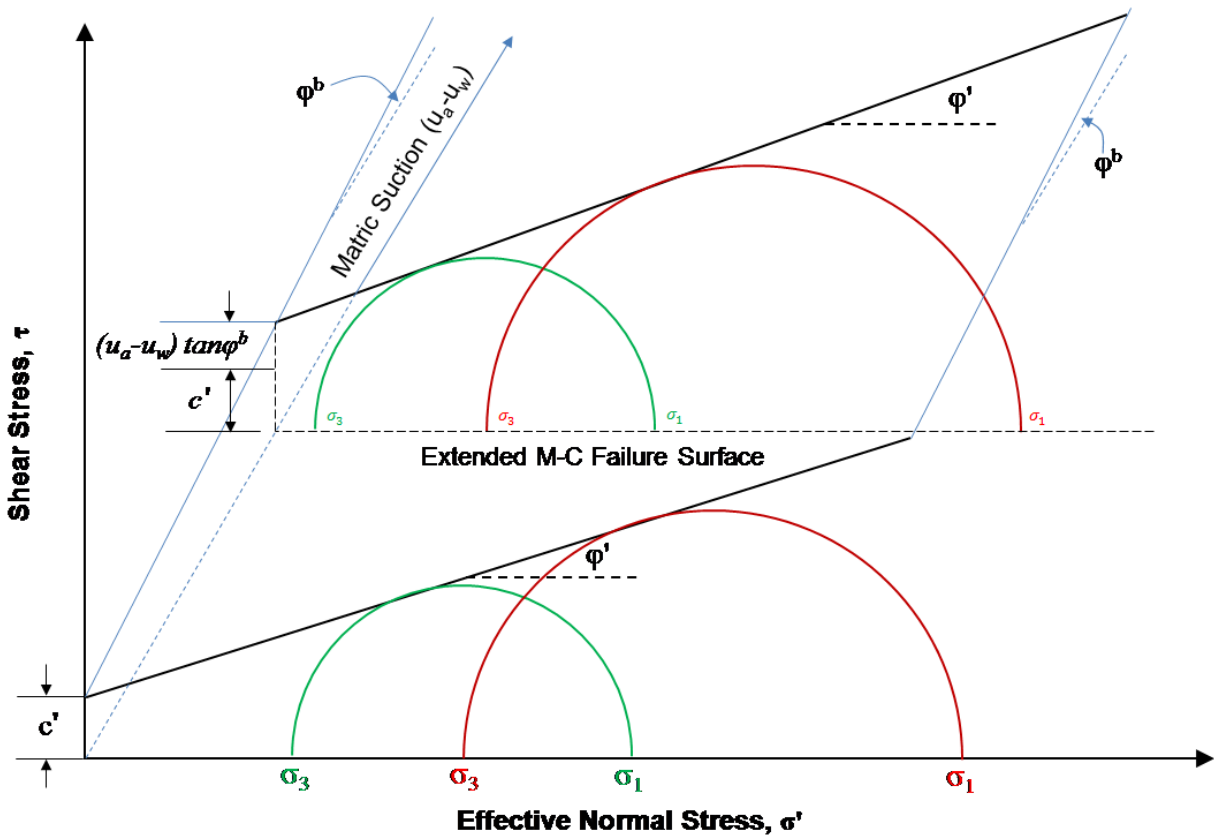


Figure 10: Extended Mohr-Coulomb Failure Criterion (Unsaturated Soil) (after Burrage 2016)

2.2.1 Typical and Correlated Values for Soils with Plasticity

Lambe and Whitman (1969) provide typical values for the drained shear strength of saturated soil based on the Atterberg limits using data by Kenney (1959). Figure 11 shows the correlation between sine of the peak friction angle and the plasticity index for normally consolidated soils. As the plasticity index increases, the drained shear strength decreases. Table 2 shows this.

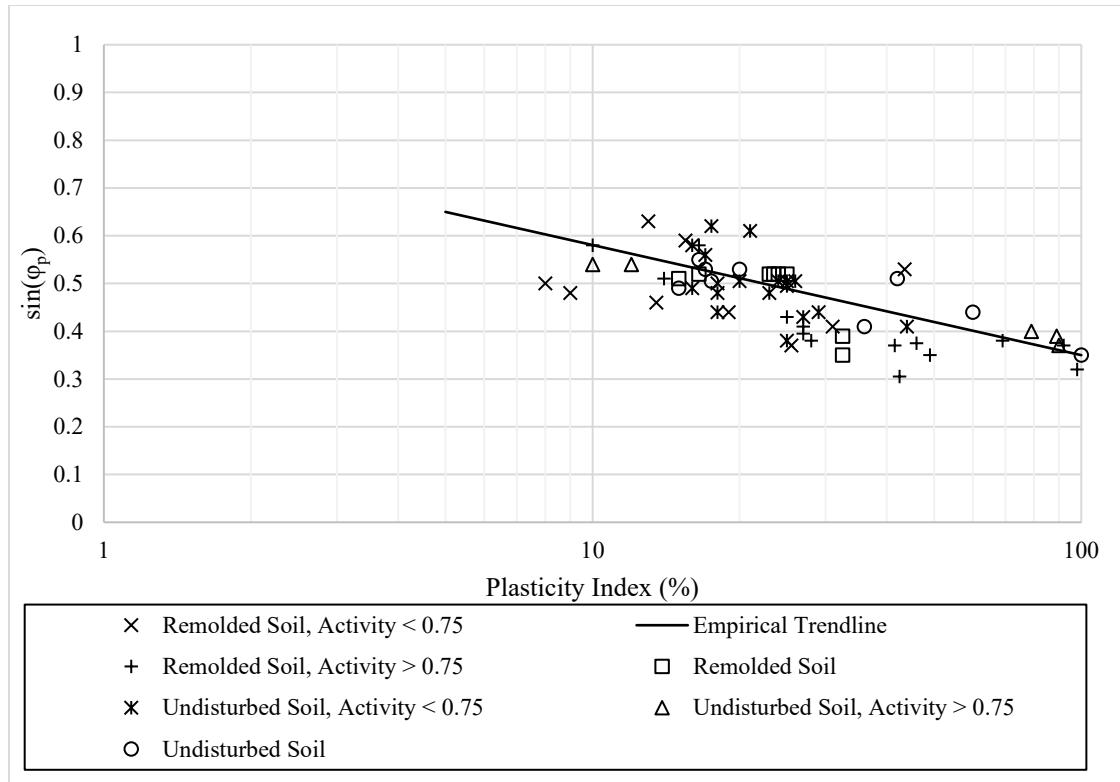


Figure 11: Relationship between $\sin \phi_p$ and plasticity index for normally consolidated soils (After Lambe and Whitman 1969, Kenney 1959)

Mitchell and Soga (2005) plotted residual friction angles as a function of effective normal stress raised to the minus one third power. This plot is shown in Figure 12 using data from Chattopadhyay (1972). In this figure, the residual friction angles are not affected when the normal stress is less than roughly 200 kPa. However, at higher stresses, the friction angle is independent of the stress and increases with larger stress values.

2.3 Volume Change in Expansive Soils

According to Fredlund and Rahardjo (1993), “[a]n unsaturated soil will undergo volume change when the net normal stress or the matric suction variable changes in magnitude... Under a constant total stress, an unsaturated soil will experience swelling and shrinkage as a result of matric suction variations associated with environmental changes.” Changes in matric suction are due to changes in the volumetric water content of the soil. As the water content of a given soil specimen increases the matric suction decreases and increases with an increase in water content. The potential of a given soil to shrink or swell, depends on its material properties: clay content,

Table 2: Summary of Friction Angle Data for Use in Preliminary Design (Lambe and Whitman 1969)

Classification	Friction Angles							
	Slope Angle of Repose		At Ultimate Strength		At Peak Strength			
	$i(^{\circ})$	Slope (vert. to hor.)	$\phi_{cv}(^{\circ})$	$\tan \phi_{cv}$	Medium Dense	Dense		
					$\phi(^{\circ})$	$\tan \phi$	$\phi(^{\circ})$	$\tan \phi$
Silt (nonplastic)	26	1 on 2	26	0.488	28	0.532	30	0.577
	to 30	1 on 1.75	to 30	0.577	to 32	0.625	to 34	0.675
Uniform fine to medium sand	26	1 on 2	26	0.488	30	0.577	32	0.675
	to 30	1 on 1.75	to 30	0.577	to 34	0.675	to 36	0.726
Well-graded sand	30	1 on 1.75	30	0.577	34	0.675	38	0.839
	to 34	1 on 1.50	to 34	0.675	to 40	0.839	to 46	1.030
Sand and gravel	32	1 on 1.60	32	0.625	36	0.726	40	0.900
	to 36	1 on 1.40	to 36	0.726	to 42	0.900	to 48	1.110

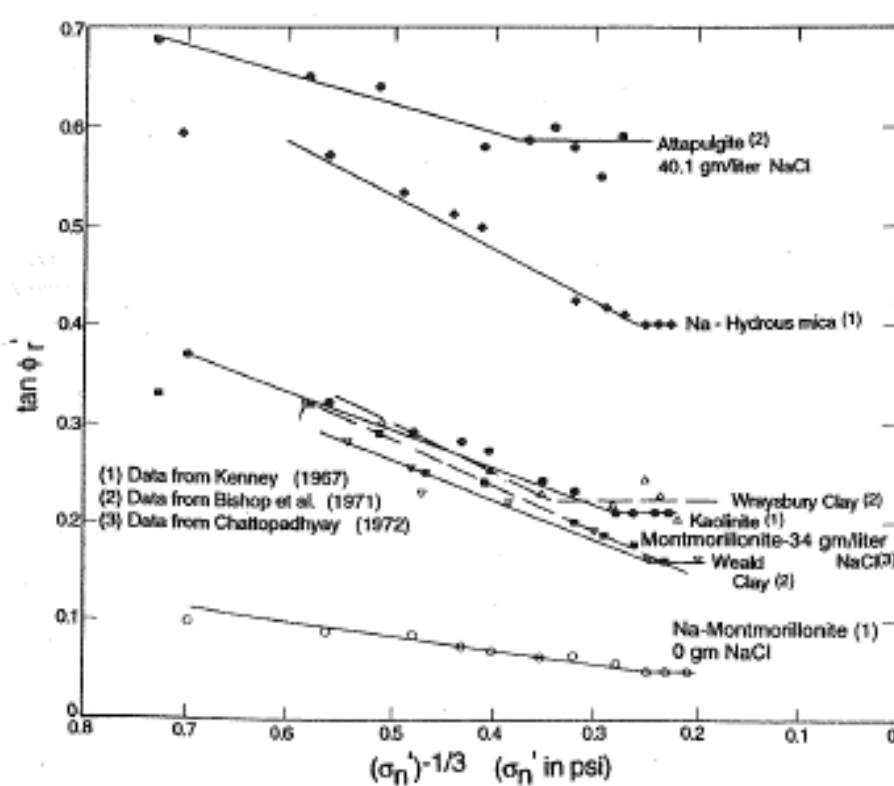


Figure 12: Residual Friction Angle versus Effective Normal Stress Raised to the Minus One Third Power (Data from Chattopadhyay 1972) (Mitchel and Soga 2005)

plasticity index, shrinkage limit, initial water content and matric suction (Fredlund and Rahardjo 1993). Holtz and Kovacs (1981) provided some guidelines for the probable expansion of a soil based on soil properties as shown in Table 3.

Table 3: Probable Expansion as Estimated from Classification Test Data (from Holtz and Kovacs 1981)

Degree of Expansion	Probable Expansion as a % of the Total Volume Change (Dry to Saturated Condition) ^b	Colloidal Content (% - 1 μ m)	Plasticity Index, PI	Shrinkage Limit, w_s
Very High	>30	>28	>35	<11
High	20-30	20-31	25-41	7-12
Medium	10-20	13-23	15-28	10-16
Low	<10	<15	<18	>15

^aAfter Holtz (1959) and U.S.B.R. (1974)

^bUnder a surcharge of 6.9 kPa (1 psi)

Montmorillonite expansive clays belong to the smectite mineral group and experience large volume changes because of the physical and chemical makeup of their mineral structure. Based on work by Casagrande (1948), Holtz and Kovacs (1981) recommend using Atterberg limits to identify active clay mineralogy. Clays with a montmorillonite composition generally plot near the U-line on Casagrande's plasticity chart, Figure 13. By using the plasticity chart to estimate mineral content, general information about the activity level of the clay can be approximated without specialized testing.

Montmorillonite is composed of an alumina octahedral sheet located between two silica tetrahedral sheets (Mitchell 1976). This configuration creates a plate-like structure with negative charges along the broad surface and positive charges along the edges of the soil particle.

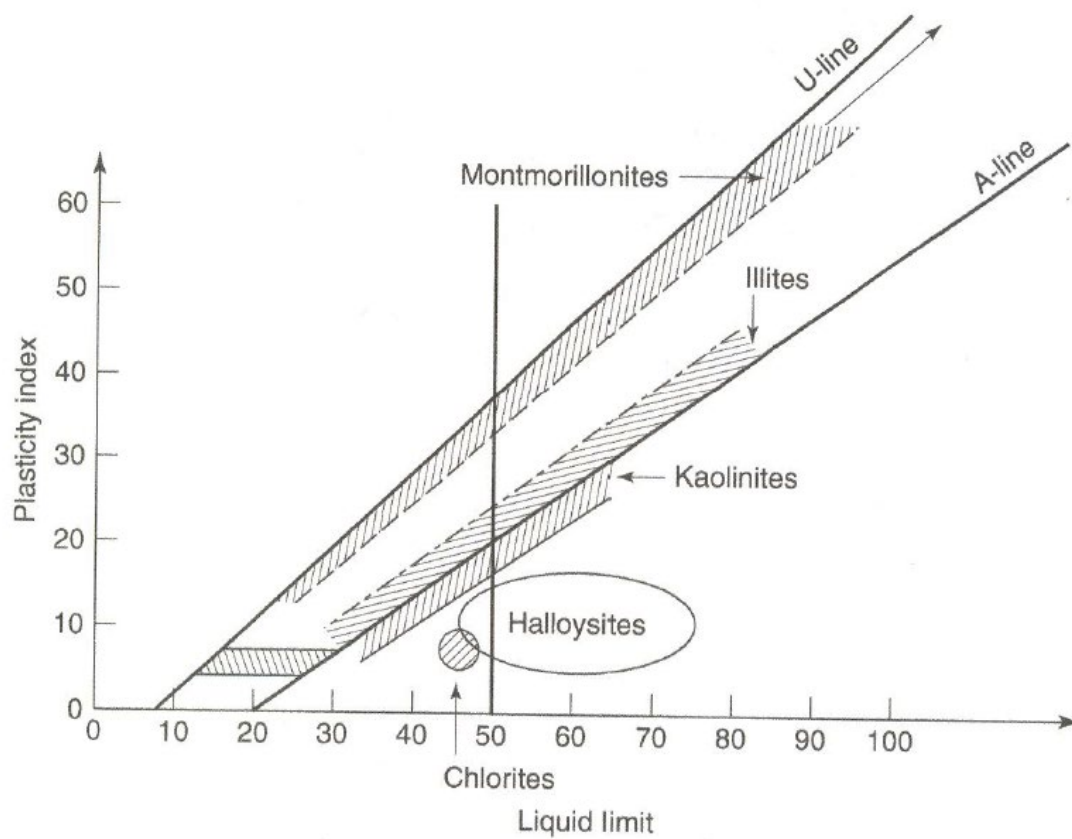


Figure 13: Location of Common Clay Minerals on Casagrande's Plasticity Chart (developed from Casagrande 1948 and data in Mitchell and Soga 2005) (Holtz and Kovacs 1981)

The polar nature of water creates an adsorptive bond between the montmorillonite soil solids and water molecules. Consequently, expansive soils have a high water storage capacity and are slow to drain. The adsorption of water around the clay particles expands the surrounding diffused water layer, forcing the particles apart (Nelson and Miller 1992). The resulting increase in volume is referred to as swelling. Shrinkage occurs when water is removed from soil matrix by desiccation, causing the diffused water layer surrounding the clay particles to shrink and draw the clay particles back together. Figure 14 depicts the swelling of smectite clays. This phenomenon does not occur in silts or sands because the individual soil particles are too large to be influenced by the polarity of water, and they are typically rounded or angular shapes.

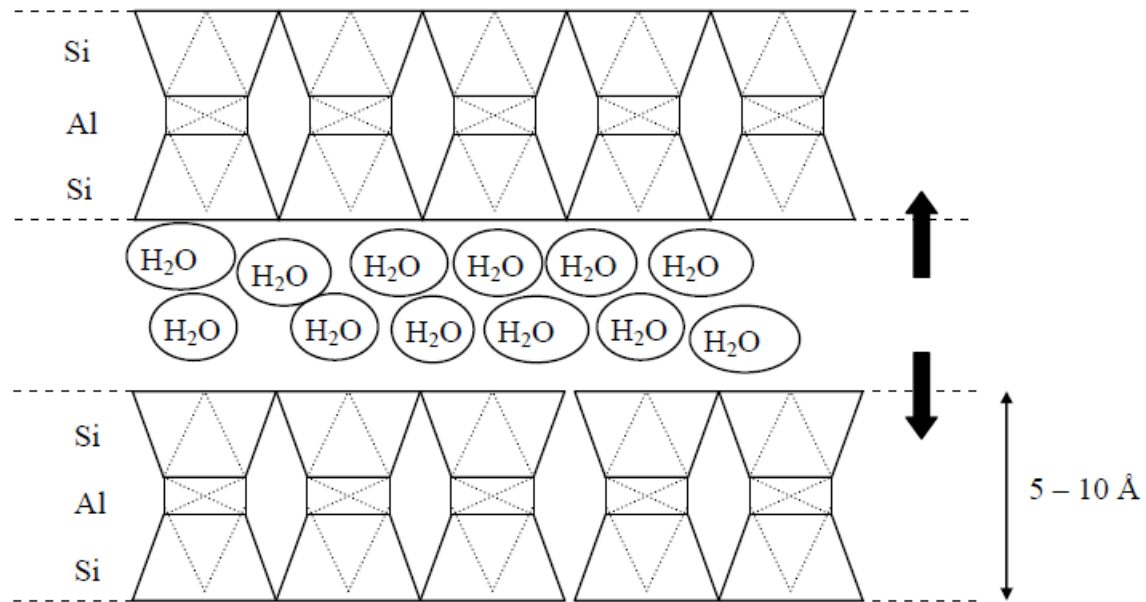


Figure 14: A Diagram Showing the Intercalation of Water Molecules in the Inter-plane Space of Clay Smectites (Taboada 2003)

The volumetric change of an unsaturated soil can be described in terms of two state variables. Fredlund and Rahardjo (1993) explain the constitutive relations between volumetric change of the solid and water phases as a function of net normal stress and matric suction. Because two state variables are required to describe the volumetric change of the solid and/or water phase, a three-dimensional surface is formed, as depicted in Figure 15, to describe the volume changes over a range of net normal stresses and matric suctions. Figure 16 depicts the changes in void ratio across a range of net normal stresses and matric suctions. According to Figure 15 and Figure 16, the volume change potential of a soil mass is limited by the net normal stress and the matric suction.

2.3.1 Soil Water Characteristic Curves

Soil water characteristic curves (SWCC) describe the constitutive relationship between matric suction and volumetric water content of a given soil mass. Low water contents correspond to high suction values, while high water contents correspond to low suction values (Lu and Likos 2004). The general shape of a soil water characteristic curve is depicted in Figure 17. It should be noted that the SWCC relationship is different for wetting and drying. This hysteresis is shown in Figure 18.

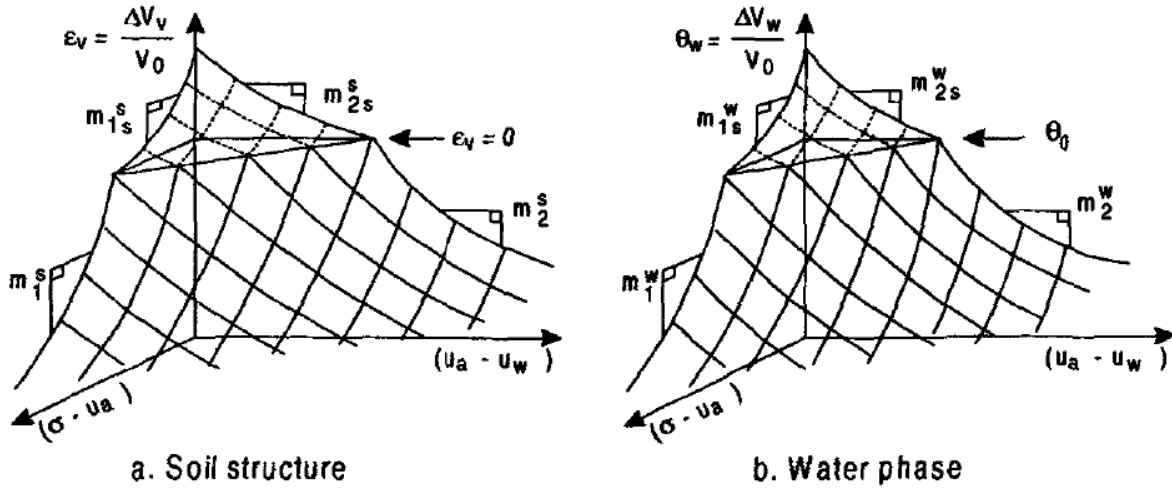


Figure 15: Three-dimensional Constitutive Surfaces for Soil Structure of an Unsaturated Soil (Fredlund and Rahardjo 1993)

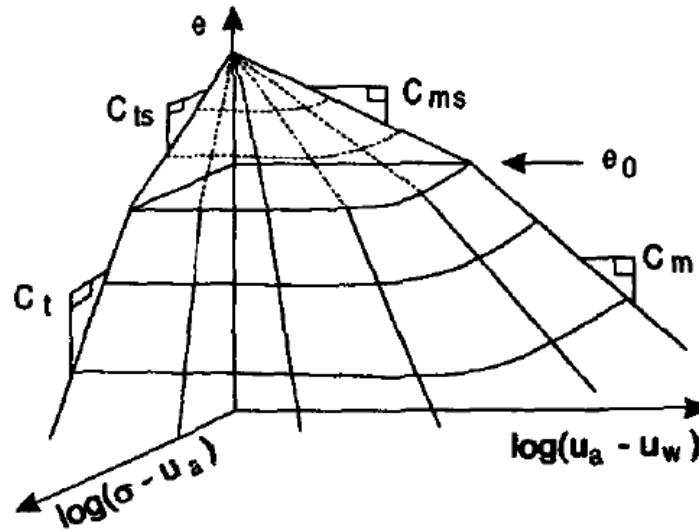


Figure 16: Semi-logarithmic Plot of Void Ratio versus Net Normal Stress and Matric Suction (Fredlund and Rahardjo 1993)

Referring back to the terminology in Figure 6, the pendular zone corresponds with the “Tightly Adsorbed” regime and the “Adsorbed Film” regime, and the “Capillary” regime corresponds to the continuous capillary zone. When the concentration of dissolved solutes is constant over the range of water contents, the osmotic suction will likewise remain constant (Lu and Likos 2004). Thus, changes in total soil suction will be due solely to changes in matric suction.

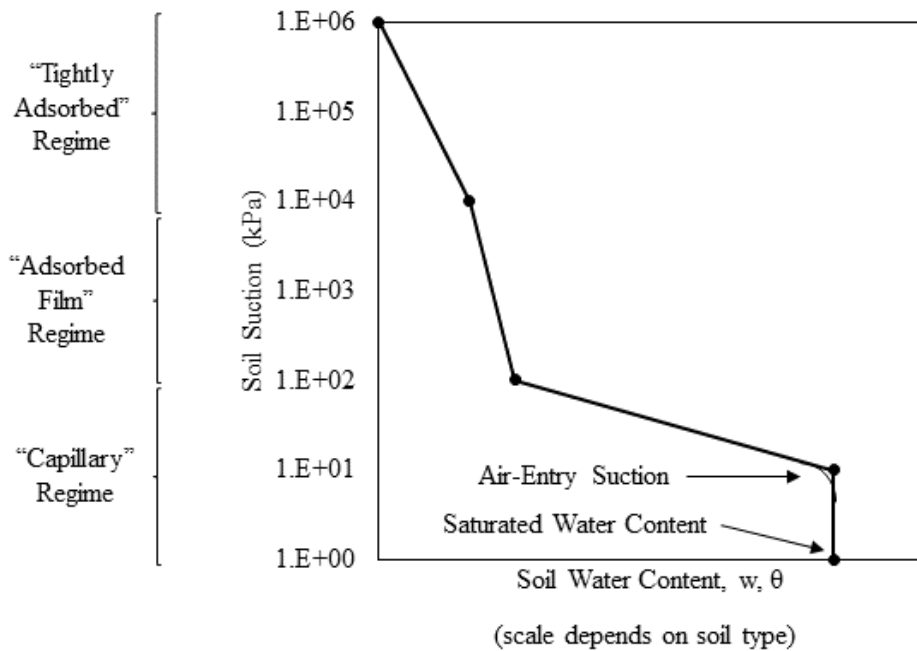


Figure 17: Illustration of McQueen and Miller's (1974) Conceptual Model for General Behavior of the Soil-Water Characteristic Curve (after Lu and Likos 2004)

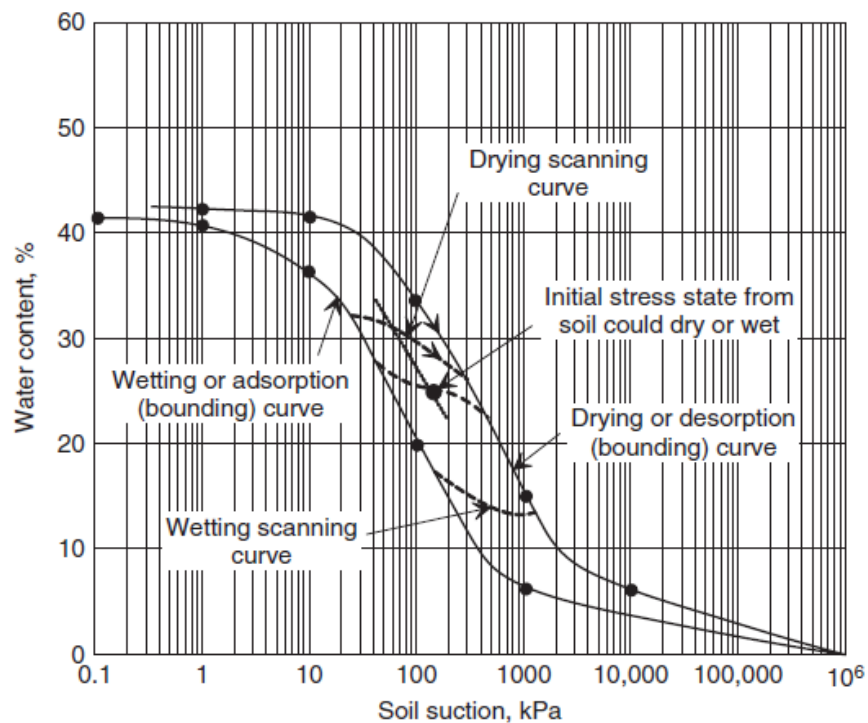


Figure 18: Hysteresis in SWCC (Fredlund et al. 2012)

The shape of a SWCC is controlled by the material properties of a given soil, including grain (pore) size distribution, density, organic content, percent clay, and mineralogy (Lu and Likos 2004). Figure 19 illustrates typical SWCCs for sand, silt and clay showing the dependency on soil type (Lu and Likos 2004). Sandy soils experience high values of matric suction over a relatively small range of water contents because of their small specific surface and limited adsorption capabilities. Clays experience high matric suction values over a wide range of water contents due to their high specific surface and charged surfaces. Non-expansive clays, such as kaolinite, adsorb less water than expansive clays, such as montmorillonite, in the tightly adsorbed and adsorbed film regimes. The SWCC is most significant for expansive clays due to their volume change capacity during the sorption process (Lu and Likos 2004).

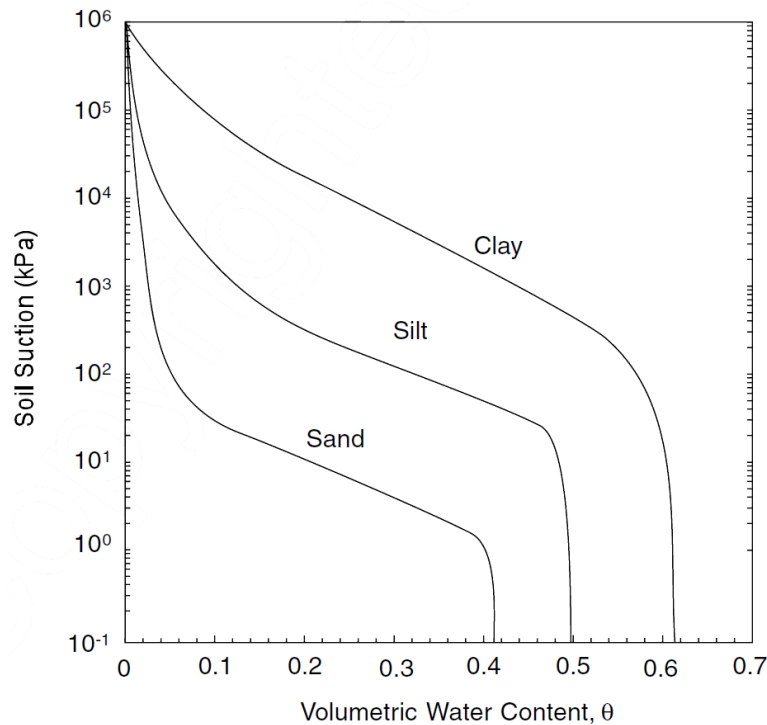


Figure 19: Representative Soil-Water Characteristic Curves for Sand, Silt and Clay (Lu and Likos 2004)

2.3.2 Effect of Swelling on Clay Strength

Case studies have proven that when a clay swells, the shear strength is negatively affected; therefore, the shear strength is variable depending on the swell potential of the material. Sixty triaxial tests were performed on expansive shale which was classified as a fat clay by the Unified Soil Classification System (USCS) (Al-Mhaidib and Al-Shamrani 2006). The samples consisted

of material 100% passing the No. 40 sieve and were remolded to form uniform remolded specimens at a predetermined water content (Al-Mhaidib and Al-Shamrani, 2006). The specimens were consolidated for approximately 24 hours under an isotropic confining pressure. After 24 hours had passed, water was introduced to the specimen and allowed to swell. The specimens could swell to 0%, 25%, 50%, 75%, and 100% of the ultimate vertical swell. When the predetermined percent swell value was achieved, the specimen was sheared to calculate the shear strength of the soil. The results were calculated in terms of the *shear ratio* which is the ratio of the shear strength of the swelled specimen and the non-swelled specimen (Al-Mhaidib and Al-Shamrani 2006), as shown in Equation 6.

$$\text{Shear Ratio} = \frac{\text{Shear Strength of swelled specimen}}{\text{Shear Strength of non - swelled specimen}} \quad (6)$$

Table 4 expresses the shear ratio values calculated for each of the swelled triaxial tests completed. The data agrees with the conclusion that the swelling of expansive clays has a large negative impact on the shear strength of the soil. Much of the shear strength was not present when the specimen could swell to the ultimate vertical swell value. As shown in Table 4 as the percentage in vertical swell increased for each specimen, the shear ratio rapidly decreased. As the shear ratio approaches zero, the strength of the swelled specimen is also approaching zero as the strength of the non-swelled specimen remains constant for each specimen.

2.4 Expansive Soils and Climate

The climate of a region is characterized by its seasonal amounts of precipitation and evapotranspiration. Evapotranspiration is the process by which water is removed from the soil by evaporation into the atmosphere and transpiration through vegetation. This process results in an upward movement of soil water through the soil matrix, desiccating the soil and increasing matric suction. Areas with excessive evapotranspiration can result in significant desiccation of expansive soils (Holtz 1983; Zornberg and Gupta 2009). In the event of heavy rains or irrigation, water moves downward through the soil matrix, increasing saturation and decreasing matric suction. Excessive precipitation in areas with expansive soils results in significant swelling (Nelson and Miller 1992). Figure 20 depicts the deformation and fluid flow phenomena in an unsaturated expansive soil (Lu and Likos 2004).

Table 4: Calculated Values for Shear Ratio for all Tested Specimens (Al-Mhaidib and Al-Shamrani 2006)

		% Vertical Swell Before Shearing			
Initial Water Content (%)	Confining Pressure (kPa)	25	50	75	100
14	25	0.32	0.09	0.07	0.04
	50	0.33	0.17	0.09	0.06
	100	0.35	0.20	0.15	0.08
	150	0.37	0.20	0.15	0.07
	Average	0.34	0.17	0.12	0.05
18	25	0.26	0.11	0.08	0.05
	50	0.26	0.16	0.11	0.08
	100	0.28	0.20	0.17	0.10
	150	0.33	0.22	0.18	0.11
	Average	0.28	0.17	0.14	0.09
22	25	0.36	0.27	0.18	0.11
	50	0.37	0.3	0.22	0.14
	100	0.39	0.32	0.27	0.20
	150	0.44	0.35	0.30	0.22
	Average	0.39	0.31	0.24	0.17
Average		0.34	0.22	0.16	0.11

As depicted, the impact of the environment on water content, and resulting volumetric changes, of the soil can cause structural heave or subsidence in foundation or pavement structure built on expansive soils. Arid regions and semi-arid regions, such as Alabama, typically have short, heavy precipitation events, which facilitate the most dramatic shrink-swell behavior (Fredlund and Rahardjo 1993; Nelson and Miller 1992). According to Fredlund and Rahardjo, an arid climate is where, “the annual evaporation from the ground surface exceeds the annual precipitation” (Fredlund and Rahardjo 1993). Seasonal changes in temperature and precipitation can exacerbate damage to structures by creating a continuous cycle of shrinkage and swelling.

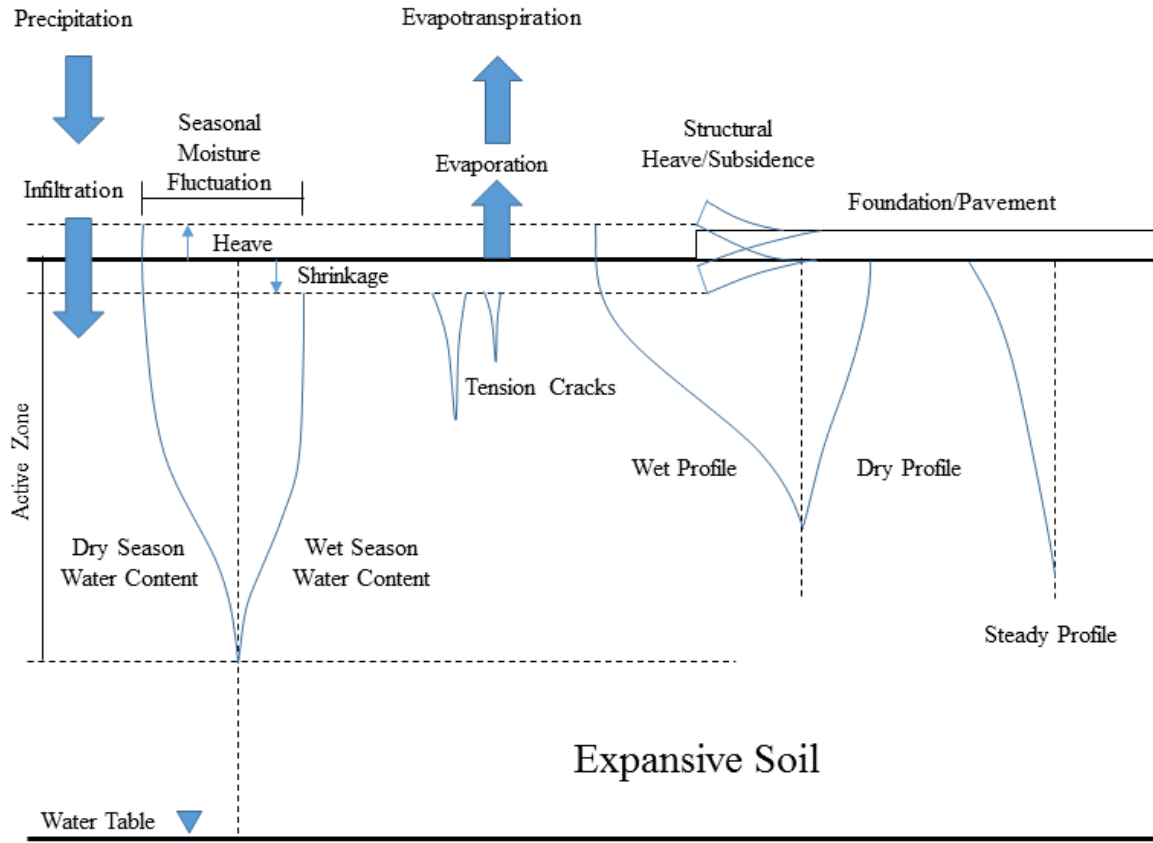


Figure 20: Deformation and Fluid Flow Phenomena in a Near-Surface Deposit of Unsaturated Expansive Soil (after Lu and Likos 2004)

2.5 Structural Damage to Pavement

Cases of structural damage to pavements constructed on expansive clays typically result in longitudinal cracking induced by moisture fluctuation. While the center of the pavement remains at a relatively constant water content, the edges are subject to water infiltration and desiccation. The longitudinal cracks are the result of flexion of the pavement due to settlements in the dry season and heave in the wet season (Zornberg and Gupta 2009). Figure 21 illustrates the formation of longitudinal cracks due to moisture fluctuation.

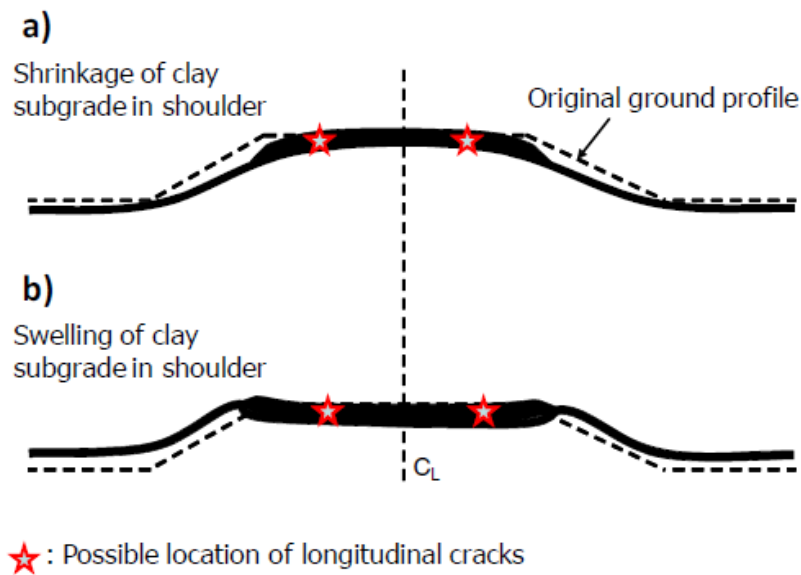


Figure 21: Formation of longitudinal cracks during (a) dry and (b) wet seasons (Zornberg and Gupta 2009)

2.6 Expansive Soils and Vegetation

Vegetation consumes water through its root systems and generates transpiration forces on soil water causing desiccation (Holtz 1983; Zornberg and Gupta 2009). The transpiration forces exerted by the vegetation occur at the root tips, generating suction pressures within the soil mass. Large plants, such as trees, develop extensive root systems and have a correspondingly larger zone of transpirational influence (Holtz 1983). The zone of transpirational influence can extend beyond the immediate vicinity of the roots (Holtz 1983). According to Fredlund and Rahardjo (1993), “Most plants are capable of applying 1-2 MPa (10 - 20 atm) [20,885 - 41,770 psf] of tension to the pore-water prior to reaching their wilting point.”

According to Biddle (2001), ninety percent of the root system of a tree is typically within 600 mm (23.6 inches) of the ground’s surface with the remaining ten percent extending deeper (Biddle 2001). “However, if the opportunistic exploitation of the soil encounters favorable conditions at any location, roots will proliferate.” The structural roots provide a radial and typically uniform foundation for the tree, distributing its weight and anchoring it into the ground. Beyond the structural root system develops a subdividing system of fine conducting roots and fine feeder roots. Water uptake only occurs in the fine feeder roots (Biddle 2001). Figure 22 depicts the soil-

plant-atmosphere relationship. In Figure 22 fine feeder roots are referred to as “active roots,” while structural roots are referred to as “main roots.”

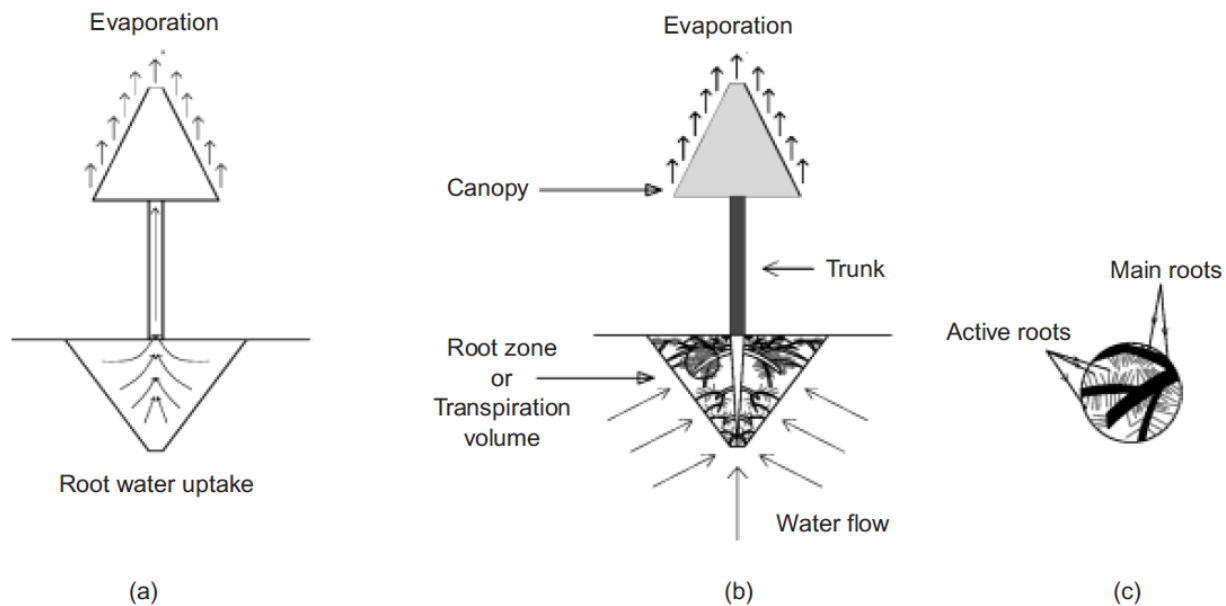


Figure 22: Schematic Sketch of Soil-Plant-Atmosphere System (a) Transpiration (b) Soil-plant-atmosphere interaction (c) Active and main roots (Indraratna et al. 2006)

These roots grow in patterns and in areas most conducive to obtain water and nutrients, typically resulting in a non-uniform distribution based on local soil conditions, elevations and the presence of water (Biddle 2001). “Roots will... proliferate near any natural water source, and, if they encounter them, will exploit deep aquifers such as bands of sand within an otherwise hostile clay soil, particularly if there is lateral inflow to replenish the source. In the same way they will exploit artificial sources of water, such as leaking drains, or the moisture condensing on the underside of paving slabs” (Biddle 2001). In general roots have difficulty penetrating soils with a bulk density greater than 1.8 g/cm^3 (112.4 pcf) (Biddle 2001). Throughout development, roots have a high mortality rate, such that a large portion of the root system dies each winter as the tree becomes dormant, resulting in a dynamic system capable of adapting to changing conditions (Biddle 2001). While it should be noted that the overall size of the crown of a tree and its root system are related, it is not possible to draw reliable conclusions about the size of the root spread based on the crown size or height of a tree because of the influence of the soil on root propagation (Biddle 2001).

Vegetation requires the use of water during photosynthesis. Thin films of water surround the cells of a leaf and aid in carbon dioxide absorption into the cells. Ultimately, the water will evaporate from the films in a process called transpiration. More than 99% of the water consumed by vegetation is lost through transpiration (Biddle 2001). The loss of water from the leaves creates a suction gradient that extends through the vascular tissue of the plant to the roots, drawing water up from the roots to the leaves (Biddle 2001). T.E. Dawson investigated water use by sugar maple trees (*Acer saccharum*) from isotopic, energy balance and transpiration analyses to determine the role of tree size and hydraulic lift (Dawson 1996). In his paper, Dawson asserts that large trees, greater than 10 meters (32.8 feet) tall have higher daily transpiration rates than small trees, 3 to 5 meters (9.8 to 16.4 feet) tall (Dawson 1996). However, small trees demonstrated sensitivity to environmental factors resulting in greater variability in daily transpiration rates (Dawson 1996). In terms of the hydraulic balance between ground water and plant transpiration, larger trees and older forest stands had a greater impact than smaller trees (Dawson 1996). The smaller trees tended to pull water from soil water close to the tree itself, while larger trees are capable of hydraulic lift (Dawson 1996). The hydraulic lift of a large tree allows it to pull water from relatively long distances from the tree trunk, re-saturate the soil within the root bulb as a shallow water reservoir, and then absorb the water for growth (Dawson 1996). The smaller trees investigated did not carry out hydraulic lift (Dawson 1996). While large trees have a greater impact on the hydrologic balance than small trees, a mixed stand of large and small trees will have the greatest impact (Dawson 1996). Figure 23 depicts the soil water potential (matric suction) and the leaf water potential at a depth of 20 cm (7.9 inches) during the 1993 growing season (Dawson 1996). These values are an average of both small and large trees, but the large trees consistently had larger leaf water potential than small trees (Dawson 1996). For Figure 23 and Figure 24, suction is negative.

Figure 24 demonstrates typical patterns of average soil water potential around the root systems of three large and three small sugar maple trees during a drought in early July (Dawson 1996). It should be noted that the matric suction is at its peak at the end of daylight hours. Changes in soil water potential between day and night around the large trees was due to nighttime soil water recharge via hydraulic lift (Dawson 1996).

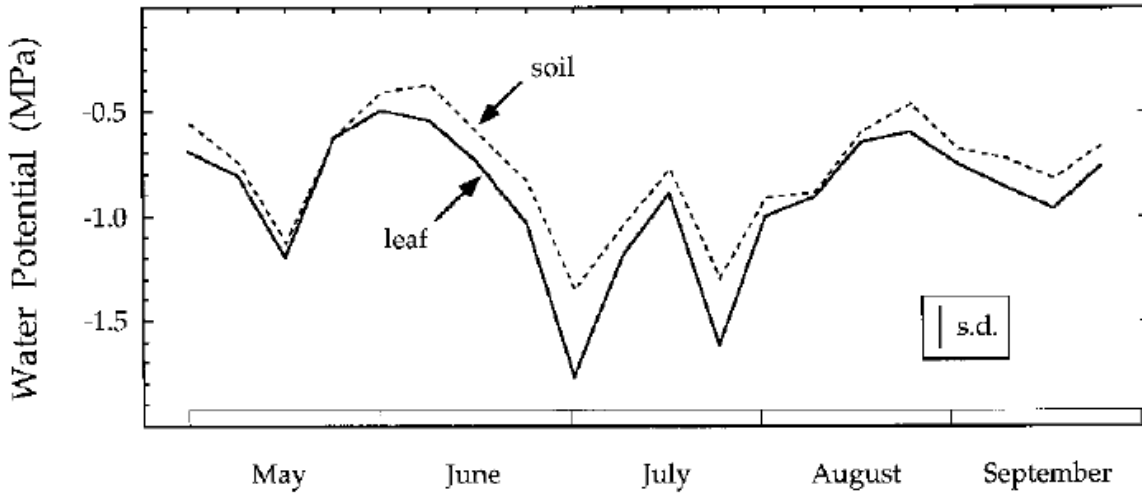


Figure 23: Average Soil Water Potential at 20cm Depth During 1993 Growing Season (Dawson 1996)

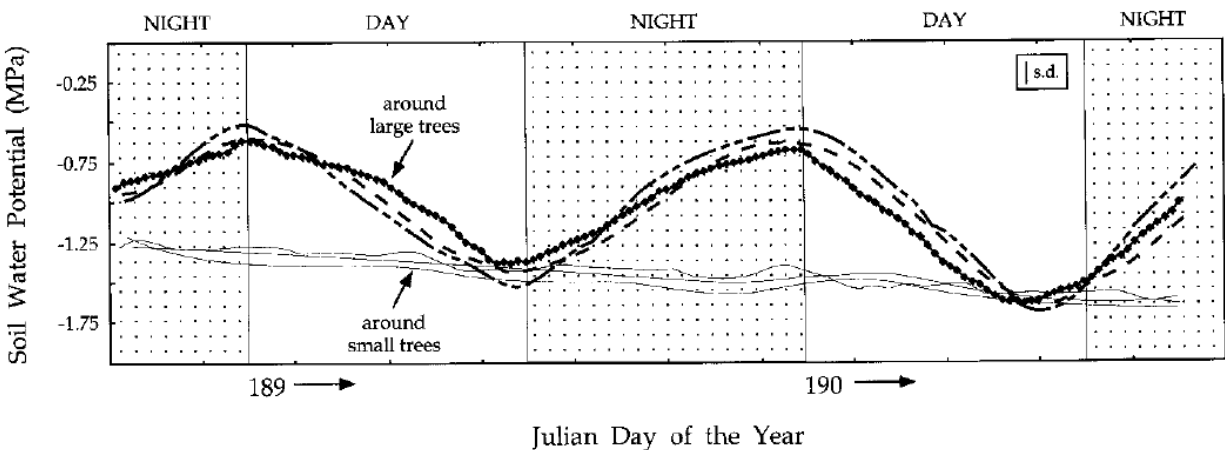


Figure 24: Average Soil Water Potential Around the Root Systems of Three Large and Three Small Trees During the Early July Drought Period (Dawson 1996)

In the case of expansive clays, the water consumption of vegetation can play an important role in the shrink swell cycle. The water demand of a plant is determined by the soil conditions and availability of water, and can be defined as “the ability of vegetation to cause drying of a clay subsoil” (Biddle 2001). Some species of trees have a higher water demand than others, because they require more water to prevent wilting and maintain good health. Figure 25 is a classification of tree genera based on water demand. It is important to notice that in the broad-leaf category, tree species in the *Quercus* and *Ulmus* genera require the highest water demand and have root systems

that extend deepest and furthest. By contrast, coniferous tree species in the *Pinus* and *Juniperus* genera have some of the lowest water demand and the shallowest and shortest root systems.

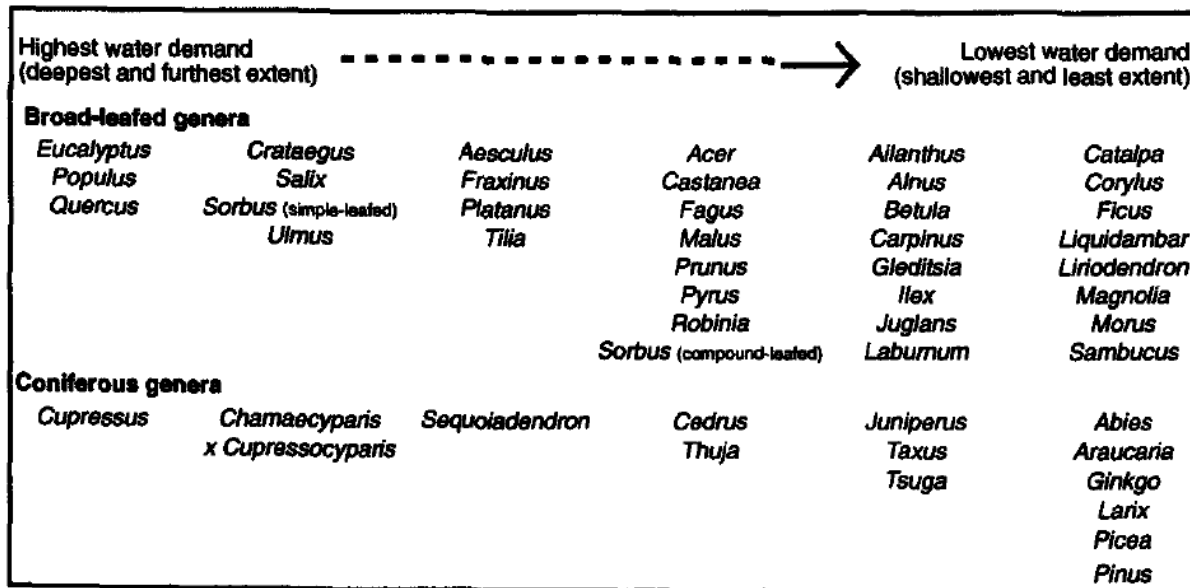


Figure 25: A Tentative Classification of the 'Water Demand' of Different Tree Genera in the UK (Biddle 2001)

2.6.1 Structural Damage due to Vegetation

Numerous cases of structural damage to buildings and pavement structures founded on expansive clays have been documented. Depending on site conditions, these damages may result purely from cycles of dry and wet weather causing the clays to shrink and swell. However, the presence of tree(s) can provide a significant addition to the desiccation of the clays, exacerbating the cycle.

In Houston a four-story steel frame office building, founded on belled drilled shafts at a depth of 9 feet, was constructed on top of expansive clays. Five live oak trees between 14 and 21 inches in diameter were located on the southern face of the building, and four live oak trees were located on the northern face of the building. Over time, significant structural damage in building and foundation settlement was observed (Tand and Vipulanandan 2011). A settlement survey of the building floor slab, Figure 26, was performed, and settlements ranged from 1 to 1.5 inches on the north face and 3 to 5 inches on the south face. The settlement of the slab resulted in significant

structural damage (Tand and Vipulanandan 2011). The author makes a strong case that the demand for water of the oak trees resulted in desiccation of the expansive soils below the slab and foundations, resulting in settlement. This argument was further supported by the removal of the oak trees on the north face and subsequent rebound of the soils.

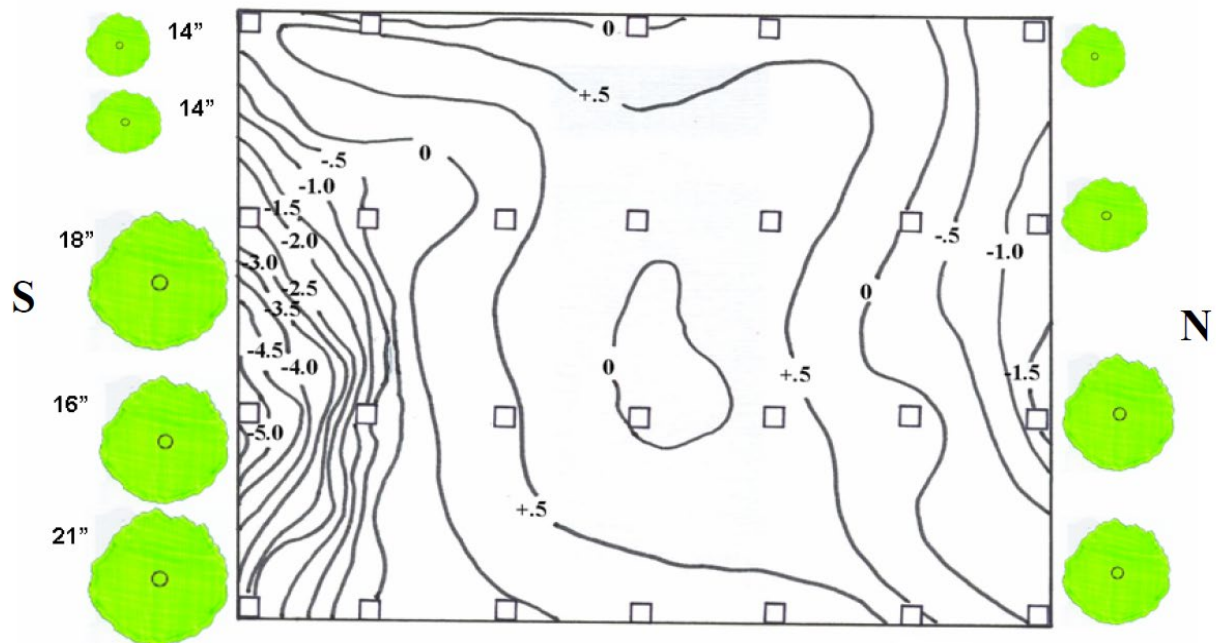


Figure 26: Elevation Contours with Trees (inches) (Tand and Vipulanandan 2011)

In central Oklahoma, significant pavement damage has been observed in the vicinity of large trees. Snethen (2001) documents three cases studies of structural damage due to vegetative influence. In the case of 32nd Street, Stillwater, Oklahoma, a 75 mm (2.95 inch) layer of hot mix asphalt (HMA) was placed on top of “gravelly clay layer created by several applications (75 to 100 mm) of crusher-run limestone gravel which was compacted into the native clay by traffic” in 1997.

Table 5 summarizes the properties of soils encountered at 32nd Street, Stillwater, Oklahoma.

Table 5: Soil Properties at 32nd Street, Stillwater, Oklahoma (Snethen 2001)

Depth (mm)	%-200	% Clay	LL	PI	Moist Density (g/cm³)	Available Moisture Capacity (mm/mm)
0-150	60-95	27-35	37-50	14-25	1.30-1.60	0.15-0.22
150-475	60-90	35-60	41-70	20-40	1.35-1.65	0.10-0.20
475-875	55-90	35-60	41-70	20-40	1.35-1.65	0.02-0.20

According to Snethen (2001), pavement damage was not observed until the summer of 1999, approximately 2 years after construction, when “arc-shaped hairline cracks” were observed near a large Chinese Elm tree (*Ulmus parvifolia*) growing at the right of way (ROW) boundary (Snethen 2001). The area experienced very dry periods in 1999 and 2000. Observed cracks were 3 mm wide with “no appreciable vertical displacement across the crack” and the “most likely cause of the crack is shrinkage of the subgrade soil caused by differential drying from the influence of the Chinese Elm tree as it disproportionately depleted the subgrade moisture during the hot, drier climatic conditions” (Snethen 2001). The cracking pattern observed on 32nd Street and relative distances to the Chinese Elm tree are depicted in Figure 27.

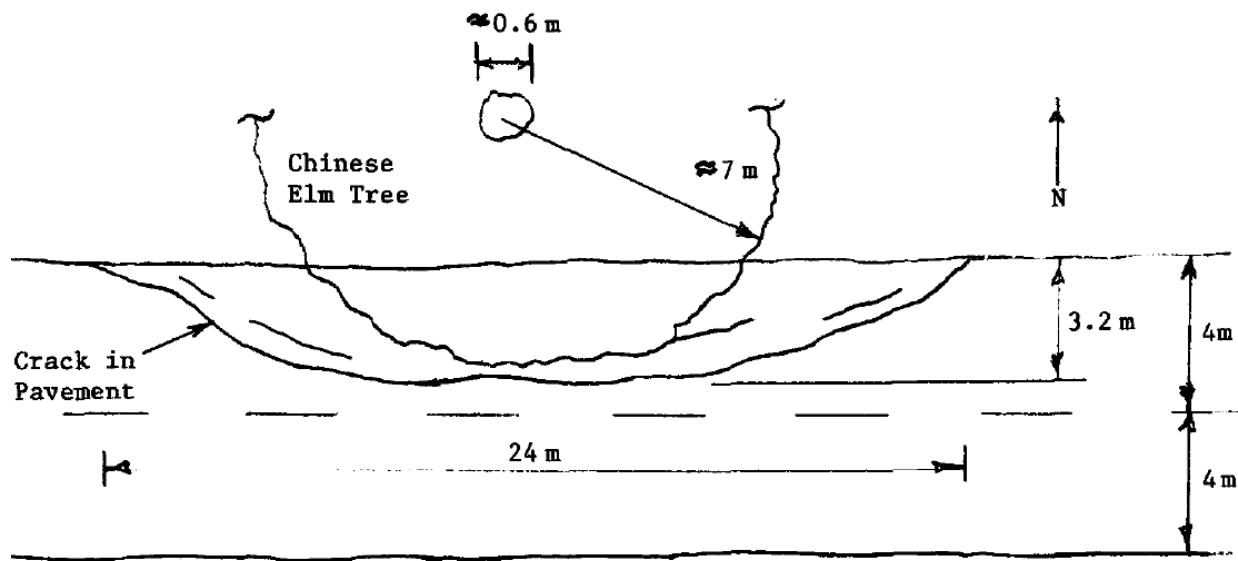


Figure 27: Arc-shaped Cracks in HMA Pavement Along 32nd Street, Stillwater, OK (Snethen 2001)

2.6.2 Remedial Action for Vegetation Related Expansion

The end effect of evaporation and transpiration is the desiccation and shrinkage of expansive soils. To mitigate the effects of transpiration Biddle suggests four solutions:

- “fell the offending tree to eliminate all future drying”
- prune the tree to reduce drying by the area of transpiration (leaves) and “the amplitude of seasonal movement”
- “control the root spread to prevent drying beneath the foundation”
- “supplementary watering to prevent the soil from drying” (Biddle 2001)

Ideally, trees that are causing structural damage to buildings and pavement structures should be cut down. Once they are cut down all transpiration will cease and the water content will stabilize (Biddle 2001). Volumetric fluctuations will be limited to those induced by climate.

When felling the tree is not an option, pruning should be considered. Before the 1970s in the United Kingdom, pruning was an effective method of controlling damage by trees (Biddle 2001). In the 1970s, the tree management policies were changed allowing trees along streets to

grow progressively larger crowns, increasing their rates of transpiration. It should be noted that unless adequate leaf area is pruned away, the treatment will be ineffective (Biddle 2001). Figure 28 and Figure 29 depicts soil/building movement if the offending tree is felled or pruned.

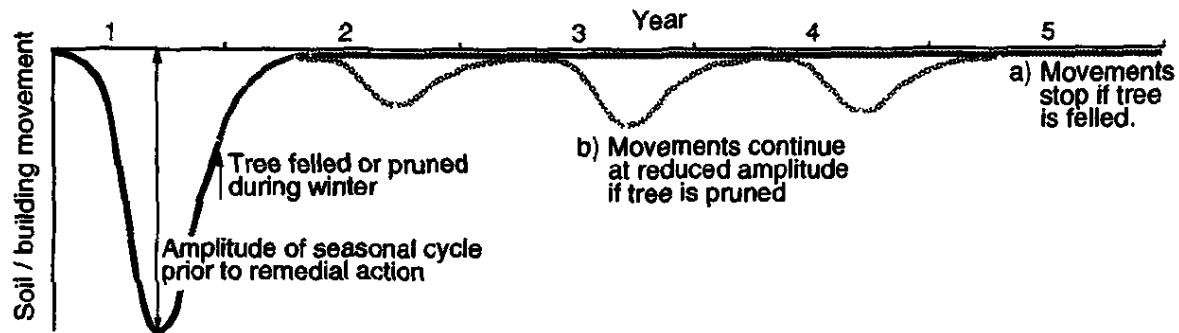


Figure 28: Diagram of Remedial Options if Drying is Predominately Seasonal (Biddle 2001)

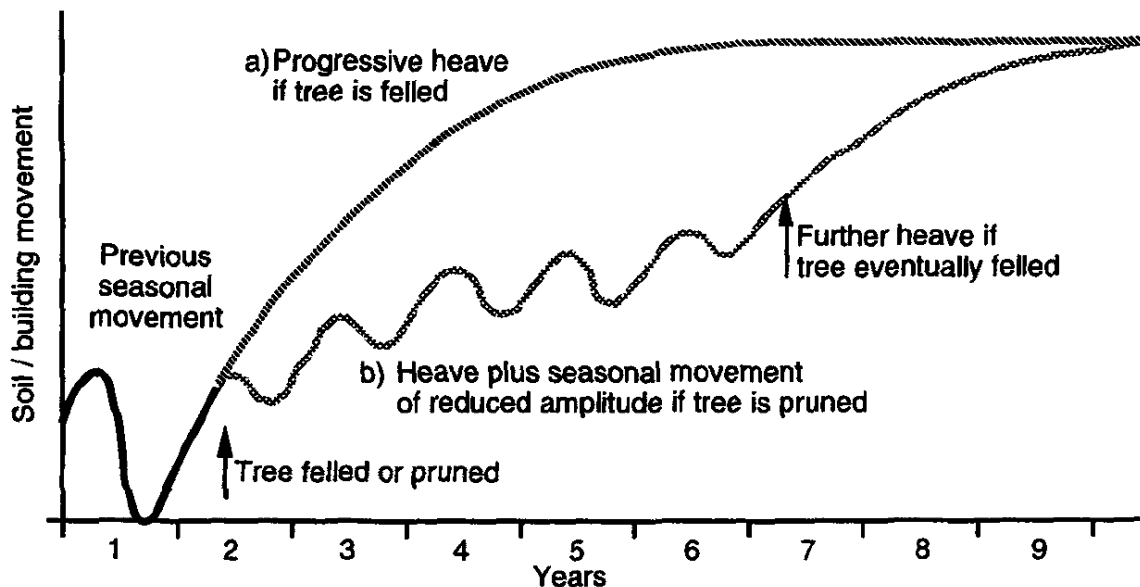


Figure 29: Effect of Pruning or Felling if there is a Significant Persistent Moisture Deficit; Stability Not Achieved (Biddle 2001)

Controlling the root spread either through root severance or vertical barriers can be difficult to implement and maintain due to the dynamic nature of tree roots. The barrier/severance must be sufficiently far from the trunk to maintain stability. Vertical barriers must be sufficiently deep so that the roots do not grow around or under them (Biddle 2001). It is also possible to prevent the

soil from shrinking through desiccation if the soil is continuously wet. However, “the quantities of water required by the tree usually make this impractical, particularly as water may not be available when it is most needed during periods of drought” (Biddle 2001).

Chapter 3. State-of-Practice Review of Shrink-Swell Soil Stabilization Techniques

Pavements damaged by expansive subgrades are commonly rehabilitated by resurfacing. This procedure is usually temporary, often costly, and typically fails to address the root of the problem. As a result, researchers and engineers have developed more economical and rational solutions that address expansive subgrades.

This review is a compilation and summary of the various solutions encountered in the technical literature for the stabilization of expansive subgrades. These procedures can be separated into four categories: (1) mechanistic designs for minimizing moisture variations, (2) chemical stabilization, (3) physical ground improvements, and (4) new and/or innovative efforts, with limited peer reviewed research or field experience. While not all the procedures that follow may be feasible apart from a closed road, the ideas involved may still be useful and are therefore reported.

3.1 Mechanistic Designs for Minimizing Moisture Fluctuations

The literature indicates that a wide variety of mechanistic strategies for minimizing subgrade moisture fluctuations exist. These strategies rely on a purely mechanistic phenomenon to minimize moisture fluctuations within the subgrade. Minimizing moisture fluctuations reduces shrink-swell phenomenon and prevents pavement damage.

3.1.1 Vertical Moisture Barriers

Vertical moisture barriers are typically composed of geomembrane sheets, geotextile coated fabrics, or fabric-sheeted laminates (Steinberg 1998). They are installed in narrow trenches dug longitudinally along both edges of a pavement. The trench depth extends through all or part of the active zone. Picornell and Lytton (1986) note that the depth of a vertical barrier should extend to the maximum shrinkage crack fabric depth, which is usually located beneath each pavement edge. Extending the barriers to a sufficient depth is important for their successful performance. Steinberg (1998) reports a case study in North Dakota in which vertical barriers installed to 4-foot depths performed poorly and suggests that the subgrade would have been stabilized if the barrier depth had been doubled.

Vertical barriers should extend beyond vegetative roots and be durable enough to resist root penetration. Experiments performed on six pavement test sections in Texas showed that sites with shallow root depths experienced greater success with vertical barriers (Jayatilaka et al., 1993).

Barriers can be protected from root penetration by sandwiching the impermeable geomembrane between two geotextile sheets.

After placement, each trench is backfilled (preferably with a relatively impermeable material), compacted, and capped. The barriers effectively seal the edges of the pavement and minimize moisture fluctuations directly beneath it. Vertical barriers greatly increase the time it takes for seepage to occur under the pavement by increasing the required length of travel for the flow of water. Furthermore, the capillary mechanics of the subgrade cause the moisture to distribute upward more evenly, reducing differential heave. The barriers also aid in the development and stabilization of the state of suction directly beneath the pavement. According to Evans and McManus (1999), “This stable suction will be the equilibrium suction that exists in the deeper foundation soils”.

In practice, it is desirable to bring the subgrade water content and state of suction to near-equilibrium conditions (i.e. wet) prior to the placement of the vertical barriers. If the barriers are placed along a dry subgrade containing a high in-situ suction, the barrier will retain and isolate water beneath the pavement until the soil suction is stabilized. This will cause swelling to occur beneath the newly placed pavement until equilibrium is reached, resulting in an initial spike in pavement roughness and cracking. Figure 30 illustrates the installation of a typical vertical moisture barrier.



Figure 30: Installation of a Vertical Moisture Barrier (Evans and McManus 1999)

The utilization of vertical moisture barriers has proven successful on several projects. In the late 1970s, the first vertical moisture barriers were installed to 8-foot depths on IH-410 and IH-37 in San Antonio, Texas. Initial moisture sensor readings indicated lower water content variations inside the barrier-enclosed areas of IH-410 (Steinberg 1980). Subsequent profilometer readings and visual observations showed reductions in IH-410 roughness and cracking (Steinberg, 1981). Observations in 1985 and 1987 indicated the longevity of the barriers in reducing roughness and cracking along both highways, and moisture sensors installed in the barrier-enclosed sections of IH-37 indicated relative uniformity of the subgrade moisture content (Steinberg 1985, Nelson and Miller 1992). Further observations of IH-37 in 1988 and 1990 indicated that no rehabilitation or maintenance work was yet needed (albeit a 1991 report indicated that two small sections required rotomilling) (Nelson and Miller 1992). It should be noted that the vertical barriers along IH-37 were installed in conjunction with the removal of the median ditch (to facilitate drainage) and the placement of a rubberized asphalt surface seal. The work on IH-37 saved approximately \$50,000 per year in maintenance costs (Steinberg, 1985 1992).

The successful performance of the vertical barriers in both of these projects prompted experiments with similar barriers on several other highway remediation projects in Texas. Steinberg (1989, 1992) summarized the installation and performance of nineteen vertical moisture barriers installed along various Texas pavements. He concluded that the barriers generally minimized moisture fluctuations beneath the subgrades and reduced long term roughness and cracking. Gay and Lytton (1988) examined the performance of an EVA (ethyl vinyl acetate)-coated fabric barrier installed at two different depths (six feet and eight feet) along IH-30 near Greenville, Texas. Notably, the barriers were placed when the state of suction in the subgrade had not reached equilibrium. Therefore, the barriers initially retained and isolated infiltrating water beneath the pavement, causing swelling to occur until the suction reached equilibrium. This resulted in an initial spike in the roughness of the pavement before subsequent resurfacings began to be more effective. The 8-foot deep EVA-coated fabric was more effective than the 6-foot deep fabric at retaining and isolating water beneath the pavement.

A study by Bredenkamp et al. (1999) indicated that vertical moisture barriers installed at four test sections along Texas IH-45 effectively reduced long-term moisture fluctuations at three of the four test sections, thereby minimizing heave damage. Evans and McManus (1999) developed a new construction procedure for vertical moisture barriers that they believe reduces

typical installation costs and overcomes some disadvantages. The procedure involves the use of a specially designed trenching boom capable of excavating a 7-foot deep trench at a minimal 3-inch width. The barrier is placed in the trench, and a low permeability, self-compacting flowable fill is poured into the trench. The low volume of required flowable fill is reported to be more cost effective than typical trenching and backfilling operations. Furthermore, the disadvantages involved with a highly permeable gravel backfill are overcome. These barriers were successfully implemented at several locations in Australia.

While vertical moisture barriers have been shown to be successful in many research and construction projects, they can be costly and require special construction. They have usually been restricted to major highways (Wanyan et al. 2008). Jayatilaka and Lytton (1997) summarized the conclusions of a study in which ten different sites with vertical moisture barriers were monitored. Based on their conclusions, they developed a method for predicting the ability of vertical moisture barriers to reduce roughness in pavements. Rojas et al. (2006) noted a lack of effort in contemporary research to analytically and rationally design vertical barriers. They developed a modeling technique with accompanying software to calculate soil suction and volumetric strains in simulation with vertical barriers.

3.1.2 Horizontal Moisture Barriers

Horizontal moisture barriers are usually constructed of geosynthetics or asphaltic sprays. They are placed horizontally along the top of the subgrade and sometimes extend over or beneath adjacent ditch lines. Horizontal moisture barriers minimize moisture flux through the top of the pavement by providing an impermeable layer. They are sometimes installed in conjunction with vertical moisture barriers. Figure 31 illustrates the detail of a typical asphalt seal horizontal moisture barrier extending to a ditch.

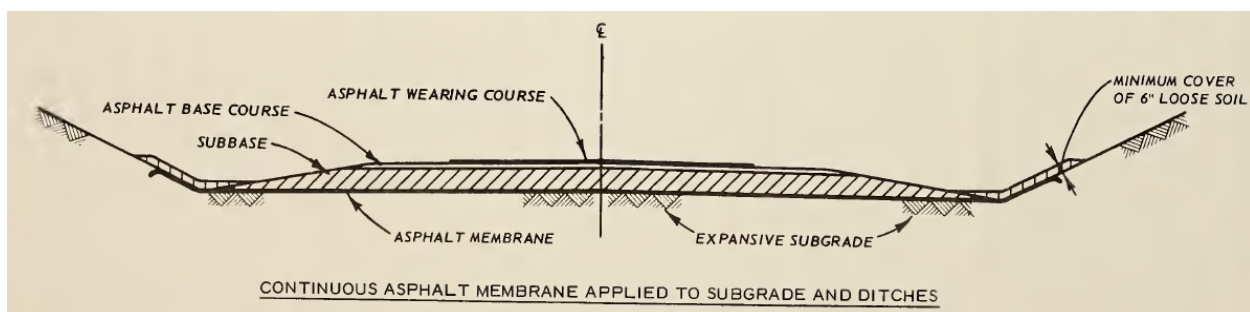


Figure 31: Detail of Asphalt Seal Extending to Roadside Ditch (Snethen 1979)

If the horizontal moisture barrier is a geosynthetic, such as a geomembrane, it is installed either prior to the construction of a pavement or on top of an existing pavement. If it is installed on top of an existing pavement, it is typically followed by sand, base, and new pavement. Each geomembrane is unrolled laterally across the subgrade, and the lap-joints are bonded together by a waterproofing admixture, such as an asphaltic spray. If base material is dumped on top of the geomembrane and spread, special care is taken not to tear the geomembrane. If the geomembrane is torn or punctured, it may be sealed with emulsified asphalt or a similar sealing agent. For portions of the geomembrane extending to the roadside ditches, a minimum cover of six inches of loose sand should be placed over them for protection. (Snethen 1979).

The reported success of horizontal moisture barriers in reducing long term pavement damage varies with different studies. One of the earliest experiments was an attempt in the 1960s to remediate pavements built on expansive subgrades in Colorado. A thin geomembrane sheet was placed between two 6-inch layers of sand, which was placed on top of the existing pavement surface. Initial findings were promising; however, several years later the Colorado DOT found that both sand layers were saturated, and the remedial efforts were ultimately regarded as unsuccessful (Steinberg 1998, 2000).

In 1976, a geomembrane horizontal moisture barrier was installed along a test section of General McMullen Drive, a San Antonio street under complete reconstruction due to damage from expansive clays. Photologging performed in 1981-1982 showed that the test section exhibited less cracking than the control sections. Further monitoring through 1985 and 1987 indicated less roughness and cracking than the control sections (Steinberg 1989). The test section required no pavement maintenance for 10 years (Steinberg 1998). Overall, the project was successful and encouraged further geomembrane rehabilitation design strategies (Steinberg 2000).

According to Steinberg (2000), the Wyoming Department of Transportation (WYDOT) oversaw 60 projects involving geomembrane horizontal moisture barriers for pavement rehabilitation purposes. Many of the horizontal barriers were installed in conjunction with vertical moisture barriers. Figure 32 illustrates a typical detail of a WYDOT horizontal and vertical geomembrane section.

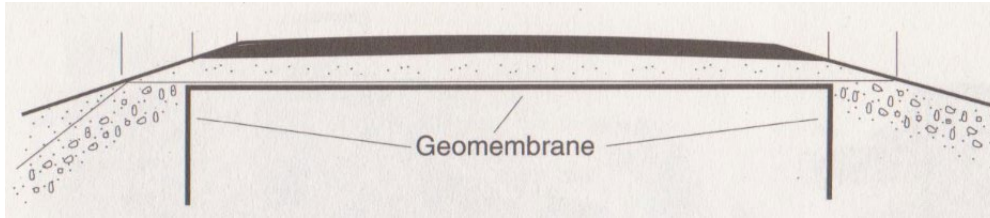


Figure 32: WYDOT Vertical and Horizontal Geomembrane Barrier Section Detail (Steinberg 1998)

One WYDOT project was the rehabilitation of IH-80 near Laramie, WY. Removal and replacement was used in conjunction with a horizontal geomembrane along a 1-mile section of the road. The original subgrade was subexcavated to a depth of 5 ft, and a geomembrane was placed horizontally at the bottom of the cut. The cut was filled with five feet of saturated backfill, base, and pavement. The geomembrane extended past the ditch line and was not installed in conjunction with a vertical barrier. A report published twelve years later indicated that the geomembrane reduced moisture fluctuations in the subgrade and minimized heave damage (Steinberg 1998).

A case study documented by Browning (1999), in which fabric coated geomembranes were installed horizontally along two sections of I-20 in Mississippi, reported poor results for the barriers. Pavement roughness and moisture fluctuations were higher for the barrier-protected sections than for the control sections. Although recommendations were made for discontinuing the use of horizontal moisture barriers, several things should be noted. First, the barriers were installed in asphalt sealed shingles rather than continuous sheets. This may have allowed water seepage to occur between poorly bonded shingle interfaces. Secondly, the barriers were not installed within 9 ft of the centerline on either side of the road. No reason is given by the author for this. However, Browning (1999) states, “A better moisture design might be using a geomembrane that is continuous under the pavement, to seal off rainwater”.

Rollins and Christie (2002) recommended a rehabilitation design for IH-15 in Utah which included a sprayed rubber asphalt liner. The design also included lime-soil stabilization, cross-drains, and gravel ditch covers. Figure 33 gives the schematic of the design.

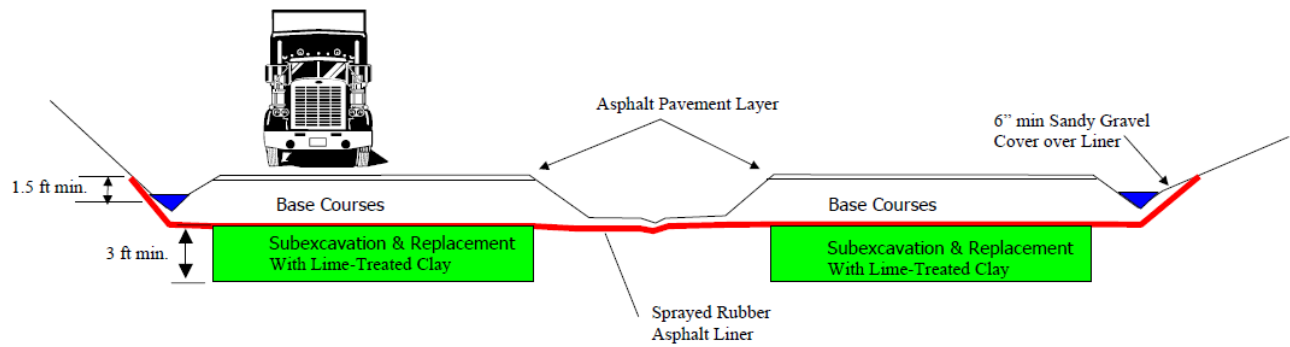


Figure 33: Cross Sectional Schematic of Design Recommendations for IH-15 in Utah (Rollins and Christie 2002)

3.1.3 Edge Drains

Edge drains are subsurface drainage systems that have been utilized to stabilize expansive subgrades. The drains are installed in shallow trenches dug longitudinally along the edges of the pavement. A perforated pipe and a clean permeable backfill are placed in the trench. These materials are typically wrapped in a geotextile, which functions as a filter that causes the passing of water and the retention of soil particles. The trench is topped with embankment fill and pavement materials. Care must be taken not to crush the pipes during backfilling and compacting operations, and construction must be performed carefully to avoid clogging. Flackenstein and Allen (2007) give an extensive overview of best construction practices for edge drains. Figure 34 is a typical schematic of an edge drain.

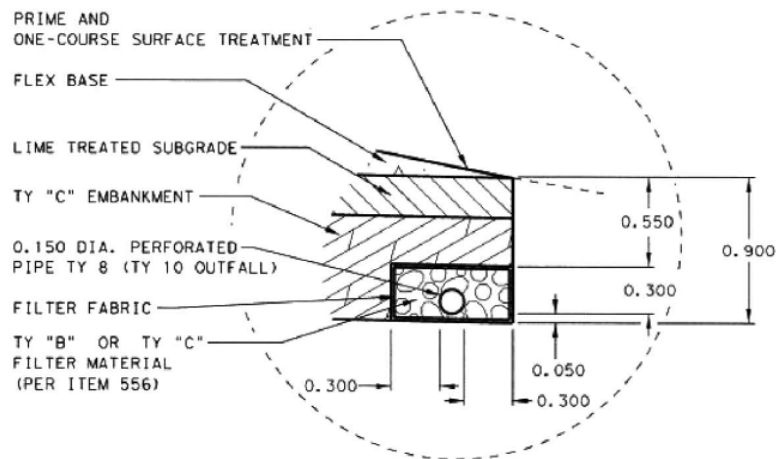


Figure 34: Typical Edge Drain Schematic (Chen et al. 2012)

Chen et al. (2012) cited the success and cost efficiency of edge drains in preventing heave damage along US-59 and SH-114 in the Atlanta (Texas) and Fort Worth districts, respectively. The installation of edge drains along US-59 resulted in excellent pavement performance for 10 years. The installation of edge drains along SH-114 resulted in excellent pavement performance for 5 years. Both roads have continued to perform well as of 2012. Regarding the edge drain installed along SH-114, Chen et al. (2012) state the following: “The District reported that water from the edge drain can be heard (even on a dry day) as it is discharged into the culvert.”

3.1.4 Ponding/Prewetting and Water Injection

The terms ponding and prewetting are used interchangeably to define the process of inundating an expansive subgrade with water in order to cause swelling to occur before a pavement is constructed. Typically, the maximum potential vertical rise (PVR) of the clay is determined through laboratory procedures, and ponding is performed on selected portions of a road with relatively high PVR values. Ponding is performed by constructing a dike around a subgrade and inundating it with water. In some instances, boreholes are drilled at a grid pattern to expedite water infiltration. The boreholes are drilled to the depth of the active zone and backfilled with free draining sand. The dike is constructed using bulldozers and motor graders, and water is obtained using water trucks or nearby wells. A section is ponded until various depths below the pavement reach ideal moisture contents. According to McKinney et al. (1974):

- a) The desired moisture content below a pavement is defined as the condition of the subgrade soil at which it will be susceptible to low amounts of volumetric swell and at the same time will have adequate bearing power to support the usual loads imposed on it.
- b) McKinney et al. (1974) provide a procedure for calculating the ideal moisture contents with respect to depth. In general, water will penetrate a subgrade in a shorter amount of time, and to a greater depth, if the subgrade has a dry, deep crack fabric. Ponding is more likely to be successful during a dry season when the expansive subgrade is desiccated. It is less likely to be successful if performed on a compacted, wet subgrade.

Ponding can be used in conjunction with other design methods discussed in this review. After being ponded, a section may be sealed with a geomembrane to retain moisture. The geomembrane may be installed as a horizontal barrier, a vertical barrier, or a combination of both.

Horizontal barriers prevent the upward escape of moisture, and vertical barriers prevent the lateral escape of moisture. Lime stabilization may also be utilized in conjunction with ponding. When lime is compacted into the upper few inches or feet of a subgrade, it provides a rigid surface during construction, increases the long-term shear strength in the upper layer of soil, and acts as a moisture seal to prevent evaporation (Little 1995). Ponded sections must be optimally compacted at the end of construction. Figure 35 illustrates the ponding procedure.

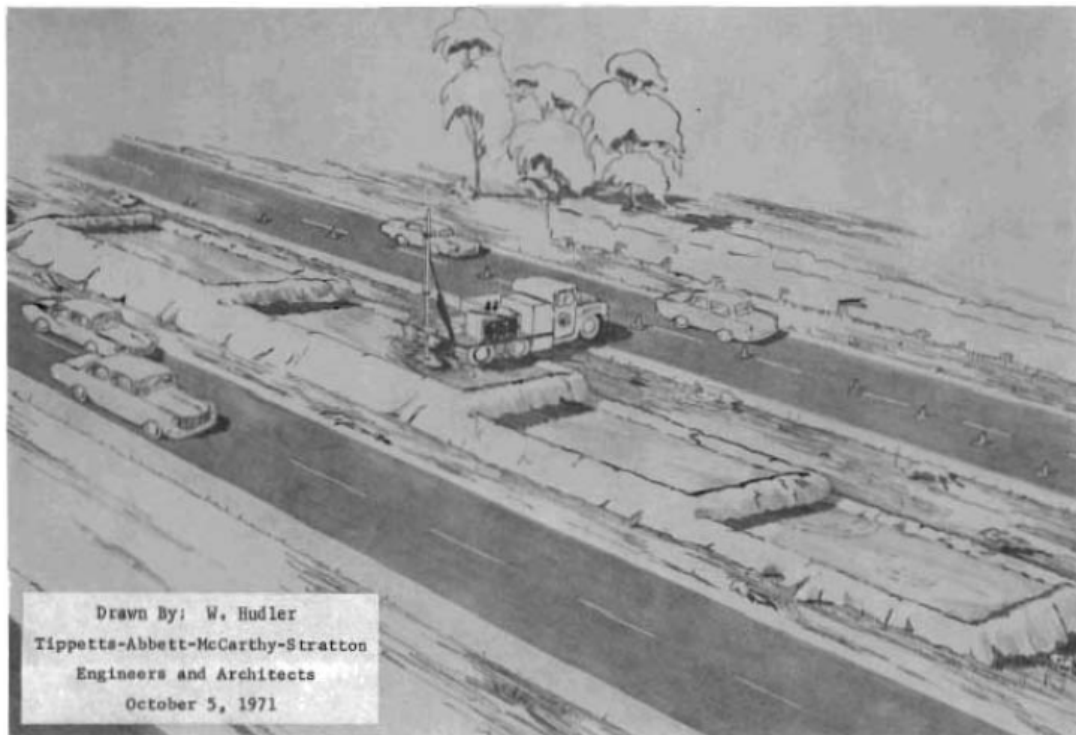


Figure 35: Sketch of a Drilling Rig in a Pond (McKinney et al. 1974)

The chief disadvantages of ponding are the long time periods required to achieve the ideal moisture contents, the unlikelihood of water penetrating to the depth through the full active zone, and the risk of losing strength properties due to over-wetting the subgrade. Nelson and Miller (1992) caution the following:

“There have been many failures resulting from loss of soil strength and the creation of unsuitable working conditions due to excessive moisture in the upper soil layers. Unfortunately, only the successes are reported in the literature and the failures tend to be suppressed.”

The ponding of expansive subgrades was the subject of much research – mostly in Texas – during the 1970s. A study by Watt and Steinberg (1972) reported the ponding of a section of US-90 in Bexar County, Texas. The section was a 25-foot long cut section with an excavation depth of 27 ft. After ponding, the water reached as high as three feet up each cut backslope. The section was ponded for 30 to 45 days, and water eventually penetrated the upper three feet of the subgrade. About 50 percent of the predetermined PVR was achieved. The subgrade surface was lime stabilized, and filtered gravel from the excavation was placed 1.5 ft above the surface as a pavement base. After five years, the ponded section required less repair work and showed less cracking than control sections (Steinberg 1977).

McKinney et al. (1974) published the results of a major ponding project in McLennan County, Texas called “The Waco Ponding Project”. This project was performed along 8 miles of IH-35 between 1957 and 1972. 18 sections, varying in length from 200 to 1,600 ft, were selected for ponding. The sections were ponded for 30 days, and water eventually penetrated the upper four feet of each subgrade. Additionally, water contents from depths of 16 to 20 ft up to the four foot level increased. This was presumably due to increased pore pressures near the surface. The ponding operation was combined with lime stabilization and a gravel base course. The operation successfully stabilized each expansive subgrade. Moisture contents below the pavement in the ponded sections remained fairly constant 13 years later, and long-term pavement roughness was drastically reduced.

A recent variation of the ponding technique is water injection. Water injection has increased in popularity in recent years (Petry and Little 2002). Water injection is similar to ponding in that it causes swelling to occur before a pavement is constructed. The procedure consists of pumping water into a subgrade using an injection vehicle equipped with injection pipes. Injections are made at 12 to 18-inch intervals to a total depth through the active zone. Injections are typically performed in a grid fashion at three to five-foot centers, and multiple injection passes may be specified (Hayward Baker 2010). Water injection overcomes the chief disadvantages of traditional ponding because it is much faster, it allows water to fully penetrate the depth of the active zone, and it is easier to control. Water injection may be used in conjunction with other design methods discussed in this review.

3.2 Chemical Treatment

The literature indicates that a wide variety of chemical additives are available to stabilize expansive subgrades (Petry and Little 2002). Chemical additives are useful because they reduce the plasticity of expansive clays (i.e. the capacity of clay to retain water) and facilitate cementitious bonding of soil particles. This in turn reduces the potential for expansive behavior. Most chemical additives also have the added advantages of improving clay workability and shear strength.

3.2.1 Traditional Chemical Stabilizers

The traditional and most frequently used chemical stabilizers for expansive clays are lime, portland cement, and fly ash. Of these three, the most popular is lime (Petry and Little 2002). Chemical stabilizers may be mixed and compacted into the upper few inches or feet of a subgrade, applied through drill-holes, or injected as a slurry.

3.2.1.1 Lime

Lime is the most frequently used chemical stabilizer for expansive subgrades (Petry and Little 2002). Lime is a term that generally denotes quicklime (CaO) or hydrated lime (Ca(OH)_2). Quicklime is produced by exposing high purity limestone to strong heat, and hydrated lime is produced by mixing quicklime with enough water to form a white powder. Lime slurry is a type of hydrated lime comprised of a homogeneous mix of fine lime particles in water (Little 1995).

Lime stabilizes a soil by replacing monovalent cations (cations with a +1 charge, such as Na^+ , Li^+ , and K^+), which are commonly present in clays, with divalent calcium (Ca^{+2}) cations. This causes a significant reduction in the size of the diffused water layer surrounding individual clay particles, which in turn reduces the capacity of a clay to adsorb water. Furthermore, the cation replacement results in the flocculation and agglomeration of clay particles, increasing clay shear strength and workability (Little 1995). Figure 36 illustrates the change in clay particles due to lime.

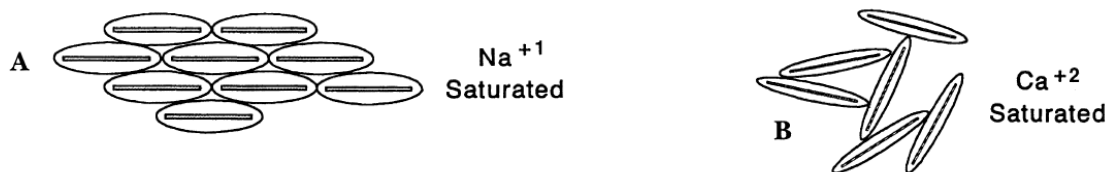


Figure 36: Change in Clay Particles Due to Reactivity with Lime (Little 1995)

Lime further stabilizes a soil by reacting pozzolanically with the silica and aluminum present in the soil to form a cementitious glue that bonds the soil particles together. Lime is a strong base. A relatively small concentration of lime will raise the pH of a water solution to a maximum of 12.454 (Little 1995). In order for lime-soil stabilization to be successful, the lime-soil environment must be maintained at a pH greater than 12.3 during mixing and curing (Chen et al. 2009). The high pH environment causes the silica and aluminum materials present in the soil to become soluble, enabling them to react pozzolanically with the lime calcium ions. Therefore, the proper concentration of lime must be determined prior to each lime-soil stabilization project in order to create and maintain an adequate pH lime-soil environment.

Nelson and Miller (1992) list the following factors that influence the reactivity of lime with clays:

- A soil pH greater than about 7 indicates good reactivity.
- Organic carbon greatly retards lime-soil reactions.
- Poorly drained soils tend to have higher lime reactivity than well-drained soils.
- Calcareous soils have good reactivity.
- Sulfates and some iron compounds inhibit the lime reaction.
- The presence of gypsum in the soil or ammonium fertilizers may increase the amount of lime required. (Nelson and Miller 1992)

Of particular concern when considering lime-soil stabilization is the possibility of high concentrations of soluble sulfates in the soil. Performing lime stabilization in clays containing high concentrations of salts with soluble sulfates (such as sodium sulfate (Na_2SO_4) and gypsum ($\text{CaSO}_4 \cdot 2\text{H}_2\text{O}$)) will trigger the formation of ettringite, a reaction product comprised of calcium, alumina, water, and sulfate (Little 1995). The formation of ettringite diminishes the lime meant to react with the soil and forms a material which contains expansive characteristics itself. Expansion caused by ettringite formation is known as lime-induced sulfate heave. Lime-induced sulfate heave may be greater than the heave of the untreated expansive clay (Mitchell, 1986). Soils containing above 1,000 ppm of soluble sulfates have been reported to react with lime to form ettringite (Little and Nair 2009). Therefore, expansive subgrades should be tested for sulfates prior to performing lime-soil stabilization. Test procedures range from simple in-situ electromagnetometer tests to more

complex laboratory tests involving small soil samples and centrifuges. Little and Nair (2009) provide a recommended practice manual for testing and stabilizing sulfate-rich subgrades.

The presence of organic matter in a subgrade can inhibit lime-soil reactivity. Organic matter affects lime in a way similar to soluble sulfates, in that it absorbs the lime meant to react with the soil. Soils containing more than 1% organic matter may inhibit lime-soil reactivity (Chen et al. 2009). Furthermore, organic matter will prevent the pH in the lime-soil environment from reaching the minimum value of 12.3 required to facilitate pozzolanic reactions, thereby reducing the lime-soil reactivity (Chen et al. 2009).

Lime stabilizers may be mixed and compacted into the upper few inches or feet of a subgrade, applied through drill-holes, or injected as a slurry. Generally, the success of lime-stabilization is dependent upon adding the correct amount of lime, properly compacting and curing the lime-soil mix, and pulverizing the lime to a proper degree. Failure to fulfill any one of these requirements can result in poor performance. Additional considerations must be made regarding temperature, since lime-soil reactions are temperature dependent (Little 1995).

When applied to the upper few inches or feet of a subgrade, lime may be applied in a dry or slurry form. When applied in a dry form, lime is typically applied in bulk through self-unloading transport trucks (Little 1995). The soil to be mixed is scarified either before or after the application of dry lime, and mixing is accomplished through blade mixing or rotary mixing. When applied in slurry form, the soil must be scarified prior to the lime application. The slurry is applied by a tank truck fitted with spray bars (Little 1995). Depending on design standards and climatic factors, the lime-soil mixture may or may not be allowed to mellow for several days to allow sufficient time for the lime to react with the soil particles. The lime-soil mixture is then compacted to optimum densities, and the pavement is constructed.

Lime may also be applied through the drill-hole technique. When the drill-hole technique is utilized, holes are drilled through the subgrade to depths of 2.5 to 4 ft at four to five-foot centers (Nelson and Miller 1992). Dry or slurry lime is then placed in the holes. If dry lime is placed, water is added to increase mobility. The pavement is then constructed. Very little research exists reporting the success of the drill-hole technique. According to Nelson and Miller (1992):

“Results of the drill-hole technique are erratic, and the authors do not encourage its use.

One factor that limits the effectiveness of the method is the inability to uniformly distribute

the lime in the soil mass. Also, the diffusion process is very slow unless the soil has an extensive network of fissures.”

The lime slurry pressure injection (LSPI) method was developed to provide a better alternative to the drill-hole technique (Nelson and Miller 1992). The LSPI method consists of pumping lime slurry into a subgrade using an injection vehicle equipped with injection pipes. The lime slurry is transported to the injection vehicle from a nearby slurry mix tank. In some instances, fly ash and/or a surfactant is mixed into the lime slurry. Fly ash will help facilitate pozzolanic reactions in the soil, greatly increasing the long-term shear strength of the soil. The surfactant will reduce the surface tension of the slurry, improving infiltration. Injections are made at 12 to 18-inch intervals to a total depth extending through the active zone. At each interval, slurry is pumped until refusal or until a target pressure is achieved. Injection depths can range from three to ten feet and are typically spaced at five-foot grid patterns (Little 1995). Figure 37 illustrates a typical injection vehicle.



Figure 37: Typical Injection System (Hayward Baker 2010)

LSPI is more likely to successfully stabilize a subgrade if the subgrade exhibits a relatively deep dry crack fabric. Upon injection, lime slurry takes the path of least resistance along crack and

fissure walls within the subgrade. Upon infiltrating the cracks, the lime encapsulates and seals off large portions of clay, reducing the capacity for capillary and seepage phenomenon. This in turn greatly reduces the potential for volumetric changes within the subgrade. Furthermore, high injection pressures can cause hydraulic fracturing within the subgrade, creating new planes of slurry infiltration. It must be emphasized that the slurry does not diffuse homogeneously “through” the bulk soil; rather, it travels along the available cracks and fissures (Snethen 1979). Therefore, if the subgrade does not exhibit a relatively deep dry crack fabric, the injection process will be performed with less confidence. The success of the procedure will be dependent upon the occurrence of hydraulic fracturing, which may be difficult to achieve and/or identify during construction. If hydraulic fracturing does not occur, the injection process may encounter refusal without a sufficient diffusion of the lime. It should be noted LSPI increases the shear strength of the soil according to the same phenomenon discussed previously.

A case study performed by Wilkinson et al. (2010) investigated the effects of a lime/fly ash pressure injected slurry on the properties of an expansive clay at a site in Breeza, New South Wales, Australia. Additionally, the quality of slurry infiltration throughout the soil was examined by digging a trench and performing visual observations. The lime/fly ash slurry was found to reduce the average swell pressures of the clays to one-fifth of their untreated values, while clay free swell values were reduced up to 4% below their original values. Additionally, cone penetration tests before and after injection indicated a strength increase in the stabilized soils. Furthermore, visual observations confirmed that the slurry infiltrated along shrinkage cracks and produced hydraulic fractures. Figure 38 gives a picture of the distribution of the slurry.

A case history cited by Koelling (1994) reported the use of a lime/fly ash pressure injected slurry along 5,000 ft of Beloit County Road in Maricopa County, AZ in 1990. It must be noted that this particular subgrade consisted of water-sensitive silt rather than expansive clay; however, the encapsulation phenomenon achieved by LSPI is the desired outcome for both soil types. It should also be noted that this road was enclosed on either side by irrigated farmland, which facilitated excess seepage and exasperated the problem. Injection was performed to four foot depths along the entire width and length of the road. After injection, the resultant network of lime/fly ash planes within the subgrade created a moisture barrier, thus stabilizing the subgrade. Soil shear strength was also increased. The slurry remaining on the surface from refusal was

scarified and compacted, providing additional moisture enclosure and increasing surface strength. Figure 39 gives a picture of the rubber tired injection machines used in the project.

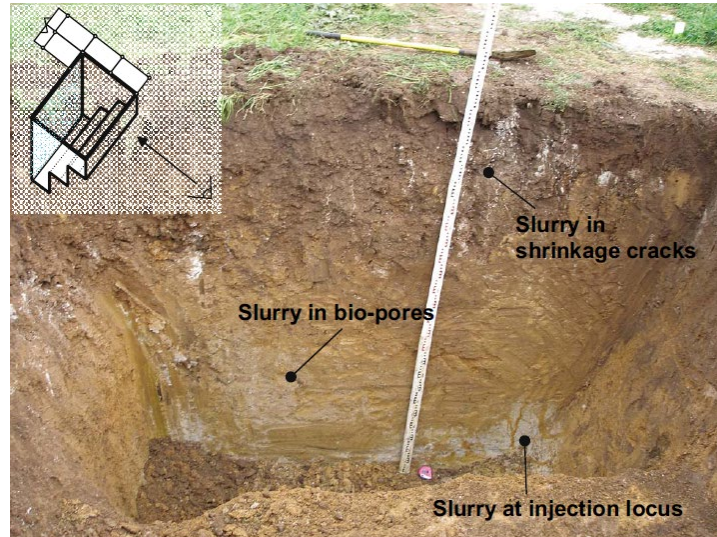


Figure 38: Distribution of Lime/Fly Ash Slurry from LSPI (Wilkinson et al. 2010)



Figure 39: Rubber Tired Injection Machines Used in the Belloat Road Project (Hayward Baker 1990)

3.2.1.2 Portland Cement

Portland cement is produced by mixing a calcareous material, such as limestone, with an argillaceous material, such as clay or shale, under special conditions in a cement plant. When combined with water, portland cement becomes two cementing compounds: calcium-silicate-hydrate and calcium-aluminate-hydrate. Additionally, excess calcium hydroxide ($\text{Ca}(\text{OH})_2$) (i.e. lime) is produced (Little et al. 2000).

Portland cement stabilizes a soil in a manner similar to lime. A cation exchange occurs between the monovalent ions present in the clays and the calcium hydroxide produced during cement hydration. This reduces the size of the diffused water layer surrounding individual clay particles. Furthermore, pozzolanic reactions may occur between the excess free lime and the soil particles, resulting in cementitious bonding. Additionally, the cementing compounds in portland cement react independently upon the addition of water to form a cementitious paste. The overall result of portland cement soil stabilization on clay is a reduction in the liquid limit, which reduces the capacity of clay to adsorb water. Additionally, portland cement increases clay shear strength.

The construction procedures for cement-soil stabilization are nearly the same as those for lime-soil stabilization (Nelson and Miller 1992). Portland cement may be mixed and compacted into the upper few inches or feet of a subgrade in a dry or slurry form as described for lime. It may also be injected as a grout slurry. In cement-stabilization, the minimum amount of cement required to achieve stabilization is determined prior to cement application. This amount may be restricted to that which is required to reduce the plasticity index of the soil to a sufficient value; it does not need to be so much as to produce a stiffened slab (Little et al. 2000).

3.2.1.3 Fly Ash

Fly ash is the residue produced by the fusing and solidification of inorganic coal materials during the combustion and cooling processes in electrical plants. Fly ash is commonly produced in two forms: Class F fly ash and Class C fly ash. Class F fly ash is a non-self-cementing, low calcium byproduct of aged bituminous coals. Class F fly ash is the pozzolanic additive commonly used with lime in lime stabilization projects, and it is dependent on the lime “activator” to produce cementitious properties (Little et al. 2000). Class C fly ash is a self-cementing, high calcium byproduct of younger subbituminous coals (Mackiewicz and Ferguson 2005). When combined with water, Class C fly ash hydrates and becomes a cementitious material that can be utilized to stabilize soil without the assistance of a lime activator. Soil stabilization with Class C fly ash has replaced lime stabilization where Class C fly ash is readily available (White et al. 2005, Mackiewicz and Ferguson 2005). A third type of fly ash is sometimes produced that contains large concentrations of sulfates. Due to hazards involving sulfates and ettringite formation, this particular type of fly ash should not be used in soil stabilization (Mackiewicz and Ferguson 2005).

Self-cementing (Class C) fly ash stabilizes a soil in three ways, two of which are similar to lime, and one of which is unique from lime. Fly ash stabilization is similar to lime stabilization in

that some free calcium ions exist in the fly ash and replace soil cations, resulting in smaller diffuse water layers surrounding individual soil particles. Fly ash stabilization is also similar to lime stabilization in that fly ash forms a cementitious paste upon the addition of water, bonding the soil particles together. However, fly ash stabilization differs from lime stabilization in that the fly ash particles mechanically stabilize a soil by replacing some of the volume held by soil particles (White et al. 2005). Therefore, fly ash stabilization may be a desirable alternative to lime stabilization because fly ash stabilization is more related to mechanical bonding than cation exchange. In other words, fly ash stabilization is less dependent on the reactivity of the soil (Mackiewicz and Ferguson 2005). It should be noted that the presence of free lime in fly ash particles can cause sulfate-induced heave in the manner described previously (White et al. 2005).

Self-cementing (Class C) fly ash stabilizers may be applied by being mixed and compacted into the upper few inches or feet of a subgrade. Fly ash has a relatively fast hydration and cementing rate (as little as ten minutes) (White et al. 2005). Therefore, delayed compaction of the ash-water-soil mixture will allow bonding to occur in a premature, loose form. This inhibits the achievement of design densities and compressive strengths (Mackiewicz and Ferguson 2005). Accordingly, compaction must be performed within one or two hours of initial mixing (Mackiewicz and Ferguson 2005). Construction involves transporting and dumping dry fly ash onto the subgrade with belly dump or tanker trucks. The fly ash is then spread, and mixing is performed by a pulvamixer (Mackiewicz and Ferguson 2005). To control the water content of the mix while avoiding delays, the mixing drum of the pulvamixer is filled with water (Mackiewicz and Ferguson 2005). A sheepsfoot or padfoot roller follows immediately behind the pulvamixer to ensure rapid compaction. The compacted mix is sealed and allowed to cure until required strengths are achieved. Regarding the economy of fly ash stabilization, Mackiewicz and Ferguson (2005) state the following:

“Most fly ash stabilization applications require fly ash contents ranging from 12 to 15% (dry weight basis); whereas, cement or lime stabilization typically requires contents ranging from 3 to 7%. Even with the addition of larger quantities of ash to achieve the stabilization required, the fly ash treatment is generally more economical than the lime and cement alternatives.”

3.2.2 Nontraditional Chemical Stabilizers

Nontraditional chemical stabilizers, such as potassium and ammonium, are used less frequently than traditional stabilizers. The use of nontraditional stabilizers is relatively new and is not supported by as much research as traditional stabilizers (Petry and Little 2002). Therefore, a higher degree of uncertainty will exist when utilizing nontraditional stabilizers.

3.2.2.1 Potassium and Ammonium

Potassium and ammonium stabilize a soil in a manner similar to lime by replacing the exchangeable cations commonly present in clays with potassium (K^+) and ammonium (NH_4^+) ions. Potassium and ammonium ions both have smaller hydration energies and radii than those of the cations commonly present in clays, such as sodium, calcium, and magnesium (Pengelly and Addison 2001). The smaller hydration radii enable the ions to move closer to the clay particle surfaces. When the ions are sufficiently close to the clay particle surfaces, the smaller hydration energies reduce the potential energy of the clay particles, resulting in reduced swelling pressures (Pengelly and Addison 2001). Potassium/ammonium stabilizers are applied in slurry form through injection vehicles equipped with injection pipes as described in previous sections. Potassium/ammonium stabilizers may be desirable for the remediation of existing subgrades because they react in such a way as to greatly limit the amount of preswelling that occurs during injection, allowing for the preservation of an existing pavement (Hayward Baker 2010).

A case study by Pengelly and Addison (2001) reported the success of a potassium/ammonium slurry-mix in stabilizing an expansive soil responsible for damaging a two-story building in Garland, Texas. Laboratory tests were performed on field samples to determine the amount of potassium/ammonium solution needed for stabilization. A potassium/ammonium slurry was injected at 16-inch intervals to a total depth of eight feet. Twenty laboratory swell tests performed after injection showed that the free swell values of the clays were reduced from 3.6-4.7 % to an average of 0.43%, indicating that the stabilization was successful. Building inspections over two years later indicated no signs of expansive clay damage.

3.3 Physical Ground Improvements

The literature indicates that expansive subgrades were stabilized through compaction and removal/replacement. These procedures physically alter the in-situ composition of the subgrade and are often utilized in conjunction with other design methods.

3.3.1 Compaction

Compaction is the process by which a soil is compressed under a specified amount of energy to achieve a desired density at a corresponding water content. Generally, a soil is spread in thin layers, and each layer is compacted as specified. Compacting an expansive clay to a low density at a water content slightly wet of optimum has been experimentally proven to reduce clay swell potential, all other things being equal (Nelson and Miller 1992). This is because a higher water content satisfies a greater amount of the potential energy of a clay, thus minimizing its potential to swell (Hayward Baker 2010). Compacting an expansive subgrade wet of optimum may be performed in conjunction with other design methods discussed in this review.

It may be feasible to rip, remold, and compact an existing subgrade as a standalone solution to expansive subgrade problems (Nelson and Miller 1992). An existing subgrade may be scarified or subexcavated and compacted to a density and water content that corresponds to a minimal swell potential. The target density and water content are determined by conducting a series of swell tests on field samples compacted to different densities and water contents. The sample exhibiting the lowest swell potential while maintaining an adequate density and water content is selected as a model for field construction.

Compaction as a standalone solution would be particularly advantageous in less active clays with shallow active zones and/or relatively dry and cracked fabrics (Nelson and Miller 1992). However, in the case of highly active clays, utilizing precise compaction alone may not sufficiently reduce the swell potential of the subgrade (Nelson and Miller 1992). Additionally, specifying water contents that are too high and densities that are too low must be avoided. Clays with relatively high water contents are difficult to compact, and a subgrade compacted to a relatively low density may have inadequate strength.

3.3.2 Removal and Replacement/Surcharging

Removal and replacement is the process by which a portion of soil is subexcavated to a certain depth, removed, and replaced with a soil more suitable for the application at hand. Removal and replacement has been utilized for expansive subgrades. The subgrade is subexcavated to a maximum practical depth of four to five feet and replaced with a nonexpansive, impermeable fill, or a nonexpansive, granular fill (Nelson and Miller 1992). If a nonexpansive, impermeable fill is readily available, it should be selected over a nonexpansive, granular fill. A nonexpansive, impermeable fill can be compacted to a higher density while minimizing moisture infiltration to

the underlying expansive clay. A granular fill would allow for water to infiltrate to the expansive clay, which could facilitate pavement distortion (Snethen 1979).

A backfilled, nonexpansive material may also be utilized as a surcharge to counteract the swelling pressures of an underlying expansive clay. Laboratory swell tests may be utilized to determine the weight of backfill needed to counteract swell pressures (Nelson and Miller 1992). Removal and replacement may be used in conjunction with other design methods discussed in this review.

A case study cited by Steinberg (1989) reported a removal and replacement operation on an expansive subgrade along IH-10 in Hudspeth County, Texas. Five feet of expansive subgrade were removed and replaced with an inactive material. The pavement performed well for ten years, after which it began to distort due to the underlying expansive clay stratum. (In 1984, vertical moisture barriers were installed to eight-foot depths along both shoulders of the road. As of 1988, there were no signs of further distress).

A case study cited by Chen et al. (2012) reported a removal and replacement operation performed on an expansive subgrade along SH-6 in the Byron District of Texas. Four feet of expansive subgrade were removed and replaced. The pavement performed well for ten years, after which roughness developed.

3.4 New and/or Innovative Designs

In this section, several relatively new or innovative designs for stabilizing expansive subgrades are introduced. These are potentially useful solutions that are not supported by as much independent research or field experience. Many of these procedures borrow concepts from the design methods discussed previously.

3.4.1 Geogrids

A geogrid is a thick plastic sheet consisting of large grid-like openings. In subgrade applications, geogrids are installed horizontally at the subgrade-subbase interface or within a layer of the pavement system itself. Geogrids are frequently installed to increase the bearing capacity of a subgrade by providing extra resistance to transmitted shear stresses (McCarthy 2007). Recently, geogrids have been utilized to minimize pavement damage caused by expansive subgrades (Zornberg and Gupta 2009). A geogrid is placed at the subgrade-subbase interface where it effectively intercepts and “shifts” incoming cracks away from the pavement (Zornberg and Gupta 2009). Figure 40 illustrates a typical cross-section of a road with geogrid reinforcement:

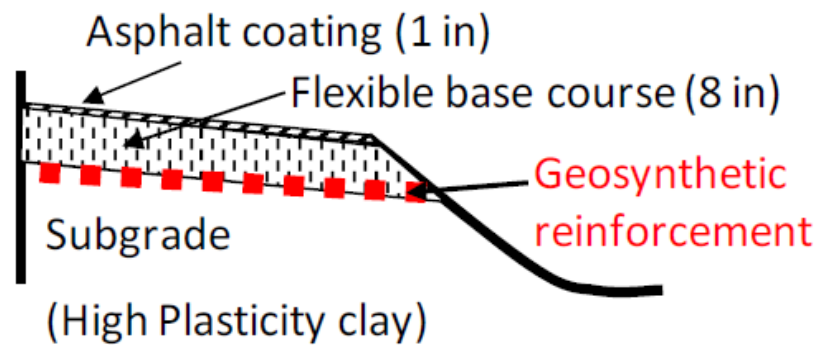


Figure 40: Cross-Section of a Road with Geogrid Reinforcement (Zornberg and Gupta 2009)

Geogrids are installed in a manner similar to horizontal moisture barriers. Each roll is unrolled laterally across the subgrade, and the lap-joints are bonded together with ties or straps. The remaining pavement system is constructed on top of the geogrid.

Zornberg and Gupta (2009) provide three case histories documenting the utilization of geogrids with expansive subgrades. In the first project, performed in Milam County, Texas, a 2.5-mile stretch of pavement exhibited severe longitudinal cracking. The entire section was lime-stabilized to a depth of nine inches and coated with an asphaltic seal. Additionally, the section was divided into three sections, two of which were geogrid-reinforced at the subgrade-subbase interface, and one of which functioned as a control section. Of the two geogrid-reinforced sections, one had an eight-inch-thick base course, and the other had a five-inch-thick base course. The type of geogrid used on both sections was the same. After a few months, condition surveys and visual inspections showed fine performance for both geogrid-reinforced sections, while longitudinal cracking was observed along the control section.

In the second project, performed in Leon County, Texas, a stretch of pavement exhibited severe longitudinal cracking. The entire width of the pavement, including the shoulder, was set apart for rehabilitation. The subgrade was lime-stabilized, and a geogrid was placed at the subgrade-subbase interface. A flexible pavement system was then constructed. Soon, longitudinal cracks were observed along a remote portion of the shoulder. A small excavation revealed that the geogrid at this particular area did not extend over the entire width of the pavement, but stopped at the exact spot of the observed longitudinal cracks. According to Zornberg and Gupta (2009):

“[This incident] provided additional evidence of the reinforcement effects of geosynthetics when placed over expansive clays. Specifically, the use of geosynthetic reinforcement relocated cracks, which may have developed within the pavement area, to a zone beyond the reinforced area.”

Figure 41 gives a picture of the excavation and the geogrid edge.



Figure 41: Picture of Excavation and Geogrid Edge (Zornberg and Gupta 2009)

In the third project, performed in Grimes County, Texas, a nine-mile stretch of distressed pavement was set apart for rehabilitation. The entire section was lime/cement-stabilized to a depth of about 10 inches, and a geogrid was placed at the subbase-subgrade interface. A flexible pavement system was then constructed. However, two separate contractors were commissioned for the work, and each placed a different type of geogrid at different sections. Both geogrids conformed to standard TXDOT geogrid specifications. Soon, longitudinal cracks were observed along pavement sections containing one type of geogrid, while the sections with the other geogrid remained stable. A small excavation revealed that the geogrid in the distressed area contained junction failures. According to Zornberg and Gupta (2009):

“Ultimately, it is clear that the currently available specifications based on tensile properties of the geogrid (both ribs and junction) may not be adequate to identify the geogrid properties that govern the performance of geogrid-reinforced pavements over expansive soils.”

It should be emphasized that for each of these projects, geogrids were installed in conjunction with surface lime-stabilization.

3.4.2 Electrochemical Treatment

The electrochemical treatment of an expansive subgrade combines the phenomenon of electro-osmosis with chemical stabilization. Electro-osmosis is the process by which a cathode-anode system generates an electric potential in a soil, causing cations and water to flow through the soil towards the cathode (Mitchell 1976). Figure 42 illustrates this phenomenon:

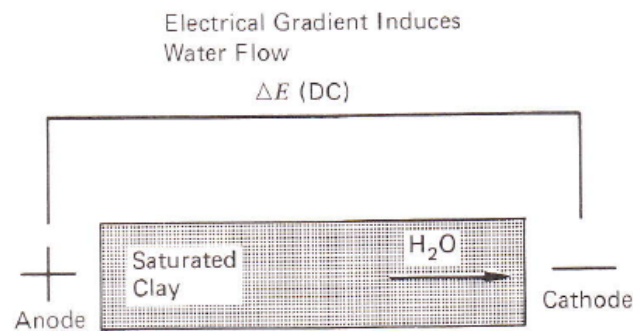


Figure 42: Electro-osmosis in Clay (Mitchell 1976)

Snethen (1979) provides a step-by-step construction process for the electrochemical treatment of an expansive subgrade. In general, longitudinal trenches are dug along both edges of the subgrade, and anodes and cathodes are placed horizontally into the exposed sides of the subgrade. Injection holes are dug at a specific grid pattern and depth – both of which are specified beforehand based on laboratory tests. An electrical connection is made between the anode and the cathode, and the injection wells are filled with a slurry solution of chemical stabilizer, such as lime or potassium. A voltage gradient is then induced, and the slurry solution is allowed to diffuse through the soil mass. The injection wells are refilled at set times for up to “3 to 4 weeks depending on electrode polarization phenomena” (Snethen 1979). According to Snethen (1979):

“The lower the initial moisture content and higher the percentage of montmorillonite, the more effective the electrochemical treatment; and electrochemical treatment is most effective on a highly localized clay mass with a high swell potential.”

3.4.3 Tire Shreds

Seda et al. (2007) were the first to study the effects of waste tire shreds on the swelling properties of expansive clays. Small particles (grade 6.7-mm minus) of waste tires were uniformly mixed (20% by weight) with clay samples from Colorado. One-dimensional swell tests were performed on the samples. The tests showed that the tire shreds reduced the original swell pressure from 2,610 psf to 647 psf, and the original free swell from 8.2% to 4.2%. At the same time, the soil-tire mixture was found to be more compressible than the original soil, presumably due to the high compressibility of rubber. However, most of the deformation took place during the initial loading of the samples and can therefore be likened to the immediate settlement experienced during construction. According to the authors, “From a practical standpoint, this means that most of the deformation should occur during construction and, thus, could be properly assessed and mitigated” (Seda et al. 2007). The authors suggest that tire-stabilization may be utilized as a standalone solution or in conjunction with other design methods.

3.4.4 Deep Soil Mixing (DSM) Columns

The use of deep soil mixing (DSM) technology is usually reserved for strengthening very soft clays and/or soils with high organic contents. A study performed by Madhyannapu (Madhyannapu 2007, Madhyannapu et al. 2009, 2010) was the first to evaluate the utilization of DSM technology for stabilizing expansive soils. Two 15 by 40-foot test sections, located in the median of Interstate 820 near Fort Worth, Texas, were selected for the placement of DSM columns. Both test sections (one containing 44 DSM columns and the other containing 65 DSM columns) were installed at different grid patterns. The columns were augured to ten-foot depths at two-foot diameters, and the center-to-center spacing was one meter. A geogrid was laid over the columns and tied to rods that were anchored into the columns. The geogrid was installed to facilitate stress transfer throughout the columns. 1.2 ft of fill was then dumped onto the geogrid and compacted using a vibratory tamper. Figure 43 gives a schematic of the final DSM design. The test sections were monitored for two years, and movements in and around the columns were found to be negligible.

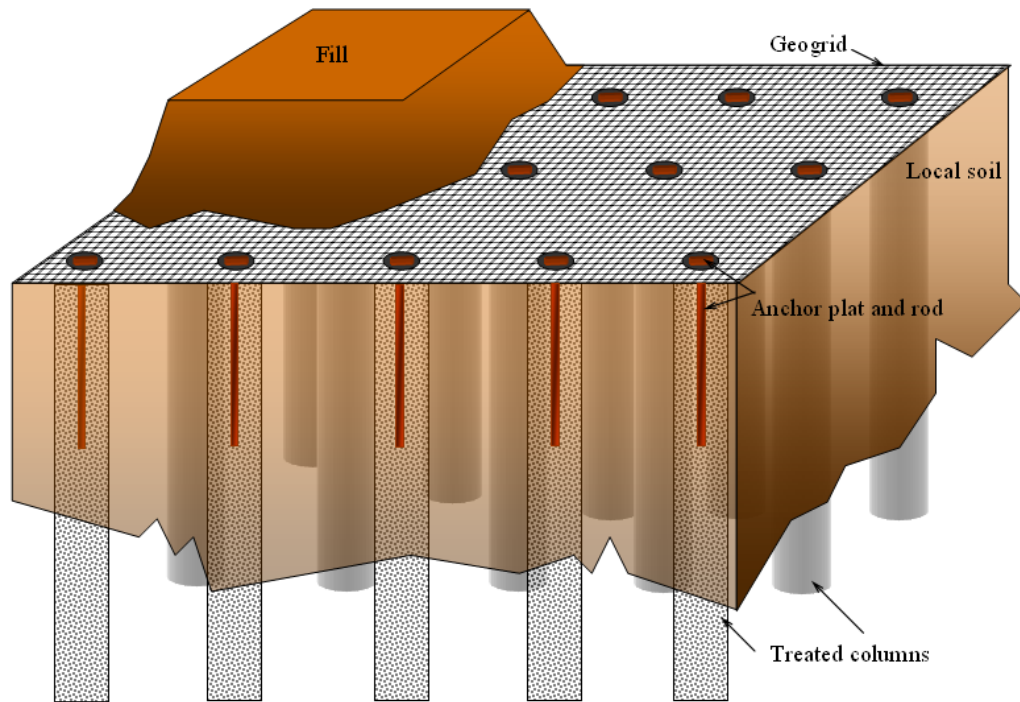


Figure 43: Schematic of Deep Mix Columns for the Stabilization of Expansive Soils (Madhyannapu, 2007)

Chapter 4. Preliminary Investigation

4.1 Desk Study

As depicted previously in Figure 3, a substantial number of highway lane miles in western Alabama are likely underlain by expansive soils. ALDOT personnel identified, in particular, Alabama state route 5 (AL 5). This project focused on a corridor of AL 5 from the Dallas County Line, mile post (MP) 50.802, to MP 54.85 in Perry County.

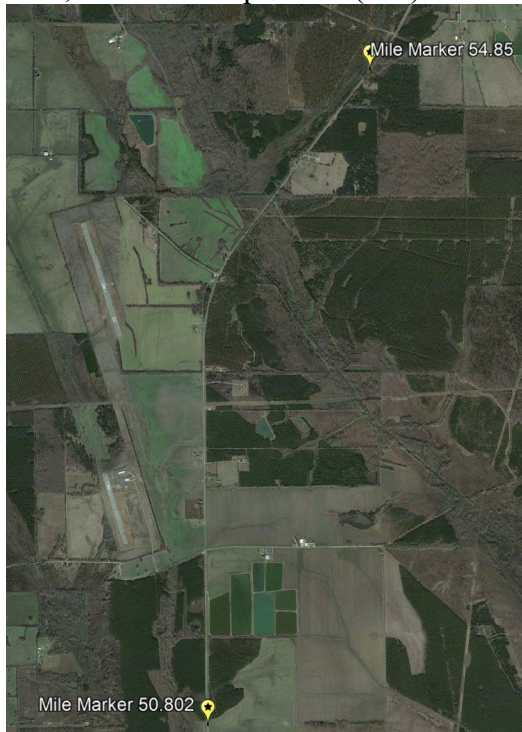


Figure 44 is an aerial image from Google Earth (2014) indicating the beginning and end of the project. Much of the surrounding land is wooded area, but significant sections consist of farmland. There is a catfish pond just east of the road near mile point 51.5. There is one bridge in the study area where AL 5 crosses over Washington Creek near mile post 53.7.

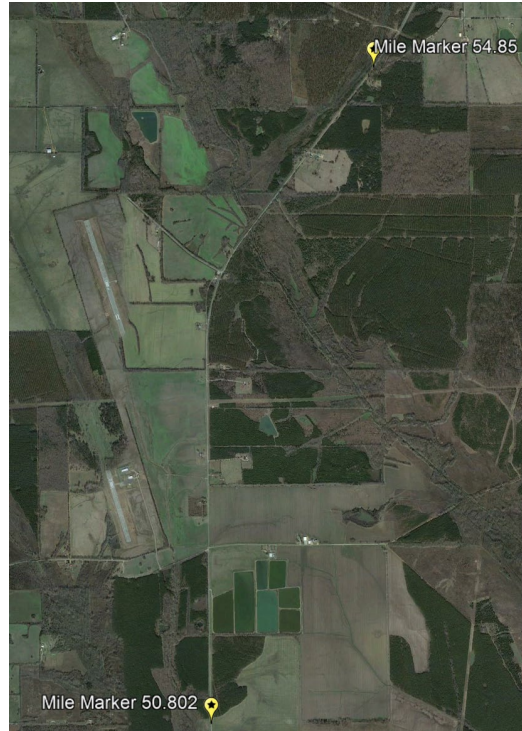


Figure 44: Google Map of Alabama Highway 5: MP 50.8-54.3 (Google Earth 2014)

Traffic data was obtained from ALDOT’s traffic database. For a traffic count station located within the bounds of the project at mile post 51.21, the average annual daily traffic (AADT) for 2014 was 1410 vehicles. Thirty-six percent of this was truck traffic (class 5 vehicles and above) meaning the average annual daily truck traffic was 508 trucks for 2014 (ALDOT 2016).

AL 5 carries heavy traffic from Mobile to Birmingham in Alabama. It is a “farm-to-market” road and it was constructed by placing pavement directly on the subgrade with little or no aggregate base. According to the approved materials report ALDOT (2014), AL 5 was last resurfaced in 1995 using approximately 125 lbs/sy of latex rubber modified bituminous concrete wearing surface under Project No. 99-305-535-005-304. Since that time asphalt patching has been required at numerous locations throughout the project and the pavement serviceability has dropped below tolerable limits.

The climate of Perry County, Alabama is primarily influenced by moist tropical air that moves north from the Gulf of Mexico and covers the area. Perry County typically has long, hot summers and cool, short winters. The average summer temperature is 79 degrees with an average daily maximum of 90 degrees. The average winter temperature is 46 degrees with an average daily minimum of 34 degrees (Harris 1998). Thunderstorms are common during the summer and the

majority of the annual precipitation falls during the summer months (April – October). Perry County experiences about 54 inches of total annual precipitation (Harris 1998). Every several years the remnants of a hurricane or tropical storm will move inland causing heavy rain for several days (Harris 1998). The NOAA National Climatic Data Center has published 30-year climate normals for Selma, Alabama from 1981 to 2010, Table 6, including total monthly precipitation, and the maximum, minimum and average monthly temperature. Figure 45 depicts these normals and demonstrates the seasonal variation in precipitation and temperature visually.

Table 6: Historical Weather Data for Selma, Alabama, 1981-2010 (NOAA National Climatic Data Center 2010)

Month	Total Precipitation Normal	Mean Maximum Temperature Normal	Mean Minimum Temperature Normal	Mean Average Temperature Normal
January	4.75	57.4	35.4	46.4
February	5.03	61.5	38.9	50.2
March	5.47	69.6	44.7	57.1
April	3.93	76.4	51	63.7
May	3.26	84	60.5	72.3
June	4.07	89.8	68.3	79.1
July	4.72	92	71.3	81.7
August	4.42	91.6	70.9	81.3
September	3.32	86.9	65.5	76.2
October	2.68	77.7	54	65.9
November	4.55	68.6	43.7	56.2
December	4.89	59.1	37.3	48.2

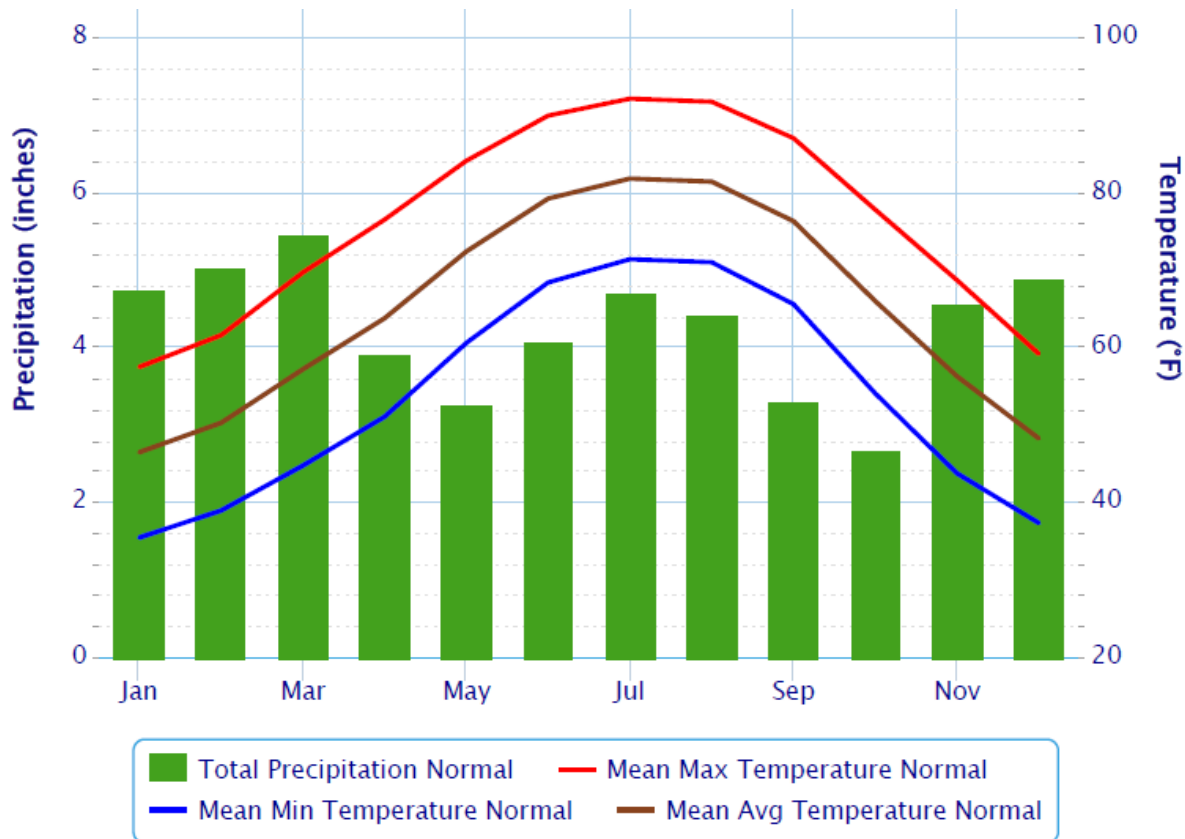


Figure 45: Historical Weather Data for Selma Alabama, 1981-2010 (NOAA National Climatic Data Center 2010)

The corridor is primarily located in the Mooreville Chalk formation, which is generally characterized by “yellowish gray to olive-gray compact fossiliferous clayey chalk and chalky marl” (Szabo et al. 1988). Figure 46 shows the project site with the USGS geologic map for the area overlain. The site lies in the coastal plain physiographic province in the Black Prairie belt (Monroe 1941). Figure 47 is a geologic map of the area. Sections near Washington Creek consist of alluvial deposits of Quaternary age. The upper and lower portions of the Mooreville Chalk vary from this with the upper 10 feet containing interbedded clay and limestone and the lower few feet containing calcareous sand (Raymond et al. 1988), but these members were not encountered in the study area.

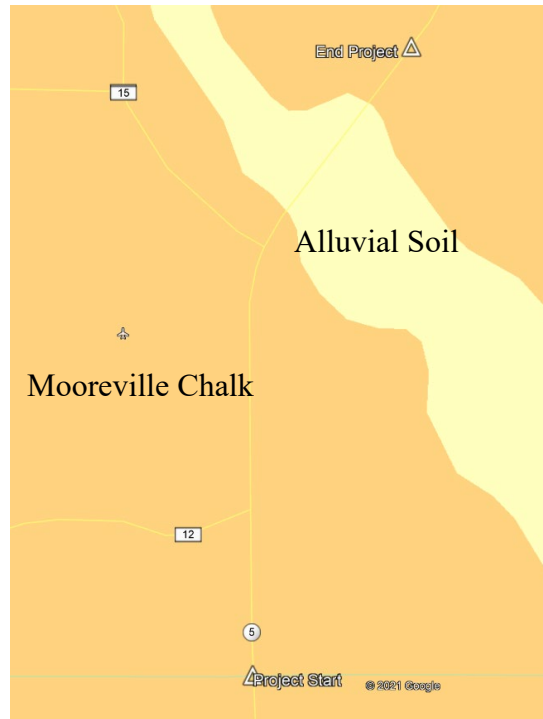


Figure 46: Google Map of Alabama Highway 5 (Google Earth 2014) overlaid with USGS Soil Survey Map (Szabo et al. 1988)

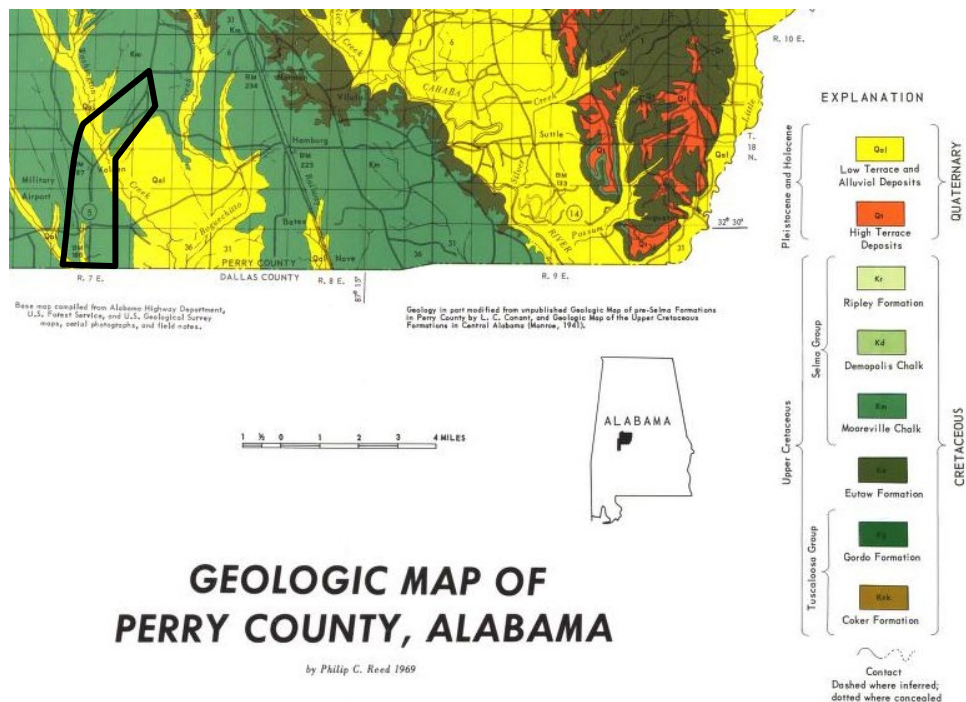


Figure 47: Geologic Map of Perry County, AL. Study Area Outlined (Reed 1969)

The United States Department of Agriculture (USDA) conducted a soil survey for Perry County in 1998 that included the research site. The general soil map from the survey is included as Figure 48. A box is shown around the study area. As seen below, the general soil type for the study area is Vaiden-Okolona-Sucarnoochee. These soils are described as somewhat poorly drained brown to olive to gray clays. The parent material of these soils is typically the underlying chalk, although some areas contain clayey alluvium (Harris 1998).

Detailed soil maps were also provided with the soil survey. According to these maps, the predominate soil types were Okolona Silty Clay Loam and Vaiden Clay with smaller sections of Kipling Clay Loam and Sucarnoochee Clay toward the northern end of the project (Test Sections 6-7). These soils are all fairly similar and exhibit moderate to very high swell potential (Harris 1998). Relevant soil properties are shown in Table 7.

Table 7: Soil Properties from USDA Soil Survey (after Harris 1998)

Type	Depth (in)	USCS Classification	% Passing 200	LL	PI	Permeability (in/hr)	Shrink-Swell potential
Okolona Silty Clay Loam	0-6	CL, CH	85-98	46-55	25-32	<0.06	High
	6-60	CH, MH	90-98	60-90	29-65	<0.06	Very High
Vaiden Clay	0-5	MH, CH	90-100	50-60	20-30	0.06-0.2	High
	5-21	CH, MH	85-100	50-90	30-50	<0.06	Very High
	21-60	CH	85-100	50-90	30-52	<0.06	Very High
Kipling Clay Loam	0-5	CL	85-95	30-45	15-25	0.06-0.2	Moderate
	5-65	CH, CL	85-95	38-70	22-45	0.06-0.2	High
	65-80	CH, CL	75-95	48-80	26-50	<0.06	Very High
Sucarnoochee Clay	0-16	CL, CH, MH	85-95	40-65	15-35	0.06-0.2	High
	16-54	MH, CH, CL	85-98	45-70	20-40	<0.06	High
	54-60	CH, MH	85-98	50-80	25-45	<0.06	High

**GENERAL SOIL MAP
PERRY COUNTY, ALABAMA**

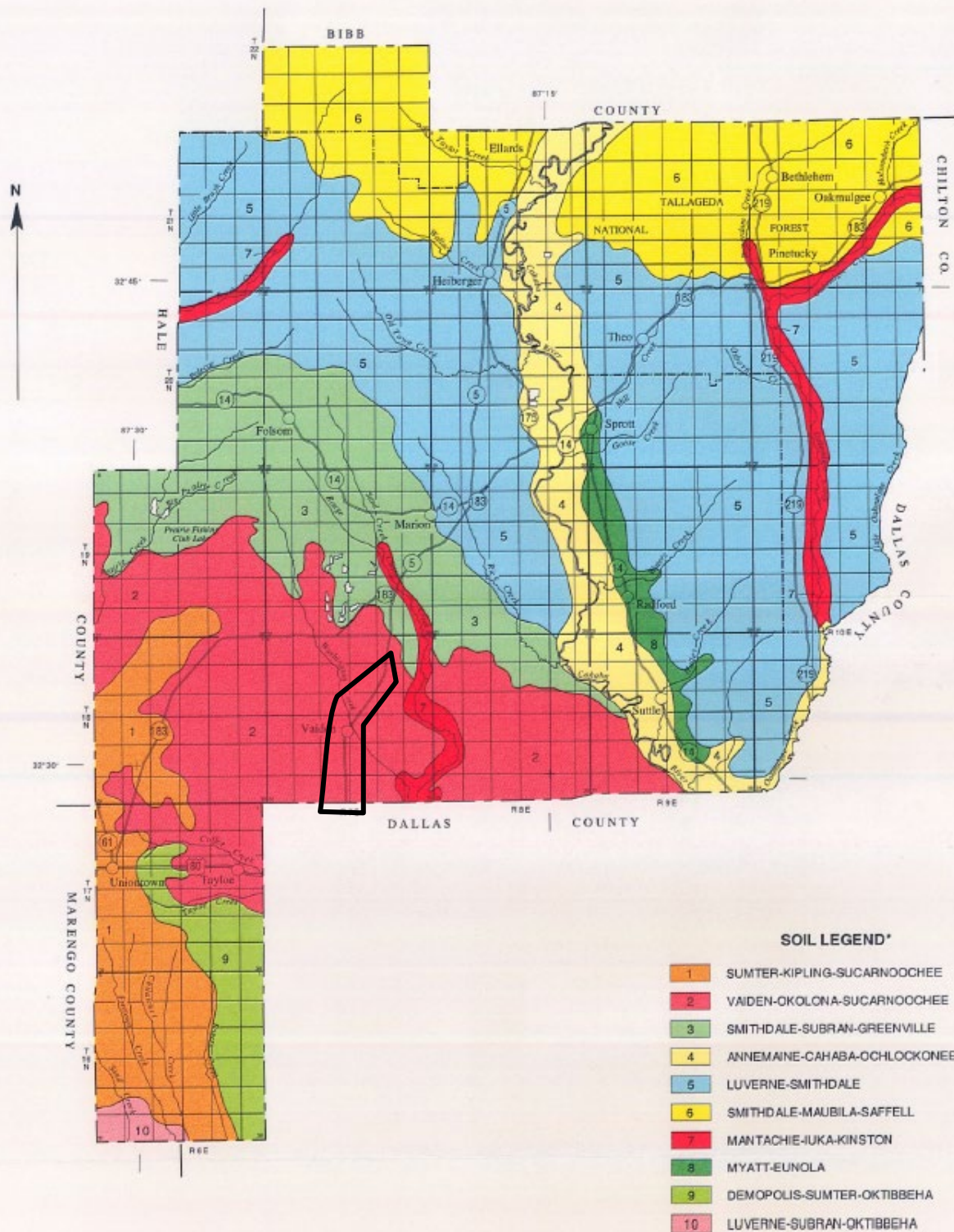


Figure 48: USDA Soil Survey General Soil Map (Harris 1998)

4.2 Soil Sample Collection and Subsurface Investigation

A subsurface investigation was performed in November 2013 and included seventeen soil test borings in the roadway. Sampling locations were spaced at approximately 0.25 mile intervals. Additional sample collections were performed in April 2015 and May 2016. The borings were performed using a CME 55 truck mounted drill rig with solid stem augers and an automatic hammer. Soils were sampled using thin-wall Shelby tube samplers and two-inch outer diameter split barrel (SPT) samplers. The soils were continuously sampled using the thin-walled tubes until the soils were sufficiently stiff to refuse further sampling by this method. A single standard penetration test was then performed, and a split barrel sample collected. Boring depths varied based on the ability to obtain undisturbed samples. Auger refusal was not encountered at any of the boring locations. Boring locations, shown in Figure 49, were approximately one quarter of a mile apart, based on GPS. Elevation information was determined using Google Earth and should be considered approximate. The drilling and sampling operations revealed 6-15 ft layers of stiff brown, gray, and blue clays underlain by soft chalk concretions. The boring logs generally showed good agreement with the soil types and profiles described in the Perry County USDA report (Harris 1998). A sample boring log is shown in Figure 50 for a borehole drilled near MP 53. Figure 51 gives a picture of several types of clay obtained from the various samples. The clay water contents ranged from moist to saturated. Boring logs with descriptions of the materials encountered are provided in Appendix A. Field testing was performed in general accordance with ASTM standards or generally accepted methods.

General geotechnical laboratory tests were performed on specimens gleaned from the thin-walled tube samples. Atterberg limits were determined for all samples. Fines fraction, in situ moisture content, dry unit weight, and specific gravity were measured for selected specimens. Table 8 through Table 10 summarize the laboratory tests.



Figure 49: Google Map of Alabama Highway 5 (Google Earth 2014) overlaid with USGS Soil Survey Map (Szabo et al. 1988)

DEPTH (ft)	SAMPLE TYPE NUMBER	RECOVERY %	BLOW COUNTS (N VALUE)	GRAPHIC LOG	MATERIAL DESCRIPTION
0					Dry Asphalt
					1.5 189.5
	SH 2.5A	100			Moist, stiff Gray Clay
5	SH 2.5B	75			
	SH 2.5C	40			5.3 185.7
	SH 2.5D	100			Moist, stiff Tan Clay
10					9.9 181.1
	SPT 2.5E	100	9-12-14 (26)		Dry, very stiff Tan Chalk
					11.0 180.0

Figure 50: Boring Log Near Mile Marker 53 on AL 5



Figure 51: Various Clays Encountered During AL 5 Sampling Operations

Table 8: Soil Properties from Laboratory Tests on Field Specimens B1A – B7A


<div style="display: flex; justify-content: space-between; align-items: center;"> <div style="text-align: center;">  <p>AUBURN UNIVERSITY</p> </div> <div> <p>SUMMARY OF LABORATORY RESULTS</p> <p>PAGE 1 OF 2</p> </div> </div>										
CLIENT Auburn University					PROJECT NAME AL-5 Research Project					
PROJECT NUMBER 99-305-635-005-401					PROJECT LOCATION AL 5, Perry County					
Borehole	Depth	Liquid Limit	Plastic Limit	Plasticity Index	Max. Sieve Size Tested (mm)	%<#200 Sieve	Classification	Water Content (%)	Dry Density (pcf)	Specific Gravity
B-1A	1.5	70	24	46						
B-1A	3.5	88	30	58						
B-1A	5.5	110	27	83						
B-1A	7.5	79	29	50						
B-1A	9.5	103	29	74						
B-1.5A	1.5	97	29	68						
B-1.5A	3.5	66	24	42	0.075	98	A-7-6 (47)	37.0	84.0	2.75
B-1.5A	7.5	91	25	66						
B-1.5A	9.5	85	24	61	0.075	98	A-7-6 (69)	32.9	87.5	2.62
B-2A	3.0	83	31	52						
B-2A	5.0	73	25	48						
B-2A	7.0	86	27	59						
B-2A	9.0	95	27	68						
B-2.5A	1.5	70	24	46						
B-2.5A	3.5	84	26	58	0.075	93	A-7-6 (62)	31.9	90.1	2.75
B-2.5A	5.5	79	32	47						
B-2.5A	7.5				0.075	98		29.2	92.4	2.72
B-3A	1.5	93	26	67						
B-3A	3.5	65	24	41						
B-3A	7.5	74	25	49						
B-3.5A	1.3	68	28	40	0.075	99	A-7-6 (47)	38.6	82.5	2.70
B-3.5A	3.3	87	28	59						
B-3.5A	5.3	84	27	57						
B-3.5A	7.3				0.075	97		41.5	77.7	2.74
B-4A	1.8	72	25	47						
B-4A	5.8	93	23	70						
B-4.5A	1.2	68	28	40	0.075	97	A-7-6 (46)	38.8	81.5	2.72
B-4.5A	5.2	97	28	69						
B-4.5A	7.2				0.075	96		33.3	84.4	2.73
B-5A	1.5	50	24	26						
B-5A	7.5	91	23	68						
B-5.5A	1.0	86	26	60	0.075	96	A-7-6 (67)	39.6	81.0	2.75
B-5.5A	7.0	88	27	61	0.075	96	A-7-6 (68)	33.3	87.7	2.70
B-Tree C	3.0				0.075	94		39.6	79.3	
B-Tree C	7.0				0.075	94		32.2	89.8	
B-6A	1.5	97	24	73						
B-6A	7.5	80	30	50						
B-6.5A	1.5									2.69
B-6.5A	3.5	71	24	47	0.075	60	A-7-6 (26)	28.2	90.2	
B-6.5A	5.5	57	18	39						
B-6.5A	7.5	50	15	35						
B-6.5A	8.8				0.075	45				
B-7A	3.5	57	17	40						

Table 9: Soil Properties from Laboratory Tests on Field Specimens B7A – B8.5A


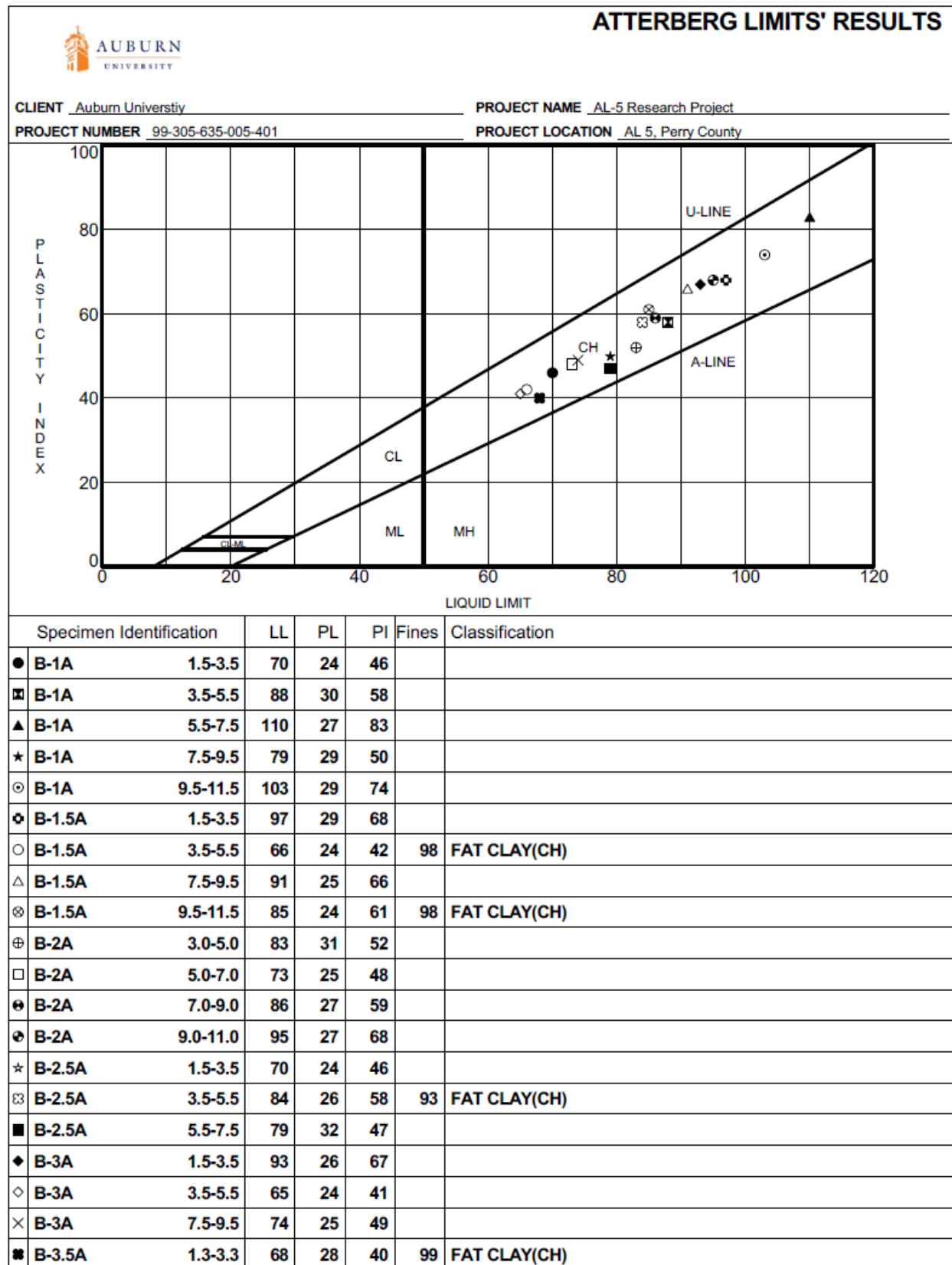
<div>  <div> SUMMARY OF LABORATORY RESULTS PAGE 2 OF 2 </div> </div>											
CLIENT <u>Auburn University</u>						PROJECT NAME <u>AL-5 Research Project</u>					
PROJECT NUMBER <u>99-305-635-005-401</u>						PROJECT LOCATION <u>AL 5, Perry County</u>					
Borehole	Depth	Liquid Limit	Plastic Limit	Plasticity Index	Max. Sieve Size Tested (mm)	%<#200 Sieve	Classification	Water Content (%)	Dry Density (pcf)	Specific Gravity	Swell Pressure
B-7A	5.5	58	20	38							
B-7A	7.5	63	21	42							
B-7.5A	5.0	67	18	49	0.075	81	A-7-6 (41)	29.2	93.9	2.72	
B-7.5A	7.0	60	18	42	0.075	78	A-7-6 (33)	27.8	95.4	2.81	
B-8A	5.0	64	16	48							
B-8A	7.0	50	16	34							
B-8.5A	1.0				0.075	90					
B-8.5A	3.0				0.075	78					

Table 10: Summary of Atterberg Limits determined from Field Specimens



4.3 Site Observations

It is hypothesized that seasonal variation in the moisture demand of large trees growing within a zone of influence of the roadway has a detrimental effect on the expansive subgrade, causing localized pavement distress. It has also been observed by the authors, qualitatively, that areas with the greatest pavement distress generally correspond to areas with large or numerous deciduous trees. To identify and track these trends over time, a survey of the trees greater than 6 inches in diameter within 60 ± 10 feet of the roadway was performed throughout the project. For each tree greater than six inches, its position longitudinally along the roadway and laterally from the edge of pavement was recorded, along with species and trunk diameter. If a tree naturally divided into a cluster of trunks sharing a single root system, it was identified and located as a single cluster, but the diameter of each off-shoot trunk was measured individually.

To qualitatively correlate the impacts of the trees on the roadway, additional qualitative observations were made regarding pavement damage and photographs taken along the length of the roadway. These observations were combined with the tree survey in a site map. As the project progresses through and beyond the construction phase, previous areas of pavement distress can be located on the map, along with areas with potentially significant damage due to trees can be identified.

During the survey, twenty-eight different species of trees were identified according to their common and scientific names. Biddle's classification of trees based on water demand indicates that trees from the genus *Quercus* – the oak trees – and *Ulmus* – the elm trees – have some of the highest water demand, and largest root systems (Biddle 2001).

4.3.1 Traffic

According to the ALDOT materials report dated February 3, 2014, the 2014 AADT was 1,410 vehicles per day with 36% truck traffic and the projected AADT for 2034 is 2,200 vehicles per day (ALDOT 2014). Equivalent Single Axle Load (ESAL) values are calculated to be 2.35×10^6 (ALDOT 2014). From the start of project to the end of project, the only intersections with AL 5 are local and county roads. There are no major routes intersecting with AL 5, that would contribute to, or detract from daily traffic volumes. For this reason, it is assumed that AADT for AL 5 is constant from start to end of project. The traffic volumes and percentage of truck traffic was visually corroborated during field work. Traffic is a primary factor in pavement deterioration along AL 5.

4.3.2 Site Observations by Damage Type

During the reconnaissance phase of the project, general information regarding the condition of the site pre-construction was collected and photographed. Several damage trends were observed at the time:

1. The severity of damage appeared to increase when deciduous trees were present.
2. Longitudinal cracking and rutting was common in areas with deciduous trees.
3. The severity of damage appeared to be unaffected by the presence of coniferous trees.
4. From the start of project, MP 50.85, to approximately MP 52.82, differential heave was observed in the roadway.
5. Various slopes throughout the project appeared to be in distress.
6. Superficial pavement damage was observed throughout the project without any apparent pattern or trend.

The following figures are used to illustrate these common observations throughout the project site.

4.3.2.1 Heave

The first 2.4 miles of the project is generally characterized by heave. For the purposes of this investigation differential heave is a general term used to describe sections of roadway that may experience different amounts of heave (or subsidence) do to varying swell potentials or availability of water. As a result, motorists may experience a rolling (over long sections) or bumpy (over short sections) ride. Figure 52 illustrates this concept as observed by the authors.

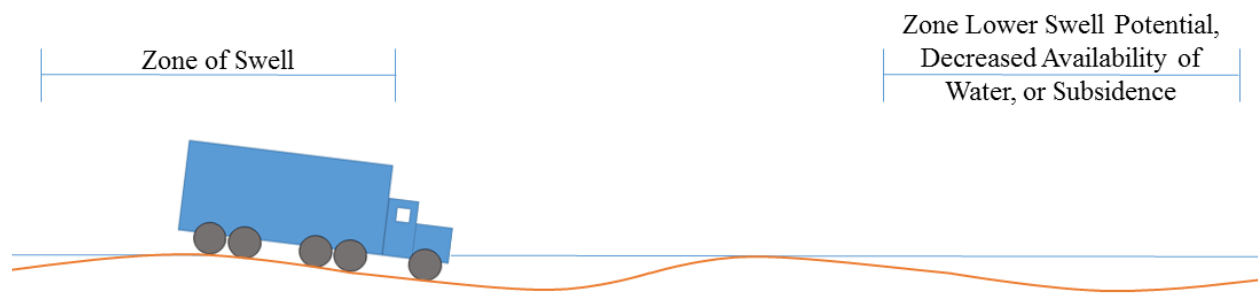


Figure 52: Illustration of Differential Heave (Not to Scale)

Figure 53 is a Google Earth image of the highway and surroundings from Boring B1.0, MP 50.85, to boring B5.0, MP52.85. The area of interest stops just short of the large deciduous trees in the image, approximately MP 50.75. It is suggested that the moisture fluctuation in this zone is significantly less varied than the rest of the project for several reasons.



Figure 53: Google Earth Image of AL 5 from Borings B1.0 to B5.0 (after Google Earth 2014)

In areas with irrigated fields and no trees, the moisture fluctuation of the soil is purely controlled by the climate and irrigation patterns of the farmers. Figure 45 shows the 30-year normal precipitation and weather patterns for Selma, AL. As indicated in the figure, April through October is the hottest and driest period for the region. Conversely, November through March precipitation increases while temperatures decrease for the region. Because the dry period is concurrent with the agricultural growth season, sections of the highway with irrigated fields should maintain the relatively constant water contents year-round. During the dry season, soil water lost by evaporation

will be replenished by irrigation and during the remaining six months, precipitation. Based on these climate and irrigation patterns it is suggested that the expansive clays will remain in a state of swell with limited shrinkage as compared to other locations onsite. Figure 54 and Figure 55 depict a section of AL 5 near boring B3.0 with irrigated fields and no trees on both sides of the roadway. Please note the lack of longitudinal cracking and rutting. Pavement damage in this section, and areas like it, was limited to superficial pavement damage and differential heave. The differential heave is due to the expansive clays swelling vertically different amounts due to varying swell potential or availability of water. The lack of longitudinal (shrinkage) cracks, can be attributed to the relatively constant water contents year round. The longitudinal (shrinkage) cracks develop due to positive and negative flexural bending forces applied to the pavement by cyclical shrinking and swelling. The cracks will form at the active zone boundary as indicated by Zornberg and Gupta (2009) in Figure 21.



Figure 54: AL 5 Facing South of Boring B3.0 MP 51.85 (Photo Taken 06/15/15)



Figure 55: AL 5 Facing North of CR 12 Intersection MP 51.82 (Photo Taken 06/15/15)

Like irrigation, the large fish ponds, located on the east side of AL 5 from boring B2.0 to B2.5, is likely to stabilize the water content of subgrade soils underneath the highway. The constant, but slow, infiltration of water from the fish ponds has the potential to partially offset evaporation rates during the dry months so that the subgrade maintains a relatively constant state of swell year round.

4.3.2.2 Longitudinal Cracking Associated with Trees

Based on visual observation during the reconnaissance phase, it appears that pine trees and trees of any type located 60 feet or more off the roadway have little to no impact on pavement damage. As indicated in Figure 19, trees belonging to the genus *Pinus*, including loblolly pines, have among the lowest moisture demand of those classified. Pine trees are also expected to have one of the smallest diameter root spread of those classified (Biddle 2001). In the case of deciduous trees, precise and reliable predictors of root spread based on canopy or trunk diameter are unavailable. However, several correlations exist and should be applied with caution when precise, accurate information is required. For the purposes of this discussion an empirical correlation will be sufficient. A ratio of root radius to trunk diameter of 38:1 has been suggested by S. Day (Day and Wiseman 2009). A six-inch diameter tree may have a root mat of 19 feet diameter and a zone of influence, to draw soil water, an unknown distance beyond 19 feet. A 14-inch diameter tree may have a root mat of 44 feet diameter and a large zone of influence. Based on the results from the

tree survey, which will be presented later in this chapter, trees 6-inches or greater in diameter were documented as close as 16 to 38 feet from the edge of pavement (EOP). On average, trees 6-inches or greater in diameter were located between 40.1 and 54.1 from the edge of pavement. Therefore, it is feasible that trees 60 feet or less could influence soils at the edge of or underneath the pavement.

Beyond 60 feet, a tree would have to be greater than 19 inches in diameter to reach the EOP. While this is possible, it is more likely that pavement damage would be driven by factors other than trees more than 60 feet from EOP, such as irrigation, trees closer to the EOP competing for moisture, climate, and variable shear strength due to moisture fluctuation.

Starting at MP 52.82, in the area of boring B5.0 on the west side of the southbound lane, a stretch of large deciduous trees runs along the Right of Way (ROW) for approximately 320 feet. The author observed longitudinal shrinkage cracks, distressed or failing slopes, and rutting in this portion of the southbound lane. Figure 56 shows the location of boring B5.0 and the surrounding area. This line of trees predominately consists of Sugarberry Trees, a member of the Elm Family, which has high water demands and large root mats (Biddle 2001).



Figure 56: Google Earth Image of AL 5 near Boring B5.0 (Google Earth 2014)

Table 11 presents descriptive statistics on the trees surveyed near Boring B5.0. The average Sugarberry surveyed has a trunk diameter of 10.2 inches. According to the previously discussed empirical correlation, the root mat may be as much as 32.3 feet in diameter on average. Trees surveyed in the section of the roadway, measured as close as 30.9 feet to EOP and averaged 40.2 feet from EOP. As a result, it is possible that root systems of some trees extend directly beneath the pavement, and probable that the zone of influence of many trees extend directly beneath the pavement.

Table 11: Descriptive Statistics on Trees Surveyed near Boring B5.0

Tree Type	Count of Trees per Type	Min of Trunk Diameter (inches)	Average of Trunk Diameter (inches)	Max of Trunk Diameter (inches)
Eastern Red Cedar	1	8.0	8.0	8.0
Sugarberry	65	6.1	10.2	26.7
White Ash	9	7.6	11.6	17.2
Willow Oak	1	41.1	41.1	41.1
	76	6.1	10.8	41.1

The largest tree surveyed at this location was a 41.1-inch diameter willow oak, Figure 57. Oak trees have among the highest water demand and largest root systems (Biddle 2001). The willow oak was located 64.7 feet off the edge of pavement, but due to its large diameter may still be able to influence water contents under the pavement.

Shrinkage (longitudinal) cracking develops at the moisture fluctuation boundary of an expansive clay subgrade. Figure 58 is an elevation view of the factors driving observed damage. The longitudinal (shrinkage) cracks develop due to positive and negative flexural bending forces applied to the pavement by cyclical shrinking and swelling. The cracks will form at the active zone boundary as indicated by Zornberg and Gupta (2009) in Figure 21. The center section of pavement stays at relatively constant water content as compared with the outer pavement sections and shoulders because of the impermeable nature of the asphalt above it. The amount of pavement subgrade that remains at a stable water content will depend heavily on the soils matric suction, negative pressure capable of drawing water, and the hydraulic conductivity of the soil. The outer sections of pavement and shoulders will gain water through precipitation and lose water through



Figure 57: Willow Oak, Diameter 41.1 inches (Photo Taken 09/13/16)

evapotranspiration. With the addition and loss of water the fine grained soils will undergo volumetric change according to the net normal pressure and matric suction.

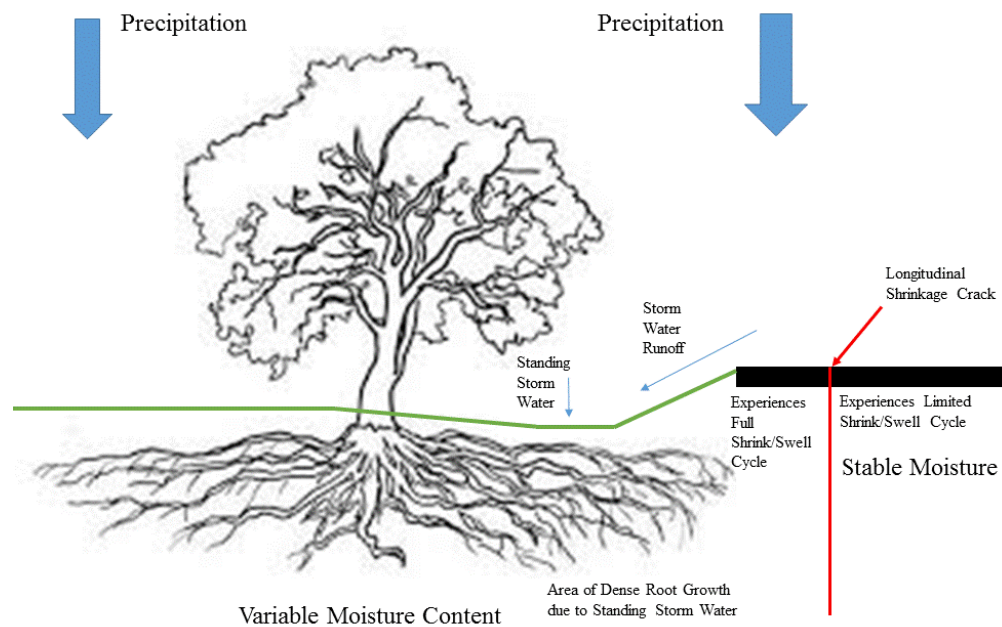


Figure 58: Driving Factors behind Pavement/Slope Damage near Boring B5.0 MP 52.85

This relationship has been described graphically in Figure 15, as the matric suction and net normal stress increase, the volumetric change of the solid and water phases will decrease. Figure 59 depicts the longitudinal shrinkage crack (Zornberg and Gupta 2009), failing shoulder slope, and ditch near boring location B5.0. The basin of the ditch was very moist at the time the photograph was taken due to recent rainfall.



Figure 59: Longitudinal Crack due to Shrink Swell near Boring 5.0 MP 52.85 (Photo Taken 06/02/15)

4.3.2.3 Slope Distress and Potential Failure

Slope distress and potential failures occurring at this and other locations on site. Based on the triaxial results presented by Al-Mhaidib et al. (2006), Table 4, it can be concluded that as the expansive soils swell and matric suction decreases the shear strength will also decrease. The variability of water content and volumetric change in the shoulder lead to a variability of shear strength. When the soils have high water contents and low shear strengths, slope failures are more likely to occur. If the soils subsequently dry, the slope failure may temporarily cease until another wet period. In Figure 59, numerous ruts from mowers are visible. The operation of heavy equipment during periods of high moisture will accelerate the slope failure process and exacerbate/create superficial surface failures. The observed slope stability issues on site provide evidence for low shear strength of subgrade soils.

4.3.2.4 Standing Water

Standing water was observed in the ditches along the right of way on many occasions throughout 2015 and 2016. Figure 60 and Figure 61 depict two such areas observed in April 2015 and July 2015. The presence of standing water off the shoulders of the roadway provides a reservoir for desiccated soils to draw water from. Recharging of the shoulder slope lead to reduction of shear strength and potential slope failure. Most of the site has at least a 4:1 slope on either side of the roadway, allowing storm water to pool in the low lying areas. The presence of standing water alongside the roadway also promotes root growth in the direction of the roadway itself, and tree roots will grow in the direction of water sources and produce the densest root system at these locations Biddle (2001).



Figure 60: Standing Water Observed in Ditch (Photo Taken 4/14/2015)



Figure 61: Standing Water Observed between Borings 1.0 and 1.5 (Photo Taken 7/10/15)

4.3.2.5 Pavement Rutting

Pavement rutting was observed at many locations throughout the site. At MP 52.85, $1\frac{3}{8}$ inches of rutting was observed between EOP and the longitudinal shrinkage crack. Pavement rutting results from permanent vertical strain in the asphalt and subgrade layer over a period of many load repetitions. Deformations occurring within the asphalt may be due to problems with the mix design or compaction during placement. Subgrade rutting occurs as the subgrade soils below each wheel path are consolidated by repeated traffic loads. As the subgrade begins to deform the asphalt layers mirror the deformations so that the ruts translate to the pavement surface. Rutting in the asphalt layers can be repaired by milling and overlaying the surface but subgrade rutting indicates much deeper problems. As shown in the boring logs, AL 5 pavements were built directly on top of expansive clays. In a few locations it appeared that a fat clay/sand mixture may have been placed as a base course. The boring logs in the appendix show specific locations. The increase in sand can potentially reduce the swell potential of soils and increase the shear strength of that layer. However, the majority of the site lacks the sand/clay mixture. It has been established that as expansive soils saturate they lose shear strength. The increase in water content and loss of shear strength will promote subgrade rutting.

Figure 62 through Figure 64, depict two different locations with sufficiently deep ruts to cause safety hazards on site.



Figure 62: Observed Rutting Near Boring 5.0 MP 52.85 (Rut Depth $1\frac{3}{8}$ inch) (Photo Taken 09/13/16)



Figure 63: Observed Rutting and Longitudinal Cracking (Photo Taken 09/14/16)



Figure 64: Observed Rutting (Photo Taken 09/14/16)

4.3.3 Site Observations by Location

Before construction, detailed site reconnaissance was performed of the entire roadway. Notes were taken on pavement damage, slope stability issues, the general surroundings, and locations. The following information is a summary of those observations according to location. Photographs have been included when available.

4.3.3.1 Location: Start of Project MP 50.802 to CR12 Intersection at MP 51.82

Observations:

- Roadway leveling occurred sometime between November 2013 and June 2014 before the start of project.

Detailed site reconnaissance was not performed before the leveling

- Figure 65 and Figure 66 depict the roadway pre-leveling

Photographs:

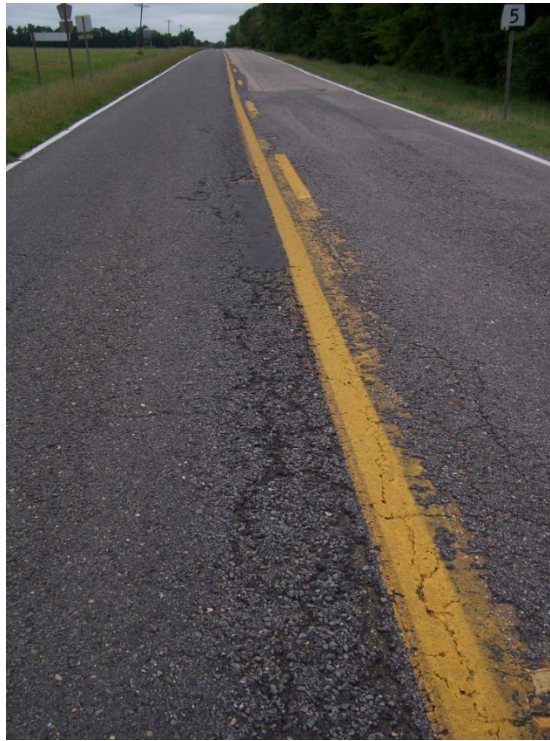


Figure 65: AL 5 Facing South MP 51.81 (Photo Taken 11/18/13)



Figure 66: AL 5 Facing South MP 51.53 Pre-leveling (Photo Taken 11/18/2013)

4.3.3.2 Location: MP 50.82 to Start of Project at MP 50.802 (Post Leveling July 2015)

Observations:

- Distressed shoulder slopes with lateral spreading at toe of slope
- Observed rutting and subsidence of pavement
- Northbound lane mild rutting of inside wheel path and raveling

4.3.3.3 Location: MP 50.82 (Post Leveling July 2015)

Observations:

- Observed fatigue cracking and rutting
- Observed severe shoulder subsidence

4.3.3.4 Location: MP 50.84 to MP 50.88 (Post Leveling July 2015)

Observations:

- Observed cracking at pavement edges
- Observed shoulder subsidence
- Northbound lane mild rutting of inside wheel path and raveling

4.3.3.5 Location: MP 50.93 (Post Leveling July 2015)

Observations:

- Standing water in ditches
- Fatigue cracking at pavement edges
- Toe of slope removed for culvert

4.3.3.6 Location: MP 50.88 to MP 50.97 (Post Leveling July 2015)

Observations:

- Observed sporadic transverse cracking
- Observed open centerline longitudinal crack
- Subsidence in southbound lane outside wheel path
- Large black willow located 28 feet off EOP with dripline 13 feet off EOP
- Northbound lane mild rutting of inside wheel path and raveling

4.3.3.7 Location: MP 50.97 to MP 51.00 (Post Leveling July 2015)

Observations:

- Observed cracking with shoulder subsidence extending to middle of southbound lane

4.3.3.8 Location: MP 51.00 to 51.03 (Post Leveling July 2015)

Observations:

- Observed cracking with shoulder subsidence
- Steep shoulder slopes
- Asphalt patch post-leveling and ongoing raveling at MP 51.00

4.3.3.9 Location: MP 51.12 to MP 51.18 (Post Leveling July 2015)

Observations:

- Observed cracking with shoulder subsidence
- Pine trees located beyond right of way
- Flat shoulder slopes

4.3.3.10 Location MP 51.18 to MP 51.21 (Post Leveling July 2015)

Observations (Southbound Lane):

- Observed cracking and shoulder subsidence at pavement edge
- Rutting in both wheel paths
- Steep shoulder slopes
- Distressed slope at MP 51.99
- Pine trees located beyond right of way

Observations (Northbound Lane):

- Damage not observed, may be obscured by previous leveling
- Shallow shoulder slopes
- Pine trees located beyond right of way

4.3.3.11 Location: CR 12 Intersection MP 51.82 to Start of Deciduous Trees at MP 52.82

Observations:

- Figure 67 through Figure 70

- Asphalt Raveling with pieces of surface layer removed, Figure 69 and Figure 70
- Rutting and longitudinal cracking not observed
- Standing water in ditches
- Ponded water at 4x4 double barrel culvert with algae growth

Photographs:



Figure 67: AL 5 Facing South of Boring B3.0 MP 51.85 (Photo Taken 06/16/15)



Figure 68: AL 5 Facing North of Boring B3.0 MP 51.85 (Photo Taken 06/16/15)



Figure 69: AL 5 Facing South of MP 51.915 (Photo Taken 06/16/15)



Figure 70: AL 5 Facing South of MP 51.915 (Photo Taken 11/18/2013)

4.3.3.12 Location: MP 51.915 to MP 52.055

Observations (Southbound Lane):

- Large deciduous trees present beyond right of way, Figure 71
- Observed Longitudinal Shrinkage Crack, Figure 72
- Observed Rutting and subsidence of pavement section, Figure 71 and Figure 73

Observations (Northbound Lane):

- Irrigated fields planted in row crops beyond right of way, Figure 71
- Observed significant lateral and longitudinal cracking but not a clearly defined longitudinal shrinkage crack

Photographs:



Figure 71: AL 5 Facing North MP 51.915 (Photo Taken 06/16/15)



Figure 72: AL 5 Facing East MP 51.915 (Photo Taken 06/16/15)



Figure 73: AL 5 Facing North MP 52 (Photo Taken 06/16/15)

4.3.3.13 Location: MP 53.11 to MP 53.28

Observations (Southbound Lane):

- Predominately pine trees with a few deciduous trees beyond right of way
- Observed rutting & cracking, Figure 77

Observations (Northbound Lane):

- Mixed deciduous and evergreen trees beyond right of way, Figure 74 and Figure 75
- Observed rutting & cracking, Figure 75 and Figure 76
- Observed slope stability problems

Photographs:



Figure 74: AL 5 Northbound Lane and Shoulder Facing South MP 53.19 (Photo Taken 06/16/15)



Figure 75: AL 5 Northbound Lane Facing South MP 53.19 (Photo Taken 06/16/15)



Figure 76: AL 5 Facing Southwest MP 53.19 (Photo Taken 06/16/15)



Figure 77: AL 5 Southbound Lane Facing North MP 53.19 (Photo Taken 06/16/15)

4.3.3.14 **Location: MP 53.28 to CR 15 Intersection at MP 53.38**

Observations (Northbound Lane):

- Mixed deciduous and evergreen trees beyond the right of way, Figure 78
- Observed rutting and pavement subsidence, Figure 78
- Observed longitudinal shrinkage cracking, Figure 78
- Observed slope stability problems
- A 4x4 single barrel culvert located at creek bed, Figure 79
- Slope subsidence toward creek bed, Figure 79

Observations (Southbound Lane):

- Marsh with standing water and cattail reeds beyond the right of way, Figure 78
- Community center located at the intersection of CR 15 and AL 5, Figure 78
- Southbound lane was previously patched obscuring any pavement observations

Photographs:



Figure 78: AL 5 Northbound Lane Facing South MP 53.38 (Photo Taken 06/16/15)



Figure 79: Northbound Lane Shoulder and Culvert MP 53.30 (Photo Taken 06/16/15)

4.3.3.15 **Location: MP 53.52**

Observations:

- Localized pavement damage, raveling at edge of pavement, Figure 80
- Pavement leveled both lanes obscuring pavement damage observations, Figure 80
- Mixed deciduous and evergreen trees beyond right of way on both sides of roadway
- Observed grass growing through cracks at pavement edge, Figure 80
- Shallow shoulder slopes
- Desiccated soils with tension cracking in shoulders

Photograph:



Figure 80: AL 5 Facing South MP 53.52 (Photo Taken 06/16/15)

4.3.3.16 **Location: Approaches to Bridge at MP 53.68**

Observations (Northbound Approach):

- Approaches to bridge leveled both lanes obscuring pavement damage observations
- Steep shoulder slopes

Observations (Southbound Approach):

- Localized pavement raveling at discreet locations with patching, Figure 81 and Figure 82
- No rutting or cracking observed
- Steep shoulder slopes, Figure 82

Photographs:



Figure 81: AL 5 Southbound Approach to Bridge Facing South (Photo Taken 06/16/15)



Figure 82: AL 5 Southbound Approach to Bridge Facing North (Photo Taken 06/16/15)

4.3.3.17 **Location: MP 54.22**

Observations:

- Four large willow oak trees observed beyond right of way with dripline extending across centerline of roadway, Figure 83
- Leveled both lanes obscuring pavement damage observations, Figure 83

Photograph:



Figure 83: AL 5 Facing North MP 54.22 (Photo Taken 06/16/15)

4.3.3.18 Location: MP 54.35 to End of Project MP 54.85

Observations:

- Observed mild rutting, fatigue cracking and longitudinal shrinkage cracking, Figure 84 and Figure 85
- Patching at various locations, Figure 85
- Mixed deciduous and evergreen trees beyond the right of way, Figure 85 through Figure 87

Photographs:



Figure 84: AL 5 Facing South East MP 54.59 (Photo Taken 06/16/15)



Figure 85: AL 5 Facing North MP 54.21 (Photo Taken 06/16/15)



Figure 86: AL 5 Facing North MP 54.58 (Photo Taken 06/16/15)



Figure 87: AL 5 Facing South MP 54.58 (Photo Taken 06/16/15)

4.3.4 Tree Survey

A tree survey was performed from CR 15 to the end of project to determine the type, size and location of large trees relative to the edge of pavement. For the purposes of the survey, a large tree is defined as one with a diameter six inches or greater. Table 12 summarizes the size and frequency of common trees surveyed by their common name. Only the most frequently occurring or mostly potentially damaging trees have been included in the summary. A comprehensive list has been included in the Appendices. According to Biddle (2001), trees belonging to the oak family have the highest water demand of those listed, with the elm family having the next highest. Please note that Sugarberry trees are a member of the Elm family and the second most frequently occurring tree onsite. The most common tree onsite belong to the Pine family. Pine trees and cedar

trees will have among the lowest water demand and potentially damaging effects. Because pine and cedar trees do not lose their leaves and go dormant in the winter time their demand for water remains relatively constant throughout the year. Even low water demand deciduous trees, such as the Sweet Gum, lose their leaves in the winter and reduce their active root zone during dormancy. This encourages soil swelling during the wet winter months and soil shrinkage during the dry summer months when the leaves and root system regrows.

Table 12: Summary of Common Trees Surveyed and Size

Tree Common Name	Count of Trunk Diameters > 6 inches (inches)	Average of Trunk Diameter (inches)	Max of Trunk Diameter (inches)
American Elm	52	12.6	32.0
Black Willow	3	11.7	20.0
Eastern Red Cedar	123	10.2	27.0
Green Ash	93	10.0	27.0
Laurel Oak	51	12.0	40.0
Loblolly Pine	538	10.8	36.0
Pecan Tree	31	12.9	42.0
Post Oak	6	14.2	18.0
Red Oak	30	15.6	32.0
Slippery Elm	130	9.1	24.0
Sugarberry	406	10.2	27.0
Sweet Gum	106	8.4	18.0
Water Oak	108	12.2	52.0
White Ash	119	9.3	24.0
White Oak	8	10.9	22.0
Willow Oak	100	14.6	54.0
Winged Elm	33	8.7	15.0
	1937	10.7	54.0

During the course of the tree survey and soil sampling, tree roots were encountered growing toward the roadway as shown in Figure 88 through Figure 90.



Figure 88: Tree Roots Observed During Installation of Sensors (Photo Taken 06/28/16)

Figure 89 depicts a 4-inch diameter structural root approximately 15 feet from the roadway that was uncovered during silt fence installation. Structural roots provide a foundation for the tree and anchor it in the ground against heavy winds and rain. While the structural roots only have limited participation in the collection and redistribution of water, a network of fine feeder roots are likely to be connected to or in the vicinity of the structural root system.



Figure 89: Tree Root (4" Diameter) Approximately 15' from Edge of Pavement

The root shown in Figure 90 was discovered in the bore hole at B4.5 during sampling. The bore hole was located in the center of the northbound lane. At this time there are not any trees near the boring location; however, its presence does indicate that it is possible for tree root systems to extend underneath the pavement. The root was approximately a half inch in diameter.



Figure 90: Tree Root Extracted from Boring Hole 4.5 (Photo Taken 5/23/16)

4.4 International Roughness Index (IRI) Surveys

The international roughness index (IRI) measures variations in a pavement surface along thin slices or profiles, Figure 91. These surface variations can produce significant vehicle vibrations and poor ride quality, safety hazards, noise, and/or drainage problems (Sayers and Karamihas 1998).

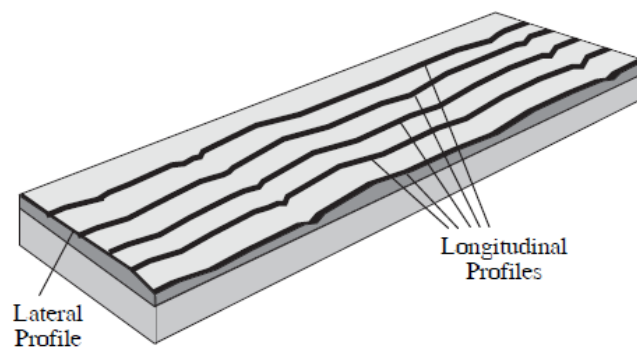


Figure 91: Pavement Profiles (Sayers and Karamihas 1998)

A pavement profile is created when elevation data is collected over a predetermined distance. For this project profile, information was collected using an inertial profiler, Figure 92, a vehicle with accelerometers and laser transducers installed for data collection. The accelerometers provide a reference elevation while the laser transducers determine the surface elevation relative to the accelerometers. The distance between each data point is then calculated from the time elapsed and speed traveled. Typically, inertial profilers develop profiles for each wheel path.

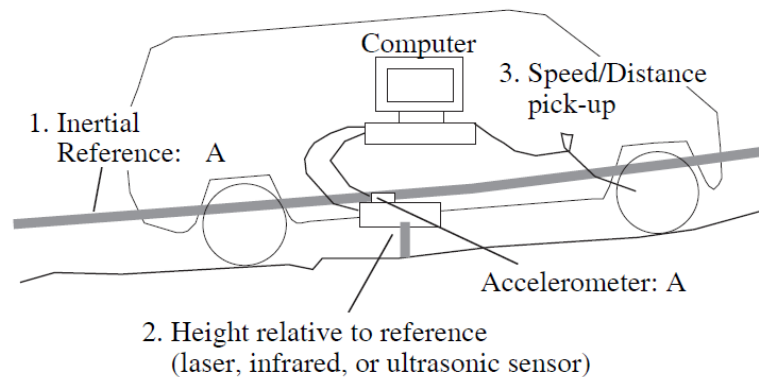


Figure 92: Inertial Profiler Schematic(Sayers and Karamihas 1998)

The National Cooperative Highway Research Program (NCHRP) developed the IRI in the 1970s as an indicator of pavement roughness, which is typically measured in units of inches per mile (Sayers and Karamihas 1998). The mathematical model is based on the “quarter car,” a reference vehicle that can convert elevation information into IRI values. According to Sayers and Karamihas (1998):

The quarter-car filter calculates the suspension deflection of a simulated mechanical system with a response similar to a passenger car. The simulation suspension motion is accumulated and divided by the distance traveled to give an index with units of slope (in/min). (Sayers and Karamihas 1998)

An IRI value can be determined over any distance. This distance is typically chosen according to project needs. For AL 5, the National Center for Asphalt Technology (NCAT) ARAN inertial profiler, determined IRIs on May 30, 2014 and November 11, 2014 to provide pre-construction baseline information. On each date four IRI profiles were developed, one per wheel path, between MP 50.8 and 54.3. Three passes along the roadway were made for each profile to

minimize error and account for variability. A single IRI value was calculated per 50-foot section of roadway, and the three passes averaged to determine the final IRI.

The Federal Highway Administration (2011) has provided IRI performance thresholds to be used in pavement evaluation, Table 13. Based on these thresholds, agencies can evaluate the resurfacing needs of many lane miles quickly and efficiently.

Table 13: FHWA IRI Thresholds (Federal Highway Administration 2011)

Category	IRI Threshold
Good	< 95
Acceptable	$95 \leq \text{IRI} \leq 170$
Not Acceptable	> 170

IRI values for AL 5 were determined using the National Center for Asphalt Technology (NCAT) ARAN inertial profiler on May 30, 2014 and November 11, 2014 to provide pre-construction baseline information. On each date four IRI profiles were developed, one per wheel path, between MP 50.8 and 54.3. Figure 93 through Figure 96 show the calculated IRI values versus distance along project where the origin corresponds to MP 50.8 for each plot. The FHWA threshold for unacceptable pavement surfaces, 170 in/mile, is also shown on the plots as a reference. Based on the IRI data, the pre-construction pavement surface is severely damaged. The majority of the surface exceeds acceptable threshold limits set by the FHWA.

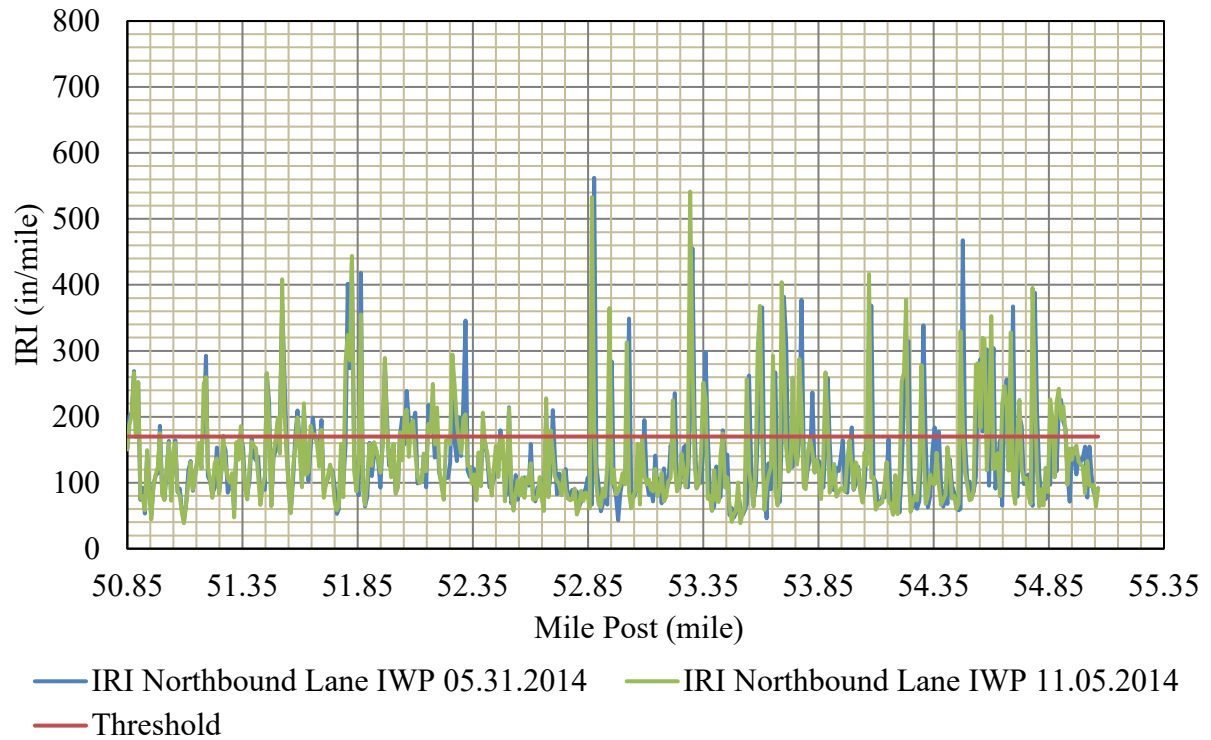


Figure 93: Northbound, Inside Wheel Path IRI Profiles for May and November 2014

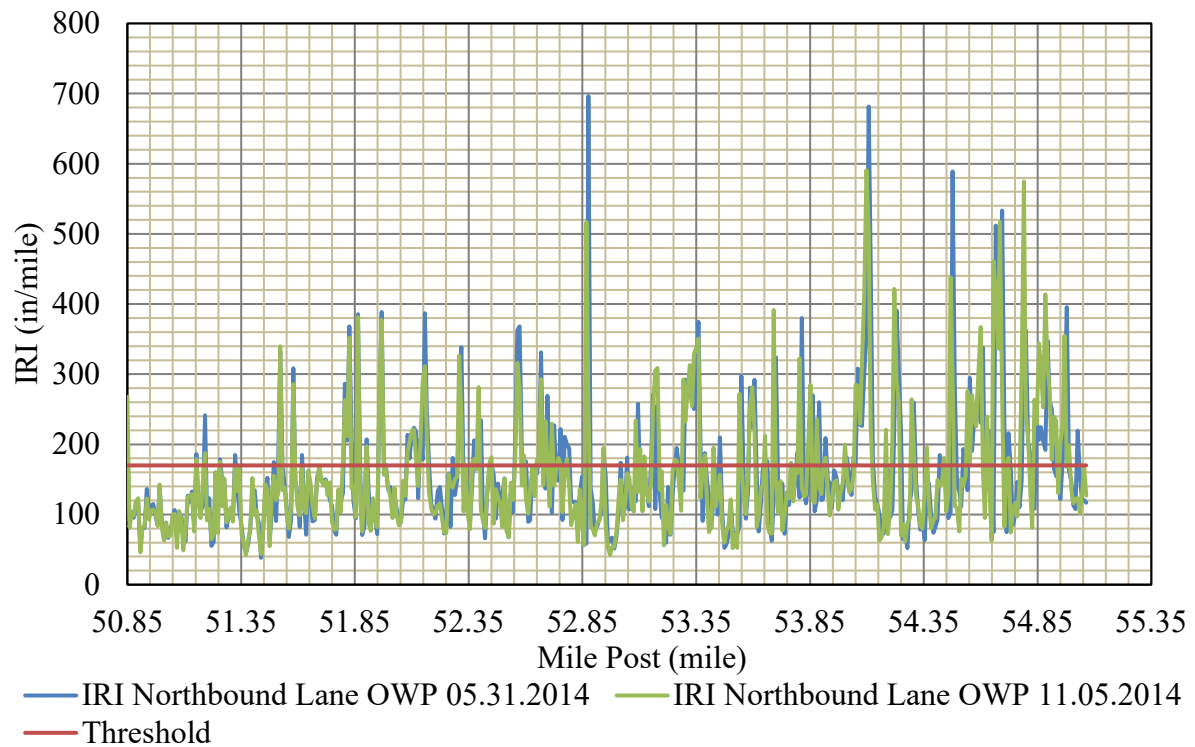


Figure 94: Northbound, Outside Wheel Path IRI Profiles for May and November 2014

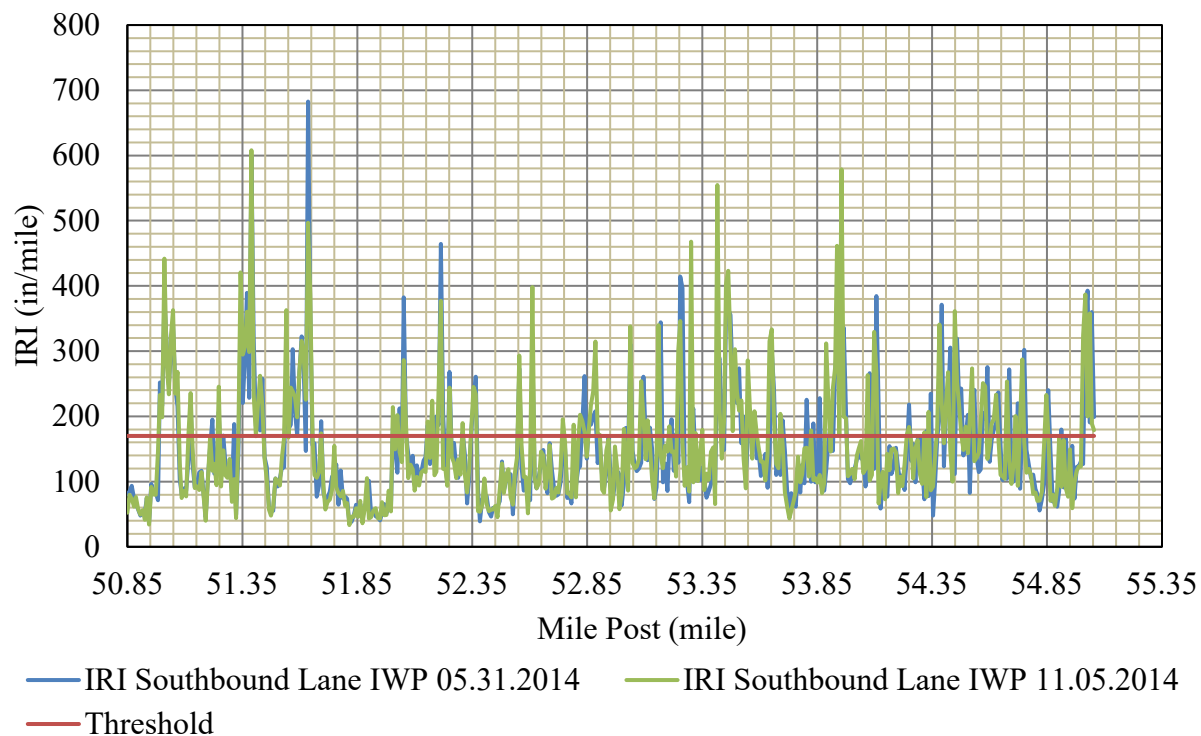


Figure 95: Southbound, Inside Wheel Path IRI Profiles for May and November 2014

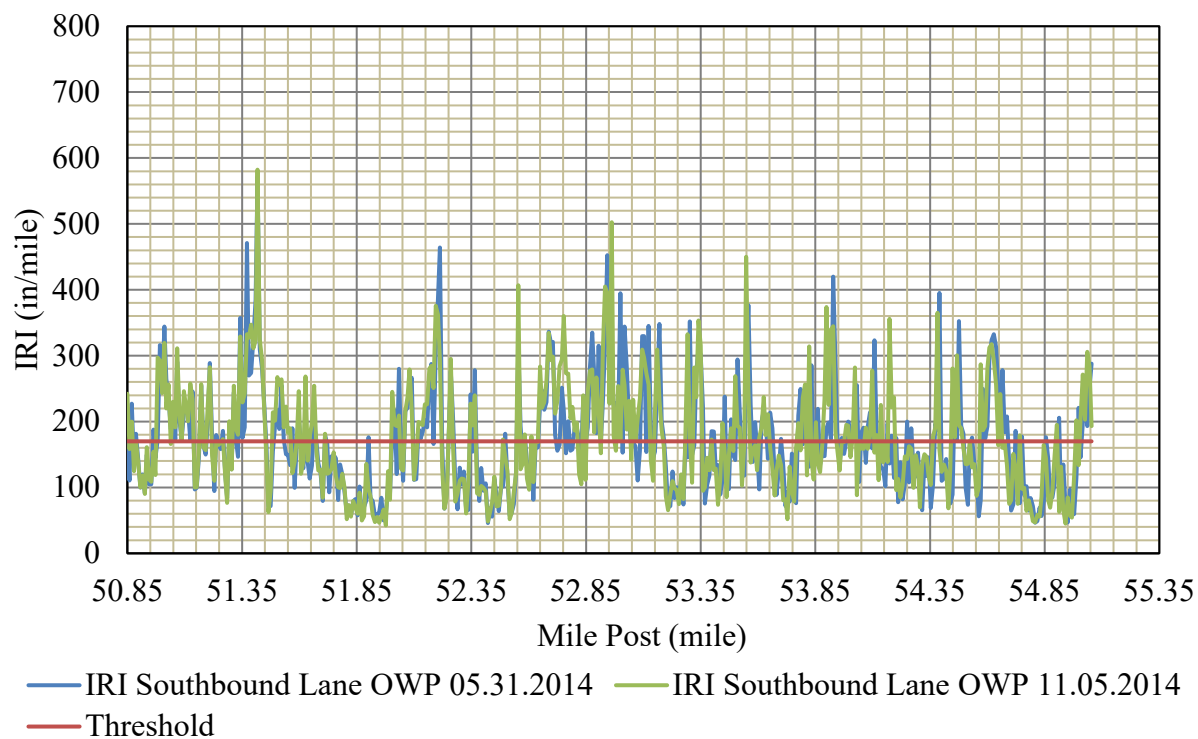


Figure 96: Southbound, Outside Wheel Path IRI Profiles for May and November 2014

4.5 One Dimensional Swell

One-dimensional swell tests were performed to determine the percent free swell and swelling pressure of the soil. The free swell value indicates the measured percent strain at the end of primary swell under a 20 psf (1kPa) vertical pressure. If the specimens were allowed to swell for an infinitely long time, additional swell would occur in some specimens during secondary swell. This is partly due to the unequal rate of swelling through the cross-section of the specimen. The clays at AL 5 in Perry County have a low hydraulic conductivity, meaning that the top and bottom of the specimen could possibly saturate and reach full swell potential before the center of the specimen. For this reason, swell tests were allowed to run until a fully developed primary swell or collapse curve was developed.

The swell pressure represents the vertical pressure required to produce zero strain when the soils are inundated. Over burden pressures greater than the swell pressure will result in collapse and lower pressures will result in swell if water is added. For each soil layer and location, the moist unit weight was determined from undisturbed samples. Table 14 summarizes the one dimensional swell test results at each boring location and layer.

At each of the boring locations, the swell pressure of layer 2 is greater than the swell pressure of layer 1, except for B6.5 which classifies as a clayey sand rather than a fat clay. Layer 1 swell pressures ranged from 508.0 psf to 1081.5 psf, and layer 2 swell pressures ranged from 207.8 psf to 1560.4 psf. In general layer 1 soils were at a higher water content, and therefore lower matric suction, than layer 2 soils, except for B3.5. As the matric suction decreases the corresponding swell pressure should also decrease and as the matric suction increases the corresponding swell pressure should increase (Tu and Vanapalli 2016). According to Fredlund et al. (1980), “the ‘corrected’ swell pressure, P'_s , equals the sum of the *in situ* net normal stress, $(\sigma_y - u_a)_{field}$, and the ‘matric suction equivalent,’ $(u_a - u_w)_e$, where σ_y is the total overburden pressure, u_a is the pore-air pressure, and u_w is the pore water pressure” (as cited in Tu and Vanapalli 2016). Thus, the reported swell pressures should be viewed as a single point on a spectrum of potential swell pressures according to the soil’s density, initial water content and matric suction. Figure 97 depicts the stress paths of a given soil mass to help visualize the relationship between matric suction, net normal stress and swell pressure.

Table 14: Summary of One-Dimensional Swell Results

Boring	Layer	Free Swell (% Strain)	Swell Pressure (psf)	Moist Unit Weight (pcf)	Approximate Depth to Overburden/Swell Equilibrium (ft)
1.5 MP 51.10	1	1.51	736.0	115.0	6.4
	2	*	1250.8	116.3	10.8
2.5 MP 51.60	1	*	912.5	118.8	7.7
	2	0.98	1588.8	119.4	13.3
3.5 MP 52.10	1	0.75	1015.5	114.4	8.9
	2	0.78	1033.9	110.0	9.4
4.5 MP 52.60	1	1.61	1069.4	113.1	9.5
	2	1.49	832.0	112.5	7.4
5.5 MP 53.10	1	*	511.7	113.1	4.5
	2	1.85	1356.6	116.9	11.6
Tree/6.0 MP 53.35	1	0.9	597.1	110.6	5.4
	2	0.79	1311.4	118.8	11.0
6.5 MP 53.60	1	0.57	570.5	115.6	4.9
	2	0.48	214.8	118.1	1.8
7.5 MP 54.10	1	*	621.2	121.3	5.1
	2	1.30	709.0	121.9	5.8

* Information cannot be determined due to error in volume measurements

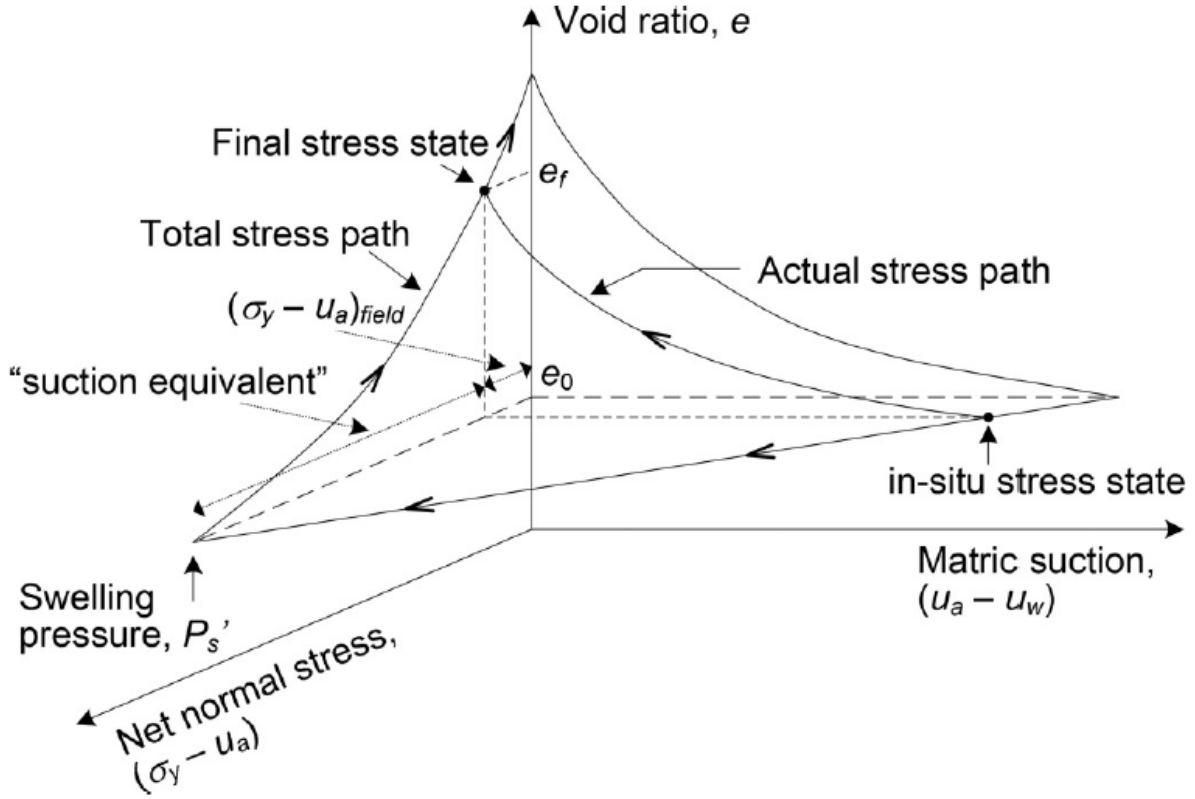


Figure 97: Stress paths of 1-Dimensional Swelling (Tu and Vanapalli 2016)

Using the swell pressure and moist unit weight of undisturbed samples the depth to overburden/swell equilibrium was calculated for each layer with the Equation 6.

$$D_{O/S} = \frac{P_s}{\gamma_m} \quad (7)$$

where:

$D_{O/S}$ is the approximate depth of overburden/swell equilibrium

P_s is the swell pressure

γ_m is the moist unit weight

This depth represents how much soil overburden with the same moist unit weight as the sample would be required to prevent the swelling of lower layers. Soils above the equilibrium depth may be subject to significant swell/shrinkage depending on the loading conditions and availability of water. This region is the active zone. The active zone may be limited to shallower

depths depending on the hydraulic conductivity of the soil and availability of water. Potentially compounding this issue is the documented hydraulic lift effects presented by Dawson (1996), which allows large trees to draw water from deep roots and recharge shallower soils for transpiration. Soils below the equilibrium depth will not undergo swell; instead they will consolidate. If the overburden pressures are relieved either through excavation or sampling the soils will undergo some swelling that cannot be accounted for with this laboratory procedure. It is important to recognize that while the *insitu* moisture content of these specimens are close to saturation, the associated swelling pressures and strains are capable of causing significant pavement damage. The moisture content and saturation data has been summarized in Table 15. Except where noted the saturation of specimens is an average of the saturation for four or more swell specimens. In a few cases swell specimens were not trimmed completely flush with the specimen ring. Because a discrepancy in the height measurement as little as 0.01 inch is sufficient to invalidate the percent saturation calculations, data with this error has not been reported.

In contrast, the potential for these soils to shrink is equally significant. These specimens are approaching saturation making the maximum potential volumetric change in the negative direction. Further testing in the form of shrinkage limits is recommended to determine the maximum shrinkage possible. Shrinkage is likely to occur during periods of drought such that the moisture losses due to evapotranspiration exceed precipitation. Ultimately, pavement damage due to expansive clays is not the result of swollen or desiccated soils in and of themselves, but rather the cyclic transition between the two states.

Table 15: Summary of Water Content and Saturation of Swell Test Specimens

Boring/MP	Layer	Free Swell (% Strain)	Approximate Depth to Overburden/Swell Equilibrium (feet)	Moisture Content of Specimens (%)	Degree of Saturation (%)
1.5 MP 51.10	1	1.51	6.4	36.97	95
	2	*	11.2	32.93	*
2.5 MP 51.60	1	*	7.8	31.92	*
	2	0.98	13.1	29.21	93
3.5 MP 52.10	1	0.75	9.1	38.59	99
	2	0.78	9.8	41.48	96
4.5 MP 52.60	1	1.61	9.6	38.81	97
	2	1.49	7.3	32.68	88
5.5 MP 53.10	1	*	7.7	39.64	94 ***
	2	1.85	11.9	33.25	95
Tree/6.0 MP 53.35	1	0.9	5.6	39.55	94
	2	0.79	11.6	32.24	97 **
6.5 MP 53.60	1	0.57	4.4	28.15	87
	2	0.48	1.8	28.77	90 ***
7.5 MP 54.10	1	*	5.0	29.20	97 **
	2	1.30	5.8	27.84	97

* Information not available

** Average of two data sets

*** Average of three data sets

4.6 Torsional Ring Shear Testing

Field observations suggested that there may be soil stability issues contributing to distress along AL 5. Built up sections of the roadway seemed to exhibit a flow like failure which could be due to clays reaching their residual strength after years of drainage. Drained torsional ring shear tests were conducted on material from AL 5 using a Controls Group (formerly Wykeham Farrance) Bromhead Ring Shear Apparatus following ASTM D 6467. Figure 98: Controls Group Bromhead Ring Shear Apparatus (Controls Group 2019) shows the ring shear testing device used for research labeled with parts.

Table 16 summarizes all the data determined using the Bromhead ring shear testing device for each test section. The data is similar for each stress level in the different test section. The peak

shear stress values have more variability than the residual stress values between the different test sections.

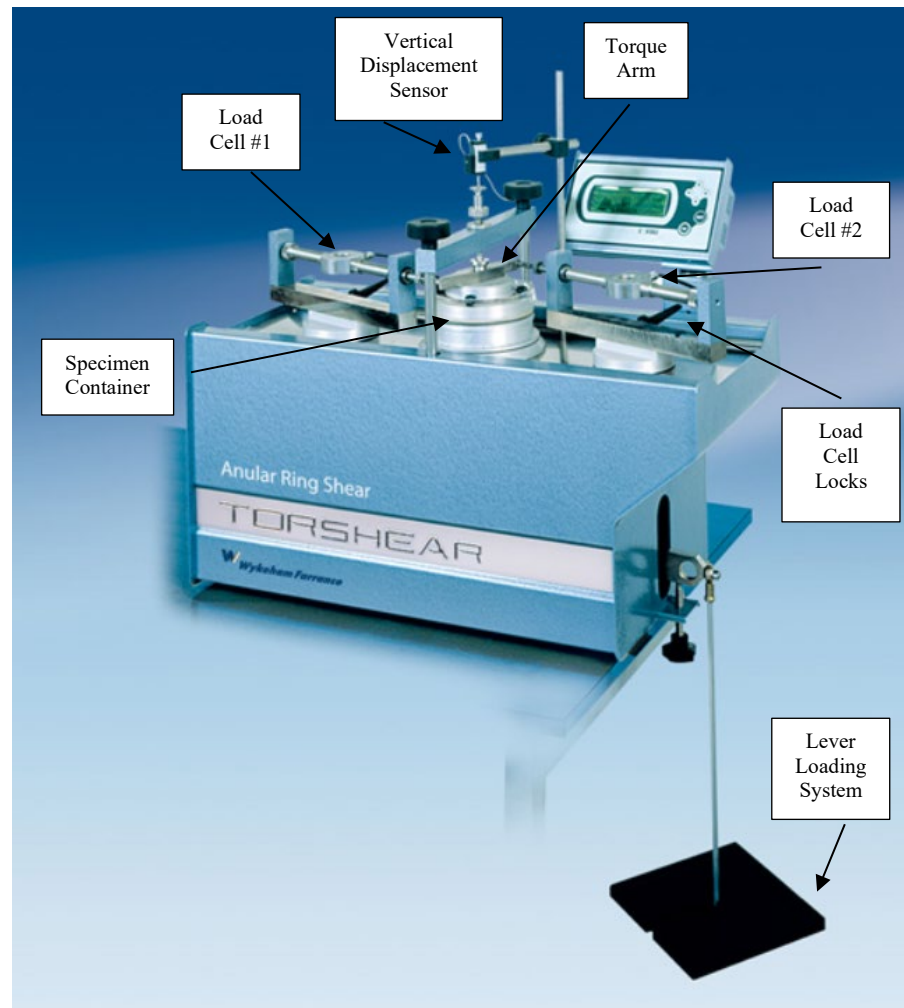


Figure 98: Controls Group Bromhead Ring Shear Apparatus (Controls Group 2019)

Using the relationship between the plasticity index and $\sin \phi$ in Lambe and Whitman (1969), Figure 99 was generated. The peak angles of shear resistance were used in this plot to compare the AL 5 ring shear data to the previous correlations determined by Kenney (1959). The peak shear strength results from the ring shear device are relatively close to the empirical trendline. The peak shear strength data produced from the ring shear testing fits well with previous research on highly plastic clays.

Table 16: Summary of Ring Shear Results

	Stress Level	Normal Stress (kPa)	Peak Shear Stress (kPa)	Residual Shear Stress (kPa)	Angle of Peak Shear Resistance, ϕ_p (°)	Angle of Residual Shear Resistance, ϕ_r (°)	Plasticity Index (%)
Control MP 50.6	1	127.1	53.02	20	-	8.94	48
	2	176.07	71.19	28	-	9.03	
	3	249.55	88.95	41	19.6	9.33	
B1.5 MP 51.10	1	127.09	72.7	32	-	14.13	59
	2	176.08	76.53	37	-	11.87	
	3	249.55	92.27	47	20.3	10.66	
B2.5 MP 51.6	1	127.1	73.04	24	-	10.69	50
	2	176.07	79.8	35	-	11.24	
	3	249.55	96.58	43	21.2	9.78	
B3.5 MP 52.1	1	127.1	62.83	24	-	10.69	52
	2	176.08	74.39	32	-	10.30	
	3	249.55	97.72	52	21.4	11.77	
B4.5 MP 52.6	1	127.09	63	24	-	10.69	55
	2	176.08	87.25	35	-	11.24	
	3	249.55	95.8	51	21	11.55	
B5.5 MP 53.1	1	127.1	61.61	24	-	10.69	61
	2	176.07	69.11	31	-	9.99	
	3	249.55	87.1	43	19.2	9.78	

Figure 99 shows different data used from Kenney (1959). There were two different types of soil tested including remolded specimens and undisturbed specimens. The activity of these specimens was then determined. If the activity of the specimen was greater than 0.75 then the specimen had a larger water holding capacity; therefore, was attracted to water more.

Referencing the typical values of residual friction angles as a function of effective normal stress by Mitchel and Soga (2005), the residual friction angles for each stress level was computed and plotted for the material from AL 5. Figure 100 shows the residual friction angle versus the normal effective stress raised to the minus one-third power. The material from AL 5 lines up very well with the residual friction angles for the material containing weald clay and montmorillonite.

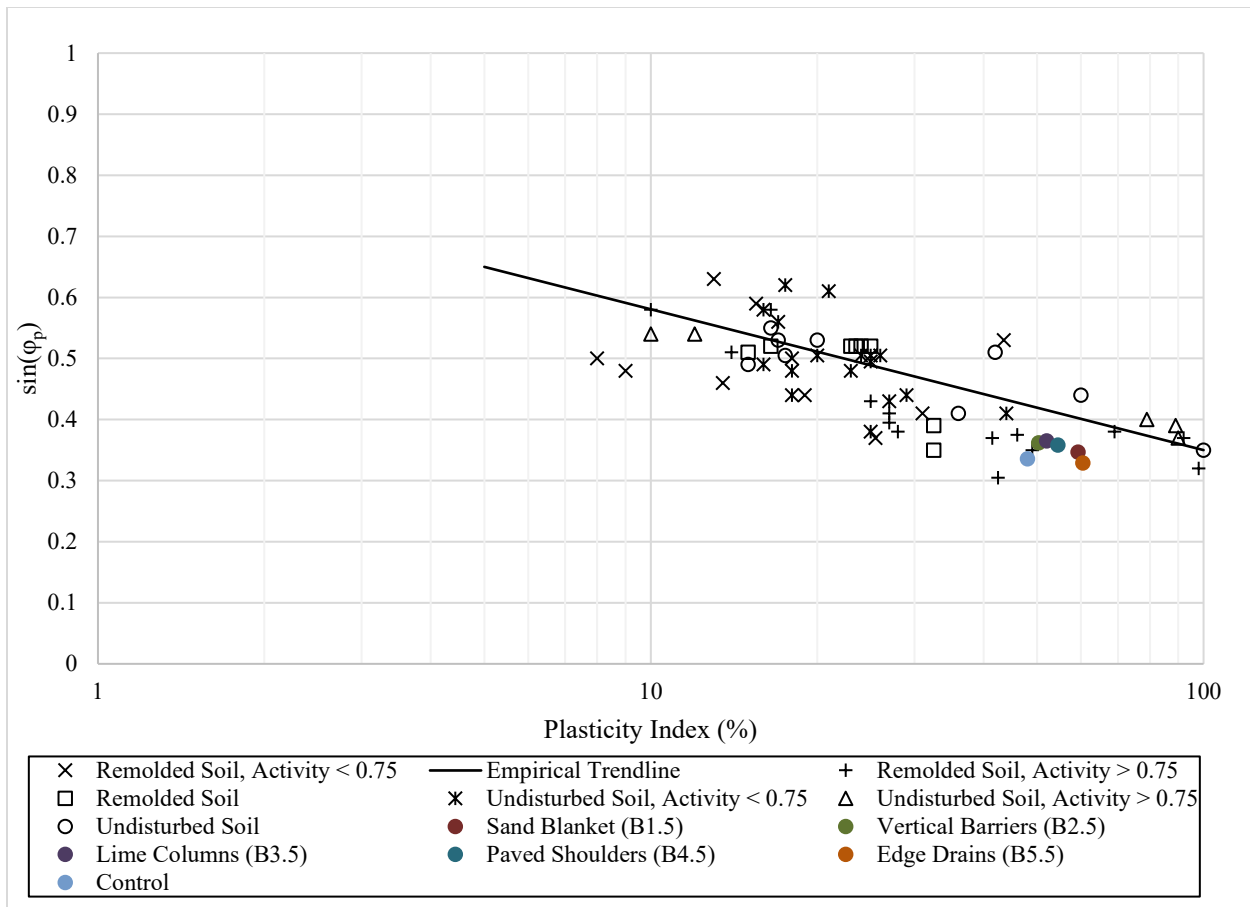


Figure 99: Plasticity Index versus $\sin \phi_p$ Using Data from Kenney (1959) (After Lambe and Whitman 1969)

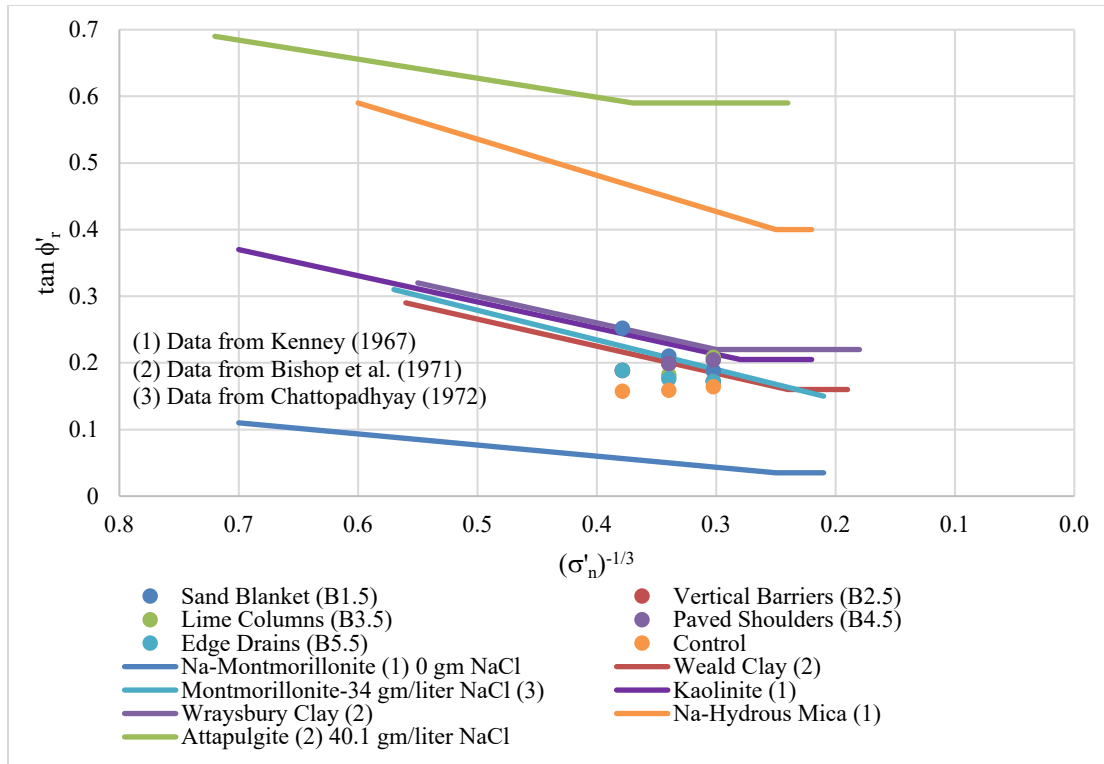


Figure 100: Comparing Residual Friction Angles versus Effective Normal Stress Raised to the Minus One Third Power from AL 5 (After Mitchel and Soga 2005)

4.7 Slope Stability Evaluation

Slope stability analyses were performed on all test sections with remediation techniques applied to them. Bishop's Method was used to analyze the road embankments using SLIDE. SLIDE is a slope stability software by RocScience (2018). The soil profiles were determined by using boring logs provided in Appendix A. The water table was placed at the bottom of the embankment because observations during site visits concluded there had been pooling water at the toe of the embankments. Suction was not accounted for above the water table for these analyses. The geometry of the embankments was determined by using the plans provided by ALDOT for each test section. An average slope of 3:1 was used for all the scenarios. Figure 101 shows a typical slope of the roadway embankment at AL 5.



Figure 101: Typical Slope for AL 5 Roadway Embankments

Figure 102 shows an example of the soil profile for the sand blanket test section using the residual strength values for the analysis. The worst case cohesion and internal angle of friction value for the asphalt concrete were estimated from work by Christenson et al (2000). Therefore, a cohesion value of 7700 psf and internal angle of friction value of 34.1° were input into the software for the material properties of the asphalt concrete. Table 17 shows the correlated undrained shear strength values for layer 2 and 3 of the boring logs. These values were correlated using the plasticity index as stated in the literature review.

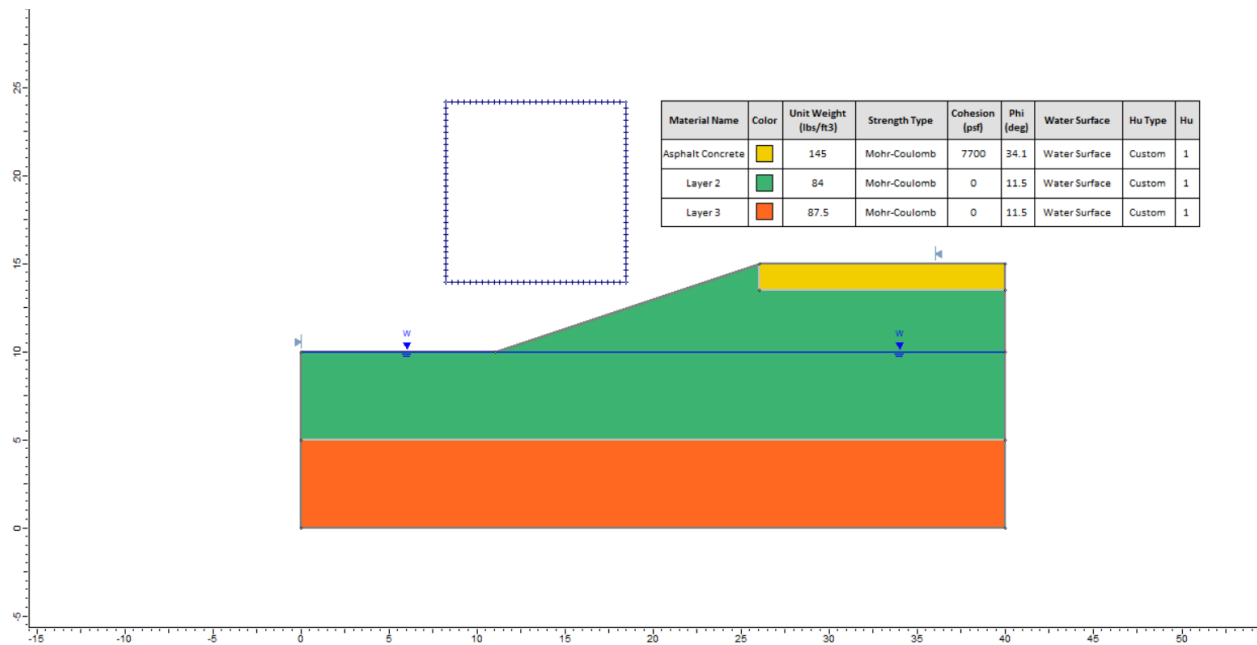


Figure 102: Example of Soil Profile for B1.5 using Residual Strength Values

Table 17: Correlated Undrained Shear Strength from Plasticity Index

Boring #	Layer	Undrained Shear Strength (psf)
1.5	AC	-
	2	164.42
	3	250.10
2.5	AC	-
	2	175.21
	3	193.70
3.5	AC	-
	2	146.17
	3	205.37
4.5	AC	-
	2	134.48
	3	209.70
5.5	AC	-
	2	167.44
	3	230.46

Three different scenarios were computed for each test section. The factor of safety was determined for the end of construction of the roadway; therefore, the undrained shear strength was inputted into the software. The factor of safety was determined under drained conditions; therefore, the peak shear strength envelope value from the ring shear testing was used and lastly, the factor of safety after localization or failure was computed. The factor of safety after failure used the

residual shear strength envelope in the software determined by the ring shear testing. Figure 103 shows the output of the analysis when the software is run. The minimum factor of safety for the residual strength values for the sand blanket test section is 0.571; therefore, the embankment is very unstable and would be expected to have slope stability problems. The software was used for each scenario for each test section and the results from the slope stability analyses are shown in Table 18.

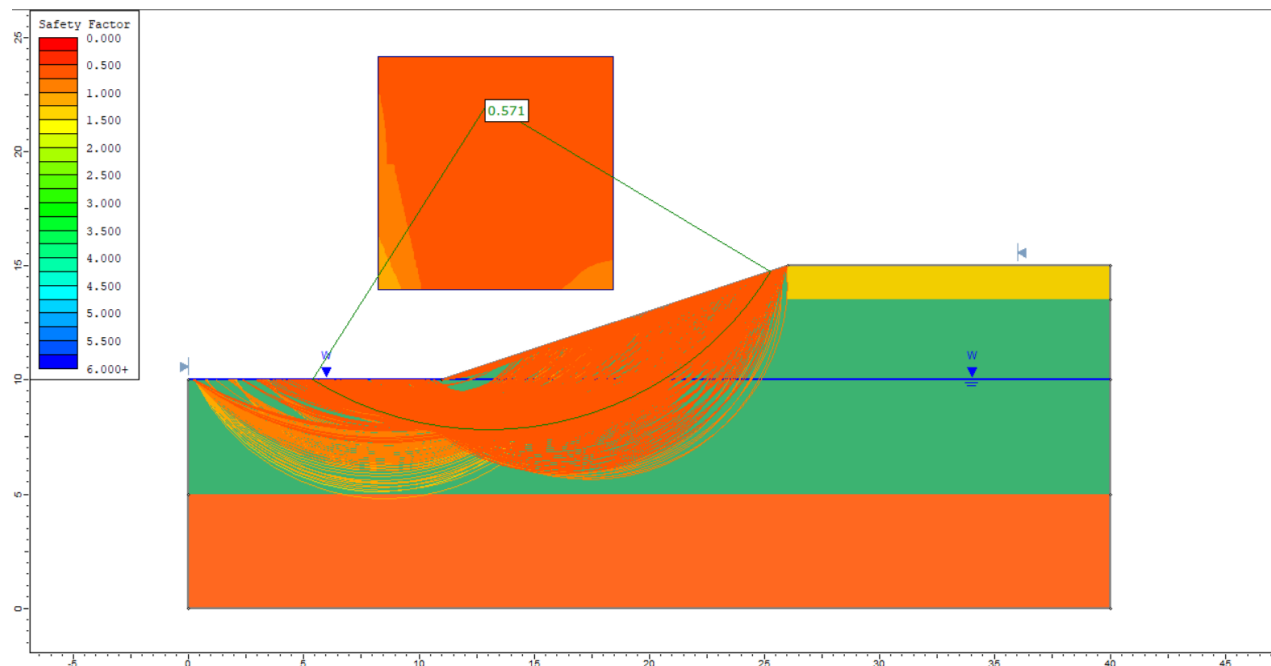


Figure 103: Minimum Failure Surfaces for B1.5 using Residual Strength Values

Table 18: Factor of Safety for Slope Stability

Location	Factor of Safety		
	Undrained Shear Strength, End of Construction (Correlated)	Peak Shear Strength, Drained	Residual Shear Strength, After Failure
B1.5 MP	3.115	1.038	0.571
B2.5 MP	3.343	1.274	0.535
B3.5 MP	2.93	1.154	0.549
B4.5 MP	2.953	1.19	0.55
B5.5 MP	3.332	1.045	0.483

As shown in Table 18, all of the slopes were stable after construction was completed with factor of safety values as high as 3.34. However, as time has passed, the factor of safety has decreased until failure of the slope or embankment was met. At the time of failure, the factor of

safeties are very close to 1. After failure, the strength value of the material was decreasing and caused the factor of safety to decrease. Using the residual strength values results in factor of safeties around 0.5; therefore, all the slopes would likely experience stability issues if the residual strength of the material was reached. These slope failures could be an explanation of the cracks seen in the pavement and the pavement distress in the travel lanes. The analyses have shown relatively deep circular failures which has been observed on the embankments along AL 5.

The preliminary slope stability analysis was completed for AL 5. Limitations and assumptions were incorporated with each analysis. The water table was assumed to be located at the toe of the embankment. The geometry of the soil profiles was very simple and was determined from the cross sections of each test section and the boring logs. Suction was not accounted for above the water table. Each layer thickness was assumed to have reached the residual strength throughout the entire layer. Another limitation was the correlated undrained shear strength values inputted into the software since undrained shear strength test were not performed in the laboratory. These assumptions and limitations should be minimized in order to produce less conservative factors of safety.

4.8 Synthesis of Preliminary Investigation

The observational, photographic and IRI surveys all point to a highly damaged roadway surface. The tree survey validates the presence, size and type of trees capable of influencing the shrink/swell cycle of subgrade soils underneath the roadway. The laboratory results also confirm the soils capacity for volumetric change and the generation of high swell pressures. Clays with very low residual strength were present in all sections. The following figures and discussion will bring the results from the different activities together according to location. Figure 104 through Figure 107 show the IRI surveys from 2014 with commentary on general site conditions overlain and corresponding to the mile post locations indicated in the survey. In theory the outside wheel path should be more susceptible to shrink swell damage than the inside wheel path because the outside edges of the pavement will be more susceptible to precipitation infiltration than the inside wheel path. Similarly, areas with large deciduous trees should show more damage than areas without. While the IRI data is suggestive of these trends, it must be recognized that before the IRI surveys were performed the roadway had been patched or leveled at various locations throughout the site and the IRI surveys do not provide an indication of damage type. However, it is clearly

established that the roadway was severely damaged before the start of project and outside the range of acceptable FHWA thresholds.

Figure 108 shows the IRI surveys overlain with the experimentally determined swell pressures and the calculated matric suction values from the trimmed swell samples. The swell pressures and matric suction correspond to a specific water content. In general, the swell and matric suction values do not correspond to specific damage observations in the IRI data or visually. However, the figure does validate that the entire site is affected by expansive clays.

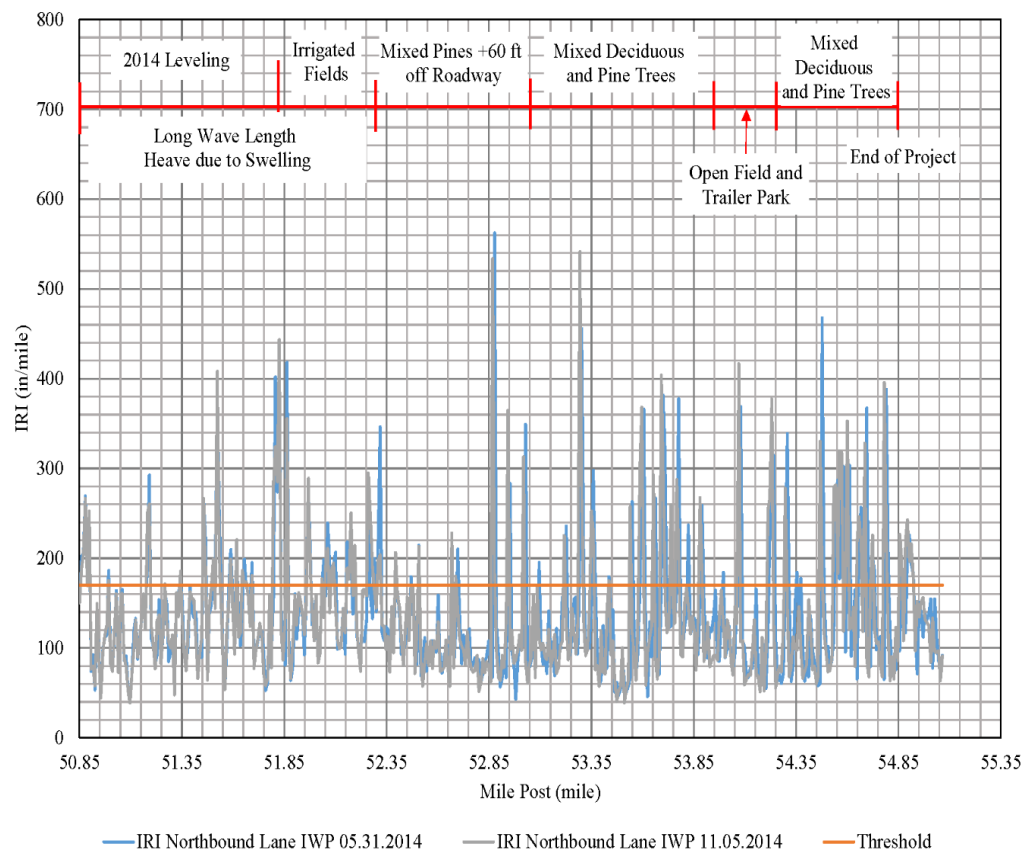


Figure 104: Northbound, Inside Wheel Path IRI Surveys with Site Conditions

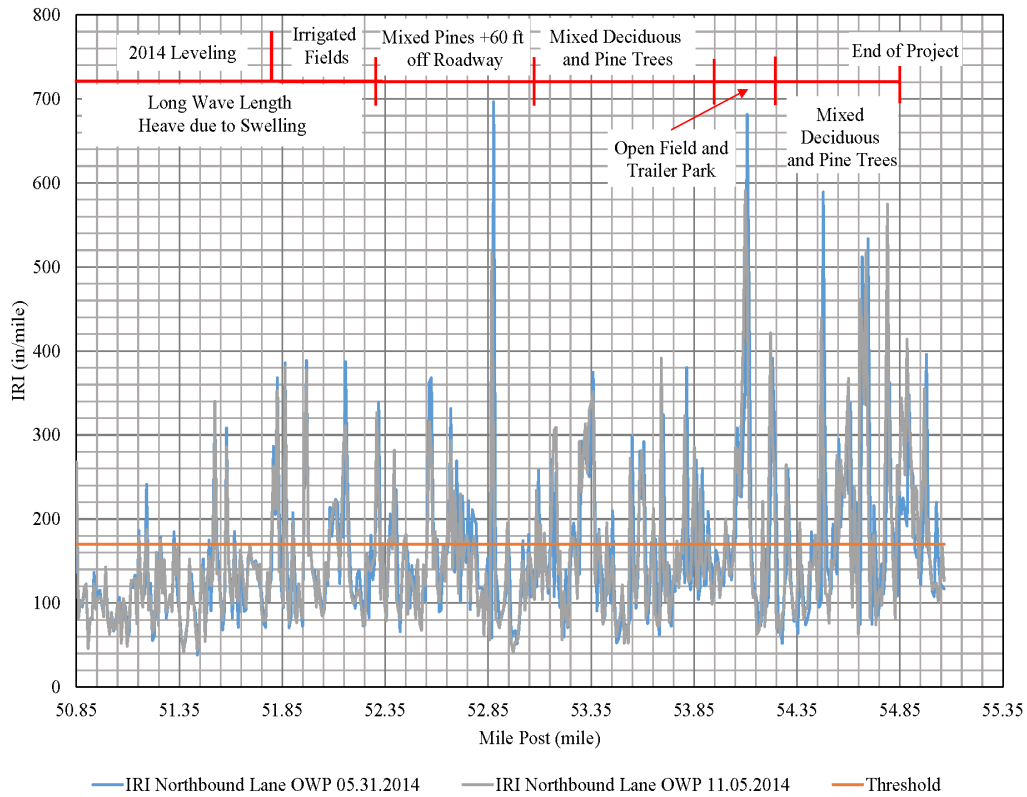


Figure 105: Northbound, Outside Wheel Path IRI Surveys with Site Conditions

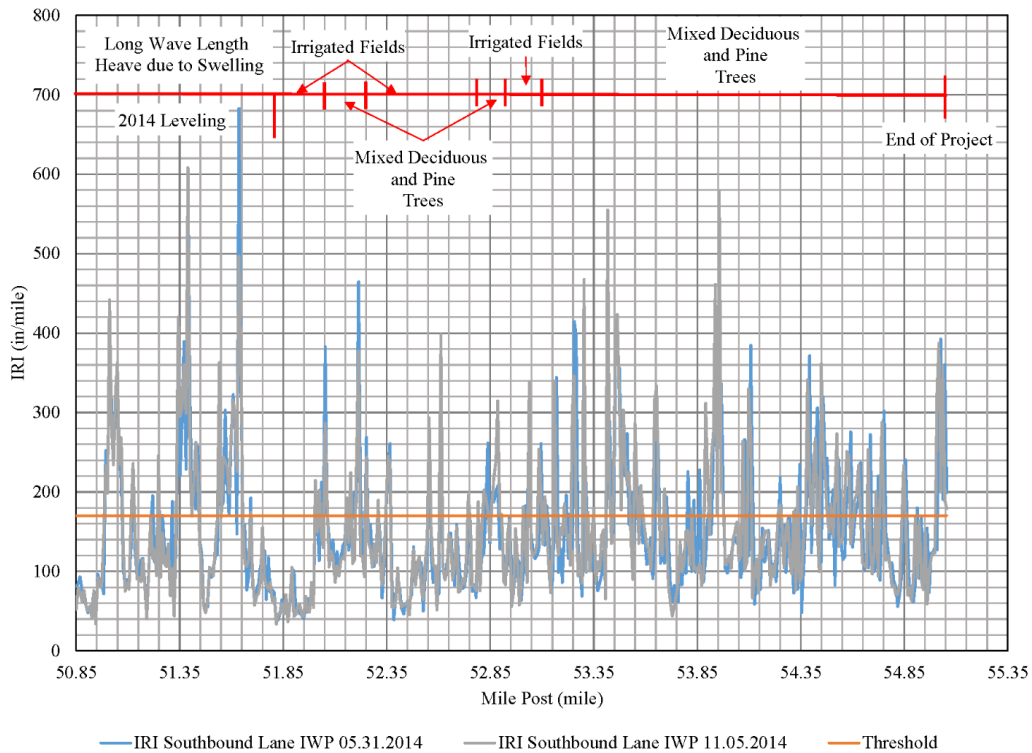


Figure 106: Southbound, Inside Wheel Path IRI Surveys with Site Conditions

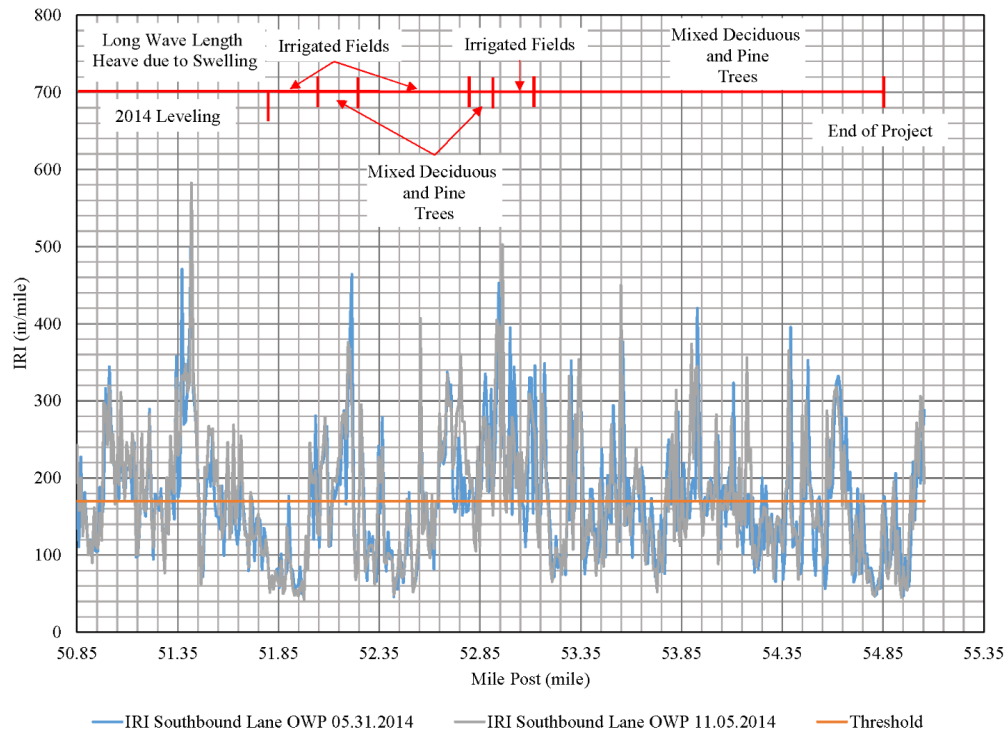


Figure 107: Southbound, Outside Wheel Path IRI Surveys with Site Conditions

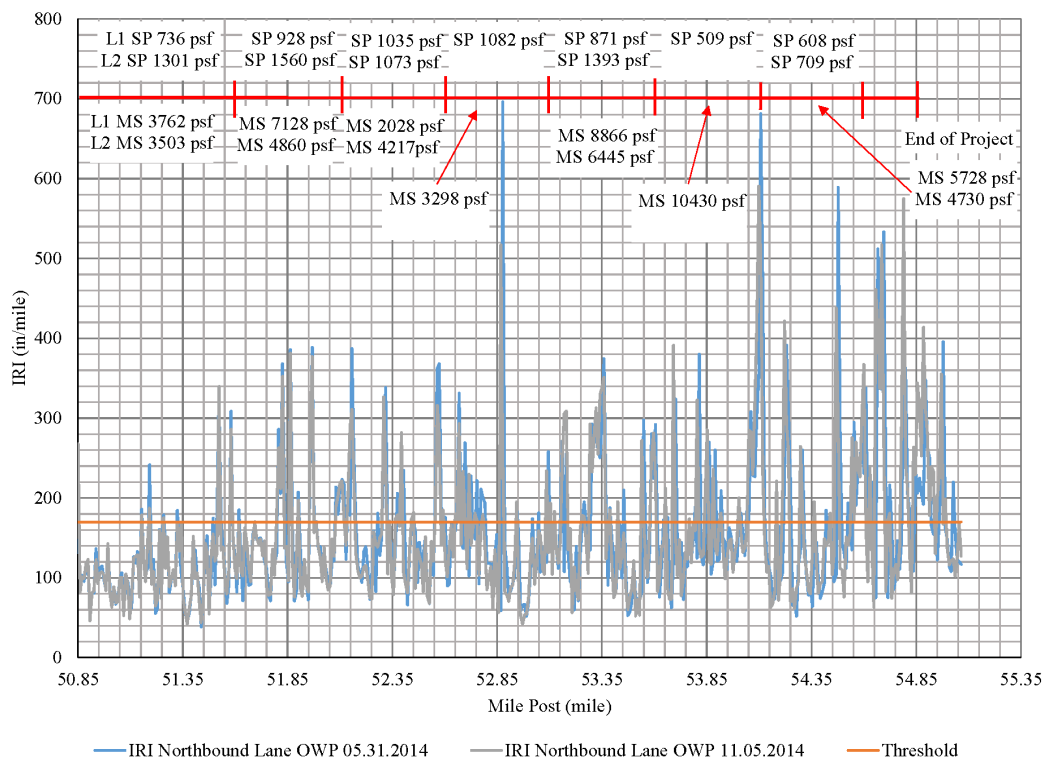


Figure 108: Northbound, Outside Wheel Path IRI Surveys Overlain with Swell Pressures and Matric Suction

Chapter 5. Implementation of Test Sections

5.1 Site Description, Layout, and Nomenclature

The study area is divided into eight half-mile test sections, shown in Table 19 and Figure 109. It was intended that each test section receive a different remediation technique. However, initial site exploration indicated that the clay layer in Test Section 8 was thinner than was typical for the rest of the project. Because of this no remediation was done in Test Section 8 and it served as an additional control section. Furthermore, Test Section 7 was also canceled due to the impracticality of the construction technique. Thus, Test Section 6, 7, and 8 all served as control sections. Due to constructability requirements and traffic control requirements, the sand blanket was only constructed in the center of Test Section 1, while the first and last 500 feet in this section received no remediation. These sections served as additional control sections. Construction and resurfacing of the test sections was completed in August 2016.

Table 19: Test Sections

Test Section	Remediation Technique	Mile post
Control	Control	50.85 – 50.90
1	Sand Blanket	50.90 - 51.21
Control	Control	51.21 - 51.35
2	Vertical Moisture Barriers	51.35 - 51.85
3	Lime Columns	51.85 - 52.35
4	6' Paved Shoulders	52.35 - 52.85
5	Edge Drains	52.85 - 53.35
6	Control	53.35 - 53.85
7	Deep Mixing - Canceled	53.85 - 54.35
8	Control	54.35 - 54.85

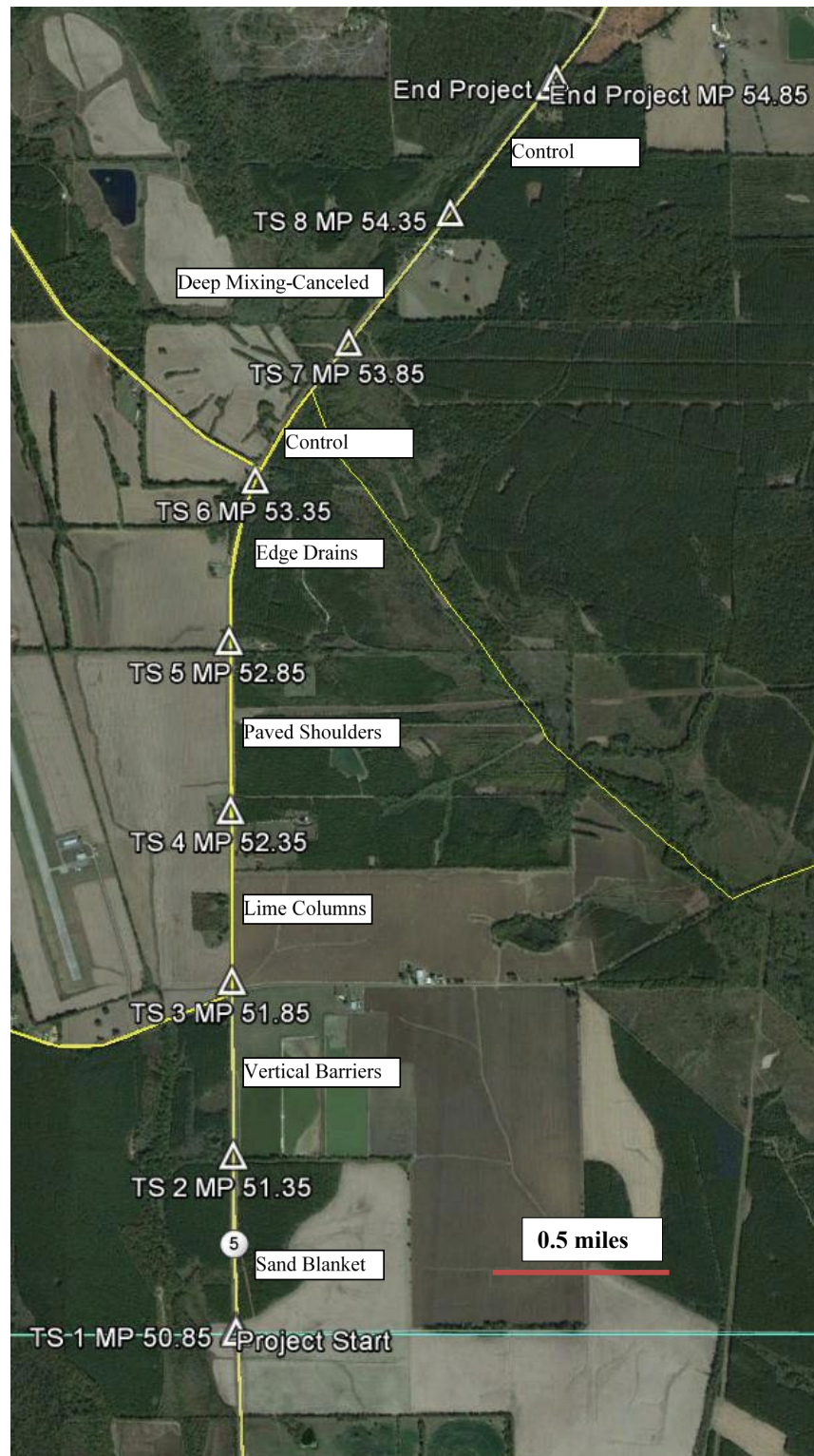


Figure 109: Layout of Research Site (Google 2014)

5.2 Remediation Techniques Implemented at AL 5

The remediation techniques mentioned above were selected by ALDOT and Auburn University based on a review of the current literature and state of practice, combined with local experience. They are described briefly below. Full descriptions and documentation of the construction procedures used will be described in a future publication.

5.2.1 Sand Blanket

A drainage layer termed a “sand blanket” was used in Test Section 1. This is essentially an underdrain that is supposed to keep the subgrade at a more constant moisture content. Construction required complete removal of the existing pavement structure. Figure 110 shows the cross-section of the sand blanket test section. Figure 111 through Figure 114 show aspects of the sand blanket construction.

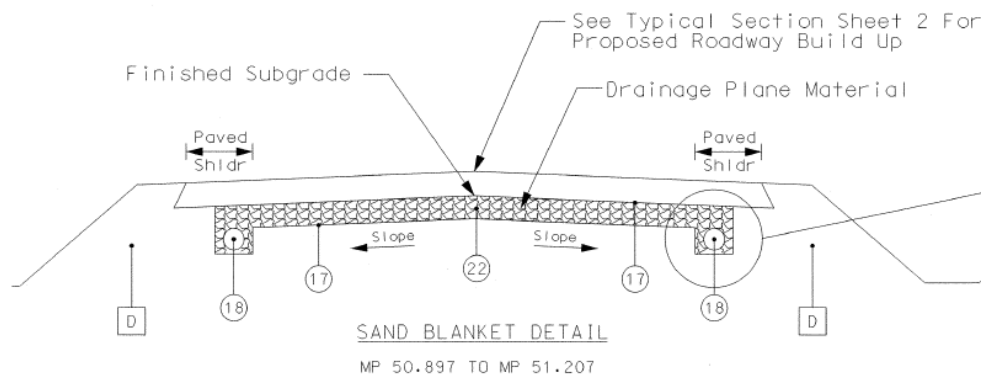


Figure 110: Sand Blanket Cross-Section (ALDOT 2015)



Figure 111: Excavation for Sand Blanket Showing Thick Pavement Over Minimal Compacted Base



Figure 112: Sand Blanket Drainage Plane Material



Figure 113: Sand Blanket Geosynthetic Layer



Figure 114: Sand Blanket Roadway Buildup

5.2.2 Vertical Moisture Barriers

Vertical moisture barriers are sheets of impervious geosynthetic material that is installed in trenches at the edge of a pavement. Figure 115 shows a typical cross-section for a pavement with vertical moisture barriers. They seek to limit the lateral flow of water into and out of the subgrade. As Nelson and Miller (1992) note, it is generally not practical to install vertical moisture barriers the entire depth of the active zone, but instead they recommend a depth of one-half to two-thirds of the active zone. Vertical moisture barriers have previously been used with some success in other areas of the country (Steinberg 1992).

The design for the AL 5 test section included two depths for the barriers six feet and 10 feet. However, due to cave-ins during construction, the ten foot barrier section was eliminated, thus the entire section was constructed with six foot barriers. Plans for the vertical barriers are shown in Figure 116. Selected photographs from vertical moisture barrier construction are included as Figure 117 through Figure 121.

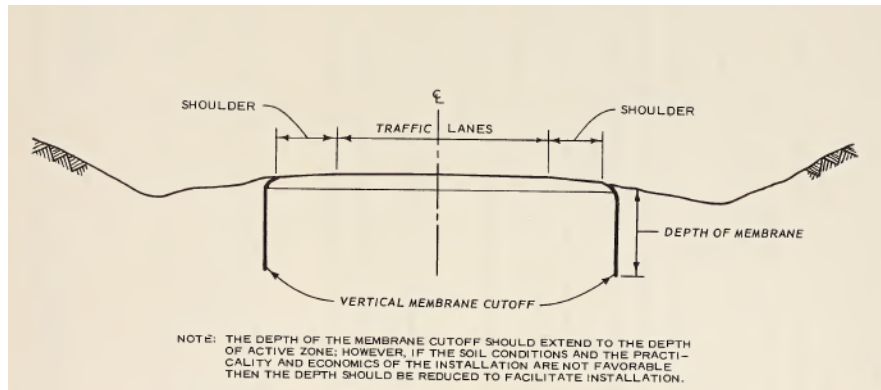


Figure 115: Typical Vertical Moisture Barrier Cross-Section (Snethen 1979)

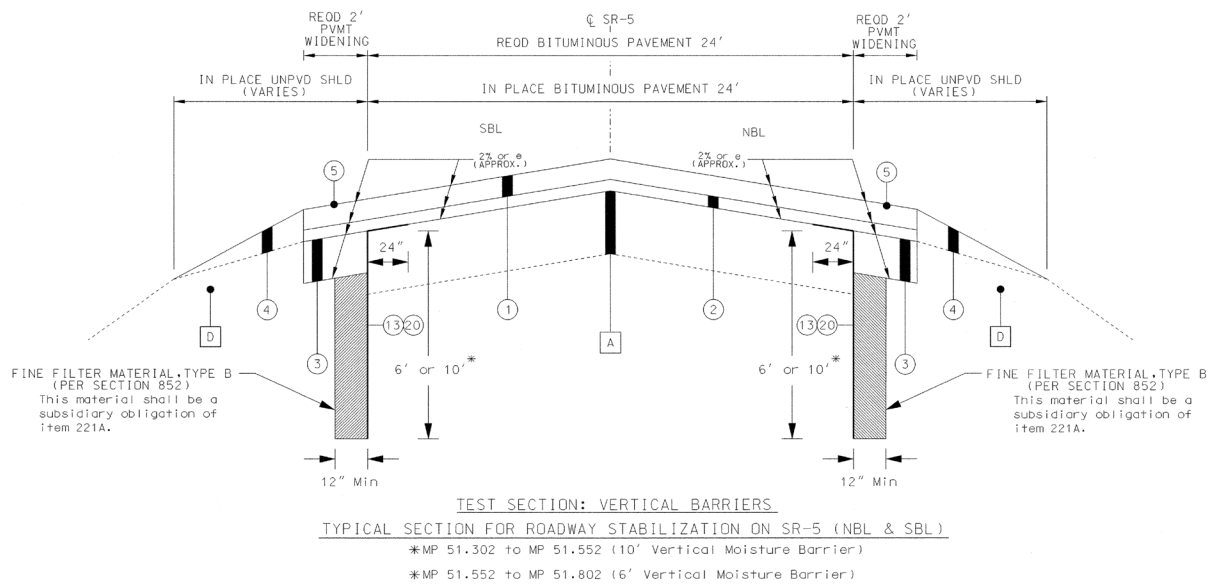


Figure 116: Vertical Moisture Barrier Cross-Section Plans (ALDOT 2015)



Figure 117: Vertical Moisture Barrier Excavation



Figure 118: Vertical Moisture Barrier Cave-In



Figure 119: Vertical Moisture Barrier Membrane Placement



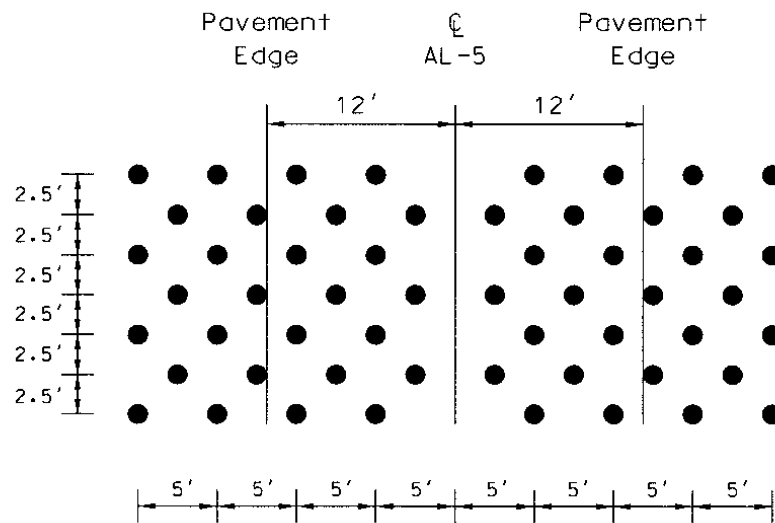
Figure 120: Vertical Moisture Barrier Filling



Figure 121: Vertical Moisture Barrier Paving

5.2.3 Lime Columns

Lime columns were implemented in an effort to chemically stabilize the subgrade. Lime is often mixed into subgrade soils during new construction to stabilize clayey soils. Lime treatment causes fine grained soils to exhibit less plasticity and improved workability (Nelson and Miller 1992). At Test Section 3 of AL 5, lime was packed into drill-holes in the pavement surface and the shoulder. Figure 122 and Figure 123 show the layout and cross-section of the lime columns. The process of drilling, packing, and patching is documented in Figure 124 through Figure 127. It should be noted that prior to the placement of the final wearing surface, the lime columns reflected through the binder course as shown in Figure 128 and Figure 129. This is most likely due to poor compaction during installation. At the time of publication of this report, the lime columns had not reflected through the final wearing surface.



Plan View Showing Spacing Of Auger Holes (Both Lanes)

Figure 122: Layout of Lime Columns at AL 5 (ALDOT 2015)

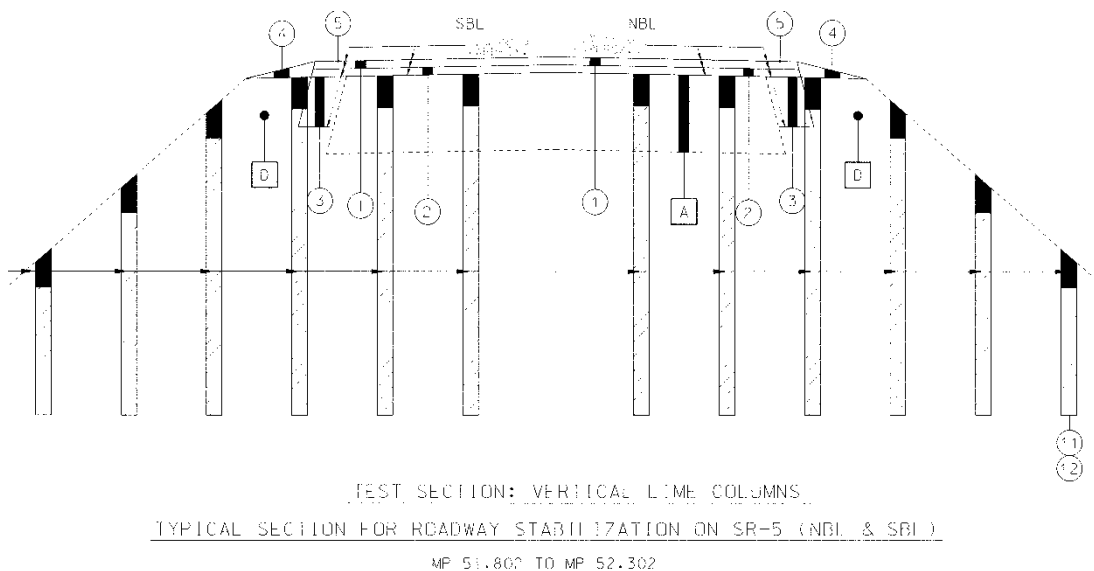


Figure 123: Typical Cross-Section of Lime Columns (ALDOT 2015)



Figure 124: Lime Column Drilling



Figure 125: Lime Column Drilled Holes



Figure 126: Packing Lime Columns



Figure 127: Cold Mix Patching Completed Lime Columns



Figure 128: Lime Columns Reflecting to Pavement Surface

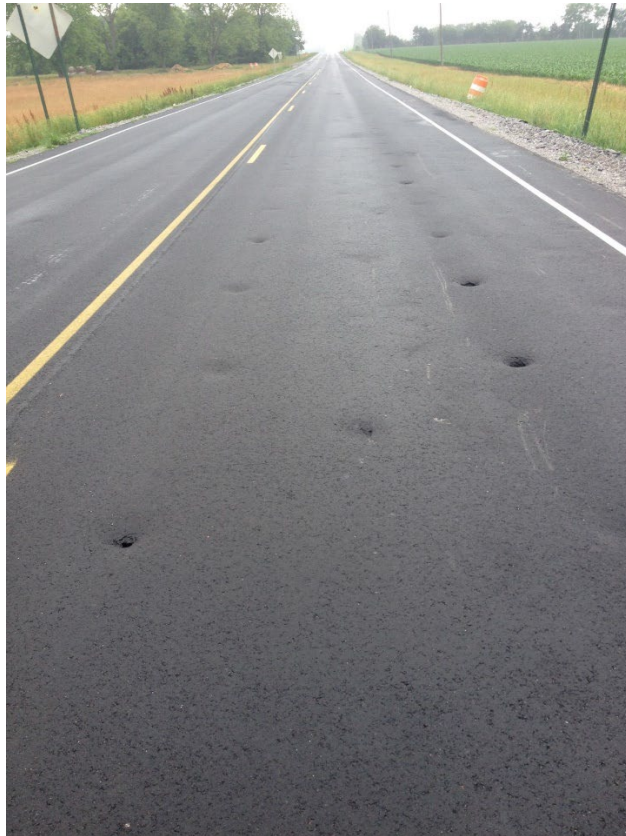


Figure 129: Lime Columns Reflected Through Binder Course and Holding Water

5.2.4 Six Foot Paved Shoulders

It was noted during field reconnaissance in Chapter 4 that large longitudinal cracks were present in several locations. This could be due to the fact that moisture fluctuation is greatest near the edge of the pavement and diminishes towards the center, causing differential movement as depicted in Figure 21. Test Section 4 employs six foot wide paved shoulders to try to shift these cracks out of the travel lane. The plans for the paved shoulder section are show in Figure 130. This has the added benefit of providing lateral support to the pavement structure.

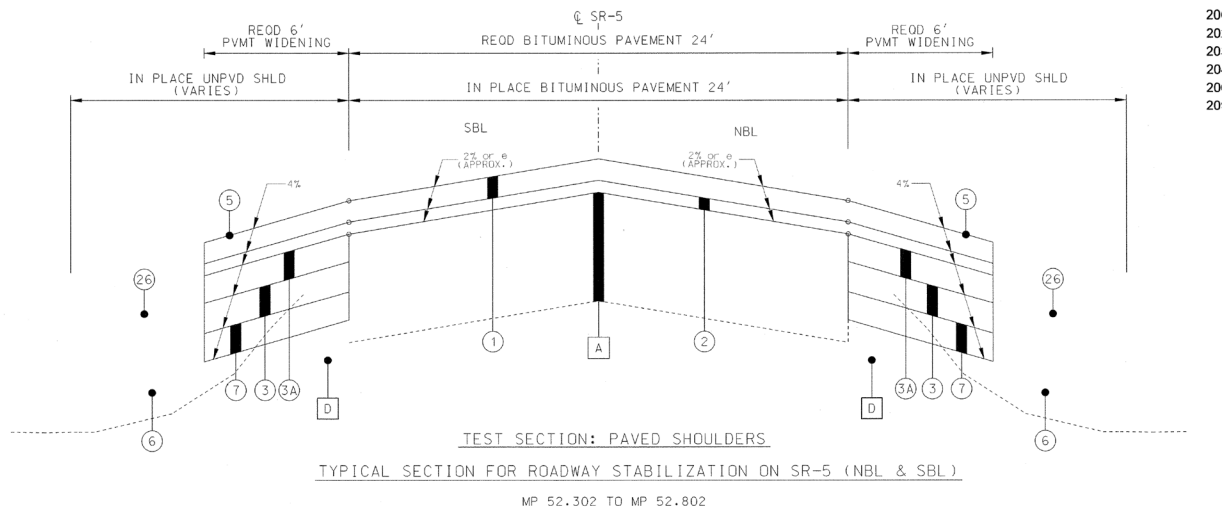


Figure 130: Paved Shoulder Cross Section (ALDOT 2015)

Longitudinal cracks observed in the paved shoulder section are shown in Figure 131. A pair of photos taken after the buildup of the paved shoulders is included as Figure 132



Figure 131: Longitudinal Cracks in Travel Lane at AL 5 Visible During Construction



Figure 132: Paved Shoulder Build-Up

5.2.5 Edge Drains

Edge drains have been used with some success to mitigate the effects of expansive soils (Chen et al. 2012). They provide drainage at the edge of the pavement to attempt to stabilize the moisture content of the subgrade, thus preventing heave damage. Figure 133 shows the typical edge drain cross-section at AL 5. Edge drains were installed in Test Section 5 at AL 5. Construction photos are included as Figure 134 and Figure 135.

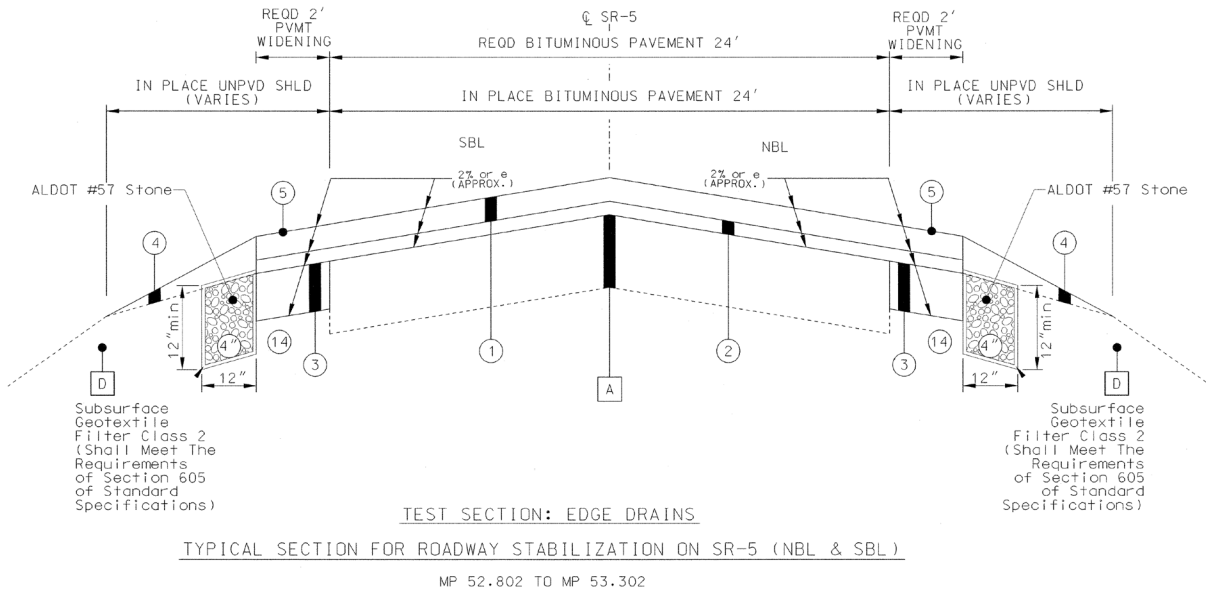


Figure 133: Typical Edge Drain Cross-Section at AL 5 (ALDOT 2015)



Figure 134: Edge Drain Excavation and Geotextile



Figure 135: Installed Edge Drains

5.2.6 Deep Mixing

Madhyannapu (2007) and Madhyannapu et al. (2009, 2010) evaluated the use of deep soil mixing to stabilize expansive soils. On two test sections in Texas, it was found that movement around the columns was negligible after two years. It was proposed that deep soil mixing be used in Test Section 7 at AL 5. The proposed layout and cross-section for the deep mix columns are shown in Figure 136 and Figure 137. During the installation of test deep mix columns, it was found that they were not practical from a constructability standpoint (Figure 138 through Figure 139). Therefore, this remediation technique was cancelled, and Test Section 7 became an additional control section.

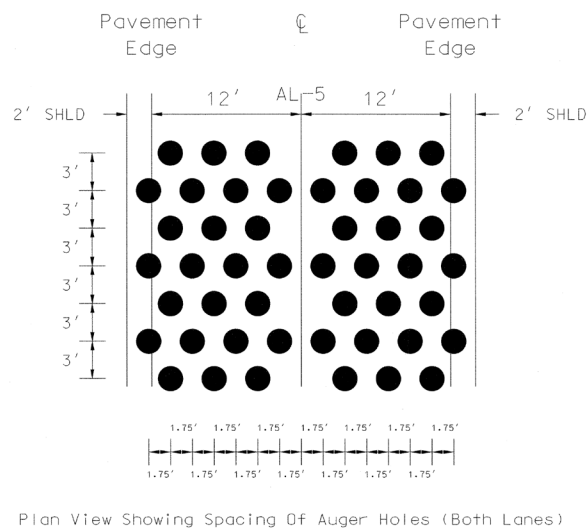


Figure 136: Deep Mix Column Layout (ALDOT 2015)

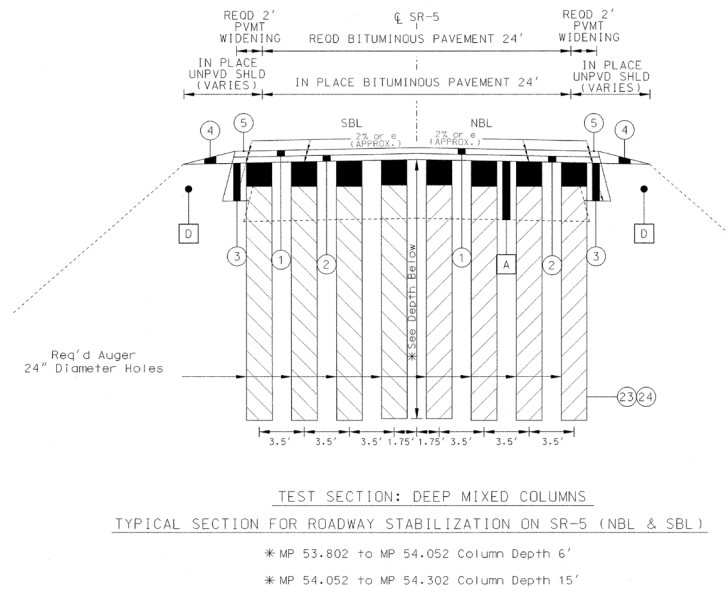


Figure 137: Deep Mix Columns Cross-Section (ALDOT 2015)



Figure 138: Deep Mix Columns Drilling



Figure 139: Deep Mix Columns Drilling and Sampling

5.3 Instrumentation

In order to monitor the subgrade behavior and evaluate the test sections at AL 5, instrumentation was installed to collect data on the soil moisture and pavement conditions. Six monitoring locations were selected along AL 5 where sensors would be placed in the pavement and subgrade as well as in the shoulder. These locations corresponded to five remediation techniques and a control section. Additional sensors were placed at a seventh location to monitor the effects of vegetation on matric suction and moisture content. Sensors were selected to measure the soil moisture content, matric suction, pore water pressure, and asphalt strain. A weather station was also installed to monitor environmental conditions at AL 5. Sensors were chosen based on cost, functionality, accuracy, durability, and the ease of which they could be installed.

5.3.1 Moisture Sensors

The volumetric water content (VWC) of the soil was monitored using Decagon Devices GS1, shown in Figure 140. The GS1 is a capacitive sensor that measures the dielectric permittivity of a soil and correlates that to volumetric water content.

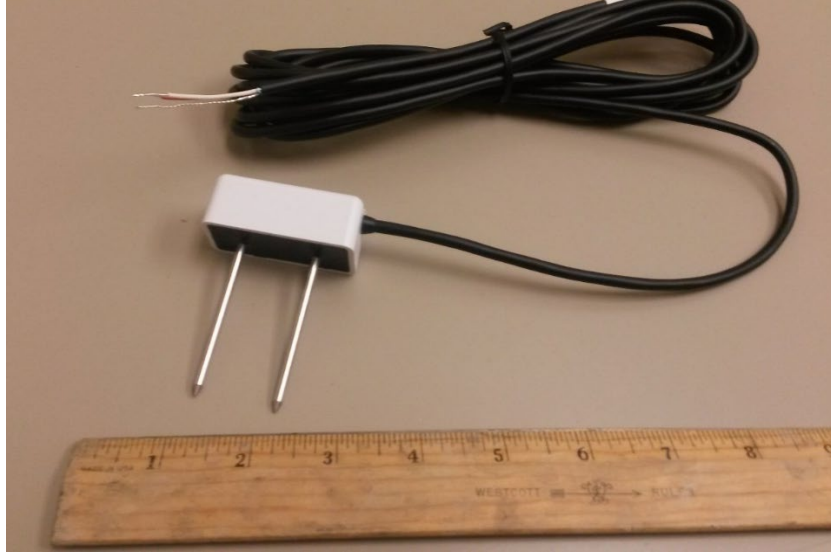


Figure 140: Decagon GS1

The GS1 functions in principle as a parallel plate capacitor with the sensor prongs being the plates and the soil being the dielectric material. The sensor measures the charging time of this capacitor formed by the sensor and soil. The charging time is proportional to the dielectric permittivity of the surrounding medium which is dependent on the amount of water present. The sensor outputs an analog voltage that strongly correlates to volumetric moisture content (Decagon Devices, Inc. 2015a).

Measurements taken by the GS1 are largely independent of soil properties and thus a single calibration, shown in Equation 10, can be used for almost all mineral soils. Decagon (2015a) states that the accuracy provided by this calibration is $\pm 3\%$ VWC. Higher accuracy can be obtained using a soil specific calibration. Because there is little sensor-to-sensor variability, a sensor specific calibration is not necessary for the GS1.

$$VWC = 0.000494 * mV - 0.554 \quad (8)$$

Where VWC = volumetric water content expressed as a decimal

mV = raw GS1 output in millivolts

The gravimetric moisture content is related to the VWC:

$$w = \frac{VWC}{S.G.} \quad (9)$$

Where w = gravimetric moisture content

S.G. = bulk specific gravity of the soil : total unit weight divided by unit weight of water.

The GS1 is very compact, giving it an advantage over TDR sensors. The prongs of the GS1 are approximately 2.25 inches long and the sensor body is approximately 2"x1"x0.75". The total length of the GS1 is only 3 inches, making it ideal to be installed in a borehole.

5.3.2 Suction Sensors

The MPS6 from Decagon Devices (2015b), shown in Figure 141, was selected to measure matric suction at AL 5. The MPS6 has a ceramic disk that is placed in hydraulic contact with the soil. The suction in the disk equalizes with the soil suction although the disk may have a different moisture content than the soil. The water content of the ceramic is measured using a dielectric technique similar to that described for the Decagon GS1. The moisture characteristic curve of the ceramic can then be used to determine the matric suction. These calculations are performed by the MPS6 and a digital output reports the matric suction and temperature.



Figure 141: Decagon MPS6

Watermark electrical resistance sensors had been successfully used in a previous study at Auburn University (Burrage 2016). However, a review of the relevant literature indicated that these sensors do not possess a high accuracy. Most suction sensors, such as thermal conductivity sensors, require calibration by the user to provide a high degree of accuracy. The equipment needed to calibrate matric suction sensors was not available at Auburn University. The MPS6 offers the advantage of being factory calibrated and was selected because of this.

Because the MPS6 was originally intended for agricultural use, the calibration focused on lower suctions that are of greater interest in agricultural applications. Each MPS6 is individually calibrated at a vacuum saturated state, an air dry state (suctions of 0 kPa and 100,000 kPa, respectively), and at four suction values between 9 kPa and 100 kPa. This leads to an accuracy of $\pm(10\% \text{ of the reading} + 2 \text{ kPa})$ over the range of 9 kPa to 100 kPa (Decagon Devices, Inc. 2015b). Decagon (2015b) reports that the MPS6 shows good accuracy to suctions of up to 1500 kPa based on Laboratory evaluations. Decagon also reports low sensor-to-sensor variability to suctions of up to 4500 kPa.

The lower limit of the MPS6 is the higher of either the air entry value of the ceramic (9 kPa) or the surrounding soil. At suctions below this the ceramic will be fully saturated and the suction will not be able to be determined.

5.3.3 Piezometers

In order to measure positive pore pressures if the soil ever became saturated, piezometers were installed in each test section. Vibrating wire piezometers from Geokon were selected for this study. These piezometers are robust and have been used in other research at Auburn University (Burrage 2016). Each 4500S piezometer has an individual calibration provided by Geokon. The Geokon 4500S is shown in Figure 142.



Figure 142: Geokon 4500S

Piezometers must be fully saturated to make measurements, so when used in unsaturated soils, a high air entry (HAE) filter must be used to separate the air and water phase. When an HAE filter is used, piezometers can measure matric suction to values of approximately 100 kPa. At suctions higher than this the water in the piezometer will cavitate and the piezometer will not be able to make measurements. In addition to this, the water compartment behind the HAE filter will

dry out over time. Once a piezometer loses its saturation due to cavitation or drying, it will not recover until it is fully saturated again.

Because of these disadvantages and the additional cost and time required to saturate HAE filters, it was decided to order piezometers without HAE filters. The piezometers will mainly be used to monitor positive pore pressures if they develop at AL 5. However, even without the HAE filters, the piezometers will remain saturated in an unsaturated soil until the air entry value of the soil is reached. This means that the piezometers can effectively measure suction up to the air entry value of the soil because the soil functions as an HAE filter.

5.3.4 Neutron Moisture Probe

In addition to the GS1 moisture sensors, a neutron moisture probe was selected to measure the water content of the subgrade. Unlike the other instruments used at AL 5, the neutron moisture probe is not automated and must be manually read on site. A Troxler Model 4300 Depth Moisture Gauge, shown in Figure 143, was acquired by ALDOT for use at AL 5. This model consists of a shield and control unit that attaches to a 1.5 inch diameter probe. The probe contains a neutron source and detector and can be lowered down an access tube to the desired depth to take volumetric moisture readings. The Model 4300 comes with a factory calibration that was performed in sand, but it is recommended that site specific calibrations be performed, especially for soil types other than sand. PVC tube was used for the hydroprobe wells and unfortunately a consistent calibration was not achieved. Therefore, the hydroprobe measurements were discontinued and not included in the report.

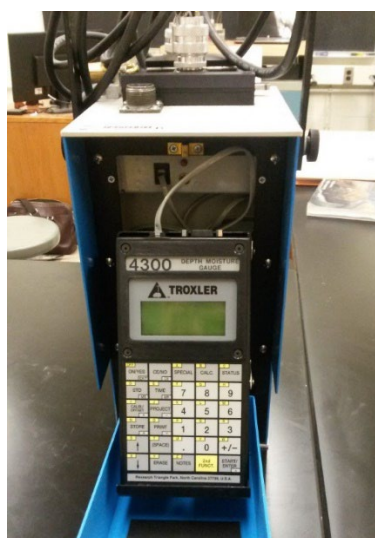


Figure 143: Troxler Model 4300 Depth Moisture Gauge

5.3.5 Asphalt Strain Gages

Asphalt strain gages were used in this study to try to continuously measure the level of pavement distress. Two types of asphalt strain gages (ASGs) were used at AL 5. The ASG-152 from CTL Group was used in Test Section 1 to monitor the sand blanket. Geocomp asphalt strain gages were used for all other sections. CTL and Geocomp ASGs are shown in Figure 144 and Figure 145, respectively.

Because the sand blanket was fully reconstructed, the ASGs were able to be installed on top of the aggregate base. Because of this, the sand blanket ASGs had to be ordered and installed several months prior to the remaining gages. CTL had the required gages in stock and could deliver them in time for installation. For the remaining gages, which were installed on a milled surface, Geocomp was able to provide a better price and had a shorter delivery time than CTL. Furthermore, CTL gages were installed during the 2015 NCAT Test Track rebuild and had very low survivability. Therefore, the decision was made to use Geocomp gages in the remaining test sections.



Figure 144: CTL Asphalt Strain Gage



Figure 145: Geocomp Asphalt Strain Gage

The CTL and Geocomp ASGs are almost identical in construction. Each gage consists of a full Wheatstone bridge circuit with four active 350 ohm strain gages mounted on a 6/6 nylon rod. A temperature resistant coating is applied to each gage to ensure it survives paving. Each gage is individually calibrated by the manufacturer.

5.3.6 Data Acquisition System and Weather Station

A CR6 datalogger from Campbell Scientific was used to monitor the sensors in each location. This datalogger is capable of reading all the sensor types used for this project without additional interfaces. The datalogger is powered by a BP12/CH200 power supply and charging regulator from Campbell Scientific. Each station is also equipped with a solar panel to recharge the batteries. Three AM16/32B multiplexers were used at each station to connect the moisture sensors, piezometers, and asphalt strain gages. Figure 146 shows the CR6, BP12/CH200, and AM16/32B. A Campbell Scientific WTX520 weather sensor was also selected to measure air temperature, barometric pressure, wind speed, wind direction, relative humidity, and precipitation. The WTX520 is shown in Figure 147.

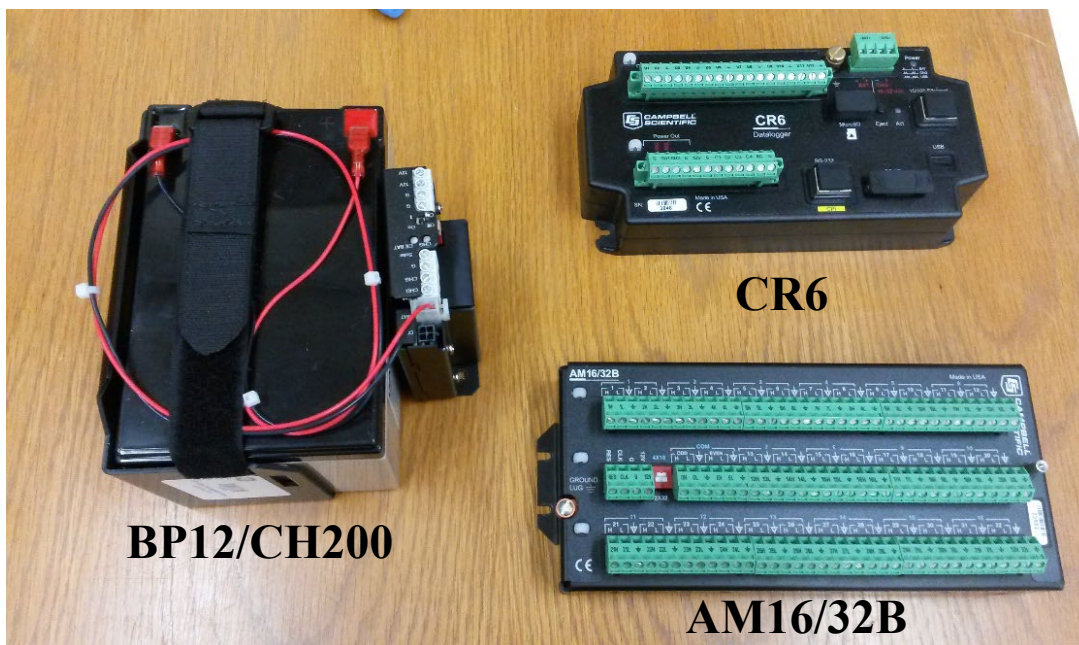


Figure 146: Campbell Scientific CR6, AM16/32B, and BP12/CH200



Figure 147: Campbell Scientific WTX520

Communication equipment was also included in the data acquisition system to allow the data to be collected remotely. This consisted of a spread-spectrum radio for communication between each station and a single cellular modem at a master datalogger that can be accessed remotely. The RavenXTV from Campbell Scientific was selected as the cellular modem. Prior to selecting radios, a test of various radio and antenna combinations was conducted. For this test, a base radio was placed at a datalogger location and a test radio was moved to the next location and communication was attempted. If communication failed, a different radio/antenna combination was tried until a combination worked. Based on the results of the radio test, RF451 radios from Campbell Scientific were selected with 0 dBd omni ¼ wave whip antennas. The RavenXTV and RF451 are shown in Figure 148.

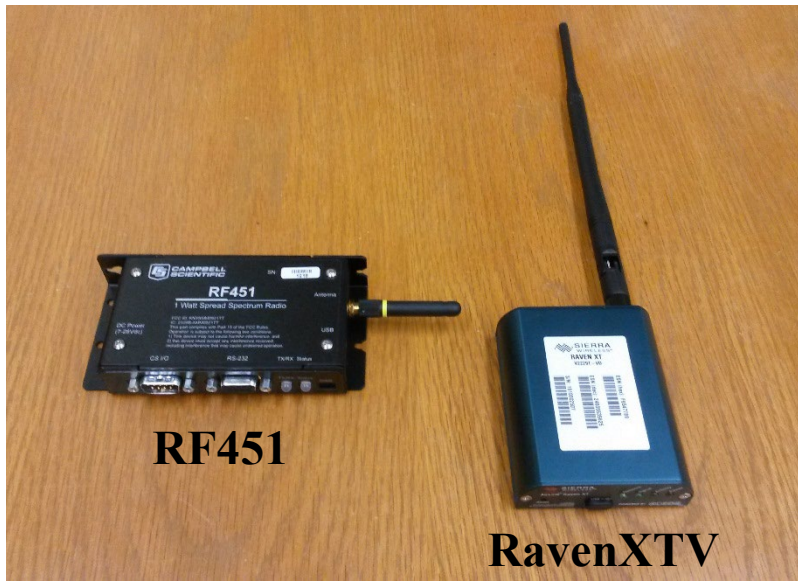


Figure 148: Campbell Scientific RF451 and RavenXTV

5.4 Sensor Installation

5.4.1 Instrumentation Locations

To measure the subgrade behavior and evaluate the remediation techniques, each test section that received remediation was instrumented with moisture, suction, pore pressure, and asphalt strain sensors. Neutron moisture probe monitoring wells were also installed near all instrument locations. The decision was made to use the first portion of Test Section 1 as the instrumented control section. This was because the soils in the remaining control sections (Test Section 6 – 8) were slightly different from the rest of the soils on the project (Stallings 2016). In

addition to the remediated test sections, the shoulder near a large tree was instrumented with moisture and suction sensors and neutron moisture probe monitoring wells. Figure 149 and Table 20 describe the locations of each set of instruments.

Table 20: Instrument Locations

Section	Mile Point
Control	50.900
Sand Blanket	51.066
Vertical Barriers	51.549
Lime Columns	52.140
Paved Shoulders	52.772
Edge Drains	53.102
Tree	53.287

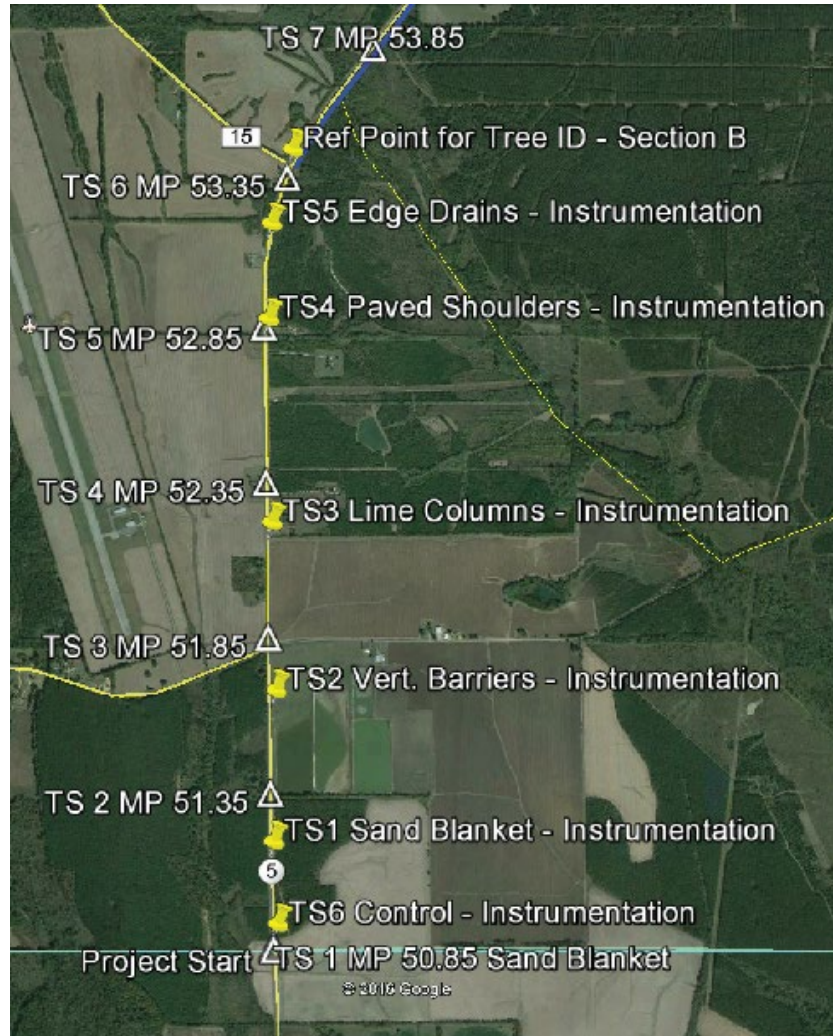


Figure 149: Instrumentation Locations

The original proposed instrument plan is shown in Figure 150. After construction considerations and other decisions, the final plan was amended. The as-built sensor layout is shown in Figure 151. To monitor moisture content, suction, and pore pressure with depth, these sensors were installed in boreholes in the pavement and shoulder. Neutron moisture probe monitoring wells were installed near each instrumented borehole. The asphalt strain gages were installed in the pavement adjacent to the borehole sensors. Data acquisition equipment was installed at each instrument location as shown in Figure 152. An effort was made to locate the instruments far enough from the test section boundaries to avoid end effects.

5.4.2 Downhole Sensors

To install the downhole sensors, a 6 inch diameter borehole was drilled to a total depth of 12 feet. The sensors were then installed from the bottom up. Four moisture sensors, four suction sensors, and two piezometers were installed in each borehole. Target depths were 2.5 ft, 5.0 ft, 7.5 ft, and 10.0 ft for the moisture and suction sensors. Target piezometer depths were 12.0 ft and 7.5 ft. The borehole was backfilled to each installation depth with native material and compacted using an inclinometer tube. The backfill procedure was monitored with a downhole camera to ensure the sensors and wires were not damaged. Because measurement volume of the moisture sensors included a portion of the borehole, it was necessary that the borehole be filled with the native material. The clay at AL 5 is also a low permeability material which will minimize preferential flow if it is compacted adequately.

5.4.2.1 Moisture Sensor Installation

The prongs from the moisture sensors had to be inserted into undisturbed soil with no air gaps. In order to insert the sensors horizontally at depths of up to 10 feet, an installation tool was fabricated at Auburn University. The tool consists of a scissor jack mounted to a half section of a six inch diameter steel pipe, shown in Figure 153. The moisture sensor was seated on the scissor jack as shown in Figure 154. As the jack extended the sensor prongs were pushed into the soil. A small piece of electrical tape was used to hold the moisture sensor to the tool while it was lowered down the borehole. Extendable rods were used to lower the tool down the borehole and operate the scissor jack. The tool was designed to rest on the bottom of the borehole and install the sensor 12 inches above the bottom of the hole. A six inch diameter borehole was required to install the moisture sensors using the installation tool.

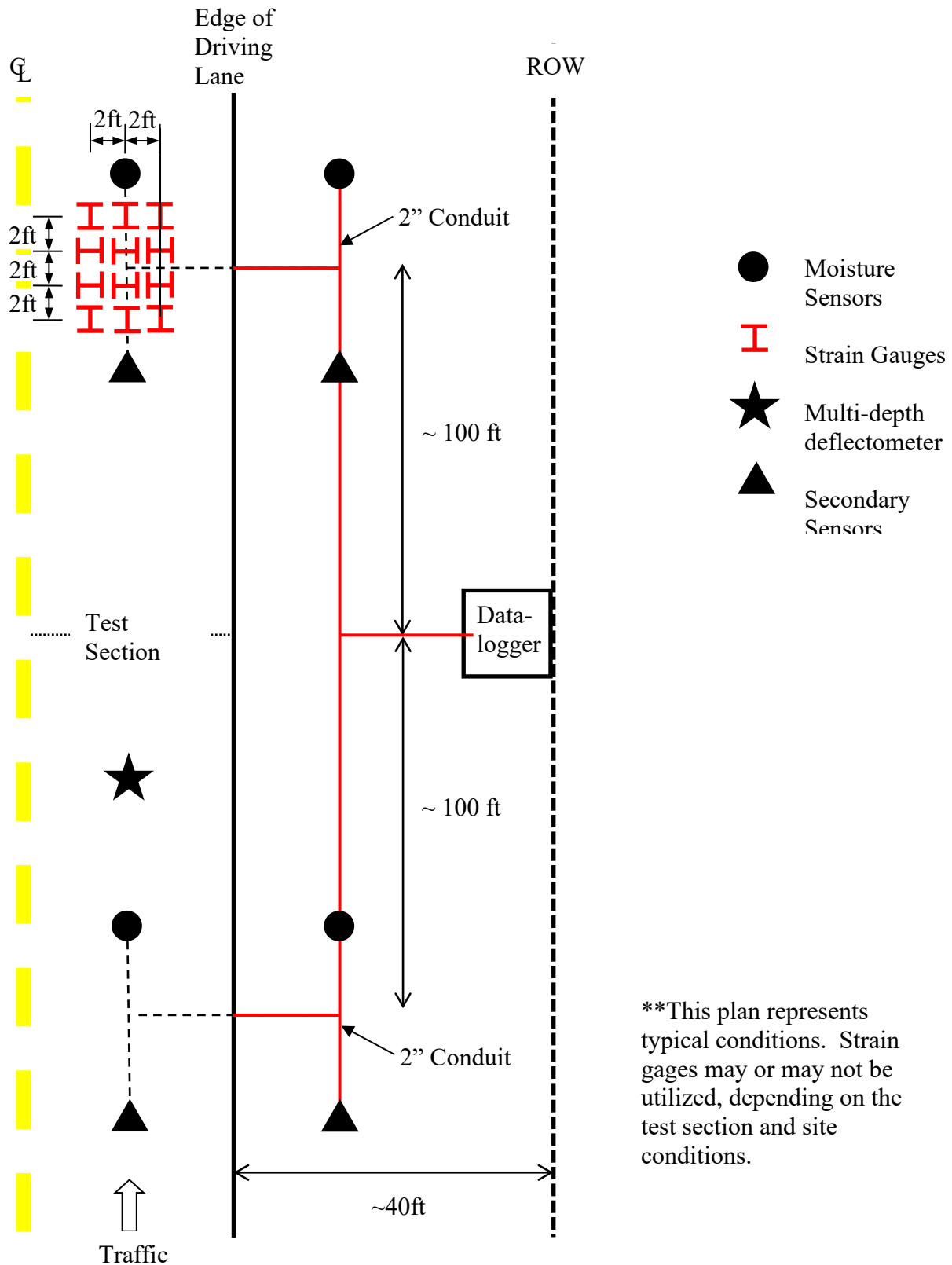


Figure 150: Proposed Sensor Locations

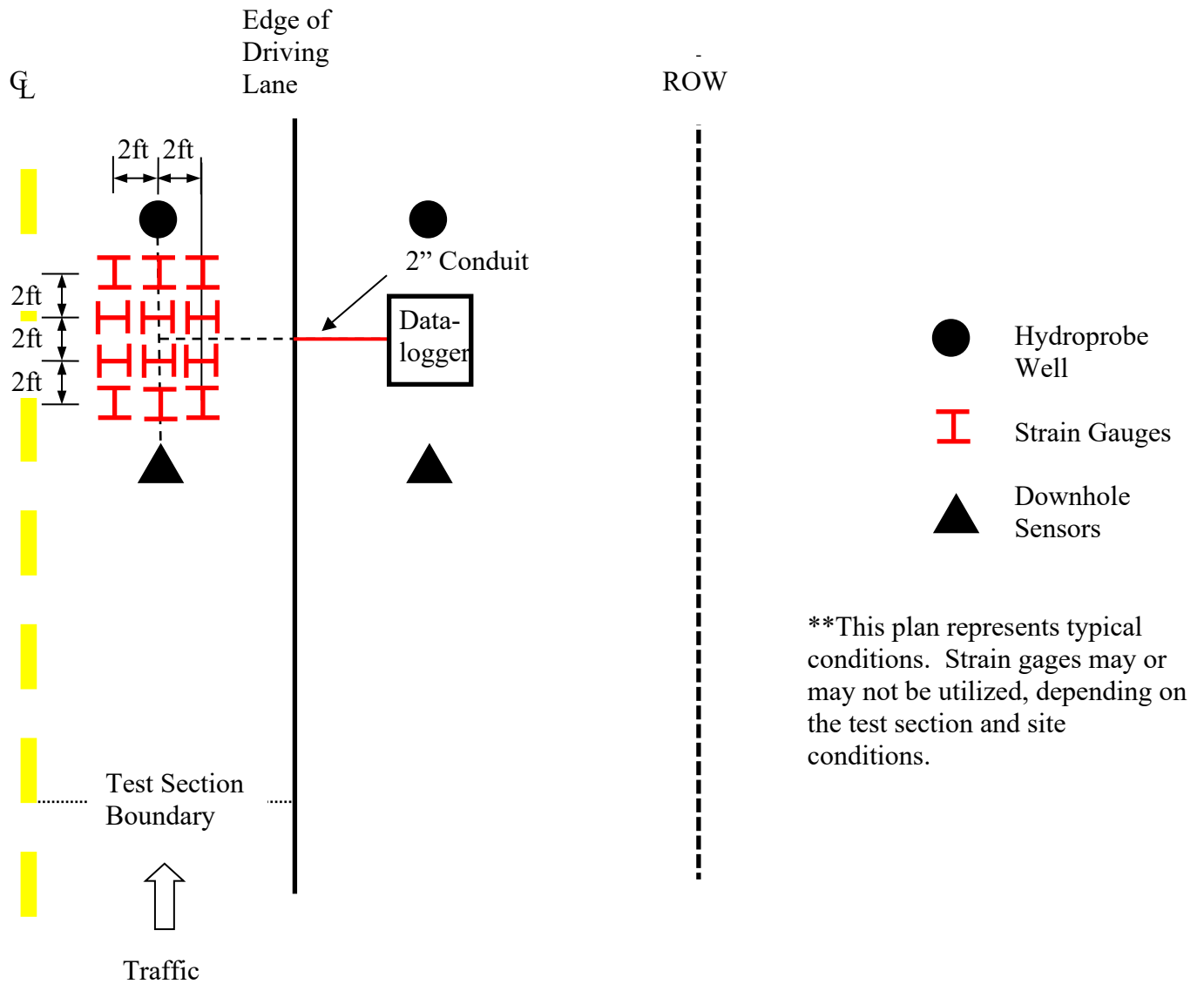


Figure 151: As-Built Sensor Locations



Figure 152: Data Acquisition Installation



Figure 153: Moisture Sensor Installation Tool



Figure 154: GS1 Seated on Installation Tool

Moisture sensor installation at AL 5 proceeded as planned for the most part. The borehole was backfilled and compacted to 12 inches below the target installation depth to facilitate the installation tool. Due to the backfill procedure used, the actual installation depths typically varied by ± 0.1 ft from the target depths. Sensor installation depths are shown in Appendix A. A downhole camera was used to verify the moisture sensor was seated on the installation tool properly and that it was fully inserted into the sidewall of the borehole without the prongs bending. Figure 155 shows a sensor being lowered down the borehole on the installation tool. Figure 156 and Figure 157 show downhole photographs of the moisture sensor installation. Care was taken to ensure other sensors and wires were outside the measurement volume of the moisture sensors, shown in Figure 140.



Figure 155: Moisture Sensor and Installation Tool being Lowered down Borehole



Figure 156: Moisture Sensor Installation



Figure 157: Fully Installed Moisture Sensor

All moisture sensors were installed as described above with the exception of the 7.5 ft sensor in the shoulder borehole of the control section. Due to a malfunction of the installation tool, this sensor could not be installed in the sidewall. Instead, the prongs were inserted into some drill shavings and the sensor was lowered down the hole, shown in Figure 158. Due to possible air gaps near the sensor, the accuracy of readings from this sensor are questionable.



Figure 158: Moisture Sensor Prongs Inserted into Drill Shavings

5.4.2.2 Suction Sensors

The suction sensors were installed according to the manufacturer's recommendations. Once the appropriate depth was reached, native soil was packed around the ceramic disk. Care was taken not to smear the soil on the disk, but to ensure good hydraulic contact. A prepared suction sensor is shown in Figure 159. This prepared sensor was lowered down the borehole to the correct depth and the hole was backfilled and compacted. A downhole camera was used to monitor the compaction process to ensure the sensor was not damaged.



Figure 159: Suction Sensor Preparation

5.4.2.3 Piezometers

Two piezometers were installed in each borehole at depths of approximately 12.0 ft and 7.5 ft. The typical procedure for installing piezometers is to place the piezometer in a large volume

sand pocket and seal the borehole with bentonite. As noted by Mikkelsen and Green (2003), this procedure was developed for stand pipe piezometers and is not necessary for diaphragm (vibrating wire) piezometers. Therefore, the piezometers were placed in a small bag full of saturated filter sand and lowered down the borehole. The hole was then backfilled and compacted with native material. Because the native material has a very low permeability, it would serve the same function as a bentonite or grout seal. Figure 160 shows the piezometer in the sand-filled bag being lowered down the hole.



Figure 160: Piezometer in Sand-Filled Bag being Lowered Down the Borehole

5.4.3 Asphalt Strain Gage Installation

Twelve asphalt strain gages (ASGs) were installed in the sand blanket and eight were installed in all other sections. The sand blanket ASGs were ordered and installed several months before the remaining sensors. When the remaining sensors were ordered, it was decided to decrease the number of ASGs to eight to minimize costs. The layout of the strain gages is shown in Figure 161 and Figure 162. These layouts provide redundancy for both longitudinal and transverse strain. The centerline of the strain gage array was at approximately the center of the travel lane.

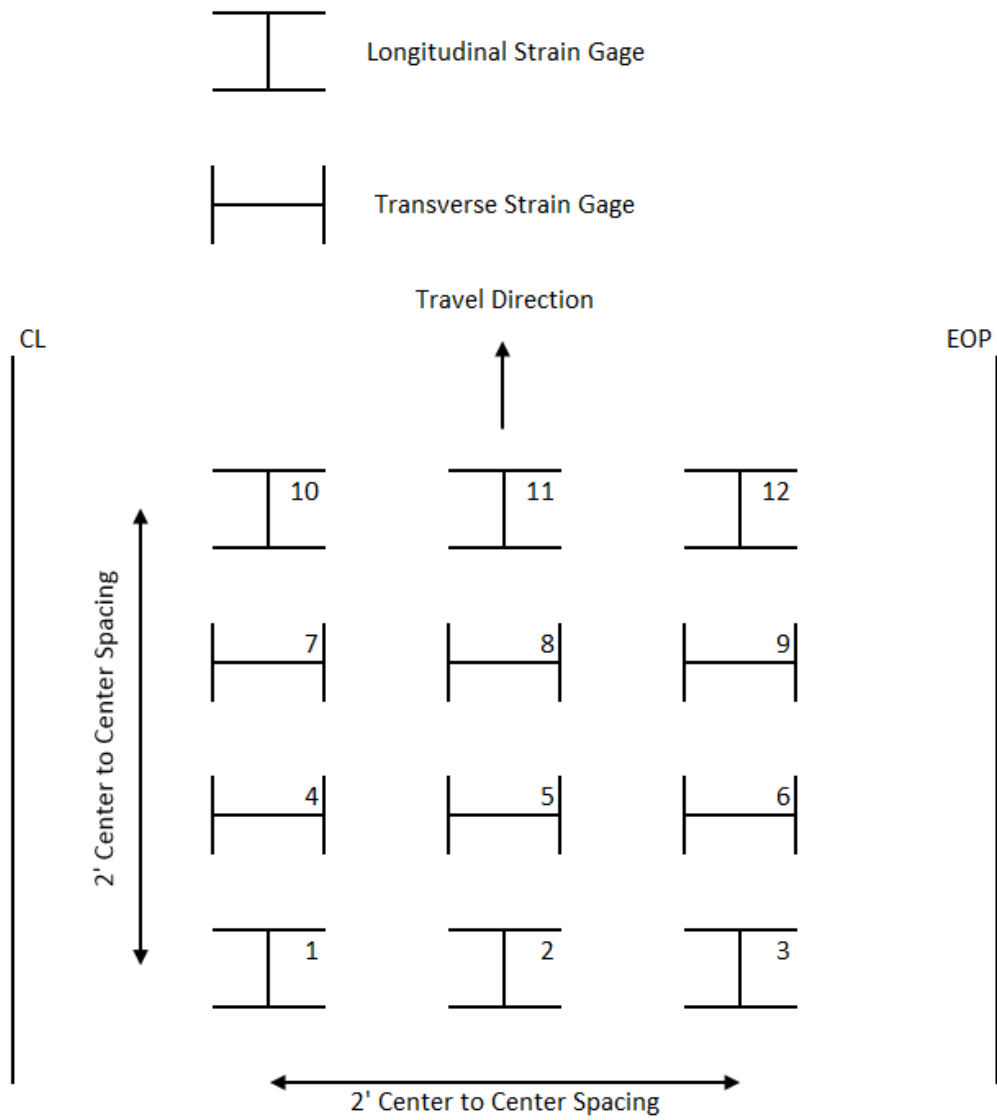


Figure 161: Sand Blanket Strain Gage Layout

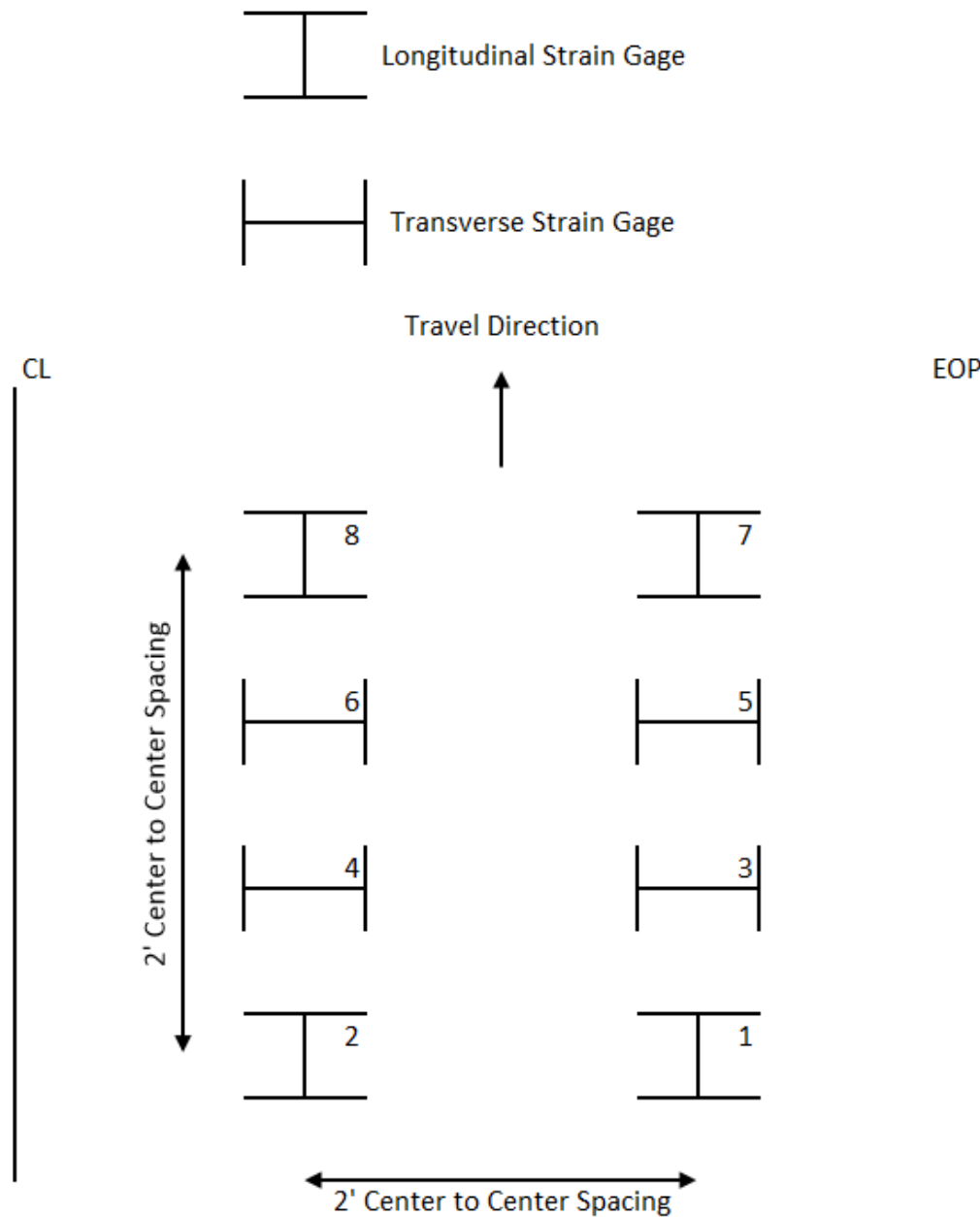


Figure 162: Strain Gage Layout for Sections Other than Sand Blanket

5.4.3.1 Sand Blanket Asphalt Strain Gages

Because the sand blanket was full depth construction, it was possible to install the asphalt strain gages on top of the aggregate base. This is the procedure that has been used at the NCAT Test Track (Timm 2009).

The gages were first laid out in the correct position and the wires were routed to the edge of the pavement. The wires were then placed in 3/8 inch flexible conduit for added protection. Small trenches were dug in the aggregate base for the wires. Once the wires were in place, the trenches were backfilled and compacted. Immediately prior to paving, the gages were tacked in place using a tack-sand mixture. This is typically done with a binder-sand mixture (Timm 2009), but the paving contractor was unable to provide binder to the site. Tacked gages are shown in Figure 163. Once the gages were tacked in place they were covered with asphalt that was screened through a ¼ inch screen. Static compaction was used to compact the mounds of asphalt over the gages. Figure 164 shows screened asphalt being placed and compacted over the gages. The paving train then passed over the gages. No vibratory compaction was used for the first pass of the roller over the gage array. The gages were monitored during the placement and compaction of the asphalt.



Figure 163: ASGs being Tacked with Tack-Sand Mixture



Figure 164: Screened Asphalt being Placed and Compacted over Gages

5.4.3.2 All Other Asphalt Strain Gages

Because the test sections other than the sand blanket only received resurfacing and not full depth construction, the strain gages could not be placed in the aggregate base. Instead, sections were milled out for the gage placement, shown in Figure 165. The sections were milled to a depth of three inches to ensure adequate coverage of the ASGs. The gages were then laid out in the proper position. Prior to paving, the gages were tacked to the milled surface using the same tack-sand mixture described above. Once again, the paving contractor was unable to provide binder to the site. After the gages were tacked, the gages and wires were covered with screened asphalt as described above. Because the wires could not be buried in trenches, they were not placed in conduit, but they were covered with screened asphalt. The wires from the borehole sensors were also covered with screened asphalt. Figure 166 shows the gage array covered with screened asphalt. The gage array was then paved over and compacted without vibration.



Figure 165: Section Milled and Cleaned for placement of ASG Array



Figure 166: Gage Array on Milled Surface Covered with Screened Asphalt

5.5 Sensor Survivability

Sensor survivability was very good at AL 5. All moisture sensors and piezometers survived and are providing reasonable outputs. Five asphalt strain gages did not survive, possibly due to over stressing during construction. A possible future point of failure for the Geocomp asphalt strain

gages is the connection of the sensor leads to the datalogger. The leads were very small and tended to break off once they were wired into the datalogger.

All suction sensors initially provided readings, but several stopped functioning shortly after baseline readings were taken. The cause of suction sensor failure in the other sections is currently unknown but is being investigated further. It is also unknown if the suction sensors are merely temporarily disabled or have permanently failed. Table 21 summarizes the sensor survivability by test section. The overall sensor survivability was 93%.

Table 21: Sensor Survivability

	Moisture			Suction		
Test Section	Surviving	Total	Percent Surviving	Surviving	Total	Percent Surviving
Control	8	8	100%	8	8	100%
Sand Blanket	8	8	100%	8	8	100%
Vertical Barriers	8	8	100%	6	8	75%
Lime Columns	8	8	100%	7	8	88%
Paved Shoulders	8	8	100%	6	8	75%
Edge Drains	8	8	100%	6	8	75%
Trees	4	4	100%	3	4	75%
Total	52	52	100%	44	52	85%
	Piezometer			ASG		
Test Section	Surviving	Total	Percent Surviving	Surviving	Total	Percent Surviving
Control	4	4	100%	7	8	88%
Sand Blanket	4	4	100%	11	12	92%
Vertical Barriers	4	4	100%	8	8	100%
Lime Columns	4	4	100%	6	8	75%
Paved Shoulders	4	4	100%	8	8	100%
Edge Drains	4	4	100%	7	8	88%
Trees	NA	NA	NA	NA	NA	NA
Total	24	24	100%	47	52	90%

Chapter 6. Results and Discussion

The sensors were monitored beginning November 2016 through June of 2020. During that period the number of active sensors generally declined. Weather data was collected continuously during the project. The pavement strain gages showed cyclic tension and compression behavior until they began to fail. Moisture sensors reflected cycles of wetting and drying. A limited number of suction sensors appeared to desaturate and show significant matric suction. Finally, the pore pressure sensors were the most robust of all installed, reflecting a rather consistent water table level. The sections that follow discuss the time series results for each sensor type, grouped by test section.

6.1 Climatological Data

Data collected using the weather station and nearby weather data from Uniontown and Selma are presented in Figure 167 in terms of rainfall and average temperature. Of note, Alabama was experiencing drought when the sensors were installed in 2016. The first appreciable rain in months occurred in November of that year. From July 2017 to July 2019, rainfall was below average. From August 2019 through the end of monitoring, the rainfall was well above normal. Temperatures were typical and unremarkable. A large number of sensors failed in early to mid-2019.

6.2 Sensor Data

6.2.1 Control

Strain gage data from the control section is shown in Figure 168. The gages showed general trends of compression and tension until majority failure in 2019. Gage 7 was the only strain gage to continuously send data to the datalogger during the monitoring period. Moisture and pore pressure data are shown in

Figure 169 and Figure 170, respectively. The moisture sensors showed fluctuations in depths 7.5 feet and shallower. The 10 ft depth sensors remained stable. The observed pore pressures were nearly constant with some fluctuations during particularly dry and wet periods. This is similar for all test sections.

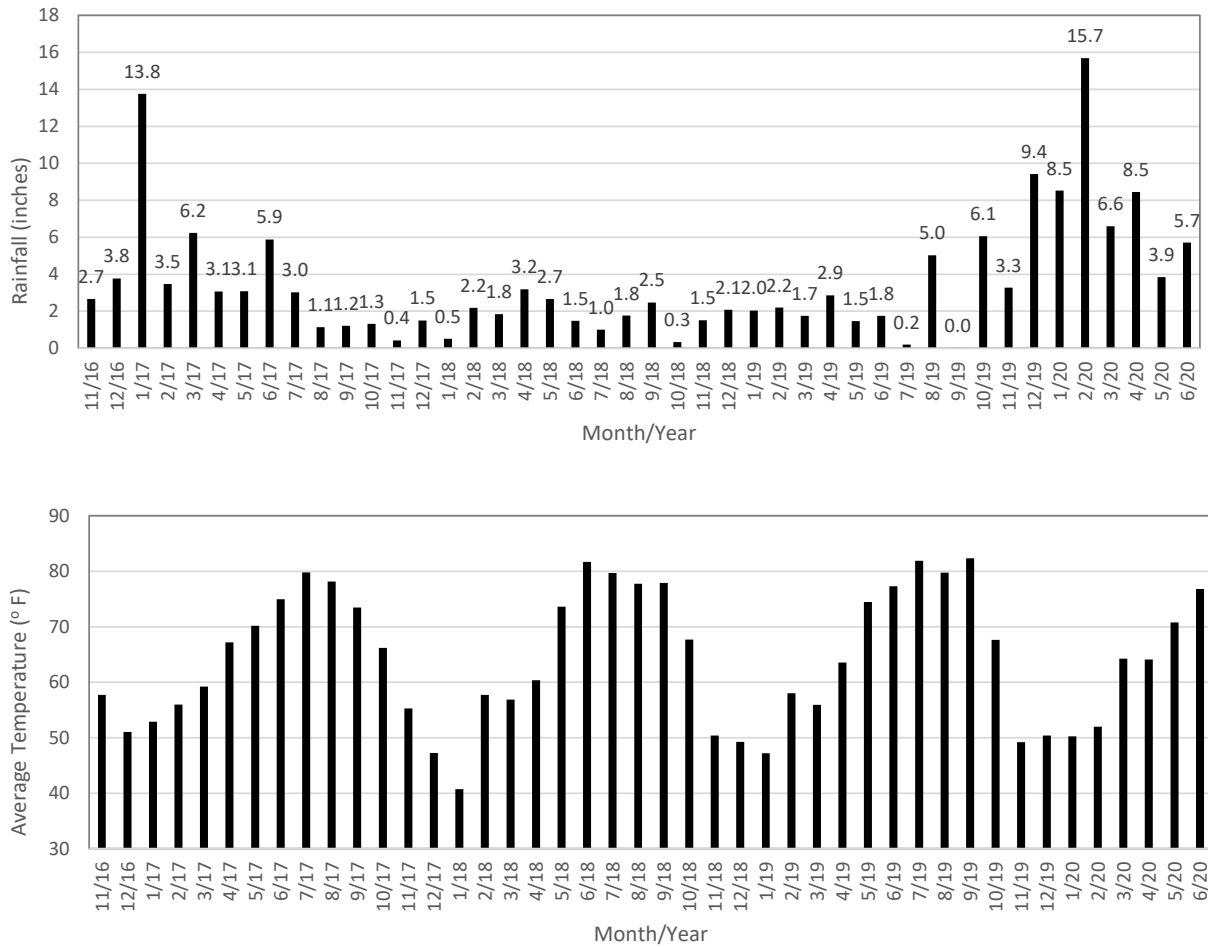


Figure 167: Climatological Data at AL 5

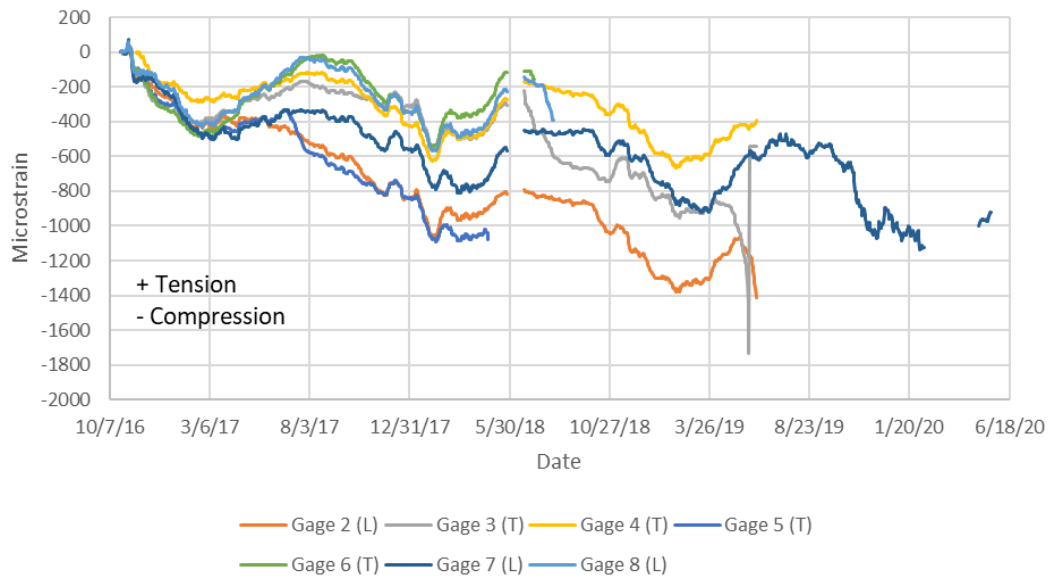


Figure 168: Strain with Time – Control

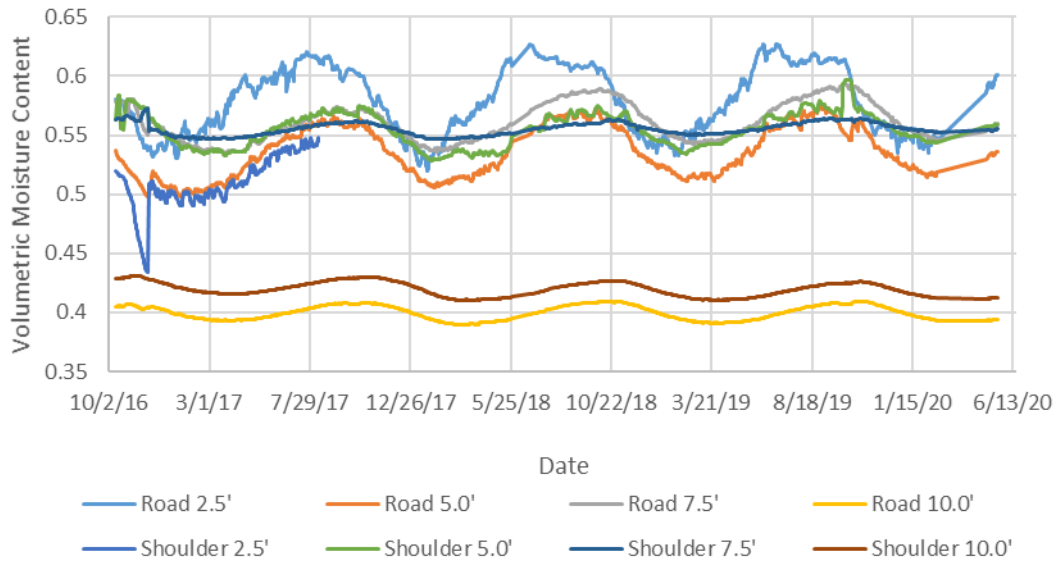


Figure 169: Moisture Content with Time – Control

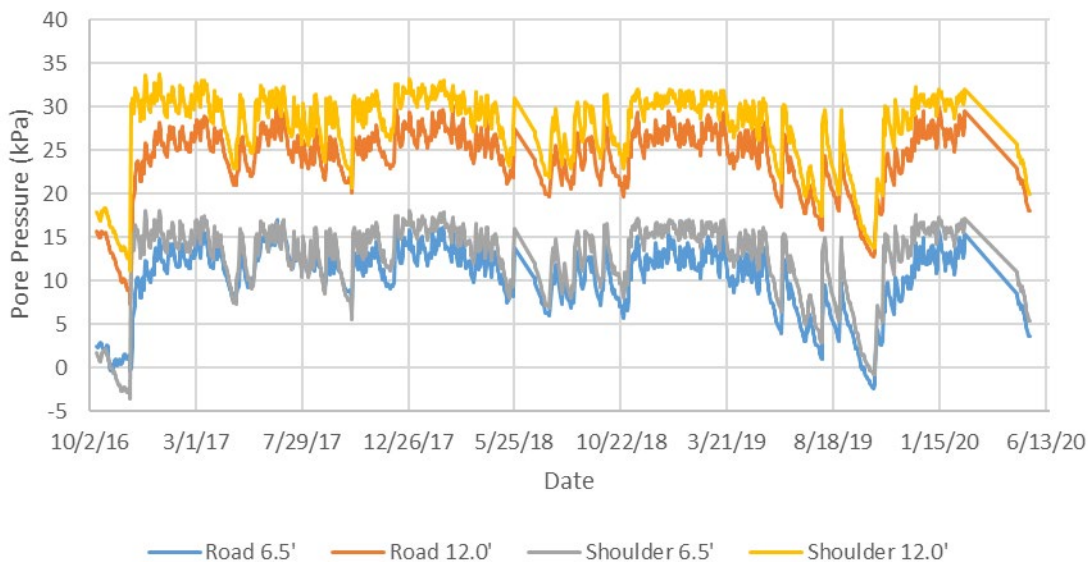


Figure 170: Pore Pressure with Time – Control

6.2.2 Sand Blanket – Test Section 1

Strain gage data for the sand blanket is shown in Figure 171. The strain gages failed during early 2020. It is worth noting that these gages were a different manufacturer than all of the other gages used in the program. Moisture and pore pressure data for the sand blanket is shown in Figure 172 and Figure 173, respectively. Note the 10 ft depth moisture sensor is replaced by an 8 ft depth

sensor under the road and the 10 ft depth sensor under the shoulder failed in 2017, but was stable before failure. Pore pressure response was similar as for the control section.

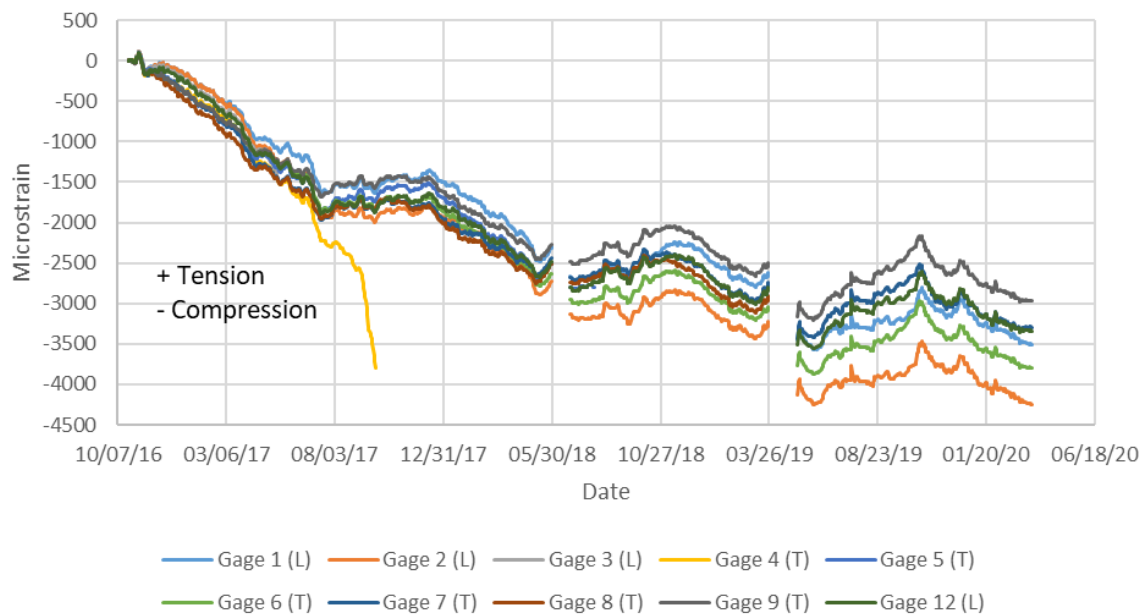


Figure 171: Strain with Time – Sand Blanket

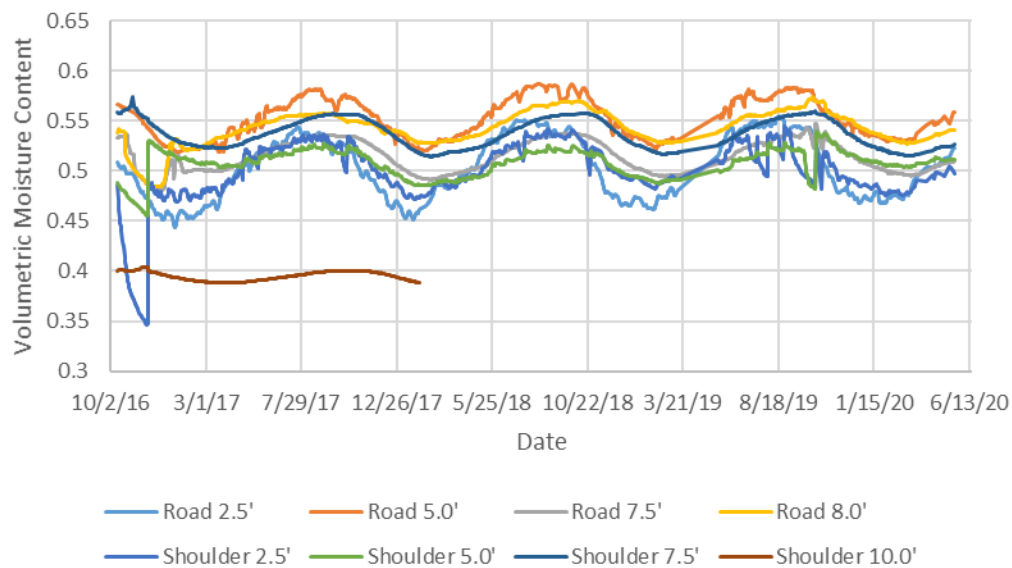


Figure 172: Moisture Content with Time – Sand Blanket

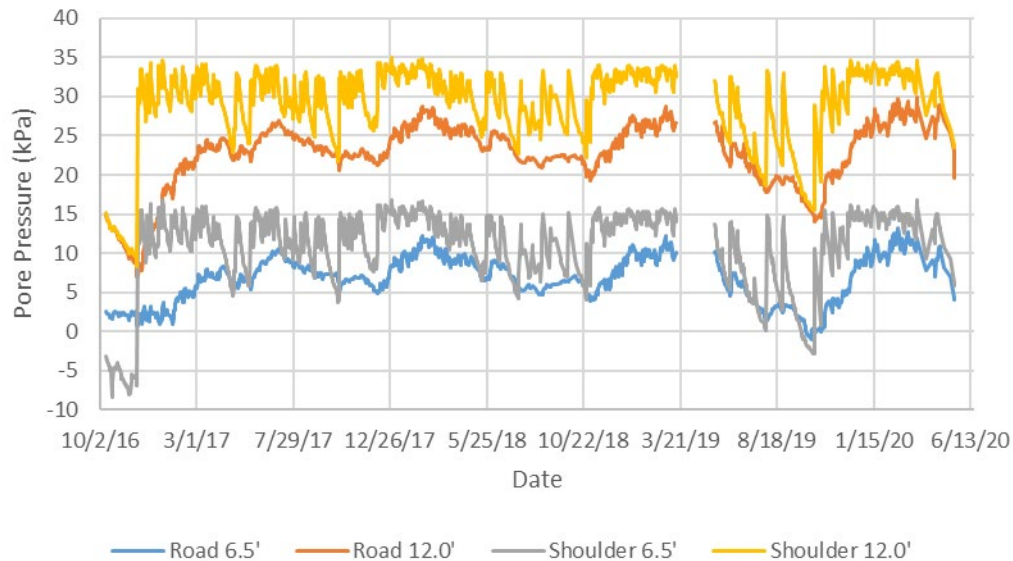


Figure 173: Pore Pressure with Time – Sand Blanket

6.2.3 Vertical Barriers – Test Section 2

Strain data for the vertical barriers test section is shown in Figure 174. The majority of gages functioned until mid-2019. Similar to other sections, some cycles of tension and compression were observed. Of the three gages still reading at the end of monitoring, the trend was toward tension. Moisture and pore pressure data are shown in Figure 175 and Figure 176, respectively. The moisture sensors stopped sending accurate data to the dataloggers in mid-2019 but showed stable values of volumetric water content while operational. Pore water pressures exhibited the same cyclic trends as other sections. The suction sensors in this section showed values below saturation near the end in 2019 following a lag in rainfall. It is noteworthy that sensors reading suction were beneath the roadway.

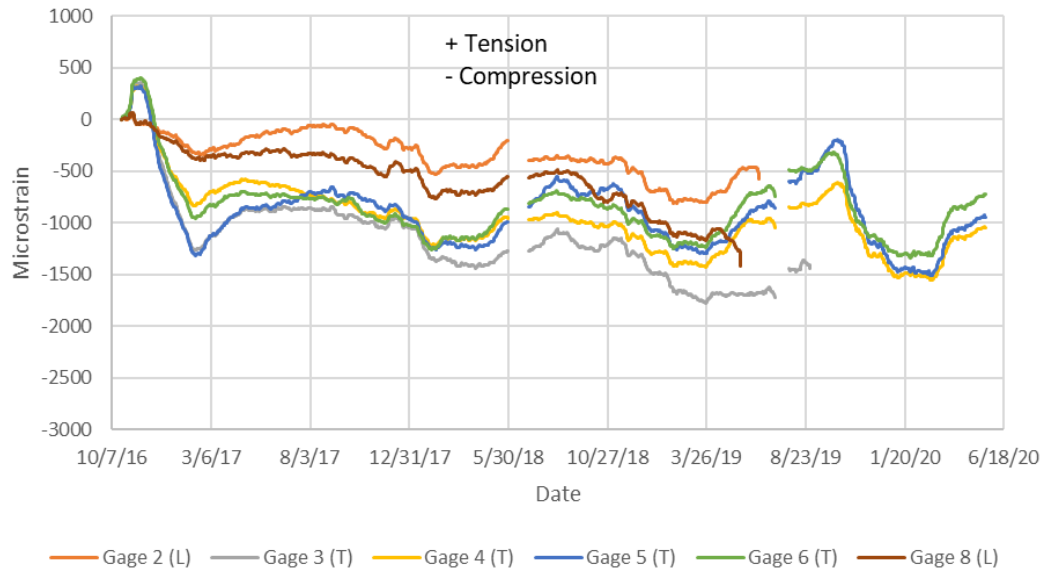


Figure 174: Strain with Time – Vertical Barriers

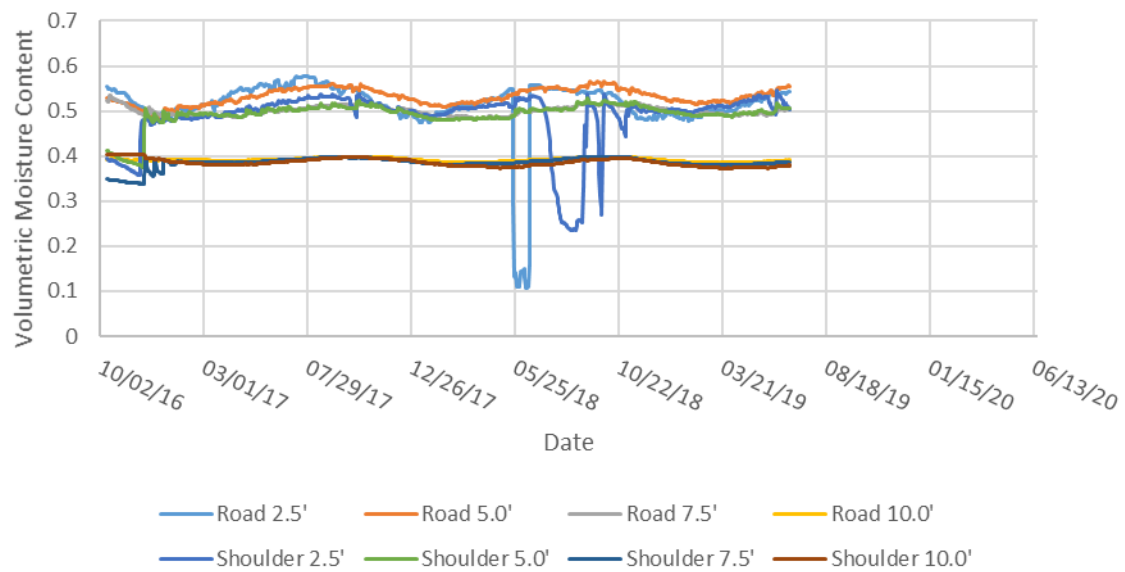


Figure 175: Moisture Content with Time – Vertical Barriers

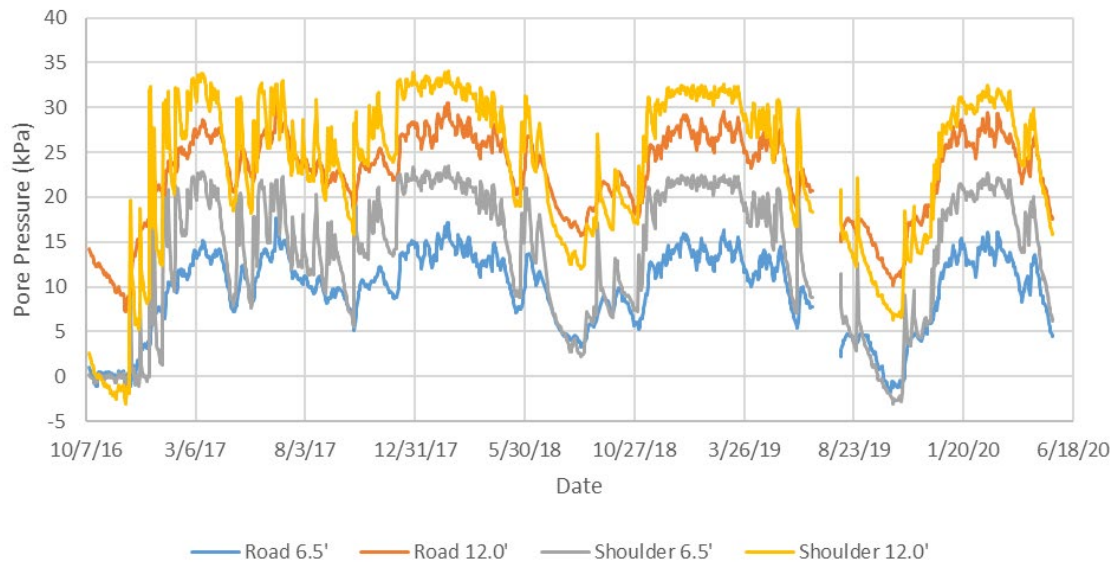


Figure 176: Pore Pressure with Time – Vertical Barriers

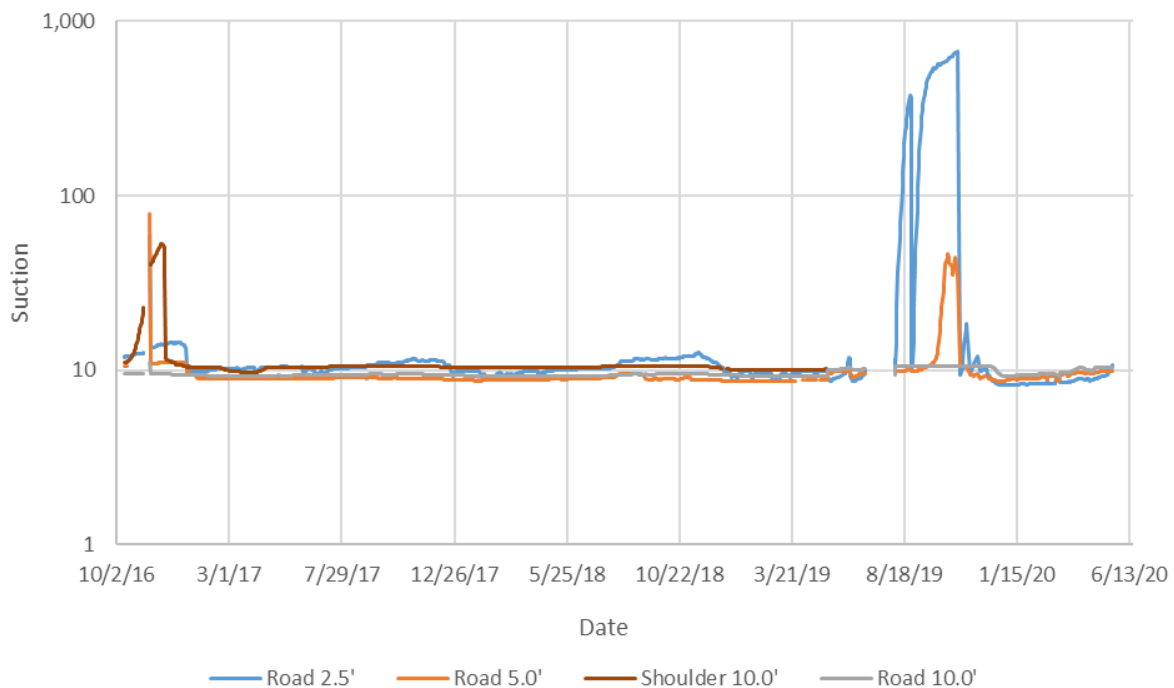


Figure 177: Suction with Time – Vertical Barriers

6.2.4 Lime Columns – Test Section 3

Strain data for the lime columns section is unchanged as shown in Figure 178. There were few gages that functioned in this section, and none of the strain gages in this section were functional as of May 2019. The placement of gages with respect to lime holes may have been a

contributing factor. Moisture and pore pressure response showed the typical time and depth distribution as for other sections and are shown in Figure 179 and Figure 180, respectively.

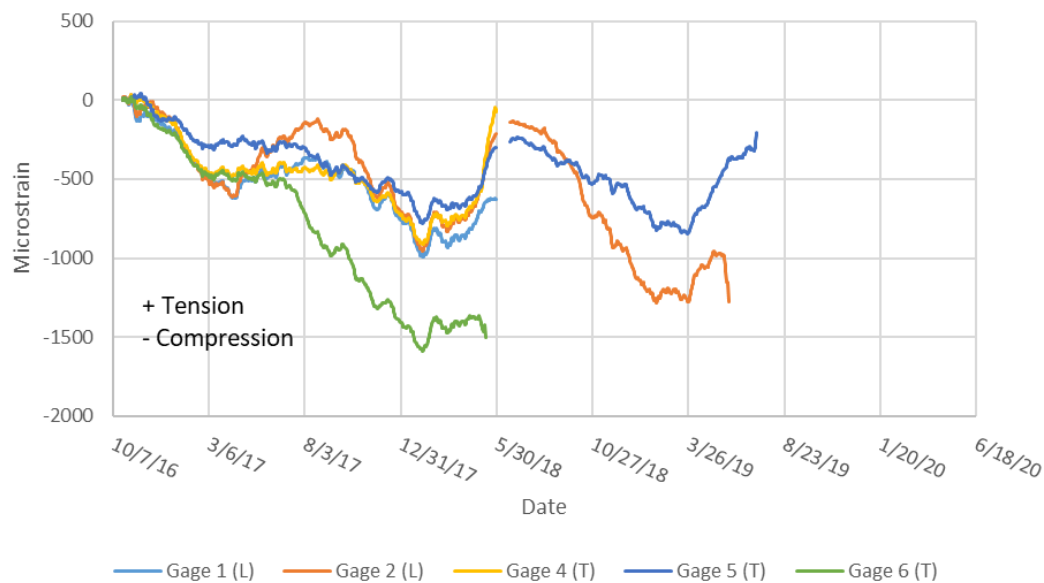


Figure 178: Strain with Time – Lime Columns

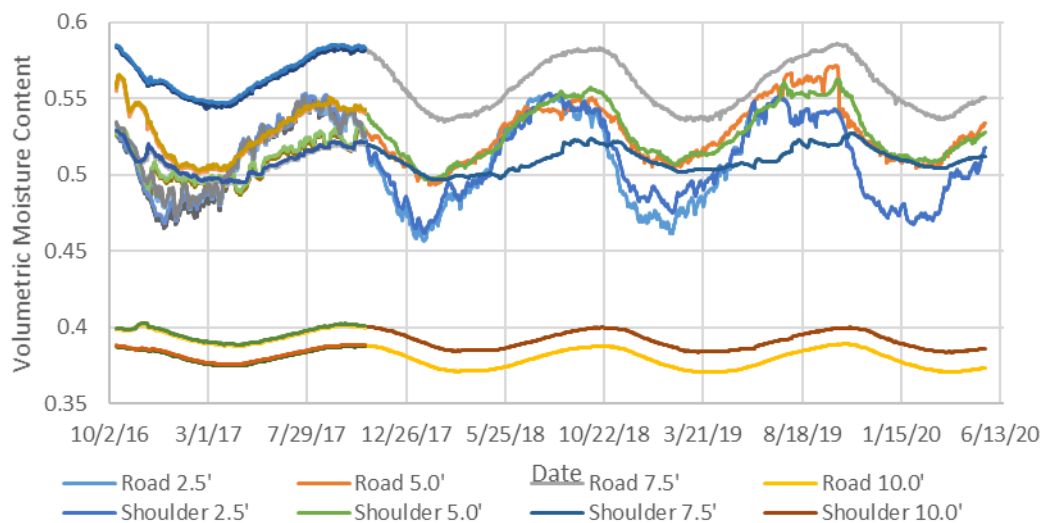


Figure 179: Moisture Content with Time – Lime Columns

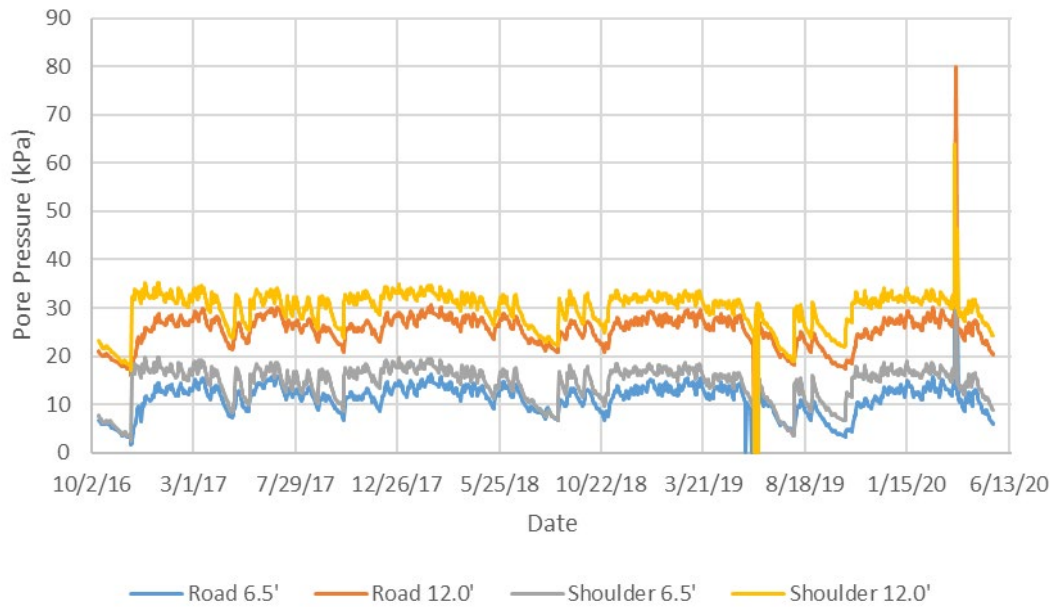


Figure 180: Pore Pressure with Time – Lime Columns

6.2.5 Paved Shoulders – Test Section 4

Strain data for the paved shoulder section is shown in Figure 181. The response was cyclic with tension and compression, but seemed to trend more toward tension than other sections. The last gage ceased function on 12/26/2020. Moisture and pore pressure data are shown in **Error! Reference source not found.** and Figure 183, respectively. As with the other sections, moisture contents were more cyclic near the surface and stable at the 10 ft depth. While there was visible fluctuation in the data, the pore pressures were stable until mid-2019 when some part of the system failed. Suction sensors showed desaturation at the 2.5 ft depths for both the road and shoulder sensors as shown in Figure 184.

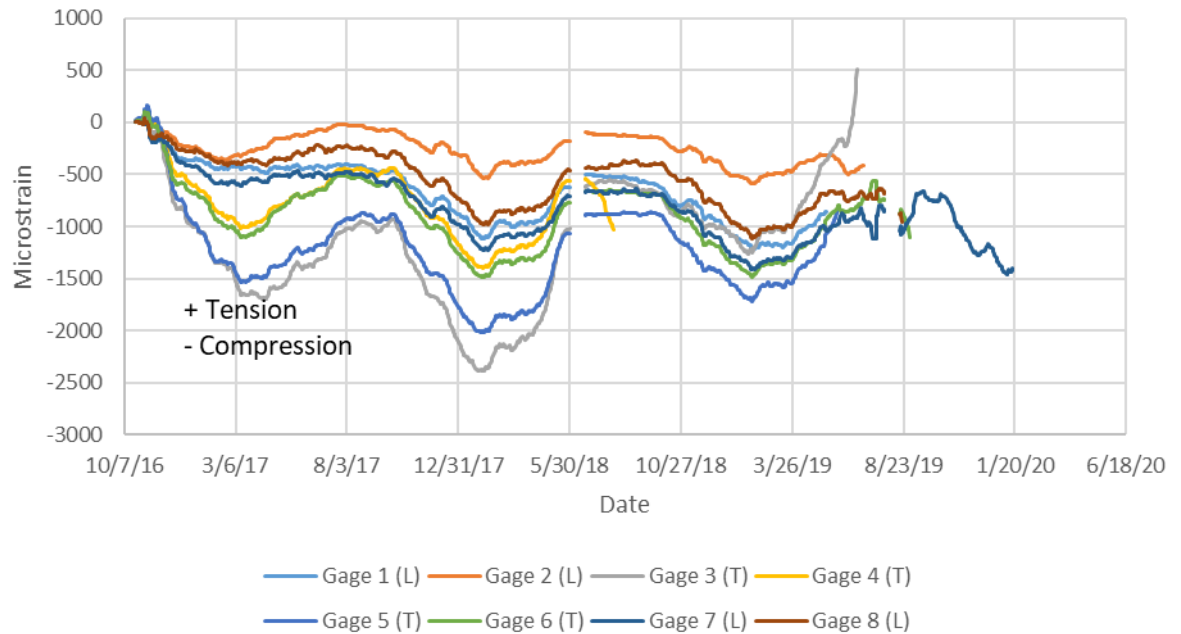


Figure 181: Strain with Time – Paved Shoulders

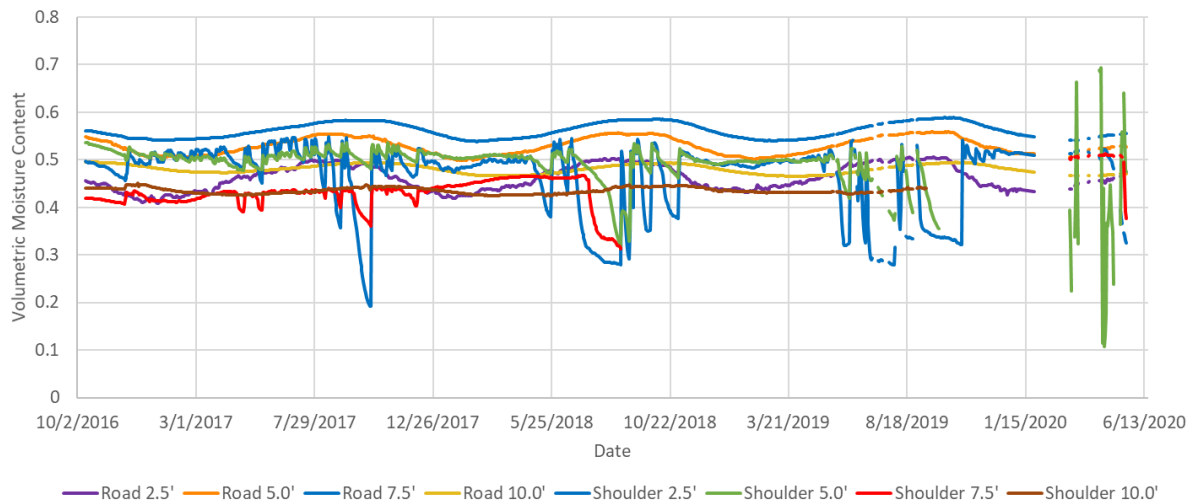


Figure 182: Moisture Content with Time – Paved Shoulders

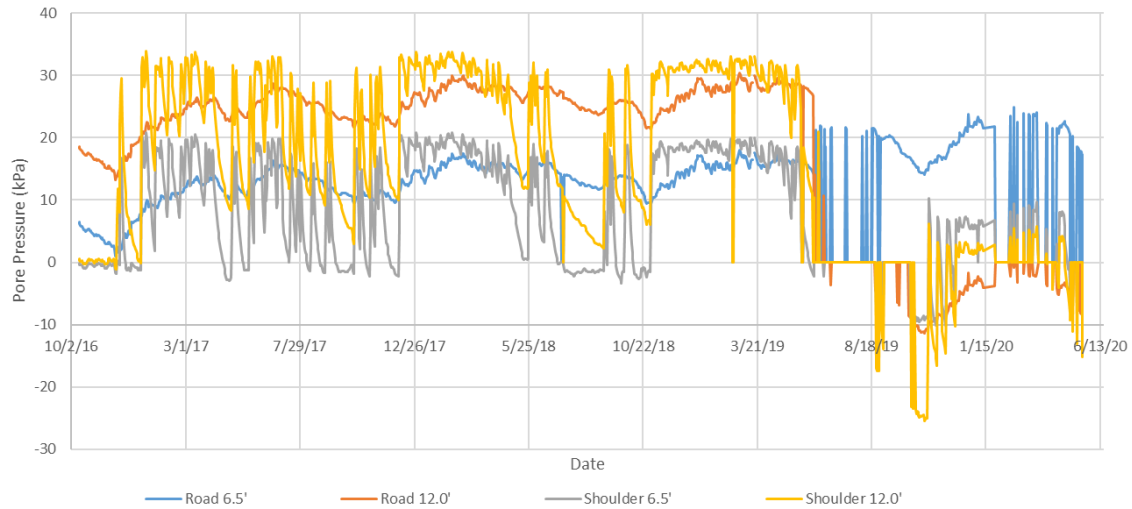


Figure 183: Pore Pressure with Time – Paved Shoulders

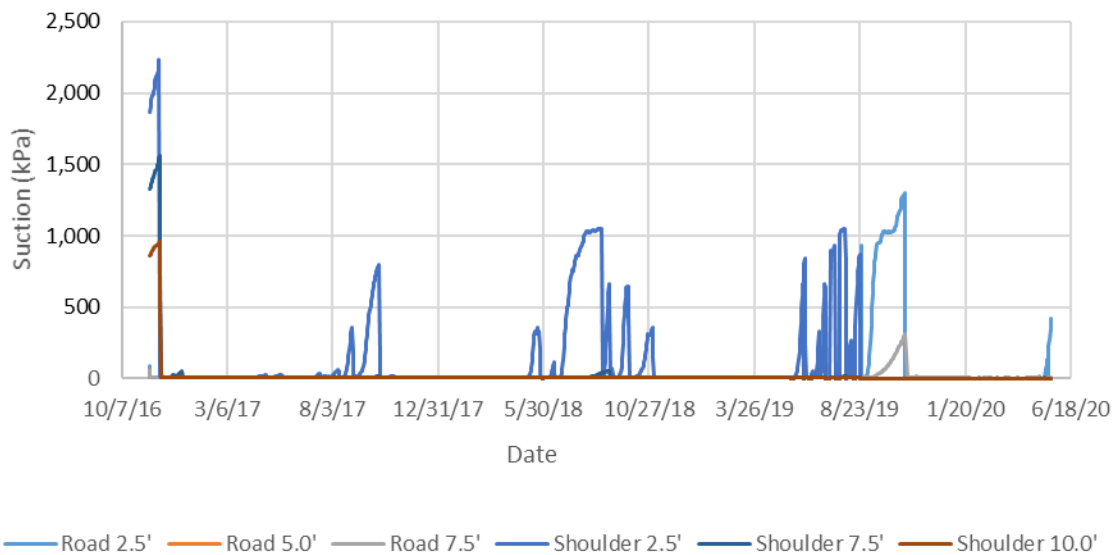


Figure 184: Suction with Time – Paved Shoulders

6.2.6 Edge Drains – Test Section 6

Strain data for the edge drain section is shown in Figure 185. The gages showed the same tension/compression trends as other sections. All strain gages in this section ceased to function in February 2019. Moisture and pore pressure data are shown in Figure 186 and Figure 187 respectively. The moisture sensors showed stable water contents up until late 2018, similar to other sections. The pore pressures showed cyclic behavior as with other sections. There were several

periods of significant, more so than the other test sections. However, the suction gages ceased operation in the fall of 2019.

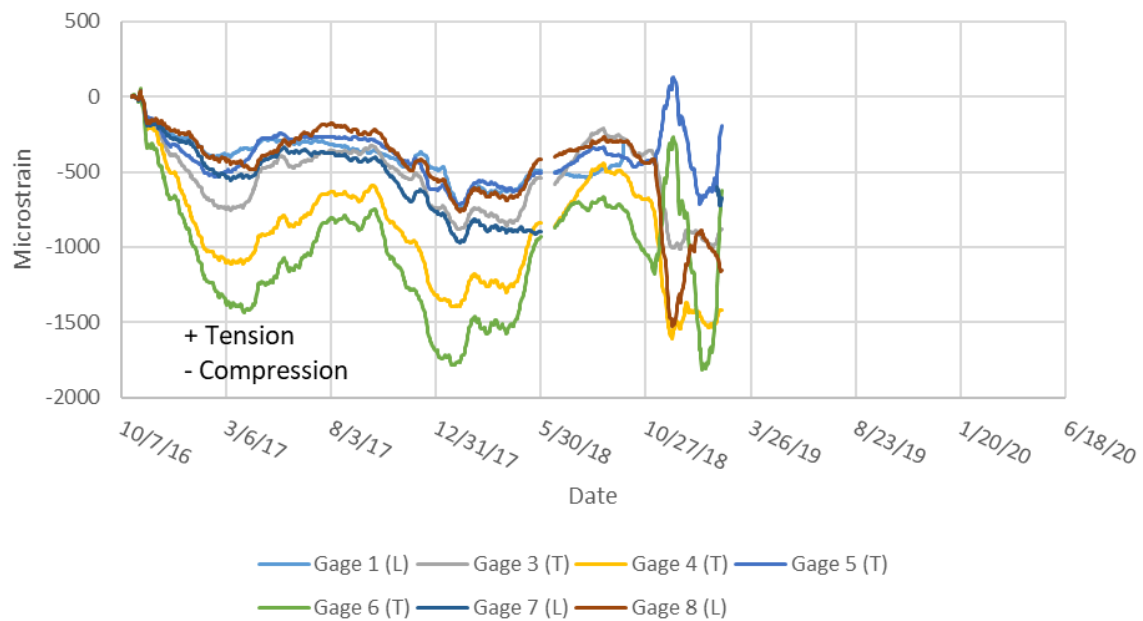


Figure 185: Strain with Time – Edge Drains

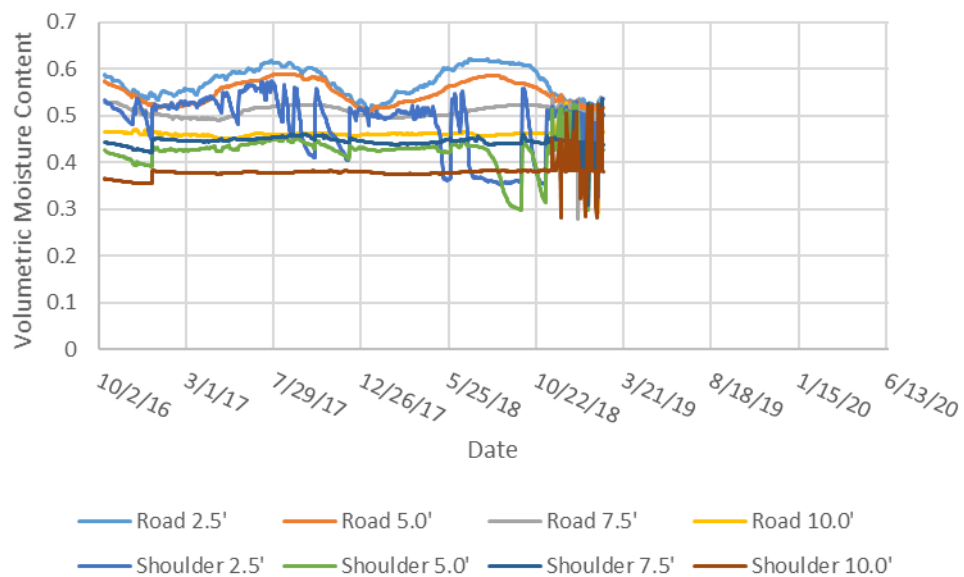


Figure 186: Moisture Content with Time – Edge Drains

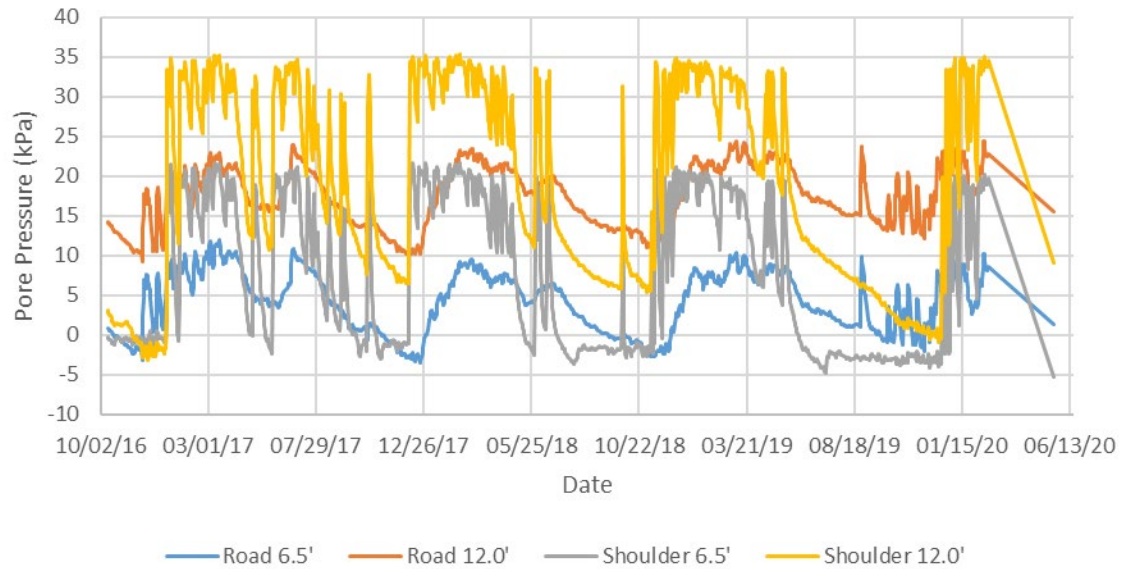


Figure 187: Pore Pressure with Time – Edge Drains

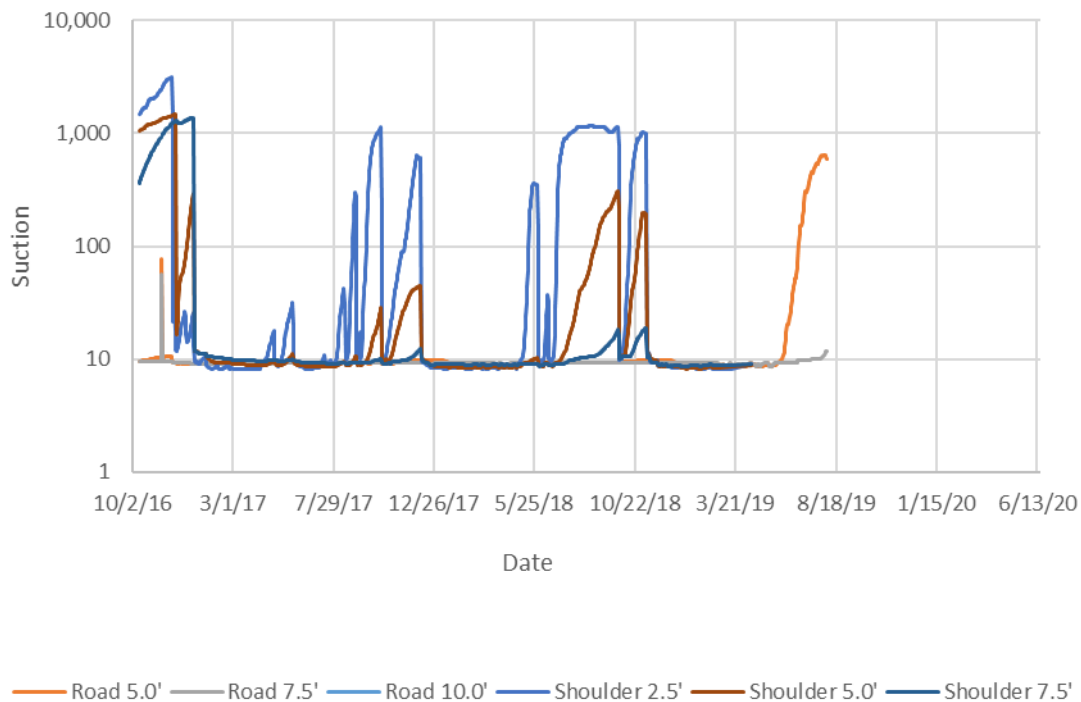


Figure 188: Suction with Time – Edge Drains

6.2.7 Trees

Figure 189 and Figure 190 show the moisture and suction data for the tree monitoring station. The moisture sensors at the tree monitoring station showed less cyclic and more climate related response unlike the other test sections. The suction data mirrored the moisture sensors.

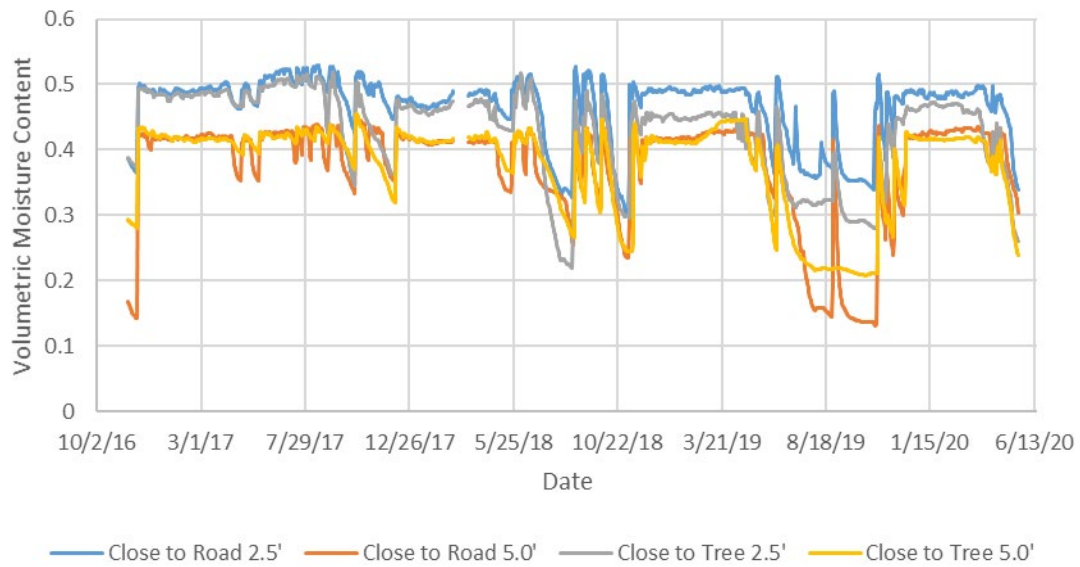


Figure 189: Moisture Content with Time – Trees

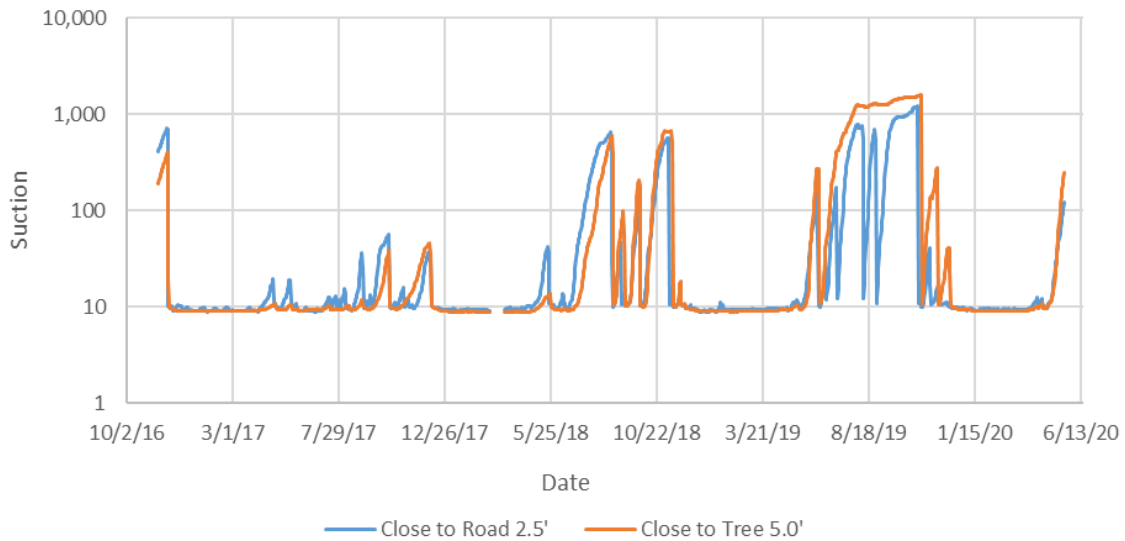


Figure 190: Suction with Time – Trees

6.3 Interpretation of Sensor Data

From the data collected over several years, figures 7, 10, 13, 16, and 19 suggest that the active zone within the AL 5 project lies between 7.5 and 10 ft. Moisture content below the 7.5ft sensor appears to remain stable and is not affected by climate or vegetation. In Figure 191, strain gage readings are plotted against the moisture content below the travel lane. The strain is most sensitive to the 2.5 ft moisture content changes, decreasing with depth of the gage.

It is also interesting to compare the suction values with strain cycles. The shallowest suction sensor in the shoulder was typically the most active of all sensors. The paved shoulders, edge drains, and trees sections sensors have consistently functioned throughout the monitoring period, shown in Figure 192. The correlation between pavement strain and suction is depicted in Figure 193 and Figure 194 for the paved shoulders and edge drain sections, respectively.

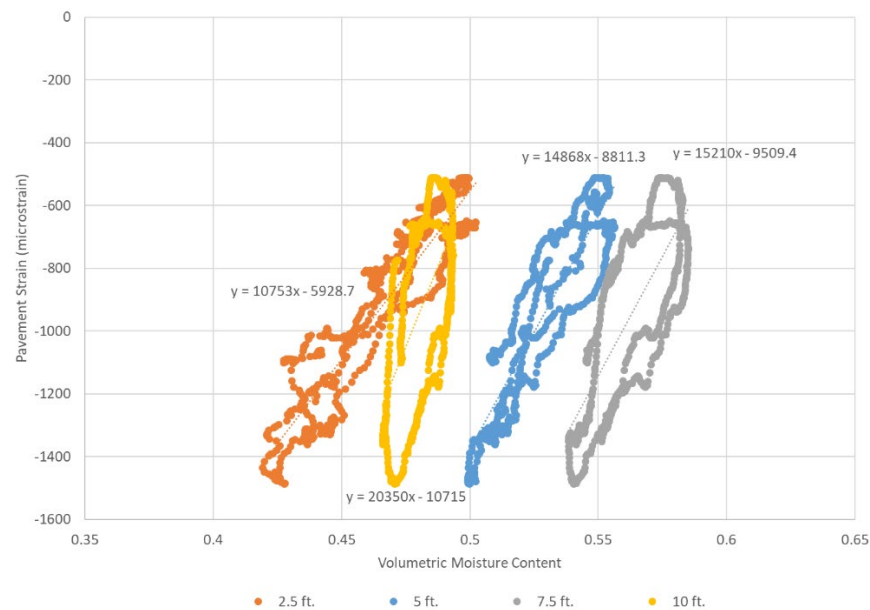


Figure 191: Relationship Between Strain and Volumetric Moisture Content from the Paved Shoulders Section

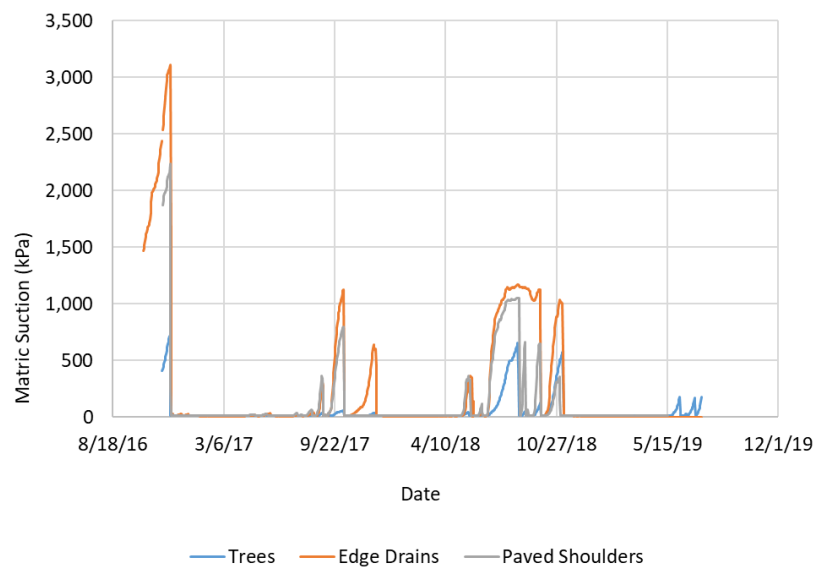


Figure 192: Comparison of Functioning Suction Sensor Measurements

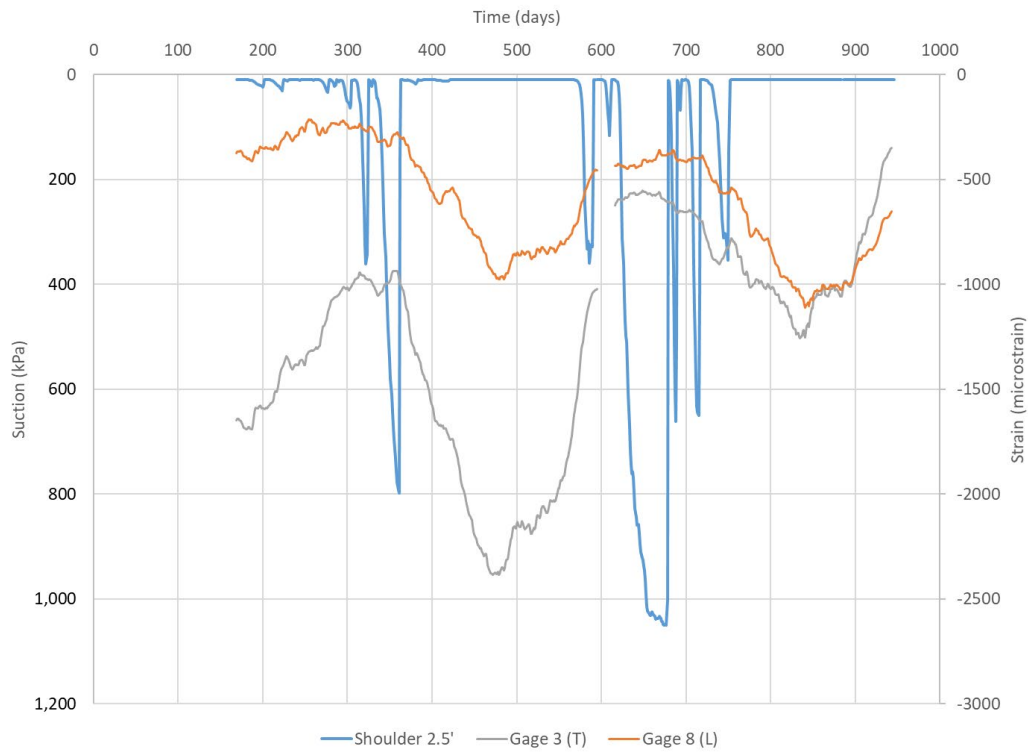


Figure 193: Suction and Strain Over Time for Paved Shoulders

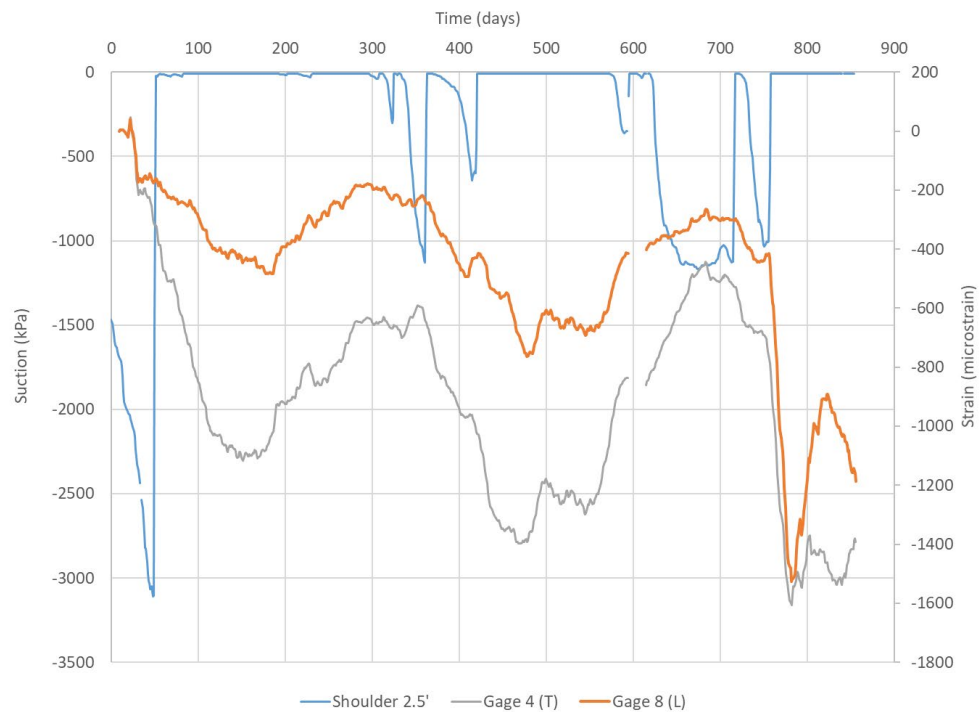


Figure 194: Suction and Strain Over Time for Edge Drains

6.4 Interpretation of IRI Tests

IRI tests were conducted periodically from construction until the end of the monitoring period. Table 22 shows the test record. Of note, the first test was conducted on May 31, 2014 and the final IRI test was conducted on June 12, 2020. The overall trend of the IRI tests show the average ride quality decreased in all sections by nearly the same amount over the monitoring period. There were no alarming changes. The comparative IRI averages are shown in Figure 195. In addition, the first IRI test conducted in 2014, the first IRI after resurfacing, and the most recent IRI are plotted together in Figure 196. It is worth noting that while the ride quality was poor in 2014, there has been an overall slight loss of ride quality in the four years since resurfacing of all sections. No one section has appeared to fare worse than another when comparing IRI results. Within the sections, there are discrete locations where the IRI values are above the threshold value, but overall, the ride quality is high.

Table 22: IRI Record for AL 5

IRI Test Date	Pre/Post
05/31/2014	Pre
11/05/2014	Pre
11/15/2016	Post
03/03/2017	Post
08/01/2017	Post
02/19/2018	Post
12/04/2018	Post
10/02/2019	Post
12/02/2019	Post
06/12/2020	Post

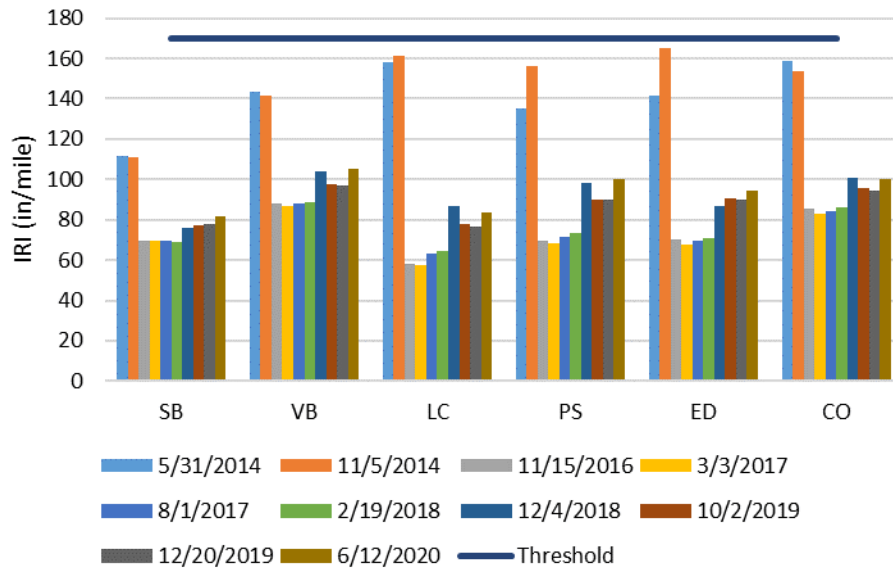


Figure 195: Average IRI by Test Section

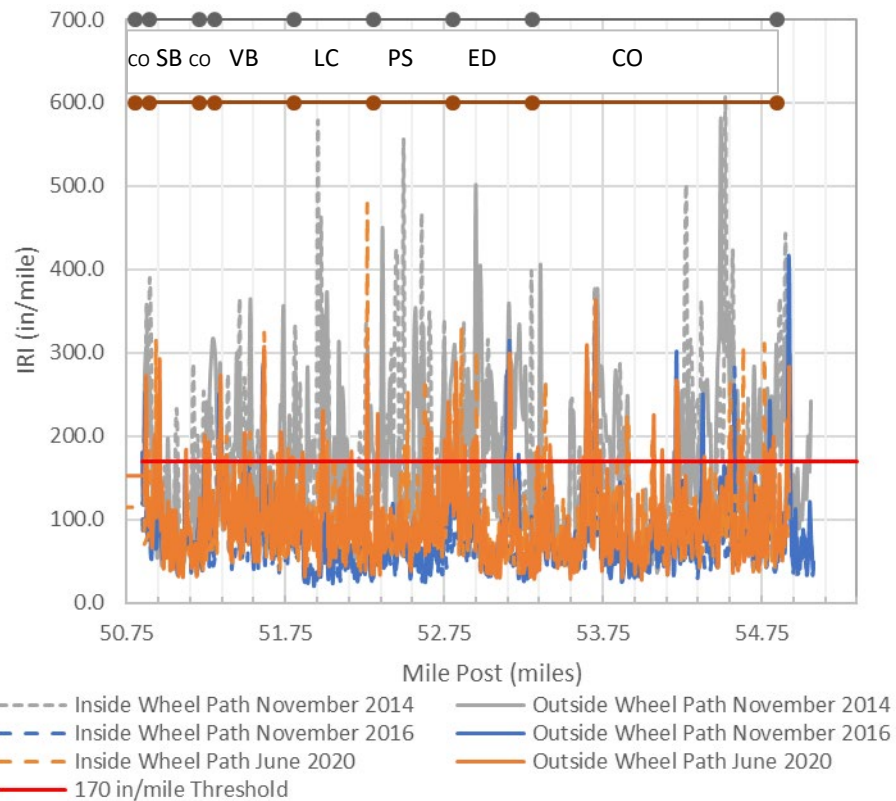


Figure 196: Comparison of IRI since 2014

6.5 Observations

In addition to the initial site survey, photographs were collected during the monitoring period. The following is a collection of images that shows performance on and off of the project after the remediation and resurfacing.

6.5.1 December 2016

During this site visit, the cracks in the safety widening of the vertical barrier sections were evident as in Figure 197. These were likely due to the folding over of the membrane barrier. Distresses were noted off project on both AL 5 in Perry County and US 80 in Dallas County. This is depicted in Figure 198 and Figure 199, respectively.



Figure 197: Longitudinal crack in Vertical Barrier section



Figure 198: Distress of pavement on AL 5 south of the Perry County line.



Figure 199: Off project distress on US80

6.5.2 December 2017

AL 5 between US 80 and the Dallas County line appeared severely distressed. Significant patching work was visible in areas where non-pine species trees encroach the roadway. This distress, shown in Figure 200, continued to be the case all along the section of AL 5 that extends to Safford. There was a section near Safford where the shoulders were paved out about 8 feet. It is interesting to note that while there was damage in areas where trees encroach, the damage was confined to the paved shoulder area. An area where trees encroach on the paved shoulders is shown in Figure 201.



Figure 200: Tree related distress on AL in Dallas County



Figure 201: Paved shoulder section of AL 5 in Dallas County

6.5.3 June 2018

During this site visit, the condition of the AL 5 test sections and surrounding roads was documented by video and continued shooting video between the Dallas/Perry County line and US 80. There was evidence of continued distress in the unimproved section in Dallas County. There were significant new patches and the ride is extremely rough. There appeared to still be a strong correlation between the presence of deciduous trees and the distress. This distress is clear in the photos included in Figure 202.



Figure 202: Observed Pavement Distress on AL 5 in Dallas County

6.5.4 November 2018

In November of 2018, the research team visited the site to maintain the dataloggers and also collect photographs. Distress was visibly noted in the paved shoulders, the lime columns and vertical barriers sections. Further, the stretch of AL 5 between the south boundary of the project and US 80 was in particularly poor condition. Figure 203 through Figure 206 that follow document the observations.



Figure 203: Cracking in the paved shoulders section



Figure 204: Visible Distress in paved shoulders section



Figure 205: Vertical barrier section crack propagation



Figure 206: Severe pavement distress south of the Dallas County line

6.5.5 October 2019

The research team visited AL 5 on October 16, 2019. Nearly two months had passed without rain, and qualitative impacts at the site were noted. The cracking in the southbound safety widening of the vertical barriers section had worsened. It appears that wide track farming equipment caused the existing crack to widen and settle, as depicted in Figure 207. Distress was

also visible in the edge drains section. There is a new crack along the southbound safety widening and within the southbound travel lane. These cracks are shown in Figure 208.



Figure 207: Vertical Barriers Crack



Figure 208: Shoulder and Lane Cracking in the Edge Drains

6.5.6 February 2020

The PI visited AL 5 on February 20, 2020. Distress was evident visually in most sections. There was cracking in the wearing surface and several instances of pavement shoving, likely from the truck traffic. For comparison, visual inspection of the portion of AL 5 from the Dallas County Line to Safford, AL showed severe distress in many stretches in that area, especially attributed to the presence of trees and also along built-up sections. Figure 207 through Figure 215 are still photos from a GOPRO inspection during the February 20 visit.



Figure 209: Edge Drains Section



Figure 210: Paved Shoulders Section



Figure 211: Lime Columns Section



Figure 212: Lime Vertical Barriers Section



Figure 213: Sand Blanket Section



Figure 214: Lime Control Section



Figure 215: Off project south of Dalla County Line

6.5.7 May 2020

During a site visit in May 2020, multiple shoving type failures were observed. There was also cracking along the safety widening of several sections. This cracking may be due to wide farm vehicles with wheels that ride along the safety widening and edge of pavement. The ride of AL 5 from the Dallas County Line to US 80 is still much rougher than the project test sections. There has been recent leveling and patching, especially along sections where broad leaf trees encroach the roadway. Figure 207 through Figure 221 are still photos from a GOPRO inspection during the May 21, 2020 visit.

The photos would lead one to believe that the sections are deteriorating, but there is little evidence from the IRI and sensor data to support that. Anecdotally, during the site visit, the ride quality was still smooth. The pavement deterioration would appear to be due to the damage of the wearing layer.



Figure 216: Cracking in Control Near Tree



Figure 217: Cracking along Safety Widening in Edge Drains Section



Figure 218: Shoving in Edge Drain Section



Figure 219: Shoving in Paved Shoulder Section



Figure 220: Opening Crack with Settlement in Safety Widening of Paved Shoulders



Figure 221: Pavement Surface Raveling in Control Section

6.6 Interpretation of Observations

The observations augment and reinforce the data collected from the sensors and IRI. Except for some isolated issues, the ride quality of the test sections was good through the monitoring period. The pavement seemed to be wearing, but at this time it did not appear to be the result of the subgrade soils. Off project observations provided an unimproved contrast to the AL 5 sections that was worth showing in this report.

Chapter 7. Decision Making and Implementation

This brief section provides guidance for the selection of remediation methods based on the results of this study. The project costs were used to evaluate the per mile investment. A decision matrix was developed with the Bureau of Materials and Tests to aid in future design.

7.1 Analysis of Cost Data

The entire project expenditure was \$7,260,921.62. This was a reduction under the original budget due to cancellation of the deep mixed columns section. The costs of the project were broken down into quantities that were unique to each section then overall items related to resurfacing. The final project consisted of 5 test sections, Sand Blanket, Vertical Barriers, Lime Columns, Paved Shoulders, and Edge Drains, and 3 controls, including the former Deep Mixed Columns. The costs for the sand blanket are also adjusted to reflect the potential cost for a 0.5 mile section for comparison. The cost breakdown is detailed in Table 23.

Table 23: Costs for AL 5 Test Sections and Overall Project

General Resurfacing Costs		\$ 3,039,237.04
Per Section, 8 sections		\$ 379,904.63

	Remediation Cost	Remediation Plus Resurfacing
1 Sand Blanket (0.31 mile)	\$750,322.89	\$1,130,227.52
1* Sand Blanket (0.5 mile)	\$1,186,260.49	\$1,566,165.11
2 Vertical Barriers	\$177,622.25	\$557,526.88
3 Lime Columns	\$1,257,761.34	\$1,637,665.97
4 Paved Shoulders	\$70,302.83	\$450,207.46
5 Edge Drains	\$55,966.28	\$435,870.91
6 Control	--	\$379,904.63
7 Deep Mixed Columns	\$1,909,708.99	\$2,289,613.62
8 Control	--	\$379,904.63

Of course, the cost of mobilizing and cancelling the Deep Mixed Columns was significant. For the remaining sections, the costs could be viewed in two tiers. The upper tier consisted of the Sand Blanket and Lime Columns. The lower tier were Vertical Barriers, Paved Shoulders, and Edge Drains.

7.2 Decision Tree for Insitu Remediation Techniques

One of the objectives of the project was to develop a decision matrix of remediation methods to aid ALDOT and other engineers in the selection of appropriate remediation methods for high volume change soils such as those present at AL 5. Based on the fact that most sections performed well, much of the decision making comes down to overall cost and construction constraints. The researcher suggests that the removal of high uptake broad leaf trees in the right of way be considered when distress is observed. The deep mixed columns are not included based on construction difficulty. The lime columns and sand blanket, while successful, were at a higher price point and were complicated to construct in terms of road closure and overall safety. Therefore, the three most economical solutions should be considered for remediation when high PI clays are verified via Atterberg limits testing. A simple decision tree, Figure 222, is offered for the selection of insitu remediation technique.

7.3 Recommendations on Remediation Options Not Investigated in the Current Study

Several techniques for remediation of expansive soils that were not utilized in this study were discussed in Chapter 3. Many of these methods were not appropriate for insitu remediation, while others were not prioritized by the PAC for investigation with the limited number of test sections available at AL 5. That being said, the following opinions are offered by the author to consider their advantages and limitations for ALDOT projects along with a relative comparison of cost.

Again, several of the methods discussed previously are only practical during new construction or complete reconstruction. The sand blanket was this case and is reflected in its relative cost to other options. The chemical stabilizers including lime, cement, fly ash, potassium, and ammonium would be implemented during construction/reconstruction, as would geogrid, horizontal moisture barriers, tire shreds, ponding, and traditional compaction. Thus, by pure cost these methods become unattractive. And again, some sort of detour would be required albeit a total closure, or single lane with remote stop light as was used by the contractor at AL 5. The other perspective is whether a specialty contractor or specialized equipment is required to perform the work. This bears out in overall increased cost magnitude and which includes mobilization and contingency. The author has summarized this as Table 24 in an effort to provide information for the use of any of the remediation methods.

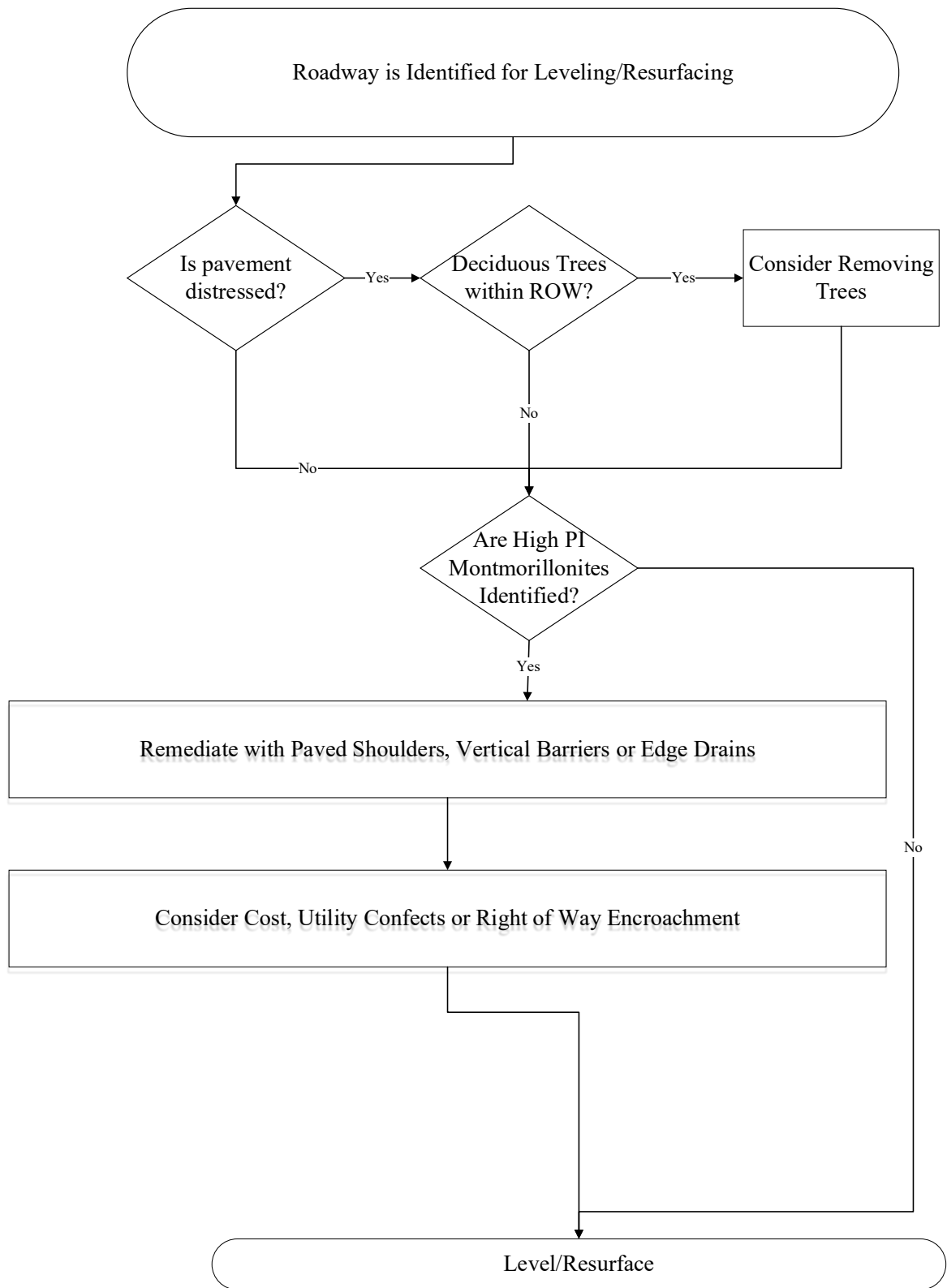


Figure 222: Decision Tree for Insitu Remediation

Table 24: Comparison of All Remediation Techniques

Remediation Method	Relative Cost	New Construction/ Total Rebuild	Pavement Patching	Specialty Contractor
Methods Considered in Present Study				
Tree Removal	\$			
Sand Blanket	\$\$\$	√		
Vertical Barriers	\$\$			
Lime Columns	\$\$		√	
Paved Shoulders	\$			
Edge Drains	\$			
Deep Mixed Columns	\$\$\$\$		√	√
Mechanical Improvement				
Compaction	\$	√		
Removal and Replacement/Surcharging	\$\$\$\$	√		
Horizontal Moisture Barriers	\$\$\$	√		
Geogrid/Geosynthetic	\$\$\$	√		
Ponding/Prewetting	\$\$	√		
Water Injection	\$		√	√
Tire Shreds	\$\$\$	√		
Chemical Improvement				
Lime Stabilization	\$\$	√		
Lime Injection	\$\$		√	√
Portland Cement Stabilization	\$\$\$	√		
Fly Ash	\$\$\$	√		√
Potassium and Ammonium	\$\$\$		√	√
Electrochemical Treatment	\$\$\$		√	√

Chapter 8. Summary, Conclusions, Implementation, and Recommendations

8.1 Project Summary

Significant lane miles of pavement in Western Alabama exhibit distress. The lifespan of these pavements is shorter than expected and the ride quality is poor. High volume change clay minerals are known to be distributed in a zone that stretches from Texas to southern Georgia. (Patrick and Snethen 1976). While the presence of clay minerals would be the obvious reason for damage, other factors including trees, clay softening, and excessive loading may have also contributed to this distress.

This study was undertaken to identify the cause of pavement distress and investigate remediation strategies that specifically did not require closure of the roadway. A literature review was conducted to examine the potential causes of soil volume change including clay mineralogy, unsaturated soil mechanics, and the impacts of vegetation on soil moisture content. Further, the shear strength of clays was investigated in both saturated and unsaturated states. A state-of-practice review was conducted to compile the techniques utilized in the remediation of expansive soils under roads.

With AL 5 identified as the subject roadway, an extensive study was conducted to determine the initial conditions including a desk study of historical documents and existing data, a site investigation with collection of undisturbed samples, an extensive effort to qualitatively and quantitatively document site conditions including pavement distress and tree location and density. International Roughness tests were initiated to provide a metric for pavement distress before remediation. Torsional shear strength tests were conducted, and the results used in slope stability analyses to determine whether shear strength was a factor for built up sections of AL 5.

Six remediation methods were chosen to be implemented in nominal 0.5 mile sections of AL 5 starting from the Perry County line proceeding north. These included a sand blanket, vertical moisture barriers, vertical lime columns, paved shoulders, edge drains, and deep mixed columns. The deep mixed columns were cancelled due to construction difficulty. The sections were instrumented with pavement strain gages along with several levels of moisture sensors, suction sensors, and pore water pressure sensors installed with depth in boreholes. A weather station was installed to monitor air temperature and rainfall along the test sections.

The sensors were monitored beginning November 2016 through June of 2020. Hourly measurements were averaged into daily values that were stored on remote dataloggers. The data was transmitted via cellular modem. Qualitative observations were made and documented using videos and photographs. IRI tests were conducted during the monitoring period to again provide a numeric measure of pavement performance.

8.2 Conclusions

In addressing the original research objectives, the following primary conclusions are offered:

- 1) The state-of-practice for shrink swell clay remediation for highway construction and maintenance was provided (chapter 3). A decision tree for their selection was developed and presented in chapter 7.
- 2) While the presence of expansive clay minerals was the primary cause of shrink swell distress, there were several mitigating factors. Atterberg limits verified the presence of montmorillonite in the test area (chapter 4). Tests to evaluate the swelling potential of these clays revealed swelling pressures up to 1500 psf with the potential to heave 10 feet or more of overburden soil. Other factors observed were frequent, overloaded trucks, and high uptake trees near the roadway (chapter 4). Further, the long term drained shear strength of the expansive prairie clays was determined and produced slope stability results with factors of safety well below 1. Thus, the distress and deterioration observed at the AL 5 test sections was due to a combination of the presence of expansive clays, the low shear strength of these clays, heavy truck traffic, and high uptake trees encroaching the roadways.
- 3) Five remediation methods were implemented at AL 5 including a sand blanket, vertical moisture barriers, lime columns, paved shoulders, and edge drains. The effectiveness of these methods was tracked with a combination of observations, instrumentation, and periodic IRI tests. No section appeared to stand out from a performance point of view among the group. Pavement damage accumulated over time, and it seems to come down to cost as a deciding factor in selection of which method to implement.

Several overarching conclusions can be made from this work:

- 1) Highly expansive clay minerals are present in the prairie clays common to western Alabama. These clays can be identified by the presence of montmorillonites that plot just below the U-Line on a plasticity chart.
- 2) These expansive clays have two important behaviors that impact pavements:
 - a. Moisture content increases can result in swelling pressures sufficient to heave the overburden soil and pavement.
 - b. The long term drained or fully softened strength of these prairie clays is low enough to result in slope failures in built-up embankment sections – even with very low slope angles.

- 3) The presence of high uptake broad leaf trees near the roadway visually correlates with pavement damage. Even at or beyond the right of way, broad leaf trees have root systems that often extend to the drip line. Pavement bounded by evergreen trees and grasses did not present damage.
- 4) Instrumentation reveals that the active zone for moisture fluctuation at AL 5 is approximately 7.5 ft below the pavement. Matric suction readings support this observation. With the average thickness of the clay layer at around 10 ft, moisture fluctuations are causing cycles of heave and settlement that contribute to pavement damage.

8.3 Implementation

The findings of this report can be integrated into ALDOT practice as follows:

- 1) When considering new construction or resurfacing, soil sampling along with Atterberg limits should be routinely used to identify the presence of expansive clay minerals.
- 2) When the minerals are identified, the following actions should be considered:
 - a. Observe the presence and types of trees and their proximity to the roadway, if they are broad leaf and within the right of way, they should be removed.
 - b. The safety widening should be increased to a minimum of 6 feet.

8.4 Recommendations for Future Research

While this study examined insitu mitigation of high volume change clays at AL 5, there are several ideas worth continued investigation:

- 1) The long term drained or softened shear strength of prairie clays should be investigated. It is clear that these materials played a role in the observed distress at AL 5, and had not been previously considered.
- 2) While the consideration of water or chemical injection was not considered for this work, the researcher believes that the practice of periodic water injection could be used to prolong the lifespan of roads such as AL 5 and should be investigated further.
- 3) Continued long term monitoring of the AL 5 sections terms of visual observation and IRI tests should be considered. It would be useful to gather data until the sections are resurfaced.

- 4) During the project, even more pronounced distress was observed on county roads that probably had less pavement structure than AL 5. Further study of the impacts of these mitigation strategies should be considered.

References

- Al-Mhaidib, A. I., and Al-Shamrani, M. A. (2006). "Influence of Swell on Shear Strength of Expansive Soils." *Advances in Unsaturated Soil, Seepage, and Environmental Geotechnics* (GSP 148).
- Alabama Department of Transportation (2014). "Materials Report for Planing and Resurfacing of SR5 from the Dallas County Line to MP 54.85, Project No. 99-305-535-005-401." Bureau of Materials and Tests, ed.
- Alabama Department of Transportation (2016). "Alabama Traffic Data." Retrieved Oct. 13, 2016 from <https://aldotgis.dot.state.al.us/atd/default.aspx>.
- Biddle, G. (2001). "Tree Root Damage to Building." *Expansive Clay Soils and Vegetative Influence on Shallow Foundations* (GSP 115).
- Bredenkamp, S., Scullion, T., Ragsdale, J., & Sebesta, S. (1999). *Evaluation of the Vertical Moisture Barrier Installed on IH 45 Near Palmer, Texas*. College Station, Texas: Texas Transportation Institute.
- Browning, G. (1999). *Evaluation of Soil Moisture Barrier*. Jackson, Mississippi: Mississippi Department of Transportation Research Division.
- Burrage, R. J. (2016). "Full Scale Testing of Two Excavations in an Unsaturated Piedmont Residual Soil." Ph.D. Dissertation, Auburn University.
- Casagrande, A. (1948). "Classification and Identification of Soils." *Transactions*, 113, 901-930.
- Chattopadhyay, P. K. (1972). *Residual Shear Strength of Some Pure Clay Minerals*. Ph.D. Thesis, University of Alberta, Edmonton, Canada.
- Chen, D.-H., Zhiming, S., & Mustafa, S. (2009). Roadway Heaving Caused by High Organic Matter. *Journal of Performance of Constructed Facilities*, 23(2), 100-108.
- Chen, D. H., Scullion, T., Hong, F., & Lee, J. (2012). Pavement Swelling and Heaving at State Highway 6. *Journal of Performance of Constructed Facilities*, 26(3): 335-344.
- Christensen, D. W., Bonaquist, R., & Jack, D. P. (2000). *Evaluation of Triaxial Strength as a Simple Test for Asphalt Concrete Rut Resistance*. Pennsylvania State University. University Park: The Pennsylvania Transportation Institute.
- Controls Group. (2019). Bromhead ring shear apparatus. Retrieved from <https://www.controls-group.com/eng/soil-mechanics-testing-equipment/bromhead-ring-shear-apparatus.php>

- Dawson, T. E. (1996). "Determining water use by trees and forests from isotopic, energy balance and transpiration analyses: The roles of tree size and hydraulic lift." *Tree Physiology*, 16(1-2), 263-272.
- Day, S. D., and Wiseman, P. E. (2009). "At the Root of It." *Arborist News*, 20-22.
- Decagon Devices, Inc. (2015a). "GS1 Soil Moisture Sensor." Operator's Manual. Pullman, WA.
- Decagon Devices, Inc. (2015b). "MPS-2 & MPS-6 Dielectric Water Potential Sensors." Operator's Manual. Pullman, WA.
- Evans, R. P., & Mcmanus, K. J. (1999). Construction of Vertical Moisture Barriers to Reduce Expansive Soil Subgrade Movement. *Transportation Research Record*(1652), 108-112.
- Federal Highway Administration. (2011). Improving FHWA's Ability to Assess Highway Infrastructure Health: Phase I Results - Final Report. FHWA. Retrieved February 18, 2015, from <http://www.fhwa.dot.gov/asset/health/phase1.pdf>
- Flackenstein, J. L., & Allen, L. D. (2007). Evaluation of Pavement Edge Drains and Their Effect on Pavement Performance. *Transportation Research Record*(1519), 28-35.
- Fredlund, D. G., & Morgenstern, N. R. (1977). Stress State Variables for Unsaturated Soils. *ASCE Journal of Geotechnical Engineering Division* GT5(103), 447-466.
- Fredlund, D. G., Morgenstern, N. R., and Widger, R. A. (1978). "Shear Strength of Unsaturated Soils." *Canadian Geotechnical Journal*, 15(3), 313-321.
- Fredlund, D. G., Hasan, J. U., and Filson, J. (1980). "The Prediction of Total Heave." *Proc., 4th International Conference on Expansive Soils*, 1-17.
- Fredlund, D. G., and Rahardjo, H. (1993). *Soil Mechanics for Unsaturated Soils*, John Wiley & Sons, Inc., New York.
- Fredlund, D. G., Rahardjo, H., & Fredlund, M. D. (2012). *Unsaturated Soil Mechanics in Engineering Practice*. Hoboken, NJ: John Wiley & Sons, Inc.
- Fung, Y. C. (1965). *Foundations of Solid Mechanics*, Prentice-Hall, Englewood Cliffs, NJ.
- Gay, D. A., & Lytton, R. L. (1988). Moisture Barrier Effects on Pavement Roughness. *ASCE National Convention: Measured Performance of Shallow Foundations* (pp. 88-107). Nashville, Tennessee: ASCE.
- Google Earth (2014). "Alabama Highway 5." Google Earth, (32°29'09.73"N, 87°22'20.08"W).
- Harris, M. C. (1998). *Soil Survey of Perry County, Alabama*. Washington, D.C.: United States Department of Agriculture (USDA).

- Hayward Baker. (1990). Injection Systems. Retrieved February 19, 2015, from Hayward Baker Geotechnical Construction:
<http://www.haywardbaker.com/WhatWeDo/Techniques/GroundImprovement/InjectionSystems/default.aspx>
- Hayward Baker. (2010). Hayward Baker Geotechnical Construction. Retrieved February 19, 2015, from Injection Systems:
<http://www.haywardbaker.com/WhatWeDo/Techniques/GroundImprovement/InjectionSystems/default.aspx>
- Herman, J. M. (2015). Damage to Pavements from Expansive Clays: A Review of Behavior and Remediation Techniques. MCE Research Paper, Auburn University.
- Holtz, W. G. (1959). "Expansive Clays – Properties and Problems." Quarterly of the Colorado School of Mines, 54(4), 89-125.
- Holtz, W. G. (1983). "The Influence of Vegetation in the Swelling and Shrinkage of Clays in the United States of America." Geotechnique, XXXIII(2), 159-163.
- Holtz, R.D. and Kovacs, W.D., (1981). An Introduction to Geotechnical Engineering. Prentice Hall, Englewood Cliffs.
- Indraratna, B., Fatahi, B., and Khabbaz, H. (2006). "Numerical Analysis of Matric Suction Effects of Tree Roots." Geotechnical Engineering, 159(2), 77-90.
- Jackson, D. T. (2016). Insitu Measurement of Pavement Distress and Causal Mechanisms in Expansive Soil along Alabama Highway 5. MS Thesis Dissertation, Auburn University.
- Jayatilaka, R., Gay, D. A., Lytton, R. L., & Wray, W. K. (1993). Effectiveness of Controlling Pavement Roughness Due to Expansive Clays with Vertical Moisture Barriers. College Station, Texas: Texas Transportation Institute.
- Jayatilaka, R., & Lytton, R. L. (1997). Prediction of Expansive Clay Roughness in Pavements with Vertical Moisture Barriers. Austin, Texas: Texas Department of Transportation Research and Technology Transfer Office.
- Jones, D. T. (2017). Moisture Content Monitoring using a Nuclear Moisture Gauge and Preliminary Findings at Alabama Highway 5. MS Thesis Dissertation, Auburn University.
- Kennedy, L.P. (2019). Drained Residual Strength of Expansive Soils Causing Pavement Distress along Alabama Highway 5. MS Thesis Dissertation, Auburn University.
- Kenney, T. C. (1959). Discussion. Journal of the Soil Mechanics and Foundations Division, 85, 67-79.

- Koelling, M. A. (1994). Ground Improvement Case Histories for Highway Construction. Proceedings of the 45th Highway Geology Symposium. Portland.
- Lambe, T. W., & Whitman, R. V. (1969). Soil Mechanics. New York: John Wiley & Sons, Inc.
- Little, D. N. (1995). Handbook for Stabilization of Pavement Subgrades and Base Courses with Lime.
- Little, D. N., Males, E. H., Prusinski, J. R., & Stewart, B. (2000). Cementitious Stabilization.
- Little, D. N., & Nair, S. (2009). Recommended Practice for Stabilization of Sulfate Rich Subgrade Soils. Texas Transportation Institute, Texas A&M University.
- Lu, N., & Likos, W. J. (2004). Unsaturated Soil Mechanics. Hoboken, NJ: John Wiley & Sons, Inc.
- Mackiewicz, S. M., & Ferguson, E. G. (2005). Stabilization of Soil with Self-Cementing Coal Ashes. 2005 World of Coal Ash (WOCA). Lexington, Kentucky.
- Madhyannapu, R. S. (2007). Deep Mixing Technology for Mitigation of Swell-Shrink Behavior of Expansive Soils of Moderate to Deep Active Depths. Dissertation, The University of Texas at Arlington.
- Madhyannapu, R. S., Puppala, A. J., Bhadriraju, V., & Nazarian, S. (2009). Deep Soil Mixing (DSM) Treatment of Expansive Soils. 2009 US-China Workshop on Ground Improvement Technologies. ASCE.
- Madhyannapu, R. S., Puppala, A. J., Nazarian, S., & Yuan, D. (2010). Quality Assessment and Quality Control of Deep Soil Mixing Construction for Stabilization Expansive Subsoils. Journal of Geotechnical and Geoenvironmental Engineering, 136(1): 119-128.
- McCarthy, D. F. (2007). Essentials of Soil Mechanics and Foundations: Basic Geotechnics (7th ed.). Pearson.
- McKinney, R. L., Kelly, J. E., & McDowell, C. (1974). The Waco Ponding Project. Austin, Texas: Center for Highway Research: The University of Texas at Austin.
- McQueen, I. S., and Miller, R. F. (1974). "Approximating Soil Moisture Characteristics from Limited Data: Empirical Evidence and Tentative Model." Water Resources Research, 10(3), 521-527.
- Mikkelsen, P.E., & Green, G.E. (2003). "Piezometers in Fully Grouted Boreholes." Symposium on Field Measurements in Geomechanics. Oslo, Norway.
- Mitchell, J. K. (1976). Fundamentals of Soil Behavior, John Wiley & Sons, Inc., Canada.

- Mitchell, J.K. (1993). *Fundamentals of Soil Behavior*. John Wiley & Sons, Inc., New York, NY.
- Mitchel, J. K., and Soga, K. (2005). *Fundamentals of Soil Behavior*. Wiley.
- Monroe, W.H. (1941). Notes on Deposits of Selma and Ripley Age in Alabama. *Geologic Survey of Alabama, Bulletin No. 48*. Tuscaloosa, AL.
- Nelson, J. D., and Miller, D. J. (1992). *Expansive Soils: Problems and Practice in Foundation and Pavement Engineering*. New York: John Wiley & Sons, Inc.
- NOAA National Climatic Data Center (2010). "Selma Alabama 1981-2010 Climate Normals." NOAA Satellite and Information Service, ed.
- Patrick, D. M., and Snethen, D. R., (1976). *Expansive Earth materials – A Survey by Physiographic Areas of Their Occurrence and Distribution*. U. S. Army Engineers Experiment Station, Vicksburg, Mississippi, 34 p
- Pengelly, A., and Addison, M. (2001). In-Situ Modification of Active Clays for Shallow Foundation Remediation. *Expansive Clay Soils and Vegetative Influence on Shallow Foundations* (pp. 192-214). Houston: ASCE.
- Petry, T. M., and Little, D. N. (2002). Review of Stabilization of Clays and Expansive Soils in Pavements and Lightly Loaded Structures - History, Practice, and Future. *Journal of Materials in Civil Engineering*, 14(6), 447-460.
- Picornell, M., & Lytton, R. L. (1986). Behavior and Design of Vertical Moisture Barriers. *Transportation Research Record*(1137), 71-81.
- Puppala A.J., and Cerato A., (2009). "Heave distress problems in chemically-treated sulfate laden materials." *Geo-Strata*, 10(2), 28-30,32.
- Raymond, D. E., Osborne, W. E., Copeland, C. W., & Neathery, T. L. (1988). *Alabama Stratigraphy*. Circular No. 140. Geologic Survey of Alabama, Tuscaloosa, Alabama.
- Reed, P.C. (1969). "Geologic Map of Perry County, Alabama." *Geologic Survey of Alabama, Map No. 118*. Tuscaloosa, AL.
- Rendon-Herrero, O., (2011). "Introduction - special issue on construction on expansive soils." *Journal of Performance of Constructed Facilities*, 25(1) 2.
- RocScience (2018). "Slide2 Program Overview." Retrieved April 12, 2020 from https://www.rocscience.com/help/slide2/program_overview/introduction.htm.

- Rollins, K. M., and Christie, R. (2002). Pavement and Subgrade Distress - Remedial Strategies for Construction and Maintenance (I-15 Mileposts 200-217). Provo, UT: Civil & Environmental Engineering Department, Brigham Young University.
- Sayers, M. W., & Karamihas, S. M. (1998). The Little Book of Profiling. The University of Michigan.
- Seda, J., Lee, J., & Carraro, J. (2007). Beneficial Use of Waste Tire Rubber for Swelling Potential Mitigation in Expansive Soils. GeoDenver 2007, New Peaks in Geotechnics: Soil Improvement, (pp. 1-9). Denver, Colorado.
- Snethen, D. R. (1979). Technical Guidelines for Expansive Soils in Highway Subgrades. Washington, D.C.: Federal Highway Administration.
- Snethen, D. R. (2001). "Influence of Local Tree Species on Shrink/Swell Behavior of Permian Clays in Central Oklahoma." Expansive Clay Soils and Vegetative Influence on Shallow Foundations, 158-171.
- Stallings, E. G. (2016). Investigation of Pavement and Subgrade Distress at Alabama Highway 5. MS Thesis, Auburn University.
- Steinberg, M. L. (1977). Ponding an Expansive Clay Cut: Evaluations and Zones of Activity. Transportation Research Board(641), 61-66.
- Steinberg, M. L. (1980). Deep Vertical Fabric Moisture Seals. Fourth International Conference on Expansive Soils (383-400). Denver, CO: ASCE.
- Steinberg, M. L. (1985). "Controlling Expansive Soil Destructiveness by Deep Vertical Geomembranes on Four Highways." Transportation Research Record, 1032: 48-53.
- Steinberg, M. L. (1989). Further Monitoring of Twelve Geomembrane Sites in Texas. Austin, Texas: Texas State Department of Highways and Public Transportation.
- Steinberg, M. L. (1992). "Vertical moisture barrier update". Transportation Research Record, 111-117.
- Steinberg, M. L. (1998). Geomembranes and the Control of Expansive Soils in Construction. The McGraw-Hill Companies, Inc.
- Steinberg, M. L. (2000). Expansive Soils and the Geomembrane Remedy. Advances in Unsaturated Geotechnics (pp. 456-466). Denver, Colorado: Geotechnical Special Publications.
- Szabo, M. W., Osborne, E. W., Copeland, C. W., & Neathery, T. L. (1988). Geologic Map of Alabama. Special Map 220. Geological Survey of Alabama.

- Taboada, M. A. (2003). "Soil Shrinkage Characteristics in Swelling Soils." Lecture.
- Tand, K. E., and Vipulanandan (2011). "Case Study of Settlement of A foundation on Expansive Clay due to Moisture Demand." Proc., Geo-Frontiers 2011: Advances in Geotechnical Engineering, American Society of Civil Engineers.
- Terzaghi, K. (1943). Theoretical Soil Mechanics, Wiley, New York.
- Timm, D.H. (2009). "Design, Construction, and Instrumentation of the 2006 Test Track Structural Study." Report No. 09-01, National Center for Asphalt Technology, Auburn University, 2009.
- Tu, H., and Vanapalli, S. K. (2016). "Prediction of the variation of swelling pressure and one-dimensional heave of expansive soils with respect to suction using the soil-water retention curve as a tool." Canadian Geotechnical Journal, 1-22.
- U.S. Bureau of Reclamation USBR (1974). Earth Manual. 2nd Ed., Denver.
- Wanyan, Y., Manosuthkij, T., Abdallah, I., Nazarian, S., & Puppala, A. J. (2008). Expert System Design Guide for Lower Classification Roads over High PI Clays. El Paso, Texas, Center for Transportation Infrastructure Systems.
- Watt, W. G., & Steinberg, M. L. (1972). Measurements of Swelling Clay in a Ponded Cut. Center for Highway Research: The University of Texas at Austin.
- White, D. J., Harrington, D., & Thomas, Z. (2005). Fly Ash Soil Stabilization for Non-Uniform Subgrade Soils, Volume I: Engineering Properties and Construction Guidelines. Ames, IA: Center for Transportation Research and Education.
- Wilkinson, A., A. Haque, and J. Kodikara. (2010). Stabilisation of clayey soils with industrial by-products: Part B. Proc. Inst. Civ. Eng. Ground Improv. 163 (3): 165–172.
- Yong, R. W. and Warkentin, B.P., (1966). Introduction to Soil Behavior. Macmillan, New York.
- Zapata, C. E., Houston, W. N., Houston, S. L., and Walsh, K. D. (2000). "Soil–Water Characteristic Curve Variability." Advances in Unsaturated Geotechnics, 84-124.
- Zornberg, J. G., & Gupta, R. (2009). Reinforcement of Pavements Over Expansive Clay Subgrades. 17th International Conference on Soil Mechanics and Geotechnical Engineering, (pp. 765-768).

